Originally Processed With FOIA(s):
1998-0004-F[2]; 2005-0336-F

FOIA Number:
S

FOIA MARKER

This is not a textual record. This is used as an administrative marker by the George Bush Presidential Library Staff.

Record Group/Collection: George H.W. Bush Presidential Records
Collection/Office of Origin: Chief of Staff, White House Office of
Series: Sununu, John, Files
Subseries: White House Offices Files

OA/ID Number: 29184
Folder ID Number: 29184-008

Folder Title:
Science and Technology (Bromley) (1991) [8]

Stack:	Row:	Section:	Shelf:	Position:
G	15	25	6	1

CONTENTS

Tab A.	**Satellite Measurements of Global Atmospheric Temperatures**
Tab B.	**Ground-based Temperature Measurements - 100-year Data Set and Urbanization Effects**
Tab C.	**Nighttime Warming versus Daytime Warming and Effects**
Tab D.	**The Ocean Conveyor Belt Theory**
Tab E.	**The Gore 6-month Temperature Update (Gore requested these authors to send him a temperature/data update every 6 months)**
Tab F.	**Schlesinger and Jiang - "Revised Projection of Future Greenhouse Warming"**

Reprint Series
30 March 1990, Volume 247, pp. 1558–1562

SCIENCE

Precise Monitoring of Global Temperature Trends from Satellites

ROY W. SPENCER AND JOHN R. CHRISTY

Copyright © 1990 by the American Association for the Advancement of Science

JUN 6 '91 10:27 FROM NASA/MSFC ESAD(ES41) TO G S WILSON PAGE.002

Precise Monitoring of Global Temperature Trends from Satellites

ROY W. SPENCER AND JOHN R. CHRISTY

Passive microwave radiometry from satellites provides more precise atmospheric temperature information than that obtained from the relatively sparse distribution of thermometers over the earth's surface. Accurate global atmospheric temperature estimates are needed for detection of possible greenhouse warming, evaluation of computer models of climate change, and for understanding important factors in the climate system. Analysis of the first 10 years (1979 to 1988) of satellite measurements of lower atmospheric temperature changes reveals a monthly precision of 0.01°C, large temperature variability on time scales from weeks to several years, but no obvious trend for the 10-year period. The warmest years, in descending order, were 1987, 1988, 1983, and 1980. The years 1984, 1985, and 1986 were the coolest.

ACCURATE ESTIMATES OF GLOBAL ATMOSPHERIC TEMPERATURES are needed for evaluation of global climate models, detection of climate changes, and a better understanding of the climate system. Global temperatures have generally been estimated from surface temperature records, but there has been much debate regarding, for example, whether these data provide evidence of recent greenhouse warming (*1*). The primary source of uncertainty is the relatively sparse distribution of thermometers over the surface of the earth. Most of the earth is covered by oceans, and vast oceanic areas go unmeasured. Even over land, the coverage is greatest where the population is greatest; therefore, remote land areas also go unmeasured. An additional problem is that urban sites, which represent only a small part of the globe but where many long-term measurements have been made, have warmed because of heat from man-made structures, and thus these records are difficult to interpret (*2, 3*). Depending upon how the thermometer data are analyzed, various answers can be expected. In contrast to surface thermometers, sensors on satellite platforms can provide nearly complete earth coverage in as little as one day and can obtain measurements from various levels of the atmosphere. Calibration of satellite sensors is particularly difficult, however. For climate temperature monitoring a precision of 0.1°C is needed, a goal that has been perceived as difficult for any earth viewing radiometer. The difficulty arises from uncertainty about the long-term stability of satellite sensors. In this article, we show that accurate long-term global temperature measurements can be obtained from satellites now operating and discuss data obtained from 1979 to 1988.

R. W. Spencer is at Marshall Space Flight Center Huntsville, Code ES43, Huntsville, AL 35812. J. R. Christy is at Johnson Research Center, University of Alabama, Huntsville, AL 35899.

Methodology. In late 1978, a series of passive microwave radiometers was launched aboard the TIROS-N series of National Oceanic and Atmospheric Administration (NOAA) satellites. These radiometers, or microwave sounding units (MSUs), are Dicke-type radiometers designed to measure the thermal emission of radiation by atmospheric O_2 at four frequencies near 60 GHz (*4*). The atmospheric concentration of O_2 is constant in both space and time (*5*), and thus O_2 provides a stable temperature tracer. The strong interaction of radiation from 50 to 70 GHz with O_2 through rotational energy transitions causes absorption and emission. As the channel frequency of the MSU approaches the 60-GHz peak in this absorption complex, higher levels in the atmosphere will be measured (Fig. 1) (*6*). We have analyzed data from MSU channel 2, which measures the temperature of the middle troposphere at 53.74 GHz. At 57.95 GHz, MSU channel 4 can be used to monitor temperatures of the lower stratosphere. MSU channels 1 and 3 are more difficult to interpret for climate purposes because channel 1 is too sensitive to surface effects on the earth and cloud water, whereas channel 3 detects radiation from a strong temperature-transition region between the troposphere and stratosphere (the tropopause). The four channels have traditionally been used to obtain vertical profiles of temperature in remote regions of the earth where weather balloon data are not available. However, because the weighting

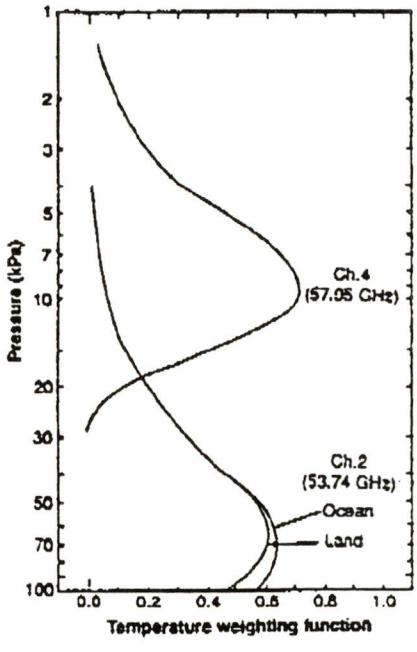


Fig. 1. Temperature weighting functions (unitless) for MSU channels 2 (mid-troposphere) and 4 (lower stratosphere). Also shown are the different channel 2 weighting functions for ocean and land surfaces, which arise because the less emissive ocean reflects more of the downwelling atmospheric radiation back upward. Sensitivity to the surface radiation itself cannot be implied from the magnitudes at the intersection of the curves with the surface. [Adapted from (*6*)]

JUN 6 '91 10:27 FROM NASA/MSFC ESAD(ES41) TO G S WILSON PAGE.003

functions for each channel are vertically broad (Fig. 1), retrieval of adequate data on the vertical temperature structure of the atmosphere that are needed for computer modeling of the weather has been difficult. The temperature measurement within a constant-pressure depth, however, rather than at traditionally measured specific pressure levels, is completely adequate, even preferable in some respects, for climate monitoring.

The MSUs are externally calibrated, after each earth scan of the instrument, by measurement of the cosmic background radiation (for our purposes, constant at 2.7 K), and a warm target in the instrument that has its temperature monitored with redundant platinum resistance thermometers. This calibration design is considered to be the best available for microwave radiometers because any temperature changes in the instrument components are canceled out. The earth-viewing measurements are then calculated as a "brightness temperature" (T_b) by interpolation between these two reference extremes. The term "brightness temperature" acknowledges that the temperature measurement is actually based upon radiative brightness and is only equal to a thermometric temperature when the emitting body is completely "black" (nonreflective). This condition is nearly true of measurements of the atmosphere from MSU channel 2.

Satellite intercomparison. Because two MSUs have usually been simultaneously operating on separate satellites, a comparison between them shows how different sensors agree in their measurements and gives an estimate of errors. The NOAA-6 and NOAA-7 MSUs were simultaneously operating during a period of nearly 2 years (29 June 1981 to 16 April 1983). These satellites are in sun-synchronous, near-polar orbits, and have constant local crossing times of 7:30 a.m. and p.m. and 2:30 a.m. and p.m., respectively. The precession rates of their orbits are quite different so that in a single day there are many differences (but also many overlaps) in the areas of the globe sampled by the two satellites. The MSUs scan across the satellite subtrack, and thus paint out swaths of coverage about 2000 km wide beneath the satellites.

We averaged the channel 2 T_b data from the separate satellites at 2-day intervals over both the Northern and Southern hemispheres in 2.5°-latitude bands with cosine-latitude weighting to account for the decrease in surface area of these bands toward the poles. We reduced contamination of the measurements by large thunderstorm complexes, which cause infrequent depressions in T_b over small areas (*6*, *7*), by excluding any scan lines that had individual footprint measurements that deviated by more than 1.5°C from their average relationship to both neighboring footprint measurements. The resulting variations in the 2-day averages are dominated by the seasonal change of temperature (*8*), termed the annual cycle. This annual cycle is sinusoidal in shape, and a smoothed cycle was computed for each satellite individually. Then this cycle was subtracted from the original 2-day time series to arrive at the anomalies in temperature, that is, the temperature deviations from the average temperature for a particular time of year. A period of data considerably longer than 2 years is necessary for a more representative annual cycle (and thus, more representative anomalies), but the short-term data are utilized only for satellite intercomparison. Several revealing observations can be made from the data (Fig. 2):

1) The standard deviation (SD) of the sums of the data from the two satellites is much larger than the SD of their differences. This relation means that both satellites were measuring nearly the same temperature variations and implies that hemispheric temperature anomalies can be measured with relatively little error from a single satellite. The 2-day average difference between these satellites was about 0.05°C, and for monthly averages, the difference improved to about 0.011°C. Similar noise was found in monthly comparisons between data acquired from sensors on (i) TIROS-N and NOAA-6 (0.012°C), (ii) NOAA-7 and NOAA-9 (0.012°C), (iii) NOAA-9 and NOAA-10 (0.006°C), and (iv) NOAA-10 and NOAA-11 (0.008°C), although much shorter overlap periods were available. Thus, we estimate that the precision of monthly satellite measure-

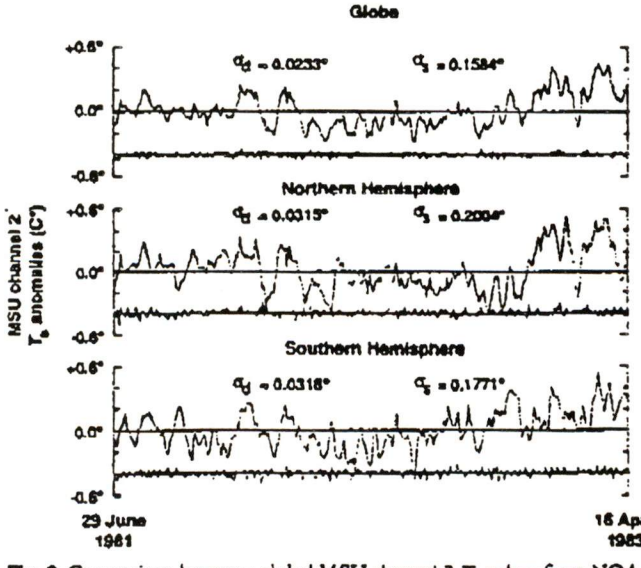


Fig. 2. Comparison between global MSU channel 2 T_b values from NOAA-6 and NOAA-7 during a nearly 2-year period (29 June 1981 to 16 April 1983) when both satellites had MSUs operating. Time series of global and hemispheric satellite averages (sum divided by 2) and differences (difference divided by 2) are shown by the large-variation and small-variation curves, respectively. The difference time series are offset −0.4°C for legibility. The SD of the two-satellite sums (σ_s) and differences (σ_d) are also listed.

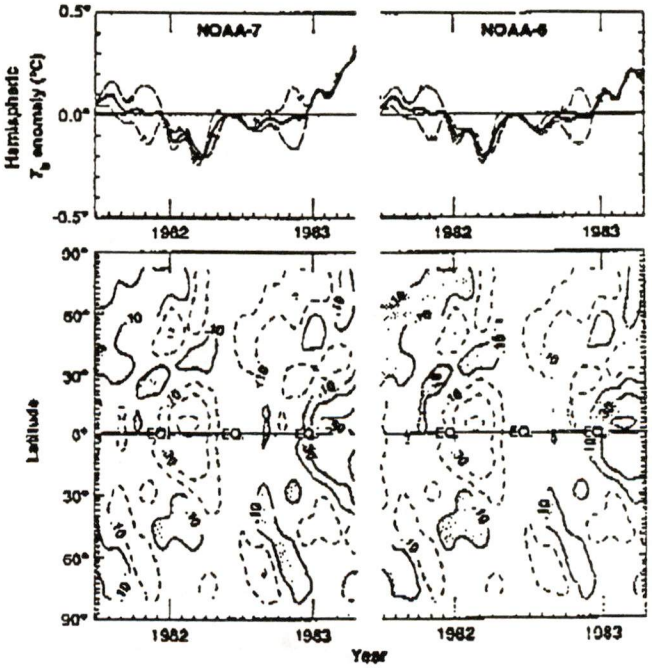


Fig. 3. Low-pass filtered hemispheric (top) and zonally averaged (bottom) MSU channel 2 T_b anomalies during the 2-year overlap period of NOAA-6 (right) and NOAA-7 (left); "N" and "S" labels represent Northern and Southern hemispheres, respectively, and the global time series is the heavy line. The time series do not agree near the beginning and end of the period because of the low-pass filter and the lack of data past the end of the period for NOAA-6 or before the beginning of the period for NOAA-7. Warm zonally averaged anomalies are stippled.

JUN 6 '91 10:28 FROM NASA/MSFC ESAD(ES41) TO G S WILSON PAGE.004

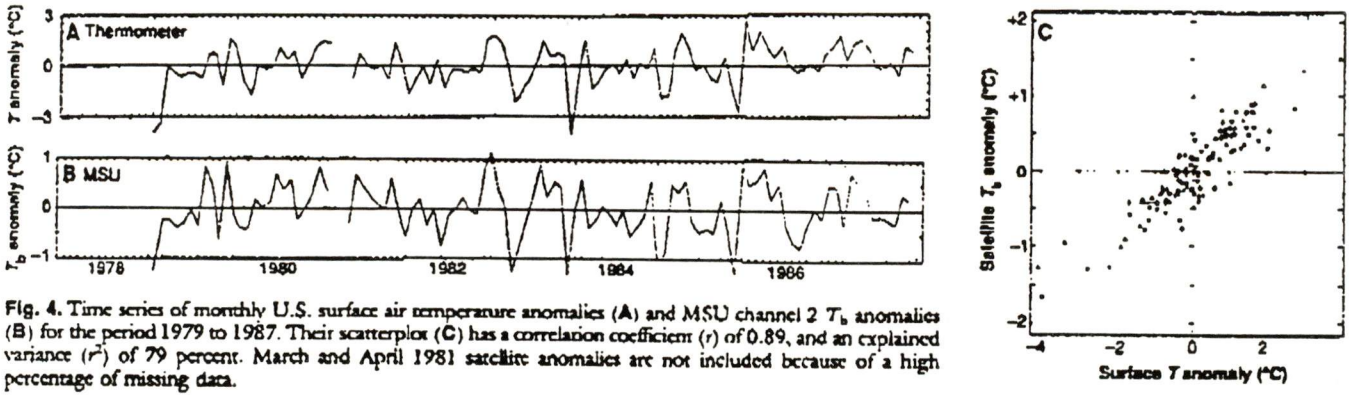


Fig. 4. Time series of monthly U.S. surface air temperature anomalies (A) and MSU channel 2 T_b anomalies (B) for the period 1979 to 1987. Their scatterplot (C) has a correlation coefficient (r) of 0.89, and an explained variance (r^2) of 79 percent. March and April 1981 satellite anomalies are not included because of a high percentage of missing data.

ments is about ±0.01°C for the globe.

2) The sums of the two sets of data reveal that dramatic globally averaged warming and cooling events of greater than 0.5°C can occur in less than 2 weeks. The warmings, representing huge energy exchanges, are possibly associated with stormy periods when large amounts of latent heat were released in precipitation of moisture previously evaporated from the sun-warmed ocean. The coolings might be from formation of widespread low-level cloudiness, which reflects significant amounts of incoming solar radiation.

3) The long-term drift of one instrument relative to the other, seen in the difference time series in Fig. 2, is so small that it is virtually unmeasurable. Any trend is less than ±0.01°C for the 2-year period. This high degree of stability was unexpected. The four other satellite overlaps mentioned above also gave no indication of drift.

Further evidence that the measurements were repeatable is shown by low-pass filtered (*9*) times series of hemispheric (and global) temperature anomalies from NOAA-7 and NOAA-6 data and the zonally averaged distribution of those anomalies (Fig. 3). The zonal averages allow examination of which latitude bands of the earth were responsible for the warm or cool events seen in the hemispheric and global time series. The zonal average patterns are nearly identical between satellites. Such agreement improves our confidence that even regional areas can be studied to find the origins of the hemispheric anomalies.

Comparisons with United States and global thermometer measurements. Although the above results indicate that the sampling provided by a single satellite is geographically extensive and that the measurements are radiometrically stable enough to be useful for monitoring climate, it still must be demonstrated that MSU measurements are closely related to temperature. Earlier investigators have made point comparisons between weather balloon data and satellite measurements (*10–12*). The differences between individual radiosonde and satellite measurements are generally less than 1.0°C. These differences are usually attributed to (i) the isolated balloon sampling compared to the large area represented by a single satellite measurement (a circular footprint 110 km in diameter); (ii) errors in calibration of the balloon thermometer before its release; (iii) the random noise of a single MSU measurement, about 0.3°C; and (iv) time mismatches between the satellite and balloon observations. We compared the 1980 through 1988 MSU observations to T_b data obtained from radiosondes launched twice daily by 66 National Weather Service offices around the United States. The T_b data were calculated with the radiative transfer equation for MSU channel 2, and thus the radiosondes had to reach a fairly high-pressure altitude, 2 kPa or less. Only MSU data within 200 km of the radiosonde location and within 3 hours of its release time were included. The comparisons revealed that there were biases of up to ±1°C between the two data sets; the biases are most easily related to the difference in time between the release time of the radiosondes (all simultaneous at 00 and 12 GMT) and the MSU observation times, which are sun synchronous. After correction for these biases on a station-by-station basis, we found no long-term trend in the 9 years of differences between MSU and radiosonde-calculated T_b values and a monthly SD of 0.068°C.

The MSU data also can be compared to records of temperature variability from near-surface thermometers. Even though they are different variables, their common variability helps to assess how well coupled the near-surface temperature variations are to the deep layer variations. Although the global distribution of thermometers is suspected by many researchers as being inadequate for accurate monitoring, the distribution over the United States is widely

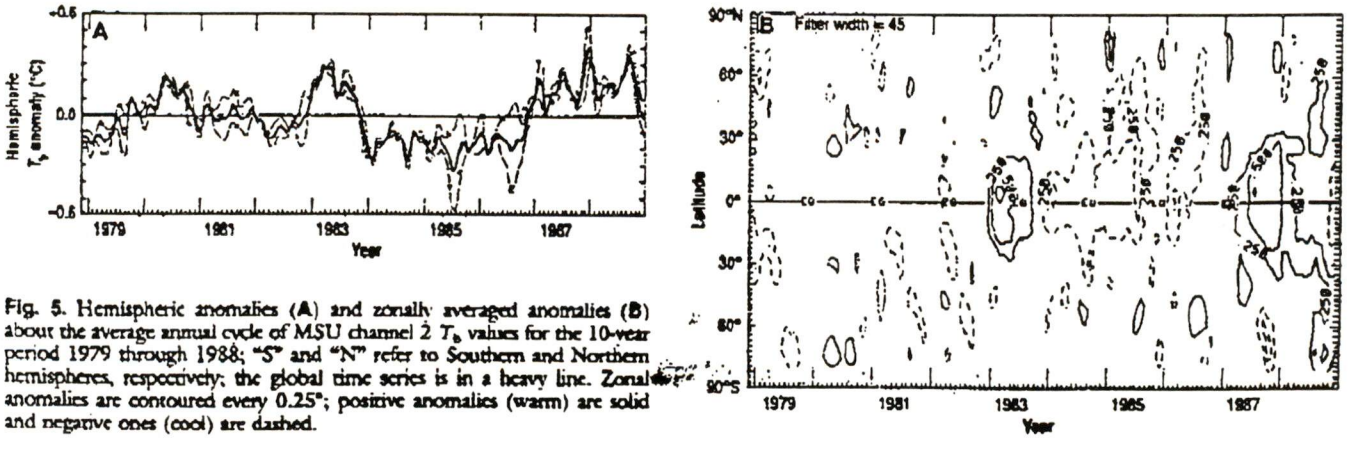


Fig. 5. Hemispheric anomalies (A) and zonally averaged anomalies (B) about the average annual cycle of MSU channel 2 T_b values for the 10-year period 1979 through 1988; "S" and "N" refer to Southern and Northern hemispheres, respectively; the global time series is in a heavy line. Zonal anomalies are contoured every 0.25°; positive anomalies (warm) are solid and negative ones (cool) are dashed.

JUN 6 '91 10:28 FROM NASA/MSFC ESAD(ES41) TO G S WILSON PAGE.005

accepted as good enough for climate work. We compared monthly temperature anomalies from thermometers over the contiguous United States for the period 1979 through 1987 (*13*) to our monthly mid-tropospheric temperature anomalies from the satellites. The resulting anomaly time series (Fig. 4, A and B) are similar, as verified by a scatterplot (Fig. 4B) and a correlation coefficient of 0.89. This correlation agrees with those between radiosonde near-surface and upper air measurements, for which monthly temperature anomalies range from 0.8 for the eastern United States to greater than 0.9 for the western United States. The surface anomalies are typically two to three times as great as the MSU anomalies. This relation is probably a result of daytime solar heating and nighttime cooling of the surface, which largely control the deeper air mass temperatures over the United States on monthly and seasonal time scales.

Two major research groups have been responsible for hemispheric calculations of temperature anomalies from thermometer measurements, and we refer to them by their leading authors names: Jones (*14, 15, 16*) and Hansen (*17*). Their results have been sufficiently different to spark debate in the climate community and have led to conflicting reports in the popular press regarding global temperature trends. We have compared our satellite-measured hemispheric anomalies to the thermometer-based anomalies from these two groups (Table 1). Again, when the separate systems are viewed as a bivariant distribution in which we wish to determine the level of common variability, these comparisons reveal that the level of agreement between the calculations by Jones and the satellite data is about 40% better than that between the calculations by Hansen and the satellite data. As might be expected for two land-dominated data sets, the Jones and Hansen data are much better correlated with each other, with an explained variance of 94%, than either is with the MSU data. The much lower explained variances for the hemispheres and globe (Table 1) compared to the United States are the result of both poor thermometer coverage over much of the earth and weak thermal coupling between the middle and lower troposphere over much of the oceans. This latter effect was deduced from radiosonde near-surface and deep layer temperature comparisons: When monthly surface temperature anomalies from radiosonde are compared to the corresponding radiosonde-calculated channel 2 anomalies for United States–controlled ocean stations, the explained variances drops to about 35% for the Caribbean, 0 to 20% for the tropical Pacific, and 25% for the tropical south Atlantic. Although there are few high-latitude ocean radiosonde stations, the data suggest that the thermal coupling increases poleward (for example, 52% in Iceland), probably because of the wider range of air mass temperatures encountered there. Thus we would not expect as good agreement between MSU anomalies and tropical ocean surface air temperature anomalies as are obtained over land, even if the oceanic thermometer coverage were adequate. This conclusion is substantiated by the somewhat poorer agreement between the satellite data and combined thermometer and sea surface temperature data from

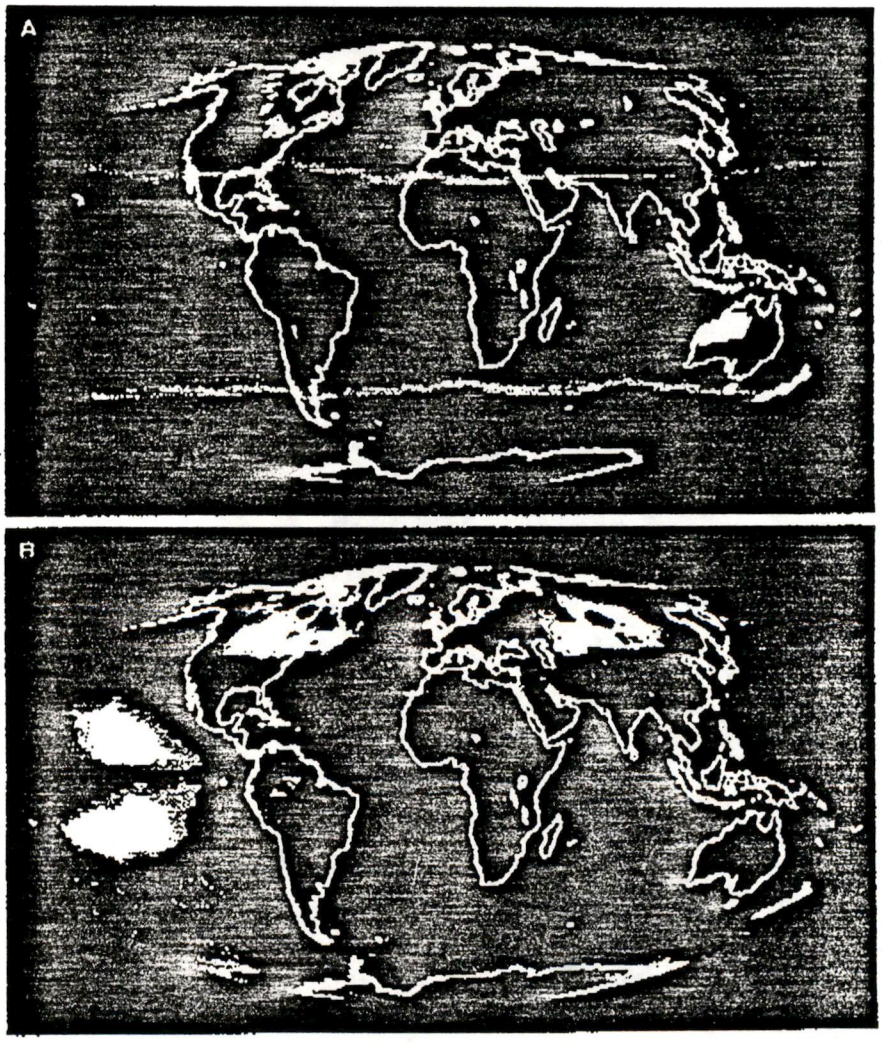


Fig. 6. Average MSU channel 2 T_b (A) during the 10-day period 26 January to 5 February and temperature anomalies (B) for the same 10-day period during the 1983 ENSO climate anomaly. Temperatures range in top image is gray, representing 235 K, to red, representing 260 K, in 1 K increments; temperature anomalies in bottom image change color every 0.25 K, the blue side of dark gray is colder, red side is warmer.

JUN 6 '91 10:29 FROM NASA/MSFC ESAD(ES41) TO G S WILSON PAGE.006

Table 1. Monthly and annual explained variances (in percent) between MSU and thermometer-measured temperature anomalies for United States (U.S.), Northern (NH) and Southern (SH) hemispheres, and the globe from 1979 to 1988. Thermometer-based calculations for the United States are from Karl (*13*); monthly and annual hemispheric and global thermometer anomalies are from Jones (*14–16*); annual anomalies are from Hansen and Lebedeff (*17*), and hemispheric and global anomalies, which also include sea surface temperatures, are from Farmer *et al.* (*18*).

Source	U.S.	NH	SH	Globe
		Monthly		
Karl	77			
Jones		33	10	35
Farmer		26	11	28
		Annual		
Karl	77			
Hansen		67	27	53
Jones		72	66	74
Farmer		77	24	69

Farmer *et al.* (*18*) (Table 1). The poor agreement raises the important issue of whether near-surface temperatures or deep layer temperatures should be monitored for detection of climate change. Because they are often different from one another over the tropical oceans, it would be best to monitor both in order to gain an understanding of how the entire troposphere behaves. Indeed, it might well be that the oceanic surface air layer is so strongly coupled to sea surface temperature variations that a deep layer mean would provide an earlier signal of possible greenhouse warming.

Global temperature anomalies 1979 to 1988. The first 10 years of satellite data reveal large fluctuations in the hemispheric and global temperatures (Fig. 5A). The Northern and Southern hemispheres trends follow each other for the slower, interannual trends, but often oppose each other on monthly to seasonal time scales. The warmest years, in decreasing order, were 1987, 1988, 1983, and 1980. There is no obvious long-term trend, and anomalies during the first 5 years nearly balance those during the last 5 years. The 1988 warm event was traced to the mid-latitudes, as was the 1980 warm anomaly. Both years included summer heat waves in the United States. The largest warm anomaly in the Northern Hemisphere for the 10-year record occurred in 1987 and 1988 (Fig. 5B). The 1987 and 1983 warm events were associated with El Niño/Southern Oscillation events [ENSOs (*19*)]. During the 1983 ENSO, transfer of heat from record-setting sea surface temperatures in the eastern Pacific to the atmosphere caused major changes in atmospheric flow that impacted weather conditions worldwide. Warming locally exceeded 2°C in two Pacific anticyclones (Fig. 6) that straddled an equatorial zone of intense convective activity caused by the warm water. This event caused globally averaged temperatures to rise more in several months than what is expected within several decades if enhanced greenhouse warming is occurring. Although the 1987 ENSO has been considered weaker than the 1983 ENSO, it was associated with higher temperatures that were more uniformly spread throughout the tropics. The mid-latitudes in both the Southern and Northern hemispheres in 1988 experienced warm conditions that appear to be coupled to the 1987 tropical warmth. The period 1984 to 1986 was dominated by cooler than normal tropical air. The 10-year time series exhibits bifurcation in that there are nine cool or warm years, and only one year (1981) that could be considered "average." This pattern makes the definition of what is "normal" for global temperatures uncertain, for as shown above normal can mean either warm or cool conditions.

The future. Our data suggest that high-precision atmospheric temperature monitoring is possible from satellite microwave radiometers. Because of their demonstrated stability and the global coverage they provide, these radiometers should be made the standard for the monitoring of global atmospheric temperature anomalies since 1979. Their use will allow relatively precise monthly determinations of the locations and magnitudes of temperature change events. The resulting data should provide a greater focus of scientific debate on why temperature anomalies occur rather than whether they occur. The advanced microwave sounding units (AMSU) will replace the MSU on NOAA satellites in the mid-1990s, and these units will allow extension of the time series into the next century. Various computerized climate models, which predict future changes through time-dependent equations representing physical processes, can now be evaluated with accurate global temperature measurements. These data should result in improved specification of processes in these models, which still require independent verification. These improvements should facilitate more informed policy decisions concerning the effects of anthropogenic greenhouse gas production.

REFERENCES AND NOTES

1. R. A. Kerr, *Science* 246, 1118 (1989).
2. R. C. Balling and S. B. Idso, *J. Geophys. Res.* 94, 3359 (1989).
3. T. R. Karl, H. E. Diaz, G. Kukla, *J. Climate* 1, 1099 (1988).
4. M. L. Meeks and A. E. Lilley, *J. Geophys. Res.* 68, 1683 (1963).
5. L. Machta and E. Hughes, *Science* 168, 1582 (1970).
6. N. C. Grody, *J. Climate Appl. Meteorol.* 22, 609 (1983).
7. R. W. Spencer, H. M. Goodman, R. E. Hood, *J. Atmos. Ocean. Tech.* 6, 254 (1989).
8. Other, smaller signals are also present in the measurements. These include a small surface temperature contribution (8 percent of the total over land, 4 percent over the ocean), wind-induced roughening of the ocean surface, cloud liquid water effects, water vapor variations, sea surface temperature changes, and soil moisture changes. The effects of variations in each of these parameters on the measured T_b values have been theoretically evaluated, and have been determined to be small for MSU channel 2 (0.01°C or less) on a hemispheric and global basis. Larger effects could conceivably occur over small regions. In contrast, MSU channel 4 is essentially unaffected by any of these changes. The radiative transfer theory involved in the analysis of these effects is covered in (*6*).
9. Low-pass filtering of the time series allows isolation of the more slowly varying temperature variations that are of interest to climatologists. Here, the filter retains 50 percent of the power of cycles having 90-day periods, progressively less power of periods shorter than 90 days, and more power of longer periods.
10. N. C. Grody, *Remote Sensing of the Atmosphere and Oceans*, A Deepak, Ed. (Academic Press, New York, 1980).
11. _____ and W. C. Shen, *NOAA Tech. Rep. NESS 88* (1982).
12. E. R. Westwater, Z. Wang, N. C. Grody, L. M. McMillin, *J. Atmos. Oceanic Tech.* 2, 97 (1985).
13. T. Karl, unpublished data.
14. P. D. Jones *et al.*, *J. Climate Appl. Meteorol.* 25, 161 (1986).
15. P. D. Jones, S. C. B. Raper, T. M. L. Wigley, *ibid.*, p. 1213.
16. P. D. Jones, *J. Climate* 1, 654 (1988).
17. J. Hansen and S. Lebedeff, *J. Geophys. Res.* 92, 13,345 (1987).
18. G. Farmer, T. M. L. Quigley, P. D. Jones, M. Salmon, *Documenting and Explaining Recent Global Mean Temperature Changes* (Climatic Research Unit, University of East Anglia, Norwich, 1989).
19. R. S. Quiroz, *Mon. Weather Rev.* 111, 1685 (1983).

20. R. Jenne and D. Joseph provided the MSU data used in this study; R. Hood provided data processing and programming support; N. Grody collaborated on portions of this research and provided general advice; F. Wentz provided updated sea surface emissivity estimates; P. Olsen, F. Soltis, and P. Swanson assisted us in obtaining technical data on the MSU; G. Wilson helped obtain the satellite data sets; discussions with J. Dodge and R. McNider led to the present research.

27 October 1989; accepted 23 February 1990

JUN 6 '91 10:30 FROM NASA/MSFC ESAD(ES41) TO G S WILSON PAGE.007

Reprinted from JOURNAL OF CLIMATE, Vol. 3, No. 10, October 1990
American Meteorological Society

Global Atmospheric Temperature Monitoring with Satellite Microwave Measurements: Method and Results 1979–84

ROY W. SPENCER

Earth Science and Applications Division, NASA Marshall Space Flight Center, Alabama

JOHN R. CHRISTY

Johnson Research Center, University of Alabama in Huntsville, Huntsville, Alabama

NORMAN C. GRODY

NOAA/NESDIS, Washington, D.C.

(Manuscript received 21 October 1989, in final form 4 May 1990)

ABSTRACT

A method for measuring global atmospheric temperature anomalies to a high level of precision from satellites is demonstrated. Global data from the Microwave Sounding Units (MSUs), flying on NOAA satellites since late 1978, have been analyzed to determine the extent to which these data can reveal atmospheric temperature anomalies on bidaily and longer time scales for regional and larger space scales. The global sampling provided by the MSUs is an important asset, with most of the earth sampled bidaily from each of (typically) two instruments flying concurrently on separate satellites at different solar times. The primary source of tropospheric thermal information is from the MSU 53.74 GHz channel. This channel is primarily sensitive to thermal emission from molecular oxygen in the middle troposphere, with relatively little sensitivity to water vapor, the earth's surface, and cloud (especially cirrus) variations. The long-term stability of the oxygen mixing ratio in the atmosphere makes it an ideal tracer for climate monitoring purposes. Lower stratospheric temperature anomalies are derived from the MSU 57.95 GHz channel.

Comparisons between monthly MSU temperature anomalies and corresponding thermometer-measured anomalies for the United States reveal a high (0.9) correlation, but hemispheric anomalies show much lower correlations. This results from some combination of poor thermometer sampling of remote regions and weak coupling of surface and deep-tropospheric temperature anomalies in tropical areas.

Analysis of data from two of the MSUs (on NOAA-6 and NOAA-7), whose operational periods overlapped by two years, reveals that hemispheric temperature anomalies measured by the separate instruments are very similar (to about 0.01°C) on monthly time scales. Their combined time series of unfiltered two-day hemispheric averages show standard deviations of their mean of 0.15°–0.20°C and standard deviations of their average difference of 0.02°–0.03°C, indicating a signal-to-noise ratio of 40 for the Southern Hemisphere and 45 for the Northern Hemisphere. The intercomparison period also reveals no evidence of calibration drift between satellites at the 0.01°C level. This was substantiated by two 15-month comparisons of NOAA-6 with rawinsonde data from 45 stations in the eastern United States, which revealed 0.013°C net difference over five years. Monthly averaged comparisons between individual rawinsonde and NOAA-6 data from 1980 through 1982 reveal a monthly standard deviation of their difference of 0.04°C. The statistical and geophysical portions of this noise are found to be about equal in magnitude, 0.03°C. The single-satellite noise due to imperfect sampling for ten-day, 2.5° gridpoint temperatures was calculated by measuring the standard deviation of the difference between two satellites with ranges from 0.2°C in the tropics to 0.4°C in middle latitudes.

The period of analysis (1979–84) reveals that Northern and Southern hemispheric tropospheric temperature anomalies (from the six-year mean) are positively correlated on multiseasonal time scales but negatively correlated on shorter time scales. The 1983 ENSO dominates the record, with early 1983 zonally averaged tropical temperatures up to 0.6°C warmer than the average of the remaining years. These natural variations are much larger than that expected of greenhouse enhancements, and so it is likely that a considerably longer period of satellite record must accumulate for any longer-term trends to be revealed.

1. Background and theory

a. The problem

Changes in the global climate system have received high level of scientific, political, and public visibility in the last several years. The possibilities of rising ocean levels and significant regional changes in climate due to anthropogenic greenhouse enhancements have captured widespread attention. Unfortunately, the potentially inadequate geographical distribution of thermometers has resulted in much uncertainty (and thus controversy) about whether temperature anomalies on a hemispheric basis can even be confidently inferred from conventional data. Sparsely populated regions are

Corresponding author address: Dr. Roy W. Spencer, ES43, NASA Marshall Space Flight Ctr., Huntsville, AL 35812.

JUN 6 '91 10:31 FROM NASA/MSFC ESAD(ES41) TO G S WILSON PAGE.008

either poorly measured or not measured at all. Changes in thermometer exposure due to urbanization are known to result in apparent warming of well populated locations (Karl et al. 1988; Balling and Idso 1989). Unfortunately, correction for this urbanization effect is difficult since the majority of land station locations have likely experienced some sort of local increase in exposure to man-made structures. Of course, most oceanic areas go unmeasured. Thus, we are faced with the task of understanding what portion of climate change is to be attributed to man versus "natural" variations, when we cannot even quantify with confidence what the background natural variability is.

b. *Satellites to monitor climate?*

In contrast to conventional measurements, satellites can provide the global coverage that is needed to monitor the earth's atmosphere. Unfortunately, the issue of satellite instrument calibration has typically been a source of great concern and uncertainty. However, possibly the best calibrated instruments in earth orbit to date have direct application to the global atmospheric temperature monitoring issue. These are the Microwave Sounding Units (MSUs), built by the Jet Propulsion Laboratory (JPL) for the National Oceanographic and Atmospheric Administration's (NOAA) operational weather monitoring needs. Because these instruments measure a vertically averaged atmospheric temperature, we feel that they have the potential for significantly augmenting the surface-based thermometer record by providing a measurement representing a significant depth of the troposphere, rather than just a thin near-surface layer sensitive to variable surface effects (urbanization, desertification, etc.). This paper provides detailed technical aspects of the MSUs utility as a climate monitoring device. A related paper (Spencer and Christy 1990) summarizes the global temperature anomalies observed during 1979–88.

c. *Theory*

The MSUs are designed to measure the thermal emission by molecular oxygen in the atmosphere at different spectral intervals in the oxygen absorption complex near 60 GHz (Meeks and Lilley 1963). Because the oxygen abundance in the atmosphere is very stable in both space and time (Warnek 1988) it makes an ideal tracer for radiometric atmospheric temperature monitoring. As Machta and Hughes (1970) state, "all reliable oxygen data since 1910 fall in the range of 20.945%–20.952% by volume," with the instrumental accuracy of in situ measurements being ±0.006% by volume. In contrast, infrared temperature monitoring methods depend upon thermal emission from CO_2, the mixing ratio of which is much more variable in space and time.

At microwave frequencies, radiance is directly proportional to the temperature of the emitting body. The radiometer output is usually converted to a "brightness temperature" (T_b). The term "brightness temperature" acknowledges that the measurement is based upon radiative brightness that equals a thermometric temperature only when the measured object is radiating as a black body (unit emissivity, and thus zero reflectivity).

While T_b is measured directly by the satellite, radiative transfer theory can be used to evaluate the different radiation emission and scattering processes which lead to the measured T_b. Conceptually, the transfer of radiation leading to the satellite measurement at the MSU frequencies involves three "sources": 1) a dominating direct (upward) thermal emission by the atmosphere; and smaller contributions from 2) an "indirect" (downward) atmospheric emission reflected by the surface back up to the satellite, and 3) a surface emission shining through the (mostly opaque) atmosphere. Based upon the theory for nonscattering atmospheres, the T_b at a given frequency, $T_b(\nu)$, depends on the vertically integrated atmospheric temperature, $T(p)$, between the satellite and the earth's surface, viz.,

$$T_b(\nu) = \int_{\ln p_s}^{-\infty} T(p)[d\bar{\tau}_\nu(p)/d\ln p]\,d\ln p + \bar{\tau}_\nu(p_s)T_s. \tag{1}$$

The integral is written in pressure coordinates, p, where p_s is the surface pressure and T_s is the surface skin temperature. For conciseness, an "effective transmittance function" is defined which is virtually independent of temperature

$$\bar{\tau}_\nu(p) = [1 - (1 - e_s(\nu, \theta)) \times (\tau_\nu(p_s)/\tau_\nu(p))^{2\sec\theta}]\tau_\nu(p)^{\sec\theta} \tag{2}$$

where $\bar{\tau}_\nu(p_s) = \tau_\nu(p_s)^{\sec\theta} e_s$ represents the surface emission term in Eq. 1, e_s is the surface emissivity, and θ is the Earth incidence angle.

Equation 2 contains the atmospheric transmittance function, $\tau_\nu(p)$, which is the exponential absorption along the vertical path between the satellite and an arbitrary pressure level. As a satellite instrument scans away from nadir (vertical), the increased absorption due to longer path lengths is accounted for by the $\sec(\theta)$ terms. Also, the contribution due to the reflected radiation by the surface is contained in the term having the factor $(1 - e_s)$. As discussed below, a compensating surface effect is contained in the surface emission term, $\tau_\nu(p_s)^{\sec\theta} e_s T_s$, in (1).

In (1), T_b is expressed as a vertically (pressure) weighted atmospheric temperature, where the weighting function is defined as $-d\tau_\nu(p)/d\ln p$ (see Fig. 1). In typical applications of the four channels of MSU data, (1) is inverted to retrieve the atmospheric temperature profile $T(p)$. We depart from this approach by interpreting the MSU channel 2 and 4 T_b for more nearly what they are, a vertically averaged temperature measurement of the atmosphere. However, to accu-

JUN 6 '91 10:32 FROM NASA/MSFC ESAD(ES41) TO G S WILSON PAGE.009

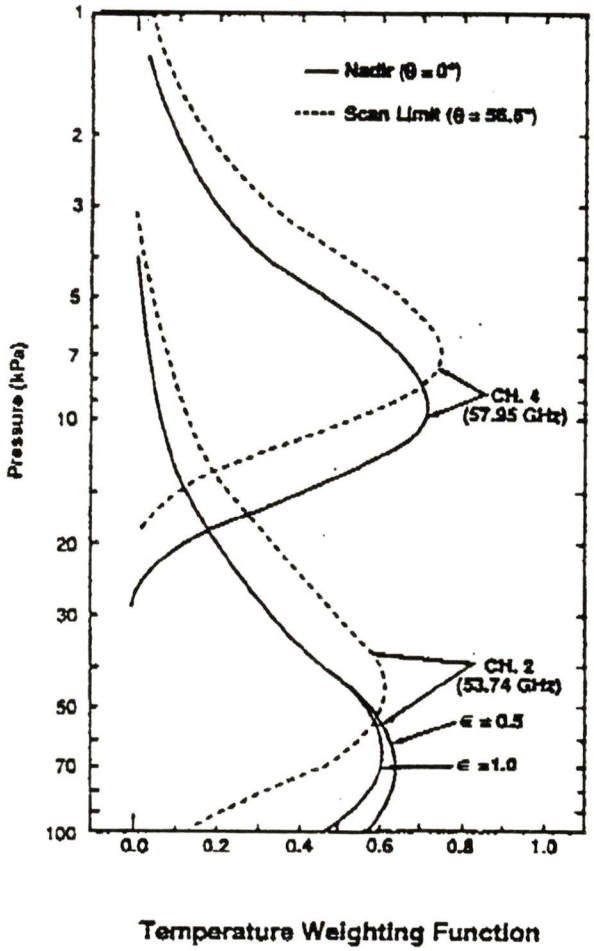


FIG. 1. Temperature weighting functions for MSU channels 2 (53.74 GHz) and 4 (57.95 GHz), for the nadir (solid) and extreme (dashed) scan positions. Also shown is the difference in the weighting functions for ocean (emissivity = 0.5) and land (emissivity = 1.0) surfaces (figure adapted from Grody 1983).

rately represent the weighted temperature, the function must have a unique pressure dependence for a given frequency. This is achieved by having channels with the following characteristics:

a) the absorption is predominately due to uniformly mixed gases, such as oxygen, whose absorption increases uniformly with pressure;

b) the absorption due to variable atmospheric constituents, such as water vapor and clouds, is very small compared to the uniformly mixed gas; and

c) the effects due to surface emissivity variations are very small compared to the T_b changes due to atmospheric temperature.

As discussed below, excluding precipitation effects, these properties are characteristic of the three highest frequency MSU channels.

MSU sampling characteristics

a. Channels

The MSUs heritage is from previous, experimental instruments on NASAs Nimbus series of research satellites (Staelin et al. 1973, Waters et al. 1975). The MSUs are four-channel passive microwave Dicke-type radiometers. Our calibration of the MSU output in terms of T_b is described in the Appendix. A T_b measurement is made by the MSU an average of every 0.4 s, each having an instrumental noise of 0.3°C.

The frequencies of MSU channels 1–4 are 50.30, 53.74, 54.96, and 57.95 GHz, respectively. Measurements made close in frequency to the 60 GHz absorption peak (e.g., MSU channel 4 at 57.95 GHz) are influenced mostly by the upper atmosphere since the absorption (and thus emission) by oxygen is so strong that the lower atmosphere cannot be "seen" by that channel (Fig. 1). Measurements made farther in frequency from the absorption peak (e.g., MSU channel 2 at 53.74 GHz) experience less atmospheric absorption and can see some of the earth's surface emission and cloud water emission "shining through" the partly opaque atmosphere. Thus, the MSU channel 2 T_b measurement cannot be ascribed totally to oxygen thermal emission, as some contributions from clouds, water vapor, and the surface exist. These effects will be addressed in more detail later. MSU channel 1 experiences only weak oxygen emission and is quite sensitive to surface and cloud effects.

The small amount of stratospheric influence on the tropospheric channel 2 and the tropospheric influence on the stratospheric channel 4 will be neglected here. Accurate correction for the overlap of these channels (Fig. 1) requires knowledge of the vertical distribution of temperature anomalies which is not generally available. Therefore, in all following analyses it must be remembered that a small portion (few percent) of a stratospheric temperature anomaly will be included in the tropospheric channel, and vice versa.

The traditional use of the MSU has been daily monitoring of synoptic tropospheric temperature structure over data-sparse regions (especially oceans) for numerical weather prediction. Their utility for this purpose has often been less than desired, due primarily to the broad vertical slice of the atmosphere sampled by each MSU channel. This characteristic has made difficult the retrieval of satellite "soundings" with acceptable vertical resolution through inversion of (1).

b. MSU viewing geometry

The MSUs are mounted underneath the NOAA TIROS-N series of satellites, which have sun-synchronous near-polar orbits at nominal local crossing times of 0730 and 1930 LST for the "morning" satellites and 0230 and 1430 LST for the "afternoon" satellites. To date, these satellites include TIROS-N, NOAA-6, NOAA-7, NOAA-8, NOAA-9, NOAA-10 and NOAA-11. The period of analysis for this study (1979–1984) will utilize TIROS-N, NOAA-6, and NOAA-7. The periods of useful data acquisition from the satellites we consider during this six-year period are illustrated in Fig. 2.

JUN 6 '91 10:32 FROM NASA/MSFC ESAD(ES41) TO G S WILSON PAGE.010

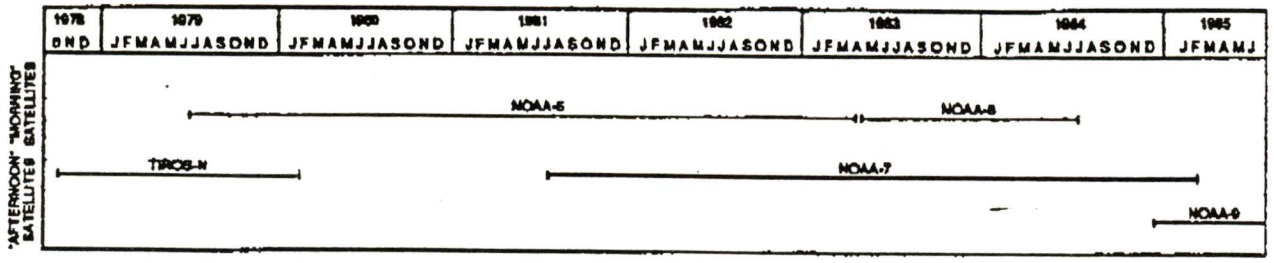


FIG. 2. Periods of useful MSU data acquisition from TIROS-N, NOAA-6, NOAA-7, NOAA-8, and NOAA-9 satellites from late 1978 through early 1985.

Each MSU scans across the satellite suborbital track through nadir (Fig. 3) such that it measures eleven "footprints" having a 3 dB (half-power) beamwidth of 7.5°. Half-power beamwidth is defined by the points on the sides of the antenna main lobe where the received energy is 50% of that at the lobe center. Due to the increasingly oblique viewing off-nadir, combined with the curvature of the earth, footprints off-nadir have increasing horizontal sizes. The 11-footprint scan lines are repeated every 25.6 seconds providing 170 km spacing between scan lines. The 7.5° beamwidth from the satellite orbital altitude of approximately 850 km results in an atmospheric footprint horizontal size (spatial resolution) at nadir of about 110 km (circular), increasing to about 180 km by 320 km (elliptical) at the scan extremes. The radiation received by the MSU is spatially weighted by the antenna beam pattern, which is dominated by the main lobe (about 2.5 times the width of the 3 dB beamwidth), outside of which only a small amount of radiation (2%–4%) is received. In stark contrast to the point measurement of a thermometer, the horizontal and vertical sampling of each MSU measurement represents approximately 100,000 km^3 of atmosphere.

For reasons to be explained below, only the middle seven of the eleven footprints are used in this study. An example of the resulting geographical distribution of two day's total number of footprints falling within 2.5° grid squares (Fig. 4) shows the orbital swath pattern and the interswath data void regions. The pattern in Fig. 4 moves eastward on a daily basis due to precession of the orbit, at a rate which varies from satellite to satellite.

3. Nonoxygen effects on the MSU channels

Small geophysical signals other than thermal emission by molecular oxygen are also present in the MSU channel 2 (and especially channel 1) measurements. These include thermal emission by the surface of the earth, cloud water, water vapor and back-scattering of the upwelling thermal radiation by precipitation-size ice. These processes have been generally ignored for MSU channel 2 because the magnitude of their effect on sounding retrievals is rarely significant. Because this paper emphasizes tropospheric temperature anomalies, which are potentially quite small (0.1° or less), we are more concerned with the extent to which these other signals can influence the satellite-observed temperature anomalies. Because our emphasis will be on anomalies (deviations from an average value for a given location and time of year), we are most interested in the variability of these small contaminations rather than their absolute magnitudes. Below, we present an analysis of

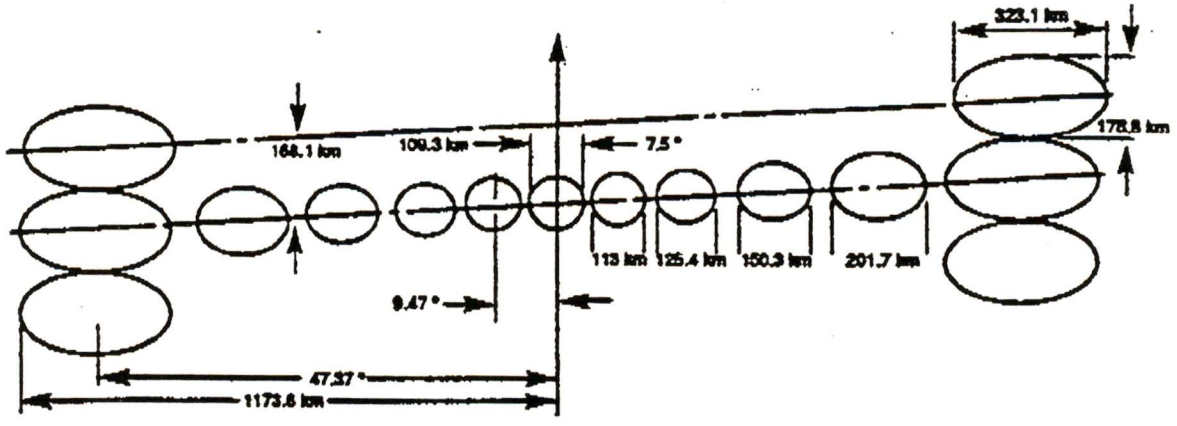


FIG. 3. MSU scan pattern and 3 dB footprint sizes assuming a nominal orbital altitude of 833 km. Angular dimensions of 7.5° and 9.47° refer to the antenna 3 dB beamwidth and along-scan footprint spacing, respectively (figure adapted from Grody 1983).

JUN 6 '91 10:33 FROM NASA/MSFC ESAD(ES41) TO G S WILSON PAGE.011

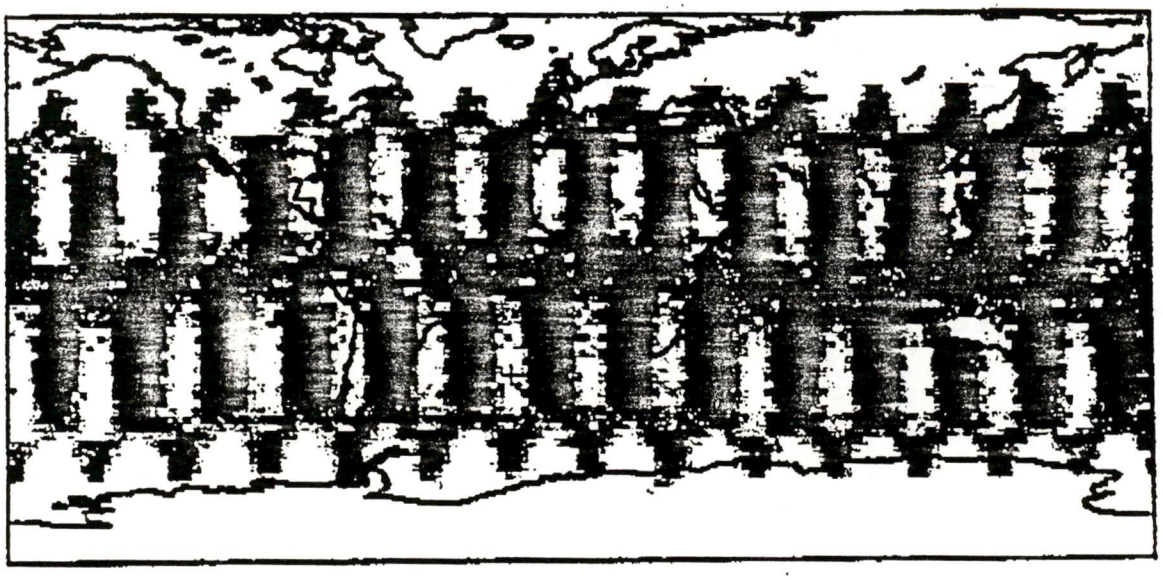


FIG. 4. Two days of earth coverage from a single MSU (NOAA-7), where 2.5° grid squares are shaded from black (zero coverage) to white (12 or more footprints).

he relative contributions to the channel 2 signal by vater vapor, surface emissions, and cloud cover changes.

a. *Water vapor emissions*

In an attempt to theoretically evaluate the relative importance of variations in water vapor alone on the MSU channel 2 measurements, radiative transfer calculations were made for the effects of varying water vapor in various atmospheres using an approximate form of (1) (Table 1). The MSU channel 2 sensitivities to water vapor changes in Table 1 are quite small, but potentially nontrivial for tropical airmasses. An interesting feature is that the T_b measured over ocean increases, while land T_b decreases, with increasing vapor content. When superimposed upon the average difference between land and ocean T_b (typically about 1°C), these opposing effects would create artificial T_b anomaly gradients when a water vapor anomaly extends across land/ocean boundaries. Thus, we can examine regional T_b anomalies for any unusual land/ocean transition characteristics that would indicate a water vapor anomaly effect. An examination of ten years (1979–88) of 10-day temperature anomaly imagery (an example of which will be discussed below) reveals no such effect.

TABLE 1. Model computed sensitivity of MSU channel 2 T_b (nadir view) to a 20% increase in water vapor concentration from the average amounts found in an average polar atmospheric profile, the U.S. Standard Atmosphere, and an average tropical atmospheric profile. Sea surface temperatures were assumed to be 0°C, 15°C, and 30°C, for polar, standard, and tropical atmospheres, respectively. Land surface emissivity was assumed to be 0.95.

	Land	Ocean
Polar	0.00°	+0.02°
Standard	−0.04°	+0.02°
Tropic	−0.09°	+0.03°

b. *Surface emissions*

Surface emission variations can arise from either temperature changes or emissivity changes. For MSU channel 2, we find that the combined surface contribution to the measured brightness temperature is 8% of the total contribution over land at sea level, increasing somewhat with elevation. This is a small, but not negligible effect. We are primarily concerned with how it might vary in magnitude and thus affect our interpretations of atmospheric temperature variability.

Most of the land surface contribution is emissive (assuming a typical emissivity of 0.95), and the remaining, much smaller part is reflection of the atmospheric downwelling radiation back upward. Theoretically, 1°C of land surface warming without any change in atmospheric temperature will cause channel 2 T_b to increase by 0.1°C. Of course, any change in surface temperature must result in an atmospheric temperature change because they are physically connected. The issue is really whether variability in the average surface/air temperature coupling for a given time of year is sufficient to cause a misinterpretation of this variability as an atmospheric temperature anomaly. This coupling might best be put in terms of the typical low-level atmospheric lapse rate. On a hemispheric scale, it would be difficult to imagine a widespread anomaly in near-surface lapse rates sufficient to impact the hemispheric temperature anomalies, especially in the ocean-dominated Southern Hemisphere. Over certain regions, however, this might well contribute to noise in our measurements. For instance, widespread anomalous drought in a region might well be associated with

JUN 6 '91 10:34 FROM NASA/MSFC ESAD(ES41) TO G S WILSON PAGE.012

steeper than normal lapse rates during solar heating, which would then cause positive channel 2 T_b anomalies. Fortunately, this would probably be, to some degree, offset by enhanced nocturnal cooling from anomalously clear skies, low water vapor contents, and the lower heat capacity of dry ground.

Emissivity anomalies for relatively unvegetated land surfaces are also a potential problem. The major factor controlling soil emissivity variations is water content, primarily standing surface water. Window frequency measurements from other spaceborne microwave radiometers (the Nimbus 7 Scanning Multichannel Microwave Radiometer, and the Defense Meteorological Satellite Program's Special Sensor Microwave/Imager) show that after a particularly intense rain system passes, a day or two of reduced surface emissivities by about 10% are possible. This is equivalent to about 20% of all surface area seen by the satellite being temporarily covered by standing water (or some smaller fraction of standing water area combined with unusually wet soil area). This decrease in surface emissivity (from 0.95 to 0.85) can cause a channel 2 T_b anomaly of about −0.2°C, which is comparable to the atmospheric temperature variability we are seeking. Fortunately, prolonged periods of anomalously wet ground usually cover only small land areas. Those areas which are frequently wet are also usually heavily vegetated, and additional moisture is not likely to reduce surface emissivities more since wetted vegetation does not have a lower emissivity than dry vegetation. Nevertheless, at this point, we must be wary that any cold anomalies in channel 2 T_b, especially if they cover a small geographical area over a short period of time, might be due to surface wetting. The net effect of land surface wetness anomalies on hemispheric channel 2 T_b anomalies, due to their limited geographic extent, will probably be very small, less than 0.01°C. Desertification might be expected to cause some contamination also, probably through slightly reduced surface emissivities which are observed over desert regions. These are due to the flatter nature of the surface and, like surface wetting, might lead to small negative biases in the T_b. This emissivity effect, however, has not been well documented.

Over the ocean, the sensitivity to surface temperature (SST) changes for MSU channel 2 is smaller than for land. Because the ocean emissivity is close to 0.5, the ocean emits only half as much energy as the land, and thus, also reflects more of the downwelling atmospheric radiation back up toward the satellite. In addition, ocean emissivity is temperature dependent, with the T_b effects of increasing SST being partly offset by decreasing emissivity. The net effect is that for each degree increase in SST, the MSU channel 2 T_b will increase by about 0.036°C for a tropical atmosphere over warm water, decreasing slightly to about 0.030°C for a polar atmosphere over cold water. Therefore, we would expect a very large SST anomaly (3°C) to result in, at most, a 0.1°C channel 2 T_b anomaly. This effect is, as for the water vapor effect, relatively small, but again it might not be negligible for regional areas experiencing large SST anomalies. As in the land case, it is the local variability in the average lapse rate between the surface and lower atmosphere that is the primary concern, since an SST anomaly would influence the temperature of the lower atmosphere.

Ocean emissivity can also change through wind-induced roughening and foam generation (Wentz 1983). Increasing winds cause increasing emissivity, ranging from 0.50 for calm conditions to about 0.56 for 20 m s^{-1} wind speeds. Southern Hemisphere mean values of surface wind speed from European Centre for Medium-Range Weather Forecasts (ECMWF) analyses for January and July 1988 show that no individual two-day period varies by more than 0.5 m s^{-1} from the monthly mean. This wind anomaly would translate into a hemispheric average channel 2 T_b anomaly of less than 0.005°C.

c. *Hydrometeors*

1) FROZEN

Most cirrus clouds are essentially transparent at MSU frequencies. This is due to both their small ice particle size compared to the wavelength of the radiation and low ice water contents. This is one characteristic of microwave observations that led us to consider them instead of infrared sounder data, which are significantly affected by cirrus clouds.

Relatively little is known about the distribution of microphysical variables within cirrus clouds, but some aircraft measurements do exist. They reveal a wide variety of ice particle sizes, shapes, and water contents. The contents usually show a decrease with altitude, as do the sizes. Ice particles, if sufficiently large and abundant, will cause T_b depressions (Wilheit et al. 1982; Spencer et al. 1983; Spencer et al. 1989). This results from the nature of the refractive index of ice at microwave frequencies. The real part of the index of refraction is large enough to cause a small portion of the upwelling thermal radiation from the atmosphere to be scattered back downward, and the imaginary part is so small that there is no ice-emitted radiation to take its place. Fortunately, in the 50–60 GHz region the ice particles must become precipitation size to cause a significant effect. Empirical evidence for this transparency is that the higher spatial resolution (15 km) data from the more ice sensitive 85.5 GHz channel of the Special Sensor Microwave/Imager (SSM/I) reveal no case of cirrus-induced T_b cooling at the 0.5°C level (Spencer et al. 1989). If, however, the cirrus are thick and the result of deep moist convection, larger T_b depressions (in excess of 1°C) do occur, which in every case have been linked to evidence of precipitation-size particles.

The influence of precipitation-size ice in thunder-

JUN 6 '91 10:35 FROM NASA/MSFC ESAD(ES41) TO G S WILSON PAGE.013

storm cores, however, can be considerable. In rare sit-
ons, 10°C depressions have been observed in the
U channel 2 T_b for midlatitude squall lines (Grody 1983). This is the largest atmospheric influence which can contaminate the MSU channel 2 oxygen emission signal. Fortunately, the larger and more intense ice precipitation events are infrequent and are easily screened out due to their isolated nature. However, we cannot rule out the possibility of an anomaly in the frequency of more subtle convective events that are below our assumed convection screening threshold. As we shall see, though, the major convective anomaly in the eastern Pacific during the 1982–83 El Niño/Southern Oscillation (ENSO) event showed a large warm, not cold, signature. This suggests that any ice contamination of the temperature signal was relatively small.

2) LIQUID

Cloud liquid water effects, to our knowledge, have always been too weak to be seen visually in MSU channel 2 imagery. Radiative transfer calculations suggest, however, that up to a few degrees impact on T_b might be expected due to cloud water variations. These effects are particularly difficult to address theoretically. This is not because the theory is not well understood, but
ause of the many combinations of cloud depth, wa-
content, altitude, and areal coverage which can exist. Like water vapor, clouds emit energy at the atmosphere's temperature, and their effect is to partly screen emission from the warmer underlying atmosphere. Thus, over land (where the surface generally emits at a brightness temperature higher than any atmospheric level), cloud water would always result in a negative T_b anomaly in MSU channel 2. Over the ocean, however, clouds below about the 65 kPa level will present a warm signal in contrast to the "cold" reflective ocean background. Therefore, we would expect anomalies in low-cloud cover, as was the case for water vapor, to generally have opposite effects over land (colder T_b) versus over ocean (warmer T_b). Deeper, cumuliform clouds extending from the 65 kPa to 95 kPa level have essentially zero impact on the T_b, although they do screen out atmospheric emission and replace it with their own emission of a near-equal magnitude. Higher clouds (above about 65 kPa) will have a cooling effect over both surfaces. The smaller water contents found in higher altitude clouds (generally below 0.1 g m^{-3}) help to reduce their impact on T_b. Some of the possible quantitative T_b effects from cloud water variations and other geophysical factors are summarized in Table 2. The cloud values, as previously pointed out, are potentially quite variable depending upon assumed cloud heights, thickness, cloud water contents and areal coverage. Hemispheric statistics on cloud water will not be affected by cloud variations nearly as much as regional statistics, which might be sufficient to influence the T_b anomalies. As was the case for water vapor anomalies, low cloud anomalies extending across land/ocean boundaries should appear as an artificial gradient in T_b anomaly along the coast, which would provide empirical evidence of their existence.

4. Method

a. *Calibration*

The MSU radiometers produce digital counts as their antennas sequentially view eleven separate earth locations, cold space, and a high-emissivity warm target. The earth-viewing counts are converted to T_b by in-

TABLE 2. Summary of the influence of various geophysical processes on MSU channel 2 T_b measurements.

Geophysical parameter	MSU Channel 2 T_b sensitivity (°C)	
Oxygen emission by the atmosphere	+0.92° per +1° (land) +0.96° per +1° (ocean)	
Land surface temperature	+0.08° per +1°	
Land surface emissivity (wetness)	−0.1° per −0.1 emissivity change	
Sea surface temperature	+0.036° per +1°	
Sea surface emissivity	+0.01° per 1 ms^{-1} incr. in wind speed	
Water vapor (land)	0.00°, −0.04°, and −0.09° per +20% in vapor in polar, standard, tropic atmos.	
Water vapor (ocean)	+0.02°, +0.02°, and +0.03° per +20% in vapor in polar, standard, tropic atmos.	
Cirrus clouds	From near 0° in thin cirrus to in excess of −1° for thunderstorm anvil cirrus near the storm core	
Precipitation size ice	in excess of 10° for the cores of large and intense storms	
Cloud water	Doubling of areal coverage or of typical cloud water contents over:	
	Land	Ocean
Low clouds: (90–95 kPa)	+0.05°	+0.1° to 0.2°
Middle clouds: (60–70 kPa)	−0.3°	−0.1°

JUN 6 '91 10:36 FROM NASA/MSFC ESAD(ES41) TO G S WILSON PAGE.014

terpolation between the cold space view (for our purposes spatially isotropic at 2.7 K) and the warm target view, whose temperature is monitored by redundant platinum resistance thermometers. The details of this calibration are contained in the Appendix.

b. *Instrumental differences*

After calibration, small (several tenths of a degree) systematic T_b differences among instruments are observed. This can be partly ascribed to the different crossing times of the morning and afternoon satellites. But even separate satellites in the same orbit have a few tenths of a degree difference between them. This is most likely attributable to antenna sidelobe pattern differences, which result in variations in the amount of energy received from colder atmospheric sources off-nadir. Because of these interinstrumental differences, each instrument's data must be addressed separately. Overlap in operational periods between successively launched instruments is necessary for adjustment to a common level. We have found that about three months is a minimum requirement for adjustment to within 0.01°C, although at least one year is preferable. We have arbitrarily chosen to adjust all satellites to the NOAA-6 level.

c. *Data screening*

Not all MSU channel 2 data are included in our analysis. As the MSU scans off-nadir, the channel 2 T_b become colder, causing the well-known "limb-darkening" effect. This is primarily due to the increasingly oblique atmospheric path viewed by the instrument, which effectively raises the weighting function (Fig. 1) to a higher (colder) level in the troposphere. This cooling increases nonlinearly with scan angle from nadir toward both scan extremes. Because spacecraft attitude roll errors of one degree or more might be expected at certain times, combined with the nonlinear nature of the limb darkening, the attitude effect could translate into small negative biases in the scan-averaged T_b if all eleven footprint locations were used. Thus, we have chosen to utilize only the middle 7 footprints of the 11-footprint scan in this study.

Each of the middle seven channel 2 T_b is checked to make sure it does not fall out of absolute bounds (190 K and 290 K). Then, each is checked against an average of its two immediate neighbors within its scan line to make sure that it does not deviate by more than 1.5°C from the average difference observed from limb darkening. If any T_b does, then the entire scan line is rejected from further processing. This procedure screens out deep convection and some large snowcovered mountain areas which also cause volume scattering-induced T_b depressions. If the data pass these tests, then the 2.5° latitude band that each footprint falls into is credited with the average T_b from the middle seven footprints.

These data are then summed and averaged at two-day intervals. Most of these two-day averages are made up of approximately 40 000 footprint locations, which at an average diameter of 120 km each (Fig. 3) corresponds to an average of 110% Earth coverage in two days (Fig. 4). Every two-day average has oval gaps (Fig. 4) in the subtropics, which are filled in as the coverage pattern precesses eastward at rate of 3° to 6° per day. A small area within 400 km of the poles is never sampled by the middle seven footprints.

5. MSU comparisons with conventional data

Before discussing the zonally averaged temperature anomalies, it is useful to demonstrate that the MSU-inferred temperature anomalies are closely related to those measured by radiosondes and thermometers.

a. *Radiosondes*

Previous investigators have made comparisons between MSU measurements and T_b calculated from rawinsonde data using the radiative transfer equation (1). Considering both land and ocean surfaces, the standard deviation of the differences between the satellite measured and rawinsonde-calculated T_b averages 0.7°C (Grody 1980; Grody and Shen 1982; Grody 1983; Westwater et al. 1985). This error is found to be independent of surface type. It has contributions from the MSU instrumental noise (0.3°C), errors in the baseline calibration of the radiosonde (0.5°), the difference in spatial coverage between an MSU footprint versus a radiosonde and space and time offsets in the satellite/radiosonde matchups.

We have compared the NOAA-6 MSU channel 2 T_b to T_b calculations from radiosonde data from 45 stations over the eastern two-thirds of the continental United States. We assumed a constant surface emissivity of 0.95 and a ground surface temperature equal to the surface air temperature for all calculations, and then removed any station-dependent biases as described below. The average of the middle three MSU footprints T_b were compared to the radiosonde-calculated T_b (from Eq. 1) when the MSU measurements were made within 3.0 h and 200 km of the radiosonde release time and location, respectively. The standard deviation of the differences between individual MSU-measured and radiosonde-calculated T_b's were found to range between 0.5°C and 1.0°C, consistent with the aforementioned 0.7°C reported by other investigators. When these results are averaged on monthly time scales, it is found that the average bias between the satellite and radiosonde measurements is radiosonde station dependent. Furthermore, this bias has a seasonal modulation of up to 1.0°C depending on the radiosonde station, with values of (MSU T_b − radiosonde T_b) falling in the summer and rising in the winter. While the station location dependence can be explained by geographical variations in emissivity due to the

JUN 6 '91 10:36 FROM NASA/MSFC ESAD(ES41) TO G S WILSON PAGE.015

presence of lakes, rivers, vegetation, etc.; the reason for the seasonal modulation at many of the stations is not clear. To isolate the monthly and annual precision with which the MSU can measure tropospheric temperature anomalies, an average annual cycle of the monthly satellite radiosonde sums and differences was removed from each of the stations individually, thus removing these station-dependent biases, as well as the signal of the average annual temperature cycle. Because each satellite period of record was at least two years, this will not cause the inadvertent removal of any evidence of interannual drift in the MSU or radiosonde systems. When the resulting monthly anomalies in individual station (satellite − radiosonde) sums and differences are averaged together, we obtain monthly time series (Fig. 5) which provide a measure of the ability of the MSU to observe tropospheric temperature variations. The monthly standard deviation of the NOAA-6/radiosonde differences, averaged over the 45 radiosonde stations, during the three year period 1980–82 is about 0.04°C, while the standard deviation of the sums is about 0.92°C, indicating a large signal-to-noise ratio, in excess of 500. The level of noise (0.04°C) is partly due to statistical noise (0.03°C) that is calculated from dividing the individual comparison standard deviation 0.8°C by the square root of the average number of monthly comparisons (about 650). The remaining portion (0.03°C) is then the estimated geophysical noise of the monthly temperature anomalies over the eastern United States, such as interannual variations in surface emissivity, precipitation contamination, etc., if the satellite measurements were made often enough to measure most of the atmospheric variability.

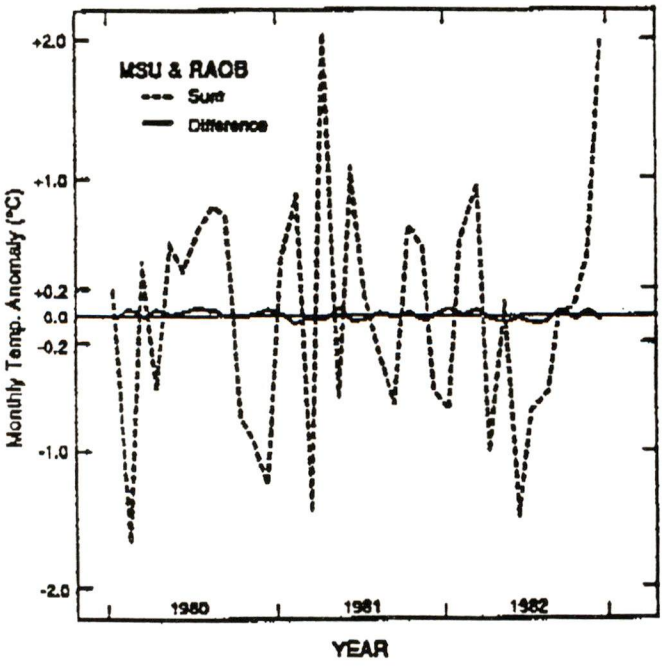


FIG. 5. Monthly anomalies in 53.74 GHz (MSU T_b + radiosonde calculated T_b) and (MSU T_b − radiosonde calculated T_b) during 1980–82. A small annual cycle in these quantities was removed from each of 45 United States radiosonde stations separately, and the resulting station anomalies were then averaged together. These time series represent signal to noise ratios of 480, 780, and 430 for the years 1980, 1981, and 1982 respectively.

To search for evidence of long-term drift, we compared a 15-month period during 1985/86 to the same subset of months during 1980/81 when the NOAA-6 MSU was operating, a time separation of five years. The difference in the 45-station average (satellite − radiosonde) between the two periods was 0.013°C, with the later period being warmer. This is approximately the expected random noise of the estimate (0.012°C), based upon division of the average single-comparison noise of 0.8° by the square root of the total number of independent matchups (about 4500). Thus, the comparison reveals no evidence of drift over the five-year period at the 0.01°C level. As discussed below, this conclusion is consistent with satellite intercomparisons with each other.

b. Surface thermometer comparisons

Monthly averaged MSU data on a 2.5° grid covering the United States were compared to monthly averaged surface air temperature data (Tom Karl, personal communication) for the period 1979 through 1984. A six-year average annual cycle was computed for each dataset and then subtracted from the original monthly values to obtain 72-month time series of temperature anomalies. The correlation between the MSU and thermometer U.S. averaged anomaly time series is 0.90. The surface air temperature anomalies average about twice the magnitude of the MSU channel 2 anomalies. This level of agreement was compared to radiosonde-only calculations, where monthly surface temperature anomalies were correlated with calculated channel 2 T_b, both from the radiosonde data. The correlations have a geographic dependence over the United States, with values of 0.7 over the extreme eastern and southeastern U.S. increasing north and westward to over 0.90 in the High Plains and Rocky Mountains, then decreasing again to 0.70 along the West Coast. Thus, it appears that the MSU versus thermometer correlation of 0.90 is about as high as can be expected for surface/deep troposphere comparisons.

The agreement between the monthly MSU and thermometer-based calculations diminishes when the above analysis is expanded in area to the Northern and Southern hemispheres. These results, based upon comparisons with calculations by Jones (1988) and Jones et al. (1986a,b), are summarized in Table 3. Whereas 81% of the variance of the monthly MSU anomalies can be explained by surface air temperature measurements over the United States, only 26% and 19% can be explained by Northern and Southern hemispheric thermometer-based calculations, respectively. To investigate the reason for this poor agreement, we again performed radiosonde-only calculations

JUN 6 '91 10:37 FROM NASA/MSFC ESAD(ES41) TO G S WILSON PAGE.016

TABLE 3. Monthly and annual explained variances between MSU tropospheric and thermometer-measured surface air temperature anomalies for United States, Northern and Southern hemispheres, and the globe. Thermometer-based calculations for the United States are from T. Karl ("K", personal communication); Jones ("J", 1988), and Jones et al. (1986a and 1986b) for monthly and annual hemispheric and global anomalies; and Hansen and Lebedeff ("H", 1987) for annual anomalies.

	U.S.	NH	SH	Globe
Monthly	0.81 (K)	0.238 (J)	0.176 (J)	0.287 (J)
Annual	0.927 (K)	0.700 (J) 0.548 (H)	0.632 (J) 0.348 (H)	0.677 (J) 0.464 (H)

of the correlation between surface and deep-layer anomalies, this time for several radiosonde stations around the world. The results show that the best coupling (highest correlation) between the surface and deep troposphere occurs over middle latitude continental areas such as the U.S. This is presumably due to the large signal of monthly anomalies that is associated with the extreme surface net radiation changes these continents go through on a seasonal basis. Low latitude explained variances ranged from about 40% around the Caribbean, to 25% at Ascension Island in the subtropical Atlantic Ocean, to 0% to 20% from Hawaii south and westward across the tropical west Pacific Ocean. High latitude maritime locations include coastal Alaska (50%) and Iceland (50%). Thus, it appears that the poor monthly hemispheric agreement between the thermometers and the MSU cannot be attributed to only poor thermometer coverage, but also to weak thermal coupling over tropical ocean regions and the smaller seasonal variability in these temperatures. The tropical ocean explained variances would probably increase if a lag in the atmosphere's response of several months were included (Reid et al. 1989).

The annual comparisons show better agreement than the monthlies, especially for the Jones et al. data. These explained variances peak at 70% for the Northern Hemisphere data of Jones but are as low as 35% for the Southern Hemisphere calculations of Hansen and Lebedeff (1987). These results indicate that annual Northern Hemispheric surface temperature anomalies are reasonably well related to the satellite tropospheric measurements, but the Southern Hemisphere relationships are only weakly correlated.

6. MSU results

a. *Precision of MSU channel 2 T_b variations*

1) HEMISPHERIC SAMPLING

Of special interest is a near 2-year overlap period when the NOAA-6 and NOAA-7 satellites simultaneously observed the Earth. An annual cycle of temperature was calculated for each satellite separately by averaging the two years' 2-day averages together, then low pass filtering this cycle to provide a more representative (smoother) cycle. Then the original two-day averages were subtracted from these smoothed cycles to give the 2-day hemispheric anomalies. The hemispheric and global anomalies for NOAA-6 and NOAA-7 averaged together are shown in Fig. 6, and immediately below them is the averaged difference in anomalies between the two satellites. Even though these separate satellites had different orbits, it can be seen that *both satellites show the same 2-day hemispheric temperature anomalies to within about 0.03°C.* The signal to noise represented in Fig. 6 (defined as the square of the standard deviation of the mean of the satellites divided by their average difference) is 45 for the Northern Hemisphere, 40 for the Southern Hemisphere, and 60 for the entire globe. Thus, these two satellites measure essentially the same 2-day hemispheric anomalies. The ragged character of the time series of 2-day averages is intriguing and shows that *jumps and dips in globally averaged temperatures of 0.5°C can occur in less than two weeks.* Because the satellites' orbits have different precession rates and substantially different daily geographical coverage, these abrupt changes are not an artifact of possible similarities in the way the two satellites insufficiently sample the earth.

Also, during this overlap period, *neither satellite record drifts relative to the other to less than 0.01°C.* Assuming that both MSUs are not drifting together in exactly the same way (that is doubtful, especially in light of the radiosonde comparisons above) this level of stability is sufficient for climate monitoring.

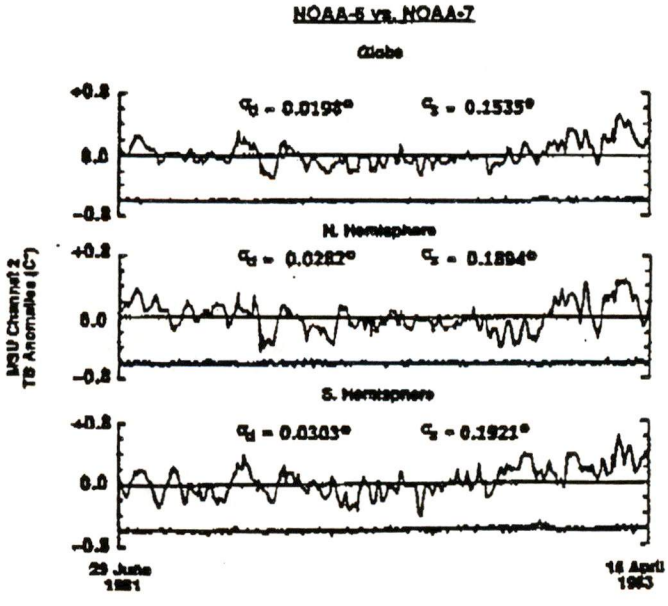


FIG. 6. Intercomparison between global NOAA-6 and NOAA-7 MSU channel 2 T_b during the near two-year period (29 June 1981 to 16 April 1983) when both satellites had MSU's operating. Time series of global and hemispheric satellite averages (sum/2) and differences (difference/2) are shown by the upper and lower curves in each panel, respectively.

JUN 6 '91 10:38 FROM NASA/MSFC ESAD(ES41) TO G S WILSON PAGE.017

2) ZONAL AVERAGES

We applied a low-pass filter having a half power point of 80 days to the NOAA-6 and NOAA-7 time series during their overlap period and similarly filtered the anomalies on a zonal basis in 2.5° latitude bands (Fig. 7). The zonally averaged anomalies seen by the different satellites are nearly identical in all their features at the 0.1°C level, and the corresponding hemispheric averages are, again, the same to approximately 0.01°C. Therefore, the zonally averaged anomalies, too, are measured with considerable precision when one deals with the longer time scales.

3. GRIDPOINT AVERAGES

Of interest to researchers examining regional climate variability is the precision with which an MSU can measure 2.5° gridpoint temperature anomalies. Whereas the zonal and hemispheric averages are not very sensitive to longitudinal gaps in satellite coverage, gridpoint estimates obviously are. A 10-day averaging period (11–20 September 1982) was arbitrarily chosen to examine the level of agreement between the gridpoint measurements made by the two satellites. While use of the middle seven footprints resulted in increased precision (decreased standard deviation of the gridpoint differences between satellites) when compared to only five footprints, the results degraded for nine or eleven footprints (full swath). Since the geographical coverage is obviously better with the wider swath, we assume that the degradation is due to the aforementioned sensitivity of the end footprint T_b to spacecraft attitude variations.

An optimized gridpoint assignment scheme was then chosen where the seven middle footprints are split into two half-subswaths (right four and left four) to preserve some of the smaller horizontal scale temperature in-

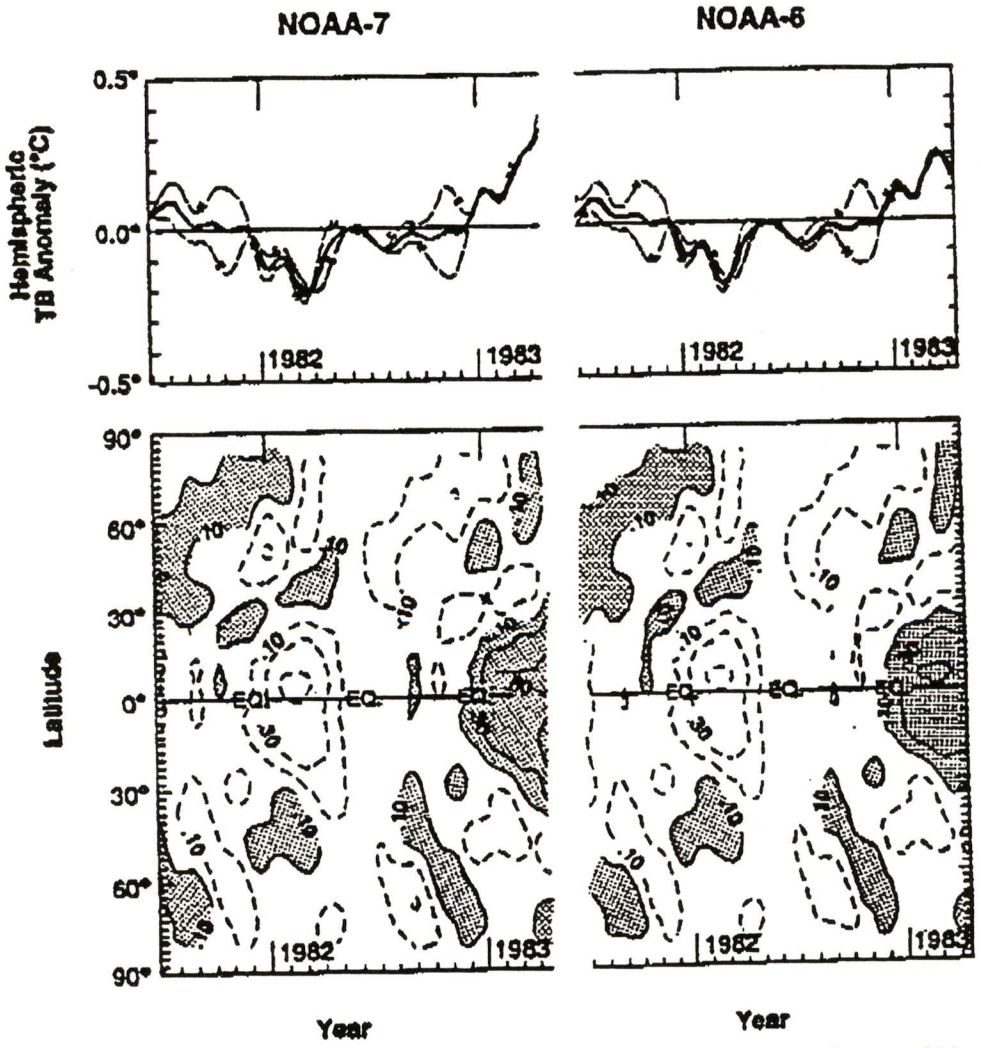


FIG. 7. Hemispheric (top) and zonally averaged (bottom) low-pass filtered (half power width = 82 days) NOAA-6 and NOAA-7 MSU channel 2 T_b anomalies during the two-year overlap period of NOAA-6 and NOAA-7. The time series do not agree near the beginning and end of the period because the low-pass filter has no data to use past the end of the period for NOAA-6 or before the period for NOAA-7.

JUN 6 '91 10:39 FROM NASA/MSFC ESAD(ES41) TO G S WILSON PAGE.018

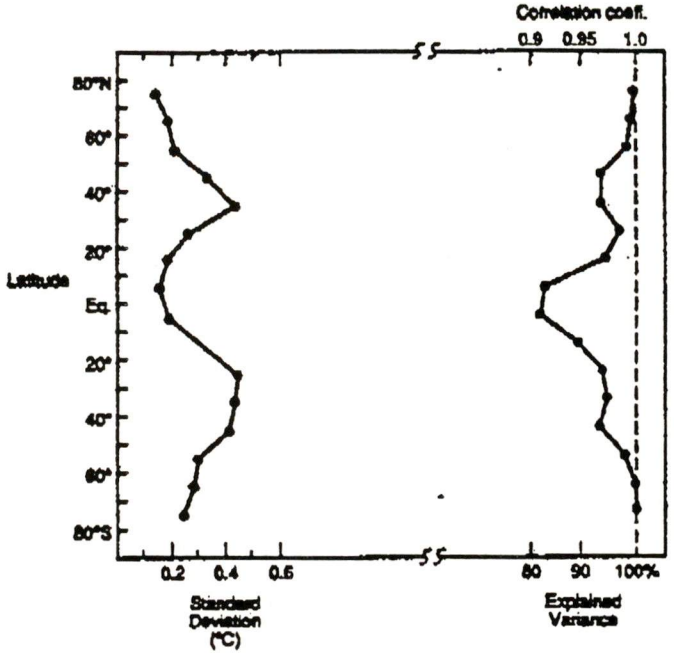


FIG. 8. Standard deviation of the difference in 10-day 2.5° gridpoint MSU channel 2 T_b between NOAA-6 and NOAA-7 (left), and the inter-satellite explained variance (right), as a function of 10° latitude band.

formation, while assigning the half-subswath averages to the full half-swath (left six or right six) footprint positions. The resulting spatial resolution being mapped onto the 2.5° grid is then about 120 km along-track by 600 km cross-track. To account for the decreasing size of 2.5° gridsquares poleward of the equator, it was assumed that a single footprint assignment would fully influence an equatorial gridsquare, while cosine-latitude weighted assignments were made to the longitudinally adjacent gridsquares as the satellite progresses poleward. This preserves the areal influence of the data independent of latitude. Figure 8 reveals the latitudinal profile of the standard deviation of the 10-day averaged differences between the two satellites gridpoint T_b measurements. This gives an estimate of the precision with which a single satellite can measure the geographic variability of 10-day averaged tropospheric temperatures. The values range from 0.15°C over the tropics to about 0.45°C at middle latitudes. Also shown in Fig. 8 is the explained variance between the two satellites' measurements, which is usually above 90%, except within 10° of the equator where it drops to about 82%. Thus, even though the precision in terms of temperature sensitivity is a maximum in the tropics,

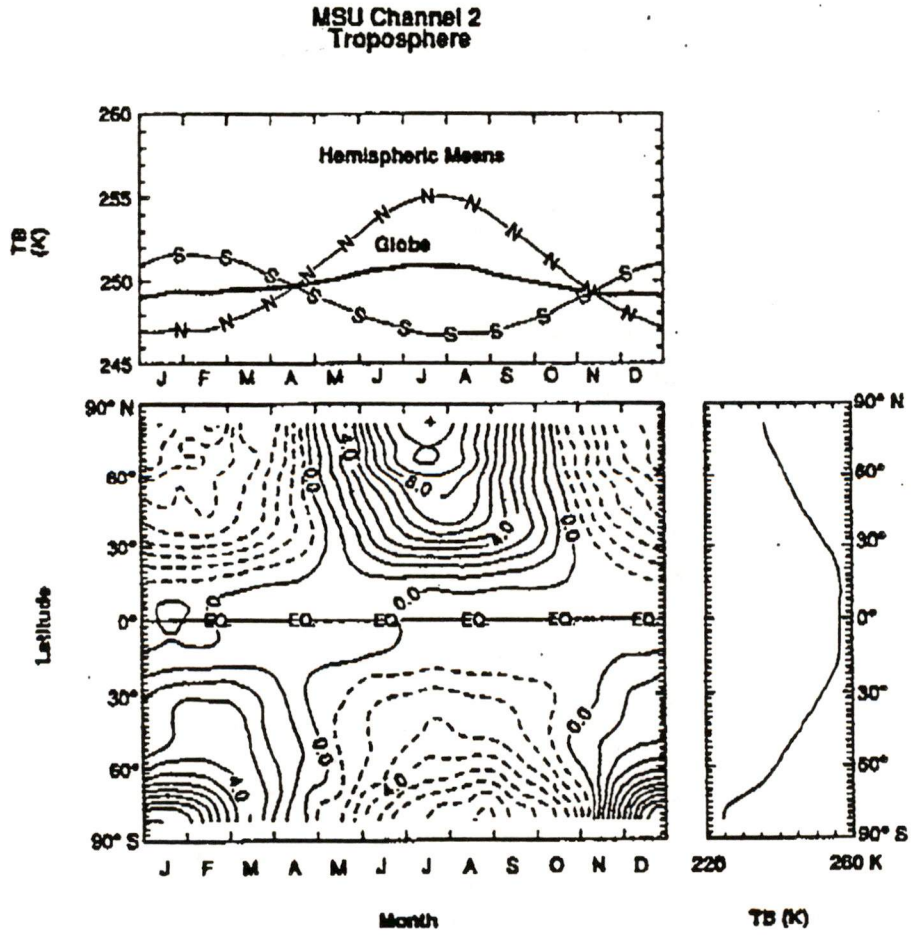


FIG. 9. Annual cycle in MSU channel 2 T_b for the globe and Northern and Southern hemispheres (top); and zonally averaged in 2.5° latitude bands (bottom left). Also shown is the year-average latitudinal profile of MSU channel 2 T_b (bottom right). The year-averaged global, Northern Hemispheric, and Southern Hemispheric T_b are 249.88 K, 250.67 K, and

JUN 6 '91 10:40 FROM NASA/MSFC ESAD(ES41) TO G S WILSON PAGE.019

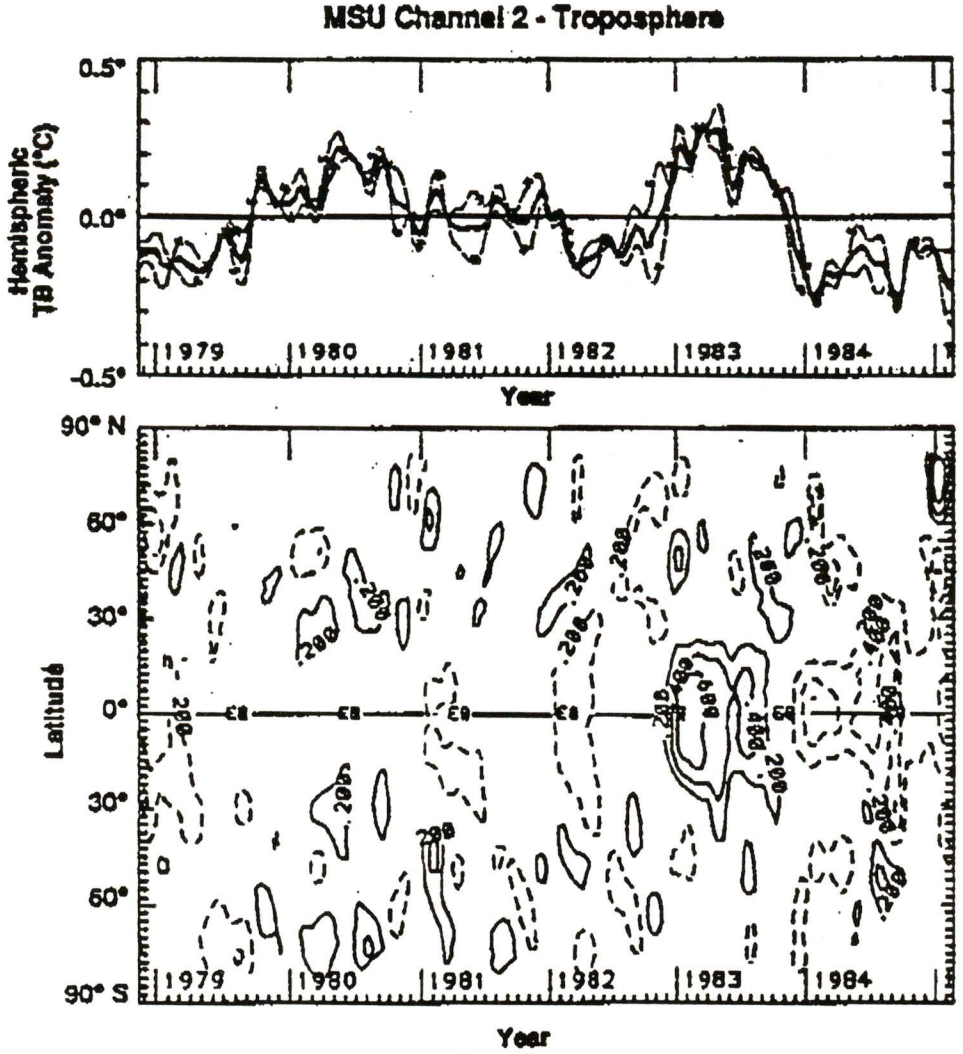


FIG. 10. Hemispheric anomalies (top) and zonally averaged anomalies (bottom) about the MSU channel 2 T_b annual cycle shown in Fig. 9 for the 6-year period 1979 through 1984.

the level of common variability measured by the separate satellites decreases there, partly due to the small signal of tropical temperature variations. These levels of precision should be adequate for many uses requiring relatively short term (10-day) estimates of atmospheric temperature variability.

b. The annual cycle in tropospheric temperatures

The combined period of useful operation of the TIROS-N, NOAA-6, and NOAA-7 MSUs was 17 November 1978–18 February 1985. The zonally averaged annual cycle of tropospheric temperature (MSU channel 2) for this 6+ year period is shown in Fig. 9. The annual range of temperature is seen to be largest at ...h latitudes, especially in the Northern Hemisphere (...ver 16°C in places) and only about 1°C within ten degrees latitude of the equator. Due to more efficient conversion of solar input to sensible heating by land masses in the Northern Hemisphere, its average annual temperature is about 1.6°C warmer than the Southern Hemisphere's temperature.

c. Tropospheric temperature anomalies during 1979–1984

When the zonally averaged low-pass filtered annual cycle for each 2.5 degree latitude band and each satellite is subtracted from the original 2-day averaged time series for each latitude band, we arrive at the anomalies in the zonally averaged tropospheric temperatures (Fig. 10), including the hemispheric averaged time series. We stress that with only six years of data these anomalies might not be representative of anomalies relative to a longer time series. The zonally averaged values have been cosine-latitude weighted to allow visual evaluation of the impact of individual latitude bands on the hemispheric values. As can be seen, the anomalies are well correlated between hemispheres for the multi-seasonal anomalies over 0.1°C. These global anomalies can usually be traced to the tropics.

The strongest anomaly during this time period was the 1982/3 ENSO event. A warm anomaly of around 0.2°C dominated the tropical latitudes during 1983 with a zonally averaged peak exceeding 0.6°C in early 1983 compared with the six-year average. A videotape

JUN 6 '91 10:40 FROM NASA/MSFC ESAD(ES41) TO G S WILSON PAGE.020



FIG. 11. MSU channel 2 T_2 gridpoint anomalies during 21–30 February 1983. The 2.5° gridpoint anomalies have been interpolated to 1.25° for display purposes.

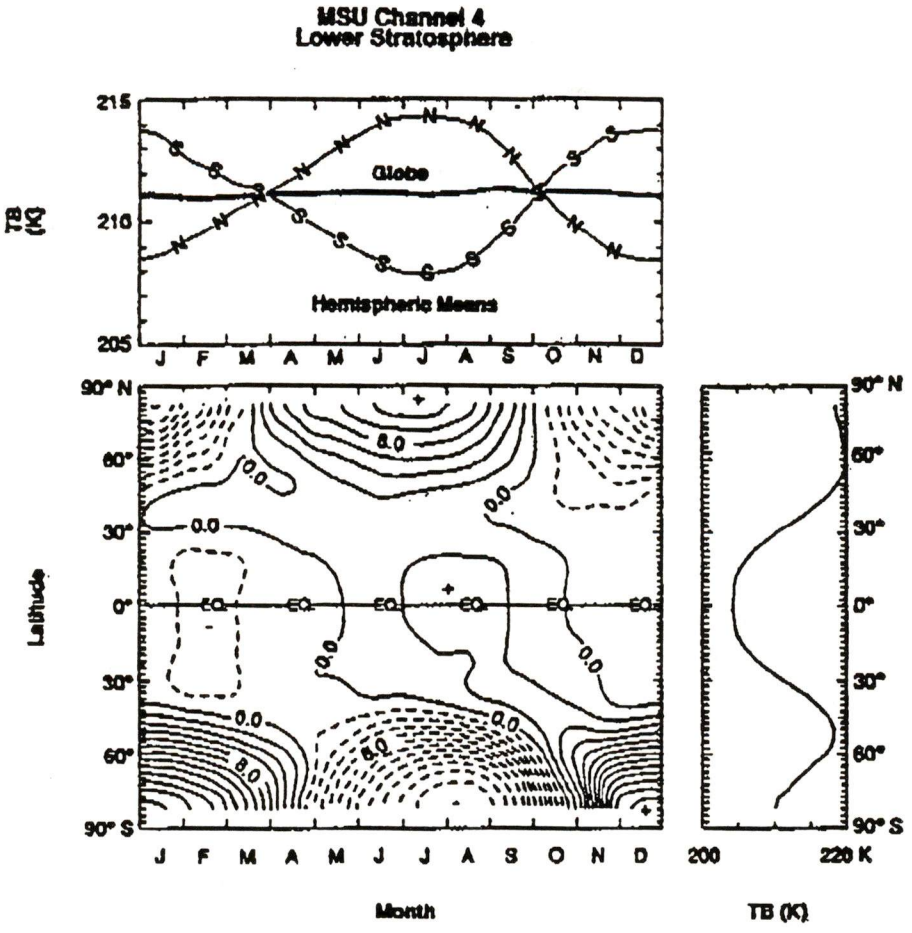


FIG. 12. Same as Fig. 9, but for the lower stratosphere (MSU channel 4). The year-averaged global, Northern Hemispheric, and Southern Hemispheric T_b are 211.13 K, 211.42 K, and 210.84 K, respectively.

of the geographic distribution of these anomalies reveals that the tropical warmth began in the eastern Pacific that rapidly peaked in intensity as a warm couplet straddling the equator (Fig. 11). This feature then weakened as the rest of the tropics became unusually warm for several more months. The zonally averaged anomaly is fairly symmetric in latitude about the equator as are the relatively cold temperatures immediately following in 1984.

d. Noise estimate of the lower stratosphere measurements

The quality of the channel 4 sampling was evaluated in the same manner as the tropospheric measurements above. The lower stratosphere (channel 4) signal-to-noise computed from the sums and differences of the NOAA-6 and NOAA-7 2-day averages during the 2-year overlap period (not shown) is even higher than for the troposphere (channel 2), with a global signal-to-noise value of 125.

e. The annual cycle in lower-stratospheric temperatures

A mean and anomaly analysis of the MSU channel 4 data completely analogous to the channel 2 analysis was performed. The resulting annual cycle of lower annual range of these stratospheric temperatures is larger than in the troposphere at high latitudes, but smaller at low latitudes. A much larger annual cycle is seen near the South Pole than near the North Pole.

f. Lower-stratospheric temperature anomalies during 1979–84

The stratospheric anomalies (Fig. 13) appear mostly uncorrelated with the tropospheric anomalies except for a period of marked tropical warmth starting six months before the tropospheric ENSO warm anomaly appeared, and similarly, beginning its decline six months before the tropospheric anomaly decline. The channel 4 anomaly during this period is impressive, exceeding a zonally averaged value of 1.2°C centered on the equator in late 1982 and early 1983. A videotape of geographic anomaly imagery for this period reveals that before the El Chichon volcanic eruption, warming of the entire Northern and Southern Hemisphere subtropics simultaneously began (early 1982) and then expanded into the tropics and intensified in mid-1982. This might have been the combined result of the eruption of El Chichon in the spring of 1982 and a tropical African volcano which erupted in December 1981. The absorption of solar radiation by the aerosols would heat

JUN 6 '91 10:41 FROM NASA/MSFC ESAD(ES41) TO G S WILSON PAGE.022

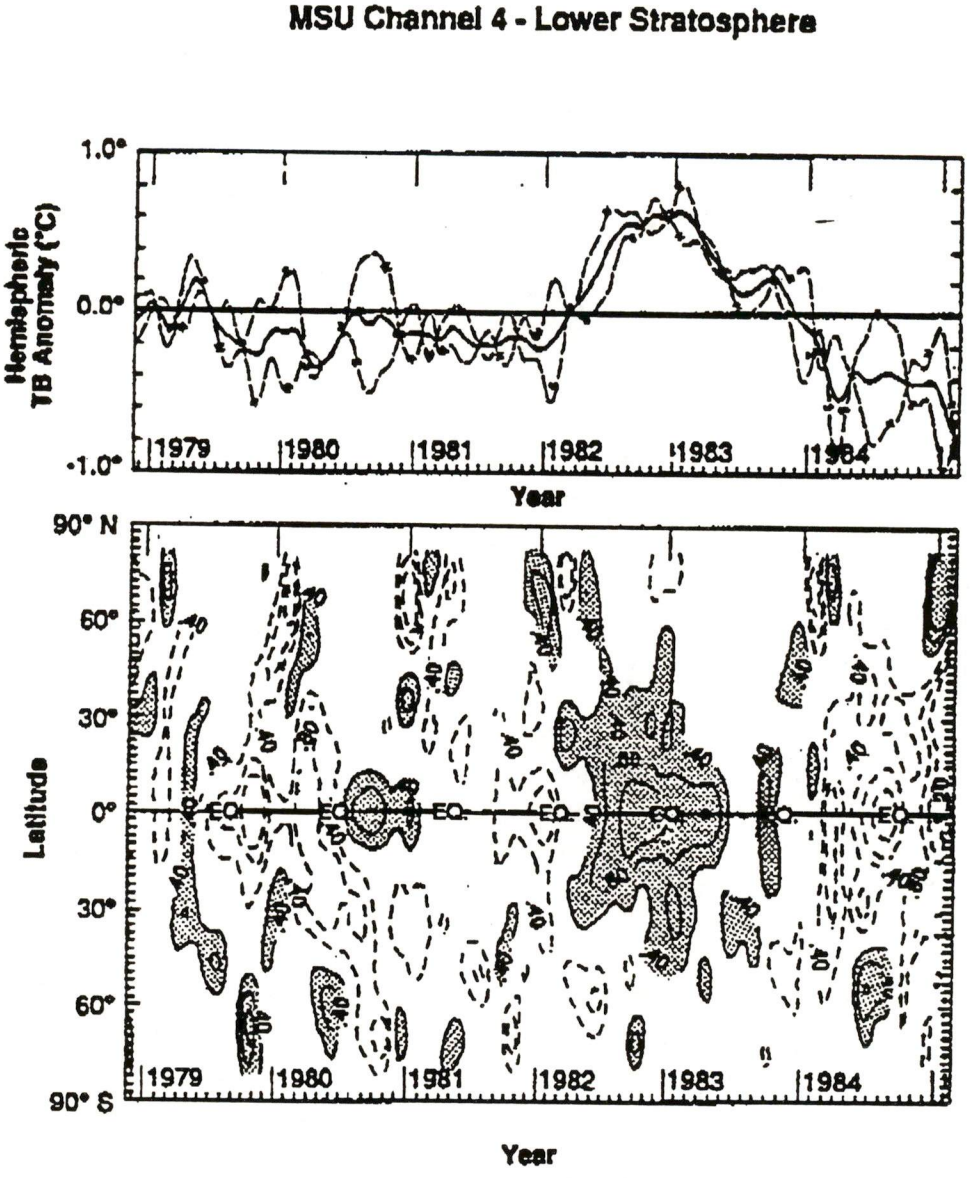


FIG. 13. Same as Fig. 10, but for the lower stratosphere (MSU channel 4).

fluence the measurements at 57.95 GHz. That the warming was probably not a manifestation of the ENSO is supported by the fact that our analysis of the 1987 ENSO (not shown) had no associated stratospheric warming.

As was the case for channel 2, the tropical anomalies are quite symmetric about the equator and contribute to a positive correlation between hemispheric anomalies on longer time scales. However, a marked negative coupling between shorter time-scale hemispheric anomalies exists (see the top panel in Fig. 13) and has time scales from two to six months. This "out of phase" behavior cannot be traced to the tropics but is instead occurring at high latitudes and might indicate some sort of inter-hemispheric exchange of mass or energy in the stratosphere or troposphere.

7. Summary and conclusions

This study has introduced the use of satellite microwave radiometry for precise monitoring of atmospheric temperature anomalies since 1979. Evidence has been presented which suggests that satellite microwave measurements of molecular oxygen thermal emission by an externally calibrated radiometer can be used to monitor tropospheric temperature anomalies on a global basis to a high level of precision. The noise associated with these measurements is 0.03°C for two-day hemispheric averages and 0.01°C for monthly time scales. This estimate is based upon a near two-year overlap period when the NOAA-6 and NOAA-7 MSU's operated simultaneously but in different earth orbits. Any long-term drift of one instrument relative to the other during this period of time was essentially unmeasurable (below 0.01°C), suggesting a high level of stability. Comparisons of the NOAA-6 MSU T_b with T_b theoretically computed from radiosonde measurements between two 15-month periods separated by five years also reveals no significant drift (0.013°C). These results, when taken together, suggest that spaceborne microwave radiometry can be used for relatively precise

JUN 6 '91 10:42 FROM NASA/MSFC ESAD(ES41) TO G S WILSON PAGE.023

** TOTAL PAGE.024 **

monitoring of global tropospheric temperature variations.

Comparisons between monthly MSU-derived hemispheric temperature anomalies and those computed from surface thermometer data show very good agreement over the United States but rather poor agreement for the hemispheres, especially the Southern Hemisphere. The poor hemispheric agreement cannot be ascribed only to sparse thermometer coverage but is found to be partly attributable to weaker thermal coupling between the ocean and deep troposphere than that which occurs over the U.S. Annual anomalies for the hemispheres show better correlations, although the level of agreement depends upon the data source used and may well change as more years are added.

The magnitude of the hemispheric temperature anomalies (relative to a 6-year mean) were between 0.1°C and 0.3°C, with time scales of close to one year. Zonally averaged data reveal that the anomalies' origins could usually be traced to the tropics. Abrupt warming and cooling events of 0.5°C occur in as little as two weeks and are verified by separate satellites.

Theoretical evaluations of the possible contaminating influence of cloud water, water vapor, and surface temperature changes on the tropospheric temperature signal suggest some possible small effects, although they would be expected to be much more significant over regions rather than hemispheres.

Our analysis suggests that the year-to-year variability of global tropospheric temperatures is so large that any enhanced greenhouse warming since 1979 will need to reach about 0.1°C before it becomes discernible in the satellite record. Therefore, we advise the continued use of satellite radiometer measurements to monitor global climate anomalies past 1985.

Acknowledgments. We are very grateful to Roy Jenne and Dennis Joseph at the National Center for Atmospheric Research who provided the MSU data used in this study; to Ms. Robbie Hood for processing of the radiosonde data and library research support; to Mr. Frank Wentz, Remote Sensing Systems, who provided updated sea surface emissivity estimates; to Pete Olsen, Fred Soltis, and Dr. Paul Swanson at the Jet Propulsion Laboratory, who assisted us in obtaining technical data on the MSU; to Dr. Gregory Wilson, who helped obtain the satellite datasets; and to Drs. Richard McNider and James Dodge, discussions with whom led to the present research; and to Dr. Richard Rosen who provided useful advice for improving the manuscript.

APPENDIX

MSU Calibration

Calibration of the MSU radiometric output (digital counts) in terms of brightness temperature (T_b) involves three general steps:

1) correction of radiometer digital counts (earth, cold space, and warm target views) for nonlinearity of instrument response;

2) conversion of warm target platinum resistance thermometer measurements (digital counts) to temperatures; and

3) interpolation between warm target counts and cold space counts to earth viewing counts and, thus, T_b.

Step 1 was accomplished by invoking the quadratic count correction equations developed by the National Environmental Satellite Data and Information Service (NESDIS), which were based upon instrument measurements made by JPL. The correction is small and of the same sign for each instrument. The general form of the NESDIS correction equation is

$$C = a_1 + C_{\text{raw}}(a_2 + a_3 C_{\text{raw}}), \qquad \text{(A1)}$$

where C is the corrected count value, C_{raw} is the raw count value, and the different values for a_i are contained in Table A1. This correction is applied to all radiometer digital counts: i.e., the cold space view counts, the warm target view counts, and all Earth-view counts.

Step 2 involves converting warm target platinum resistance thermometer (PRT) digital counts to resistances, then converting these resistances to temperature. Two redundant circuits in the MSU each monitor the output of one thermometer in each of two warm calibration targets. Target #1 is seen by MSU channels 1 and 2, while Target #2 is seen by channels 3 and 4. There have been no failures of these circuits to date out of seven MSUs successfully launched and operated. Our target temperatures were computed as an average of both thermometer outputs in each target, unless there was more than 2°C disagreement between the two PRTs in which case the entire scan line was skipped. The conversion from thermometer digital counts to resistance requires the following equation:

$$R = k_0 + k_1[(C_{\text{target}} - C_{\text{cal lo}})/(C_{\text{cal hi}} - C_{\text{cal lo}})], \qquad \text{(A2)}$$

where R is resistance: k_0 and k_1 are 495.6 and 107.8, respectively, and the same for all MSUs; C_{target} is the radiometer digital counts (corrected) during target viewing; and $C_{\text{cal hi}}$ and $C_{\text{cal lo}}$ are precision reference resistor digital counts in each of the separate redundant

TABLE A1. MSU digital count nonlinearity correction coefficients for channels 2 and 4.

	a_1	a_2	a_3
TIROS-N (ch. 2)	26.85	0.939964	0.0000172642
(ch. 4)	22.2317	0.964907	0.00000965909
NOAA-6 (ch. 2)	22.0408	0.927569	0.0000167910
(ch. 4)	36.5099	0.935564	0.000016923
NOAA-7 (ch. 2)	26.061	0.9438	0.00001626
(ch. 4)	21.736	0.9598	0.00001124
NOAA-8 (ch. 2)	18.71	0.9589	0.000012800
(ch. 4)	15.14	0.9533	0.0000146528

JUN 6 '91 10:42 FROM NASA/MSFC ESAD(ES41) TO 6 S WILSON PAGE.024

Precision and Radiosonde Validation of Satellite Gridpoint Temperature Anomalies, Part I: MSU Channel 2

by

Roy W. Spencer

ES43 Earth Science and Applications Division

NASA Marshall Space Flight Center

Alabama 35812

John R. Christy

Johnson Research Center

University of Alabama in Huntsville

Huntsville, Alabama 35899

Manuscript Still in Review

submitted to

Journal of Climate

April 1991

ABSTRACT

In Part I of this study, monthly 2.5° gridpoint anomalies in TIROS-N Microwave Sounding Unit channel 2 brightness temperatures during 1979-88 are evaluated with multiple satellites and radiosonde data for their climate temperature monitoring capability. The monthly gridpoint agreement between concurrently operating satellites is generally better than 0.1°C in the tropics and better than 0.2°C at higher latitudes. Monthly anomalies in radiosonde channel 2 brightness temperatures computed with the radiative transfer equation compare very closely to the MSU measured anomalies in all climate zones, with correlations generally from 0.94 to 0.98 and standard errors of 0.15°C in the tropics to 0.30°C at high latitudes. Simplification of these radiative transfer calculations to a static weighting profile applied to the radiosonde temperature profile leads to an average degradation of only 0.02° in the monthly skill. In terms of a more traditionally measured quantity, the MSU channel 2 anomalies match best with either the 100-20 kPa or 100-15 kPa layer anomalies. No significant spurious trends were found in the ten-year satellite dataset. Thus sequentially launched, overlapping passive microwave radiometers provide a useful system for monitoring intraseasonal to interannual climate anomalies. The Appendix includes previously unpublished details of the MSU gridpoint anomaly data set construction. Part II of this study addresses the removal from channel 2 of the temperature influence above the 30 kPa level, a layer which often experiences considerably different trends than those measured by radiosondes below 30 kPa.

1. Background

The potential of externally calibrated microwave radiometers for precision monitoring of climate change was demonstrated by Spencer and Christy (1990, hereafter SC) and Spencer et al. (1990, hereafter SCG) in the context of deep tropospheric and lower stratospheric brightness temperature (T_b) anomalies. Satellite intercomparisons between simultaneously operating Microwave Sounding Units (MSUs) on morning and afternoon TIROS-N satellites revealed agreement to 0.01°C for monthly, globally averaged T_b anomalies, and instrument stability to better than 0.01°C over a two year overlap period. Whereas these results addressed the precision of the satellite measurements on hemispheric and global scales, we now extend this evaluation to the 2.5° gridpoint scale, and incorporate radiosondes as an independent tool for verifying their quality.

A fundamental question often asked is, what do the channel 2 T_b anomalies represent? First let us address the deep-layer nature of the measurement. The channel 2 weighting function (Fig. 1) is vertically broad and represents the vertical distribution (in $\log_e p$ coordinates) of the satellite-measured radiation over a layer extending from the surface to above 30 kPa. The bulk of this microwave radiation is thermally emitted by molecular oxygen with an intensity directly proportional to temperature. A much smaller contribution is from water vapor thermal emission. Oxygen is an ideal temperature tracer for climate monitoring because it occupies a large fraction of our atmosphere (20.95% by volume), is uniformly mixed, and its concentration is very stable in time. Therefore, MSU channel 2 measurements are dominated by the vertically weighted air temperature through a deep tropospheric layer of air. In typical satellite sounder "retrieval" schemes, this deep layer measurement is combined with other channels having overlapping weighting functions (such as MSU channels 1,3, and 4 in Fig. 1) in order to deconvolve these weighting functions into an "averaging kernel" (see Conrath, 1972, and Grody, 1980) which is considerably sharper than the individual channel weighting functions. However, we rapidly approach a

practical limit in our ability to sharpen the averaging kernel because of the finite number of channels, each having a certain amount of measurement noise. Therefore, based upon current theoretical and engineering limits, the satellites simply can not measure the many levels a radiosonde system measures. Thus, even though satellite temperature retrievals often relate the measurements to temperature at a specific level in the atmosphere, this assignment is ultimately based upon certain average statistical relationships which occur in the atmosphere which are, by their assumed time-invariant nature, irrelevant to the climate monitoring issue.

A second issue concerns much of the satellite-measured signal is contaminated by non-oxygen emission. Based upon theory (see SCG) we expect the MSU channel 2 T_b anomalies to have small contaminating influences from interannual variations in precipitation-size ice in deep convection, cloud water, water vapor, and surface emissivity. However, the magnitudes of these contaminants are difficult to quantify without knowledge of interannual variations in these variables. Theoretical evidence was presented by SCG to support interpretation of the T_b anomalies as dominated by thermometric temperature to about $0.01^{o}C$ for globally averaged monthly anomalies, although regional areas might experience contaminating influences exceeding $0.1^{o}C$.

Therefore, at this point we hypothesize that the channel 2 anomalies are dominated by thermometric temperature variations over a layer represented by the channel 2 weighting function. However, theory alone is insufficient for rigorous evaluation of the satellite temperature monitoring technique. Here we will present results of comparisons between ten years of monthly radiosonde thickness anomalies to the MSU channel 2 anomalies, in atmospheric environments ranging from tropical to polar. If it can be demonstrated that individual gridpoint anomalies in MSU channel 2 T_b closely match anomalies in radiosonde measurements, then we will have increased confidence that the full global 2.5^{o} gridpoint dataset can be successfully utilized for intraseasonal to interannual climate studies. Furthermore, if there is

little or no ten year trend in the difference between the radiosonde and satellite time series, then the satellite system will be supported for long-term monitoring (e.g. of potential global warming).

2. Some limits of radiosonde precision for gridpoint climate monitoring

Before gridpoint comparisons with radiosonde data are carried out, it is useful to address the capability of a single radiosonde station to measure monthly anomalies in different layers, as well as for long-term trends.

a. monthly radiosonde precision

Individual radiosonde temperature profiles are generally considered to have about a 0.7°C random error in the absolute calibration of the sonde. If a station makes sixty observations per month, then that station's precision in the measurement of a monthly temperature anomaly is $(0.7/(60)^{1/2})$, or about 0.1°C. The fact that each measured profile might not accurately represent the larger scale environment will produce an additional source of error for climate monitoring which is related to temperature variability on the micro- and mesoscale. Let us assume this error component to be about 0.2°C. Assuming these errors to be uncorrelated, we arrive at an RMS error of somewhat over 0.2°C for a single station's ability to measure monthly temperature anomalies.

We have chosen two pairs of tropical western Pacific Ocean stations which are closely spaced to see what level of agreement is experienced for monthly temperature anomalies. These are Yap and Koror Islands; and Truk and Ponape Islands. The tropical environments were chosen to avoid significant horizontal gradients in the monthly anomalies. The distances between these station pairs are 450 km and 700 km, respectively. In Figure 2a we have plotted the agreement between these station pairs in terms of correlations and standard errors of estimate for different layers' thicknesses. We see that the agreement between stations is about 0.2°C, which is consistent with our *a priori* estimate.

b. ten year trends

When we plot the ten-year trends of the layer temperatures for these station pairs (Fig. 2b) we see disturbingly large differences of 0.2^{o} to 0.5^{o}C for the period 1979-88. If we also examine two other western Pacific stations, Guam and Majuro, we find somewhat less disagreement and a tendency towards zero trend. Whatever the reasons for such large variability in single station trends, it appears that decadal trends calculated from a single radiosonde station should be viewed with extreme caution. If this station-to-station variability is random in nature, then many-station averages might be more confidently related to real atmospheric temperature trends (as we will see below). In any event, any disagreement we later find in the satellite comparisons to decadal radiosonde trends at the 0.1^{o} or 0.2^{o} level probably falls in the realm of noise.

3. Satellite gridpoint dataset construction and precision

a. limb correction and gridpoint assignment

The MSU measures at eleven scan angles as it scans across the satellite subtrack every 9.5^{o} from 47^{o} left to 47^{o} right of nadir (see SCG for more information regarding the MSU sampling geometry). Each scan position measurement was calibrated as a T_b according to the procedure in SCG. After calibration, regression-derived limb correction equations were applied to all ten non-nadir scan positions data to correct for the off-nadir T_b being an average amount colder than the nadir T_b. This relative coldness is due to the off-nadir weighting functions being slightly higher in the troposphere than the nadir weighting function caused by the increased atmospheric path length of the radiation off-nadir. These limb correction equations have the form

$$T_{bL} = aT_b - b, \qquad (1)$$

where T_{bL} is the limb corrected T_b for an individual MSU scan position, and the regression coefficients constants "a" and "b" were derived as a function of satellite, 10^o latitude band, and scan position. Approximately 6,700 scans were chosen from each of twelve calendar months of the separate satellites for certain years, i.e. TIROS-N (1979), NOAA-6 and NOAA-7 (1982); NOAA-9 (1986); NOAA-10 and NOAA-11 (1990). For it to be included, each scan had to exhibit little evidence of horizontal (synoptic scale) temperature gradients, with the difference in the T_b from opposite ends of the scan line not exceeding a few degrees. For each satellite, all twelve months of data (80,000 scan lines) were partitioned according to which 10^o latitude band each occupied (assigned by the nadir scan position). Both northern and southern latitude bands were combined together to avoid averaging biases arising from a single scan position usually being on the warmer (tropical) or colder (polar) side of the nadir footprint. The resulting limb corrected T_{bL} for the first (#1) and last (#11) scan positions were quite noisy, so they were not included in any further processing of the data.

Next, each T_{bL} was binned into the appropriate 2.5^o grid square according to the latitudes and longitudes provided with the raw data by NESDIS. This was done on a daily basis for each satellite separately and for ascending and descending satellite passes separately. At the end of each day, a simple (1/distance) interpolation was performed to empty 2.5^o grid squares for ascending and descending grid fields separately with the nearest non-zero grid data in the east and west directions, out to a maximum distance of fifteen grids. These interpolated ascending and descending T_{bL} fields were then averaged together to provide a single daily T_{bL} field for each satellite. At the end of each month, a time interpolation was performed (+/- 2 days) to any remaining empty grid squares. The daily fields were then averaged together within each month. Further references to the averaged fields will always assume the limb correction procedure was applied to the calibrated data (T_{bL}), so for brevity we will now refer to the data as simply T_b.

b. gridpoint anomaly calculation

Production of monthly gridpoint T_b anomalies would be a simple procedure if a single satellite had been operating for the full period of the satellite record. This would have involved computing, say, a ten-year average for each of the twelve calendar months at every gridpoint and then subtracting this average from individual months within the ten year period. Unfortunately, there are two complications which must be taken into account.

First, the satellite record is made up of seven satellites (six of which we use, see Fig. A1), all of which have calibration biases relative to each other by up to several tenths of a degree. The second complication is the existence of not one, but two separate orbit times alternating throughout the satellite record. Because MSU channel 2 has a small surface sensitivity to diurnal variations in land surface heating, the gridpoint averages are dependent upon the satellite orbit time (2:30 or 7:30) and the local strength of the diurnal heating cycle, which is a function of geography and time of year.

The procedure for the merging of all six satellites' data records into a single time series of anomalies is described in the Appendix. This is the same procedure which led to the global time series reported by SC and SCG, but some details of which have been previously undocumented.

c. gridpoint precision

The precision of the satellite T_b anomaly measurements at the gridpoint level can be readily demonstrated without the satellite merging procedure described in the Appendix. Because the TIROS-N satellite system occasionally had two satellites simultaneously operating in separate orbits (7:30 and 2:30) for more than one year, we can compare their measurements of interannual variability in two successive years. (This, of course, provides an interannual anomaly measurement since any multi-year mean assigned for those two years cancels out in the difference.) Then we can compare the results from the separate satellites to evaluate how well a single satellite can measure monthly grid-

point anomalies in T_b. If this procedure is followed for the month of February from 1982 and 1983, we find remarkable agreement between the NOAA-6 and NOAA-7 satellites (Fig. 3a and 3b, respectively). For this single month, the gridpoint correlation between satellites in each 2.5° latitude band ranges from 0.95 in the tropics to over 0.99 at the higher latitudes, with the standard deviation of the satellite difference ranging from generally less than 0.1°C in the tropics to generally less than 0.2°C at middle and high latitudes. Note that this level of gridpoint agreement between satellites is as good or better than the accuracy provided by adjacent tropical radiosonde stations, as previously discussed. Further, since these are single-satellite precision, the error is reduced even further (by 0.7) when two satellites are operating.

If we utilize the full gridpoint dataset (assembled according to the procedures in the Appendix) we can evaluate monthly gridpoint precision for many more months when the satellite operating periods overlap. A map of the standard deviation of the monthly inter-satellite differences between NOAA-6 and NOAA-7 (Fig. 4) shows the level of monthly anomaly agreement for an overlap period of twenty months. Note that most areas have gridpoint T_b agreement to better than 0.1°C, mainly in the tropics, with almost all other non-tropical areas exhibiting better than 0.2°C agreement. Degradation of a few hundredths of a degree is seen over land areas, noise which is probably introduced by the diurnal variations in the surface as seen by the morning and afternoon satellites. A few small areas of mountainous terrain (the Andes, Himilayas, Tibetan Plateau, and portions of Greenland and Antarctica) show poorer agreement between satellites due to enhancement of this surface influence as the terrain protrudes up into the channel 2 weighting function.

4. Radiosonde comparisons

While the above results demonstrate there is great precision in the ability of a single MSU to precisely monitor monthly gridpoint anomalies in channel 2 T_b, it still remains to be

demonstrated that these anomalies are dominated by a temperature signal. We will address three kinds of radiosonde comparisons to MSU measured anomalies: 1) channel 2 T_b computed from the radiosonde profiles of temperature and humidity with the radiative transfer equation (see Grody, 1983), 2) a much simpler method where an assumed constant weighting function is applied to the radiosonde temperature profile only, and 3) comparisons to traditionally measured thickness anomalies for various standard atmospheric layers.

a. radiosonde data processing

The channel 2 T_b anomalies from the merged multi-satellite dataset at specific 2.5^{o} gridsquares were compared to radiosonde measurements for individual stations within those grid squares. The radiosonde data utilized for our intercomparisons is a quality controlled dataset provided by NCAR. The stations are United States (U.S.)-controlled and include, in addition to the mainland United States, scattered Pacific, Caribbean basin, and Alaska locations. Of approximately 120 stations which have fairly complete ten year records, here we will present the results from six stations representing various climate regimes (Table 1). Also, comparisons to several stations from each of these six regimes are composited together to provide regionally averaged comparisons.

In the first type of radiosonde comparison, the radiative transfer equation (Grody, 1983) was used to compute a T_b with the temperature and water vapor information provided by the radiosonde. All radiosonde ascents were included which went above 10 kPa, with the most recent radiosonde data above 2 kPa (usually not more than one or two days old) being inserted if the current profile did not go above 2 kPa. Each sounding was capped by an artificial temperature of 250 K at 0.01 kPa level. These T_b computations throughout the 10-year period were averaged on a monthly basis. The ten-year (1979-88) monthly averages were then subtracted from the individual monthly averages to arrive at a 10-year time series of monthly anomalies.

Secondly, a simpler method of computing T_b was used which avoids the computational intensity of the radiative transfer equation. Because the temperature dependence of the oxygen absorption and the water vapor absorption are both small, a static weighting function can be applied to just the temperature profile without risking great error. The channel 2 weighting function for a U.S. Standard Atmosphere (Fig. 1) was applied to the radiosonde temperature profiles to provide a vertically weighted T_b estimate, i.e.

$$\hat{T}_b = \frac{\sum_{i=1}^{N} w_i T_i \log_e(p_1/p_2)}{\sum_{i=1}^{N} w_i \log_e(p_1/p_2)} \qquad (2)$$

where the ith layer of N radiosonde profile layers has an average temperature (T_i), an average weight (w_i) from Fig. 1, and bounding pressures (p_1 and p_2).

Third and lastly, comparisons were made to all combinations of thickness layers having bases at 100 kPa or 85 kPa, and tops at 70, 50, 40, 30, 25, 20, 15, and 10 kPa. Because virtually all of the correlations were somewhat lower for layers having bases at 85 kPa, only the results for the layers having 100 kPa bases are presented here.

b. single station gridpoint correlations

The levels of agreement between the satellite measurements and each of the six stations are presented in Figures 5 through 10 in terms of correlation coefficients (R) and standard error of estimate (SE) of the radiosonde temperature anomalies. The first half of these figures (a) shows the time series of comparisons to radiosonde-computed channel 2 T_b, while the second half (b) shows R and SE for various thickness layer temperature anomalies.

In Cold Bay, Alaska (Fig. 5a) we find a monthly correlation of 0.98 between the satellite-measured and the radiosonde-calculated T_b, with a corresponding SE of 0.24°C. The yearly anomaly correlation is just under 0.99. Use of the simplified T_b computations with Eq. 2 results in R=0.96 and SE=0.28°C, which is only a slight degradation in performance for the monthly

anomalies. The best monthly agreement between the satellite and a traditionally measured thickness layer (Fig. 5b) is with the 100-20 kPa layer (R=0.94) which is not quite as good as with the other measures. Most of the stations we examined (of over 100 in number) indicated the 100-20 kPa layer as having the best agreement of all traditionally measured thickness layers. This should not be surprising considering the channel 2 weighting function distribution in Fig. 1.

In St. Cloud, Minnesota (Fig. 6a) we find similar results to those of Cold Bay, with a monthly correlation of 0.98 and SE of 0.24°C. Use of Eq. 2 gives only slightly degraded results with R=0.97 and SE=0.27°C. These figures are slightly better than the correlation with the 100-15 kPa layer (R=0.96) in Fig. 6b.

The comparisons to radiosonde-computed channel 2 for Oakland, California (Fig. 7a) reveal R=0.95 and SE=0.25°C. Interestingly, the results with Eq. 2 are slightly better than those obtained with the radiative transfer equation, with SE=0.23°C. As with the other stations, these are both slightly better than with the thickness layer of best agreement (100-20 kPa) for which R=0.94 (Fig. 7b).

At Lihue, Hawaii (Fig. 8a) the radiative transfer calculations with the radiosonde data show a 0.96 correlation and SE=0.16°. With Eq. 2 these measures become R=0.95 and SE=0.18°C, again revealing the utility of a simple vertically weighted average of the temperature profile with a constant weighting function. Compared to a traditionally measured layer, best agreement is seen in the 100-20 kPa layer, with R=0.95 and SE=0.23°C (Fig. 8b). Note that we are now reaching the limit of agreement (0.20°C) between adjacent tropical radiosonde stations measuring the same layers shown in Fig. 2. In fact, comparison between the Lihue and Hilo, Hawaii radiosonde stations, despite their relatively close proximity to each other, yields *poorer* agreement (the circles in Fig. 8b) than the satellite shows with Lihue. This casts some doubt on the regional representativeness of isolated radiosonde stations when used to construct "global" temperature anomalies. Of some interest are the low correlations

between the MSU channel 2 anomalies and the lower tropospheric temperature anomalies at Lihue. This illustrates very little coupling between the lower and middle troposphere in this oceanic region.

The agreement with the satellite anomalies at San Juan, Puerto Rico (Fig. 9a) is about the same as was found in Hawaii, with R=0.95 and SE=0.15°C. Using Eq. 2 for the radiosonde computations, we once again obtain only slightly poorer performance, with R=0.93 and SE=0.20°C. In the comparisons to thickness anomalies (Fig. 9b), for the 100-25 kPa layer R=0.95 and SE=0.21°C. Again, these levels of agreement approach the precision inherent in the sampling provided by a single radiosonde stations.

Guam, in the tropical western Pacific (Fig. 10a) reveals a somewhat lower correlation (R=0.85), but an excellent standard error (SE=0.14°C). This reflects the very weak signal of monthly temperature anomalies in this region of the world. Note that the correlation is no worse than that between the adjacent radiosonde stations in Fig. 2. The constant weighting method (Eq. 2) gives R=0.81 and SE=0.17°C, again only a slight degradation from using the full radiative transfer equation. Considerably worse results are revealed for the 100-15 kPa layer anomalies, where R=0.74 and SE=0.25°C. This degradation is the result of low natural interlayer correlations within the troposphere which makes comparison with the correct vertical weighting profiles very important.

c. composite station correlations

When satellite-radiosonde comparisons are grouped by region, the levels of agreement improve further (Table 2). We see the largest improvement in correlation for the tropical western Pacific, for which Guam was 0.85, and now a six station composite correlation increases to 0.94, with the SE improving to 0.09°C. These station composites thus reveal that the radiosonde (and satellite) noise at individual gridpoints is reduced when several gridpoints are averaged together.

d. trends

Table 3 shows the ten year trends for these station composites as well as the satellite measured trends. Note that the differences are well within the levels of disagreement seen in Fig. 2b between closely spaced tropical Pacific radiosonde stations. Thus the ten year trends in the multi-satellite record of monthly anomalies, when compared to regionally averaged radiosonde station measurements, show no obvious evidence of drift. Unfortunately, these radiosonde station groupings are probably not sufficient to measure drifts to better than 0.1°C.

5. Conclusions

Radiosonde comparisons support the use of satellite passive microwave temperature measurements for precise deep layer temperature monitoring, even at the 2.5° gridpoint scale. Inter-satellite comparisons of monthly TIROS-N MSU channel 2 T_b anomalies at the 2.5° gridpoint level reveal remarkable agreement, generally better than 0.1°C in the tropics and better than 0.2° at high latitudes. Since these are single-satellite precisions, the precision of the gridpoint values with two satellites is improved even further. Comparisons between MSU-observed and radiosonde calculated monthly anomalies in channel 2 T_b reveal correlations generally around 0.95 and standard errors from 0.15°C in the tropics to 0.25°C at high latitudes. This performance degrades by an average of only 0.02°C if a simple vertical weighting is applied to the radiosonde temperature profiles, instead of using radiative transfer calculations. This simple method is recommended for quantitative comparisons to other multiple layer temperature datasets. Compositing of four to fifteen radiosonde stations together in specific regions improves the satellite-radiosonde agreement to 0.10°C in the tropics to about 0.20°C at high latitudes. Thus, the satellite precision approaches that of individual radiosonde stations in their ability to measure monthly temperature anomalies, which we estimate to be 0.2°C from intercomparisons of closely spaced tropical oceanic stations in the Pacific. In terms of traditionally measured

layers, the highest satellite correlations exist for the 100-20 kPa layer or the 100-15 kPa layer. These correlations are only slightly poorer than for the channel 2 weighting profile, except over the tropical Pacific where natural inter-layer correlations are low, making the correct weighting of the radiosonde profile very important.

We find no evidence of instrumental drift in the ten years of MSU channel 2 measurements (1979-88) to our ability to measure it with multiple-station radiosonde data.

Acknowledgments

We thank Roy Jenne and Dennis Joseph at NCAR for provision of the raw MSU data sets and radiosonde data. Robbie Hood assisted in the processing of the radiosonde data and radiative transfer modeling. Norm Grody (NOAA/NESDIS) and Shelby Tilford (NASA Headquarters) provided useful advice during the course of this study.

APPENDIX

Merging of Multi-Satellite MSU Data for Climate Monitoring

The TIROS-N series of sun-synchronous polar orbiting satellites have provided a continuous monitoring of the Earth since late 1978. Each satellite has a operational lifetime of one to three years. Nominally two satellites are operated at the same time, one in a morning orbit (7:30) and one in an afternoon orbit (2:30), although a few periods have existed when only a single satellite has been available. Launches of new satellites alternate between morning and afternoon.

If a single satellite had always been operated (and its sensors remained sufficiently stable), then computation of monthly brightness temperature anomalies from this single satellite would have been a simple process of averaging all data into monthly bins for some multi-year period sufficient to observe a representative annual cycle (say 1979-88), and then subtracting this average from the individual single-month averages to arrive at a time series of monthly anomalies. Unfortunately, we must deal with multiple satellites with slightly different sensors in different orbits. As a consequence, merging of the data from these overlapping satellites into a continuous time series requires the removal of two basic sources of differences between satellites. First is the absolute calibration differences between different MSUs, for which we find a very small latitudinal dependence in our two primary channels of interest (2 and 4). The second source arises from the different solar times of the morning and afternoon orbits. MSU channel 2 has some sensitivity to the surface, and so the 2:30 afternoon channel 2 T_b observations over land can be considerably warmer than either the 7:30 a.m. or 7:30 p.m. T_b. This effect becomes stronger as one moves toward the equator and higher elevations, e.g. 5-10^{o}C over the United States, 10-15^{o}C over the Sahara Desert. Therefore, removal of an annual cycle for anomaly computation is not only a function of the different satellite orbits, but also of geographical region.

Following are the specific steps performed in the time series construction:

We first compute an average annual cycle from the monthly grid fields described in Section 3 for a single overlap period between two concurrently operating satellites. We chose 1982 when there was a full-year overlap between NOAA-6 (morning) and NOAA-7 (afternoon), using NOAA-6 as a base period due to its long (7+ year) lifespan.

The morning and afternoon satellite annual cycles were then used as bases from which anomalies for all the other satellites were computed, a simple subtraction of the gridpoint annual cycles ~~the~~ from the monthly averages obtained from the other morning and afternoon satellites. The anomalies at this point are based upon only the 1982 annual cycle of either NOAA-6 or NOAA-7, without any correction for inter-satellite differences.

To make the inter-satellite correction, the anomalies from different satellites were compared during all periods of overlap between satellites (Fig. A1) to find the time- and gridpoint-averaged offsets relative to NOAA-6, which were then individually removed from each satellite's anomalies. At this point, we have anomalies which are intercalibrated between satellites, but are still relative to only a single year's annual cycle (1982).

Finally, the average of 12 years of each month's anomalies was forced to zero by adding an appropriate offset to each anomaly, thus removing the 12-year mean annual cycle.

Table A1 lists statistics of the inter-satellite comparisons and adjustments, including the route of adjustment to a common level (NOAA-6); the dates of overlap between satellites used in the adjustments; the daily standard deviation of the difference (single satellite "error") between the overlapping satellites globally averaged channel 2 T_b anomalies; the daily signal to noise ratio (the sum of the overlapping satellites daily ch. 2 T_b anomaly divided by their daily difference, squared); 30-day statistics; the globally-averaged adjustments necessary to bring that satellite to the NOAA-6 level; and the net trend in the time

series of the daily differences between overlapping satellites T_b anomalies. NOAA-8 had many operational problems and was not used in any of our statistics.

References

Grody, N.C., 1980: Analysis of satellite-based microwave retrievals of temperature and thermal winds: Effects of channel selection and a-priori mean on retrieval accuracy. *Remote Sensing of the Atmosphere and Oceans*, A. Deepak, Ed., Academic Press, 381-410.

Grody, N.C., 1983: Severe storm observations with the Microwave Sounding Unit. *J. Climate Appl. Meteor.*, **22**, 609-625.

Spencer, R.W. and J.R. Christy, 1990: Precise monitoring of global temperature trends from satellites. *Science*, **247**, 1558-1562.

Spencer, R.W., J.R. Christy, and N.C. Grody, 1990: Global atmospheric temperature monitoring with satellite microwave measurements: Method and results, 1979-84. *J. Climate.*, **3**, 1111-1128.

List of Figures

Figure 1. Weighting functions for MSU channels 1 (50.3 GHz); 2 (53.74 GHz); 3 (54.96 GHz); and 4 (57.95 GHz) for a 22° view angle through a U.S. Standard Atmosphere.

Figure 2. Monthly temperature anomaly agreement (a) and decadal trend agreement (b) between closely spaced tropical Pacific radiosonde stations for different thickness layers.

Figure 3. Gridpoint MSU channel 2 T_b anomaly differences for February 1983 minus February 1982, as measured separately by NOAA-6 and NOAA-7.

Figure 4. The standard deviation of the MSU channel 2 gridpoint anomaly differences (°C) between NOAA-6 and NOAA-7 for a twenty month overlap period, resulting from the satellite intercalibration procedure outlined in the Appendix.

Figure 5. Time series (a) of MSU channel 2 anomalies and radiosonde-calculated channel 2 anomalies; and correlation and standard errors (b) with radiosonde thickness temperature anomalies for Cold Bay, Alaska during 1979 through 1988. In (a) the solid line is MSU-measured, the dashed line is radiosonde-measured, and the correlations (R) are for the monthly and yearly anomalies, respectively. In (b) the solid line shows the best agreement possible based upon MSU channel 2 T_b being computed from the radiosonde data, and the dashed line shows the satellite-measured agreement with the radiosonde thickness temperature anomalies.

Figure 6. As in Fig. 5, except St. Cloud, Minnesota.

Figure 7. As in Fig. 5, except Oakland, California.

Figure 8. As in Fig. 5, except Lihue, Hawaii. Also shown in (b) is the level of agreement between Hilo, Hawaii and Lihue, Hawaii.

Figure 9. As in Fig. 5, except San Juan, Puerto Rico.

Figure 10. As in Fig. 5, except Guam.

Figure A1. Periods of operation and overlap between MSUs during 1979-90. Gaps indicate one or more days of less than 85% global data. The authors do not yet have March 1989 data in their dataset.

Table 1. Radiosonde stations from various climatic regimes chosen for comparison to the satellite gridpoint temperature anomaly dataset.

Station	Climatic Type	Location
Cold Bay, Alaska	Polar	55.2°N 162.7°W
St. Cloud, Minnesota	Continental	45.6°N 94.2°W
Oakland, California	Mid-latitude	37.7°N 122.2°W
Lihue, Hawaii	Sub-tropical	22.0°N 159.3°W
San Juan, Puerto Rico	Sub-tropical	18.4°N 66.0°W
Guam	Tropical	13.6°N 144.8°E

Table 2. Station composite correlations and standard errors of satellite versus radiosonde monthly anomalies in channel 2. Numbers in parentheses are the corresponding single-station values from the stations represented in Figs. 5-10.

Region	R	SE
Alaska(15)	.98(.97)	.17°(.24°)
Great Lakes(6)	.98(.98)	.22°(.24°)
West Coast(4)	.97(.95)	.18°(.25°)
Caribbean(6)	.97(.95)	.10°(.15°)
West Pacific(7)	.94(.85)	.09°(.14°)

Alaska:(15) Anette, Yakutat, Kodiak, King Salmon, Cold Bay, Adak, St. Paul Island, Anchorage, Fairbanks, McGrath, Bethel, Kotzebue, Nome, Barter Island, Barrow. **Great Lakes:**(6) Sault Ste. Marie, MI; International Falls, MN; Green Bay, WI; St. Cloud, MN, Huron, SD. **U.S. West Coast:**(4) Quillayute, WA; Salem, OR; Oakland, CA; San Diego, CA. **Tropical West Pacific:**(7) Koror, Yap, Majuro, Wake, Guam, Truk, Ponape. **Caribbean:**(6) Christ Church, Barbados; Santo Domingo, Dominican Republic; Piarco, Trinidad; San Juan, Puerto Rico; Curacao, Netherland Antilles; Roberts, Cayman Islands

Table 3. Ten year trends (^{o}C, for the decade 1979-1988) in MSU-observed and radiosonde-computed channel 2 T_b anomalies for the regional station composites listed in Table 2. The number of stations is each group is shown in parentheses.

Region	Radiosonde Ch. 2 Trend	MSU Ch. 2 Trend	(Raob-MSU)
Alaska(15)	-0.67^{o}	-0.64^{o}	-0.03^{o}
Great Lakes(6)	+0.33^{o}	+0.43^{o}	-0.10^{o}
U.S. West Coast(4)	-0.03^{o}	+0.18^{o}	-0.21^{o}
Caribbean(6)	-0.01^{o}	+0.10^{o}	-0.11^{o}
West Pacific(7)	+0.14^{o}	+0.08^{o}	+0.06^{o}
Weighted Average			-0.06^{o}

Table A1. Global statistics of all satellite overlaps between MSUs for MSU channel 2 data.

Satellite	Method	Overlap Dates	#days	daily error	daily S/N	30-day error	30-day S/N	Global Adj.	1-yr trend*
TIROS-N	to NOAA-6	7/1/79-1/19/80	164	.033°	24.4	.013°	48.9	+.068°	+.074°
NOAA-6	BASE								
NOAA-7	to NOAA-6	6/26/81-4/16/83	596	.028°	36.7	.006°	577.4	-.002°	+.007°
NOAA-9	to NOAA-6	10/30/85-11/4/86	284	.028°	71.4	.006°	183.0	+.067°	+.015°
NOAA-10	to NOAA-9	11/26/86-3/7/87	98	.030°	47.4	.006°	361.7	-.281°	-.068°
NOAA-11	to NOAA-10	10/23/88-10/31/90	641	.030°	29.2	.011°	114.0	+.240°	+.004°

*Due to slightly different crossing times in afternoon satellites, there seems to be a very slight difference in annual cycles between TIROS-N versus NOAA-7. This is also seen in NOAA-7 versus NOAA-11, however, the two year overlap between NOAA-10 and NOAA-11 eliminates any trend due to an annual cycle in the satellite difference time series.

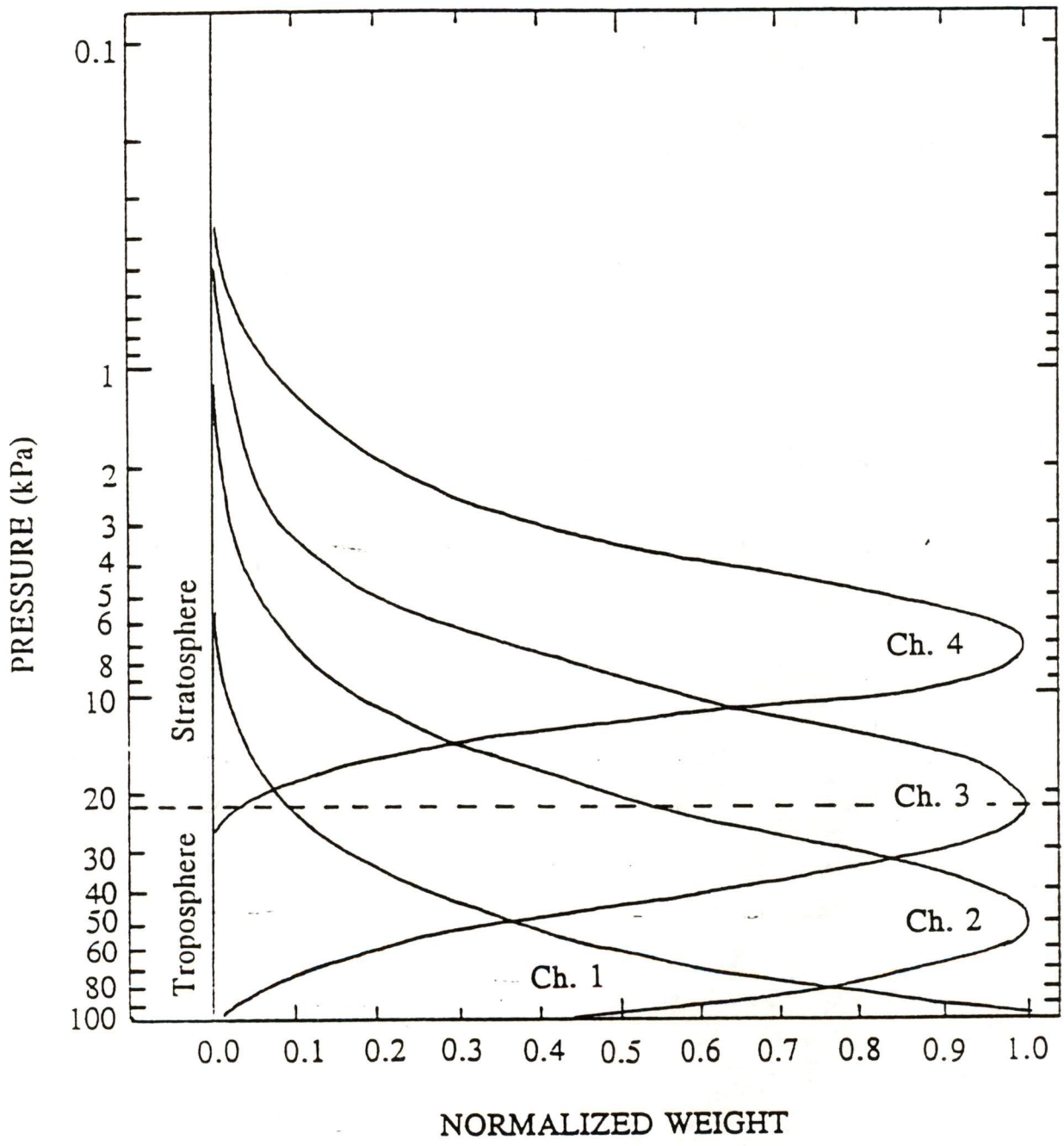
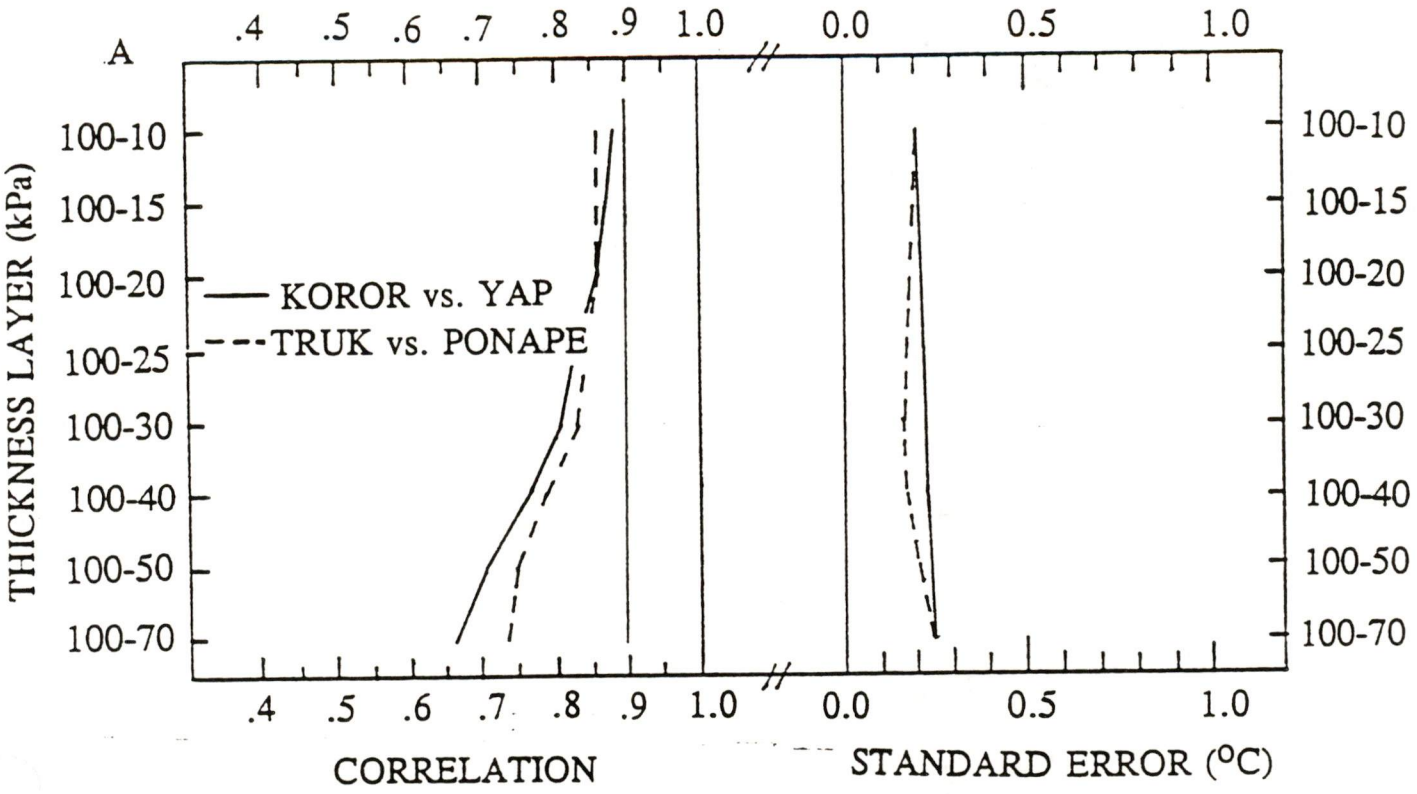

PRESSURE (kPa)
0.1
1
2
3
4
5
6
8
10
20
30
40
50
60
80
100
Stratosphere
Troposphere
Ch. 4
Ch. 3
Ch. 2
Ch. 1
0.0
0.1
0.2
0.3
0.4
0.5
0.6
0.7
0.8
0.9
1.0
NORMALIZED WEIGHT

Fig. 1


A
.4 .5 .6 .7 .8 .9 1.0 0.0 0.5 1.0
100-10
100-15
100-20
100-25
100-30
100-40
100-50
100-70
KOROR vs. YAP
TRUK vs. PONAPE
THICKNESS LAYER (kPa)
CORRELATION
STANDARD ERROR (°C)

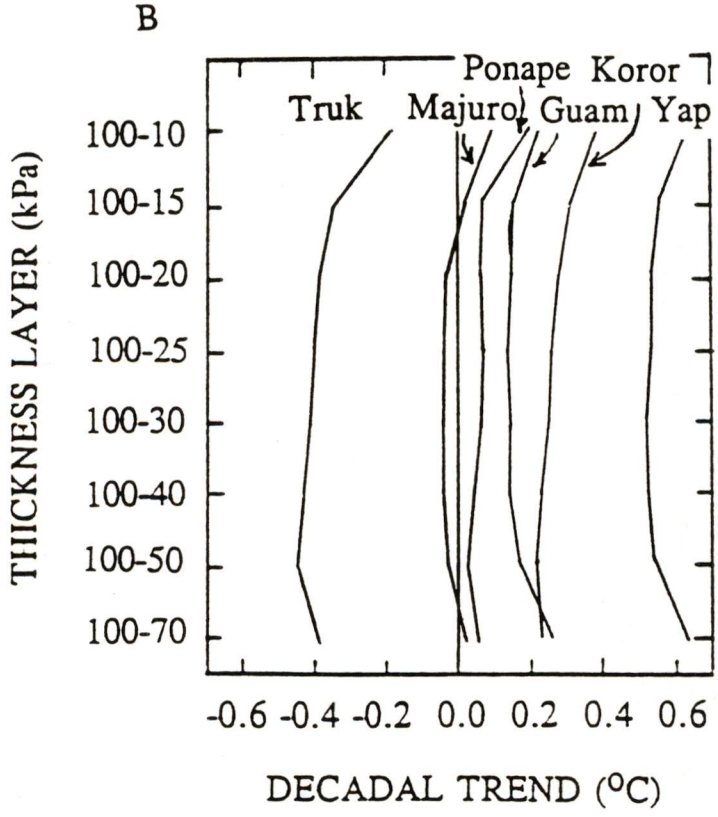

B
Ponape Koror
Truk
Majuro
Guam
Yap
100-10
100-15
100-20
100-25
100-30
100-40
100-50
100-70
THICKNESS LAYER (kPa)
-0.6 -0.4 -0.2 0.0 0.2 0.4 0.6
DECADAL TREND (°C)

Fig. 2a,b

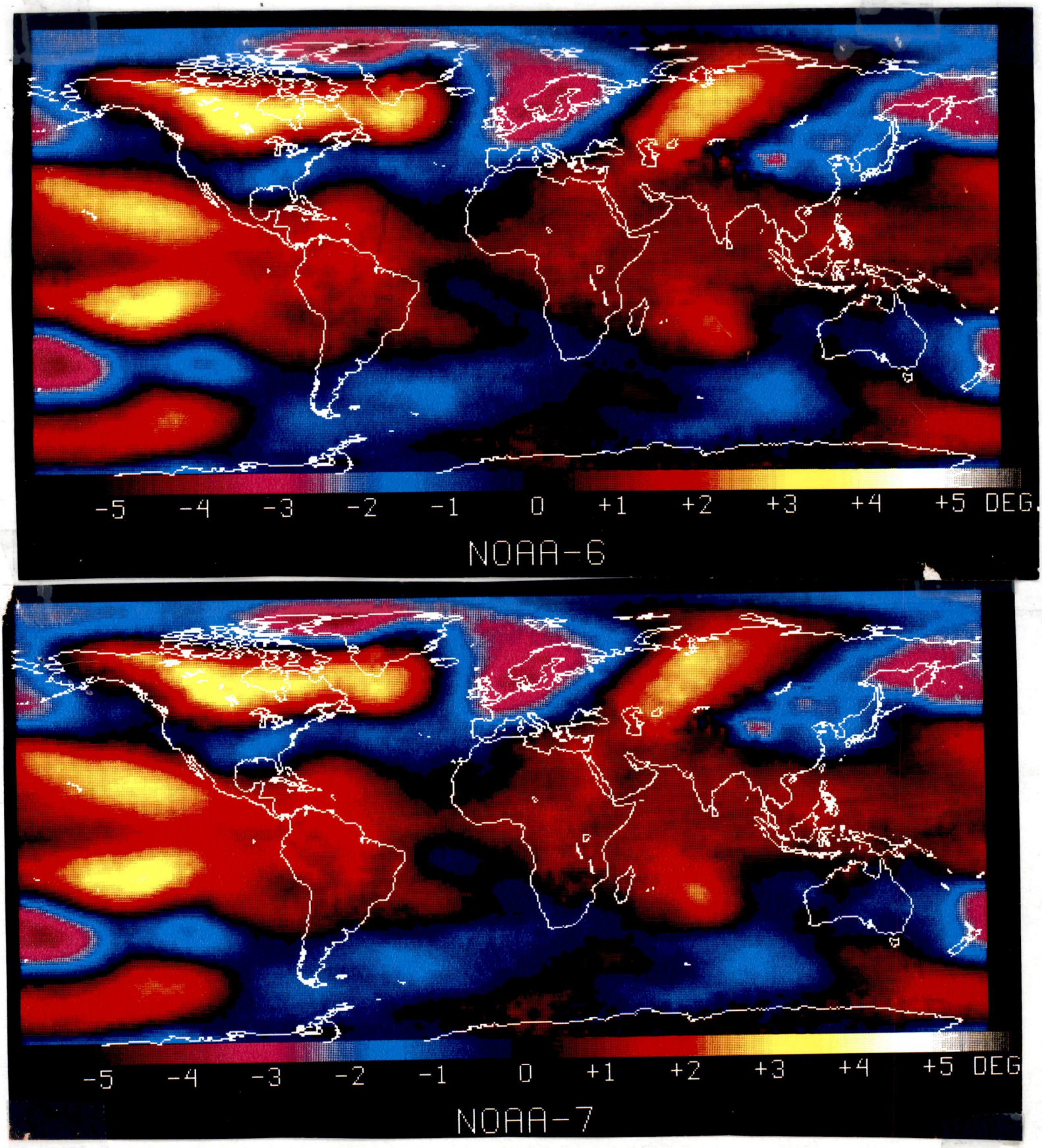


Fig. 3 a,b (overlay)



Fig. 4

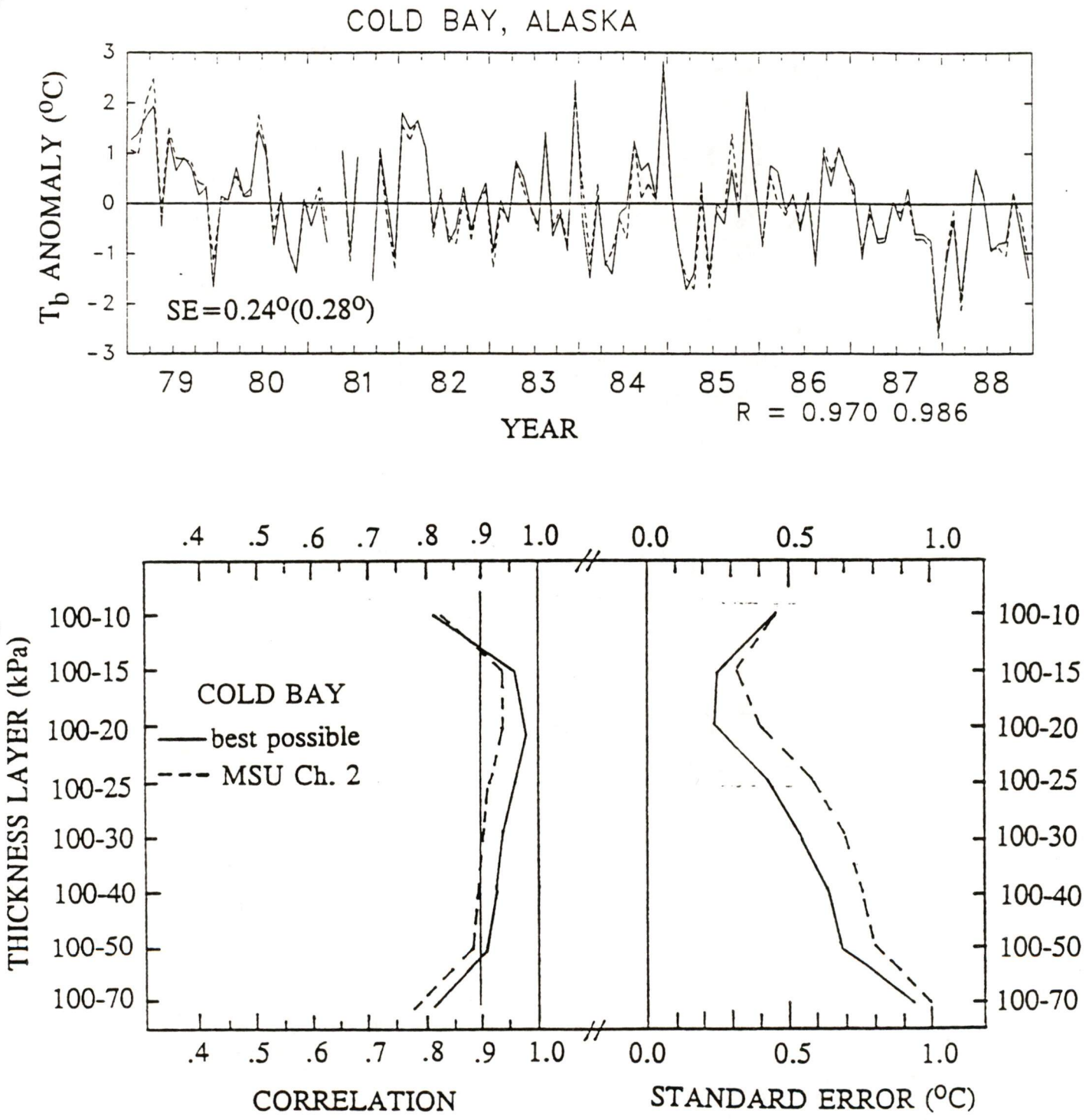

COLD BAY, ALASKA
T_b ANOMALY (°C)
3
2
1
0
-1
-2
-3
SE=0.24°(0.28°)
79
80
81
82
83
84
85
86
87
88
YEAR
R = 0.970 0.986
.4
.5
.6
.7
.8
.9
1.0
0.0
0.5
1.0
THICKNESS LAYER (kPa)
100-10
100-15
100-20
100-25
100-30
100-40
100-50
100-70
COLD BAY
best possible
MSU Ch. 2
CORRELATION
STANDARD ERROR (°C)

Fig. 5

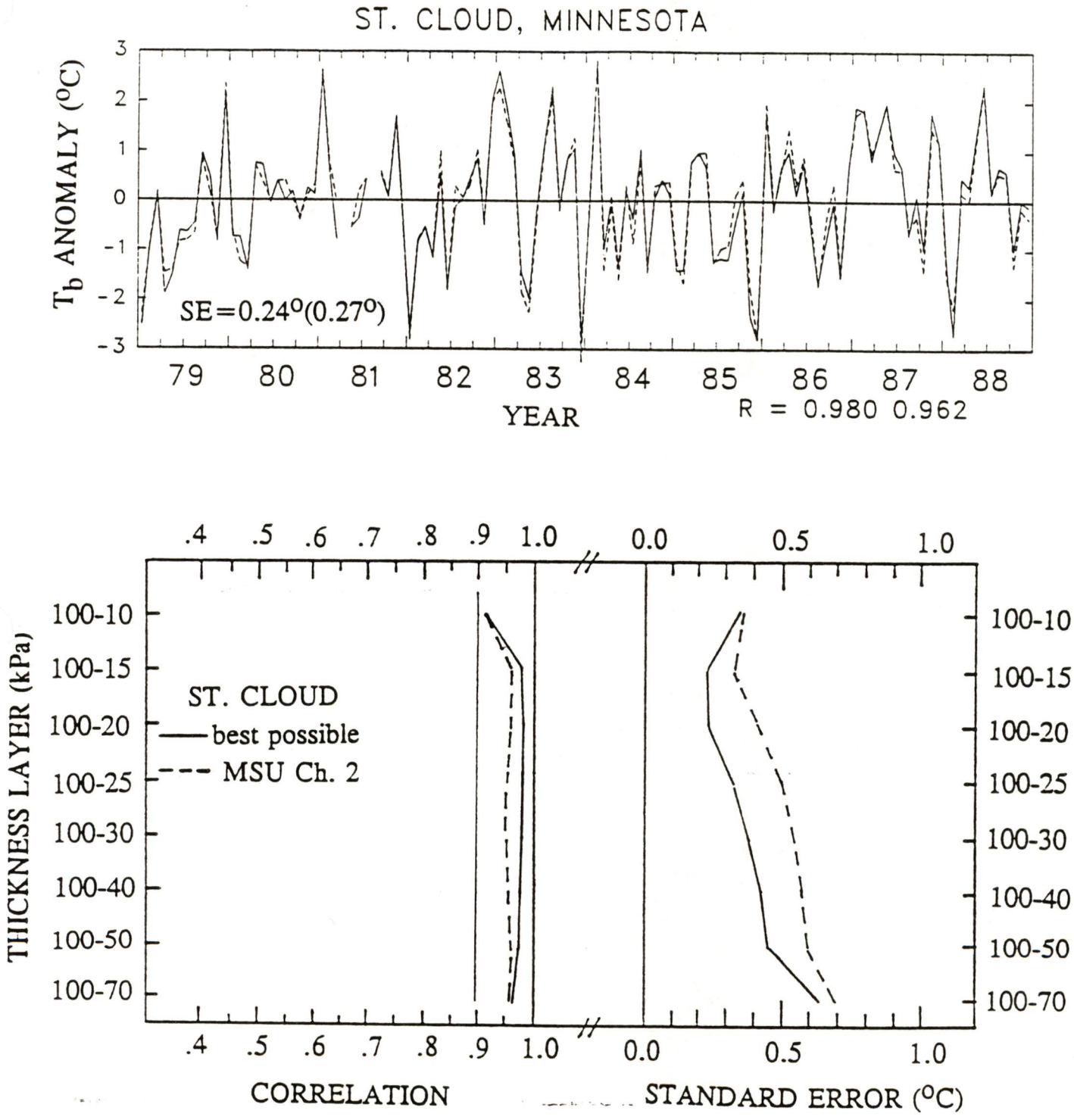
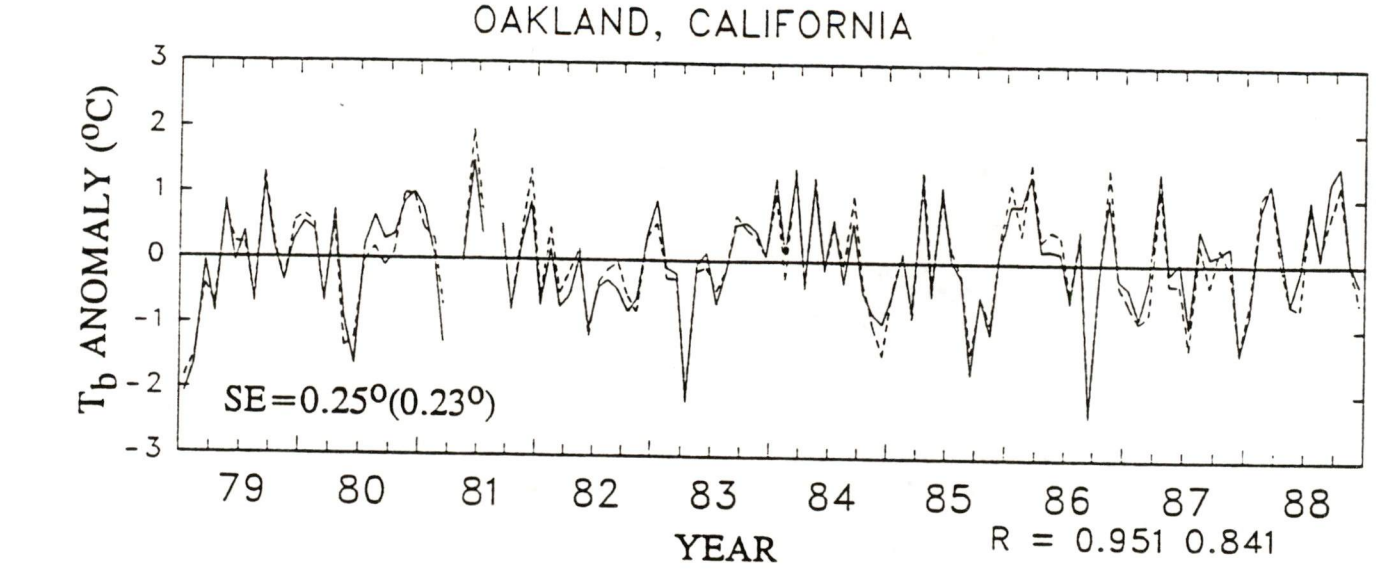

ST. CLOUD, MINNESOTA
T_b ANOMALY (°C)
3
2
1
0
-1
-2
-3
SE=0.24°(0.27°)
79
80
81
82
83
84
85
86
87
88
YEAR
R = 0.980 0.962
.4
.5
.6
.7
.8
.9
1.0
0.0
0.5
1.0
THICKNESS LAYER (kPa)
100-10
100-15
100-20
100-25
100-30
100-40
100-50
100-70
ST. CLOUD
best possible
MSU Ch. 2
CORRELATION
STANDARD ERROR (°C)

Fig. 6


OAKLAND, CALIFORNIA
T_b ANOMALY (°C)
3
2
1
0
-1
-2
-3
SE=0.25°(0.23°)
79
80
81
82
83
84
85
86
87
88
YEAR
R = 0.951 0.841

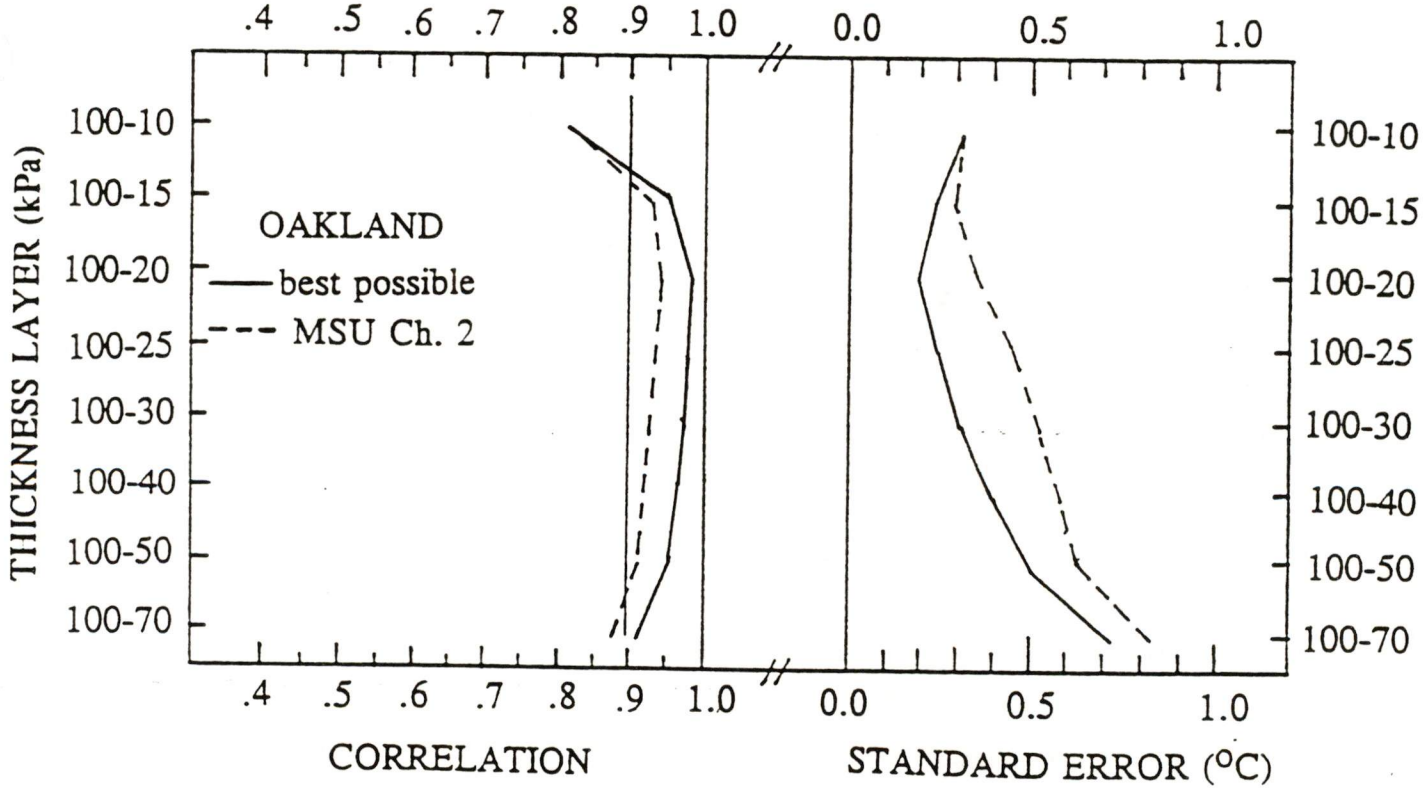
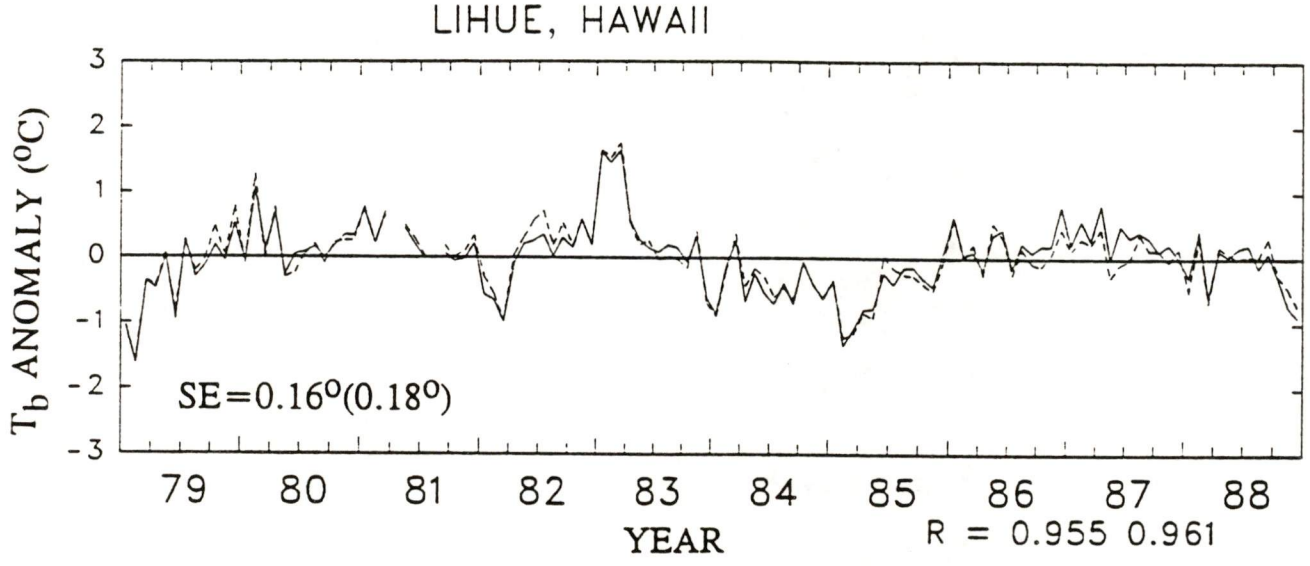

.4
.5
.6
.7
.8
.9
1.0
0.0
0.5
1.0
THICKNESS LAYER (kPa)
100-10
100-15
100-20
100-25
100-30
100-40
100-50
100-70
OAKLAND
best possible
MSU Ch. 2
CORRELATION
STANDARD ERROR (°C)

Fig. 7


LIHUE, HAWAII
T_b ANOMALY (°C)
3
2
1
0
-1
-2
-3
SE=0.16°(0.18°)
79
80
81
82
83
84
85
86
87
88
YEAR
R = 0.955 0.961

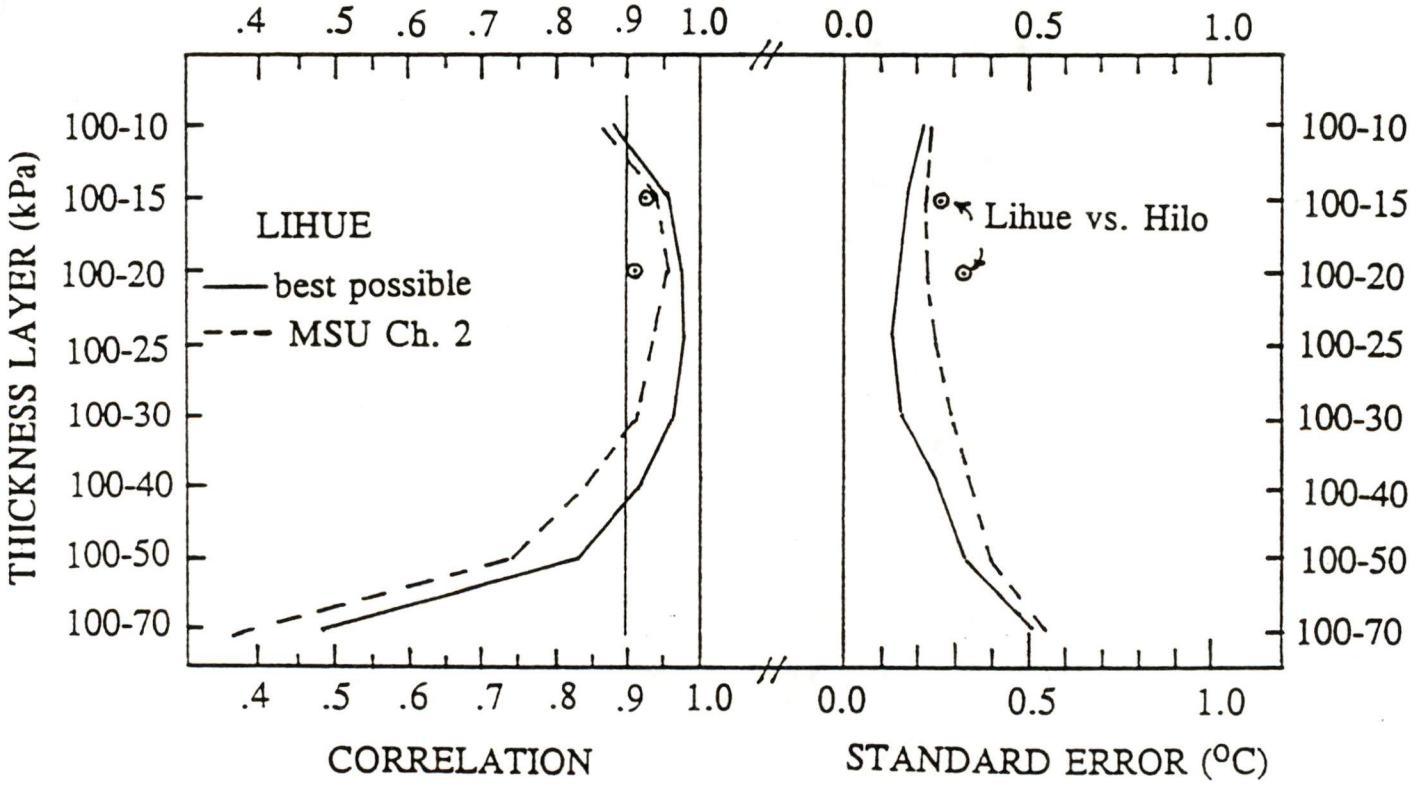

.4
.5
.6
.7
.8
.9
1.0
0.0
0.5
1.0
THICKNESS LAYER (kPa)
100-10
100-15
100-20
100-25
100-30
100-40
100-50
100-70
LIHUE
best possible
MSU Ch. 2
Lihue vs. Hilo
CORRELATION
STANDARD ERROR (°C)

Fig. 8

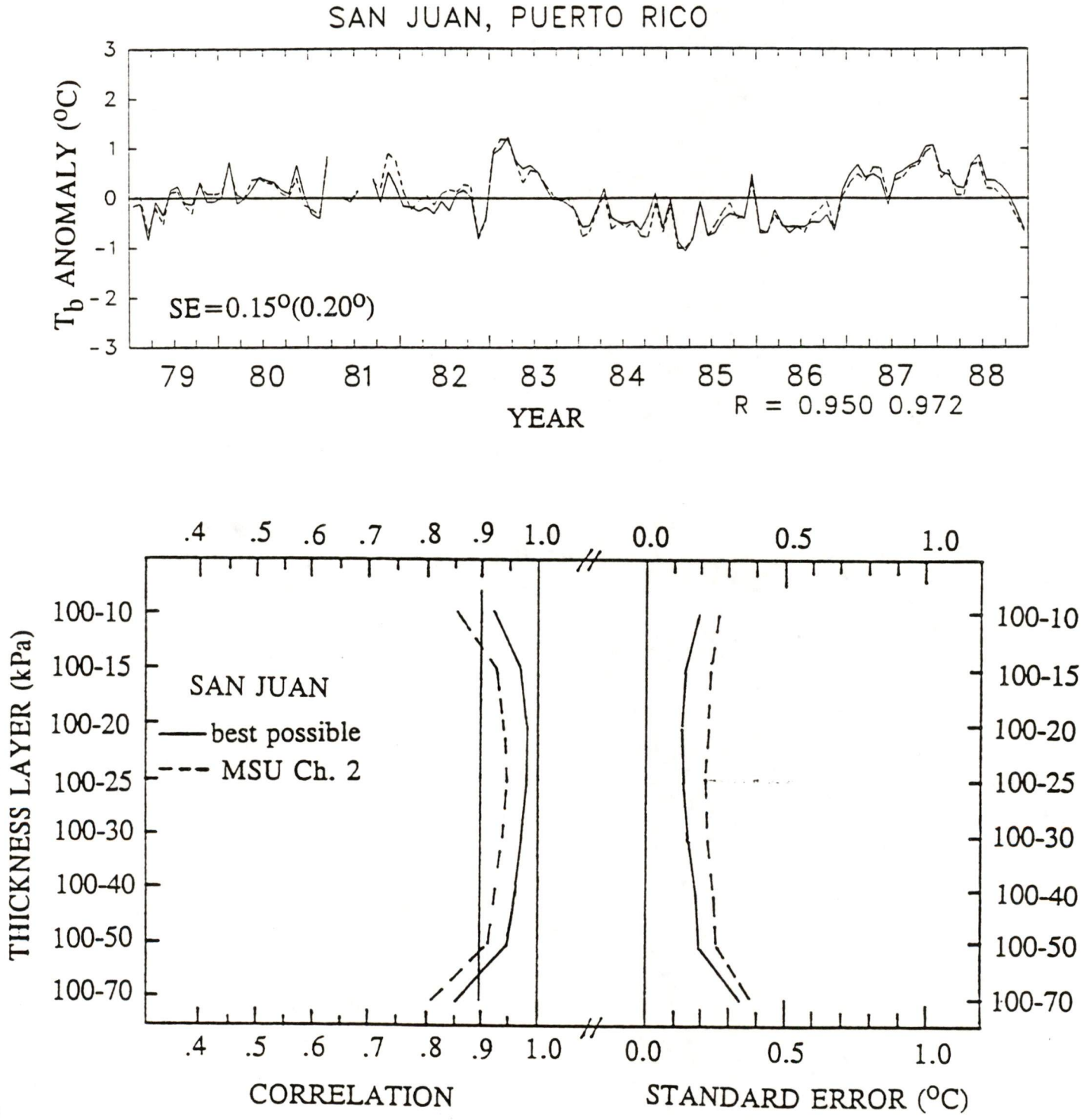

SAN JUAN, PUERTO RICO
T_b ANOMALY (°C)
3
2
1
0
-1
-2
-3
SE=0.15°(0.20°)
79
80
81
82
83
84
85
86
87
88
YEAR
R = 0.950 0.972
.4
.5
.6
.7
.8
.9
1.0
0.0
0.5
1.0
THICKNESS LAYER (kPa)
100-10
100-15
100-20
100-25
100-30
100-40
100-50
100-70
SAN JUAN
best possible
MSU Ch. 2
CORRELATION
STANDARD ERROR (°C)

Fig. 9

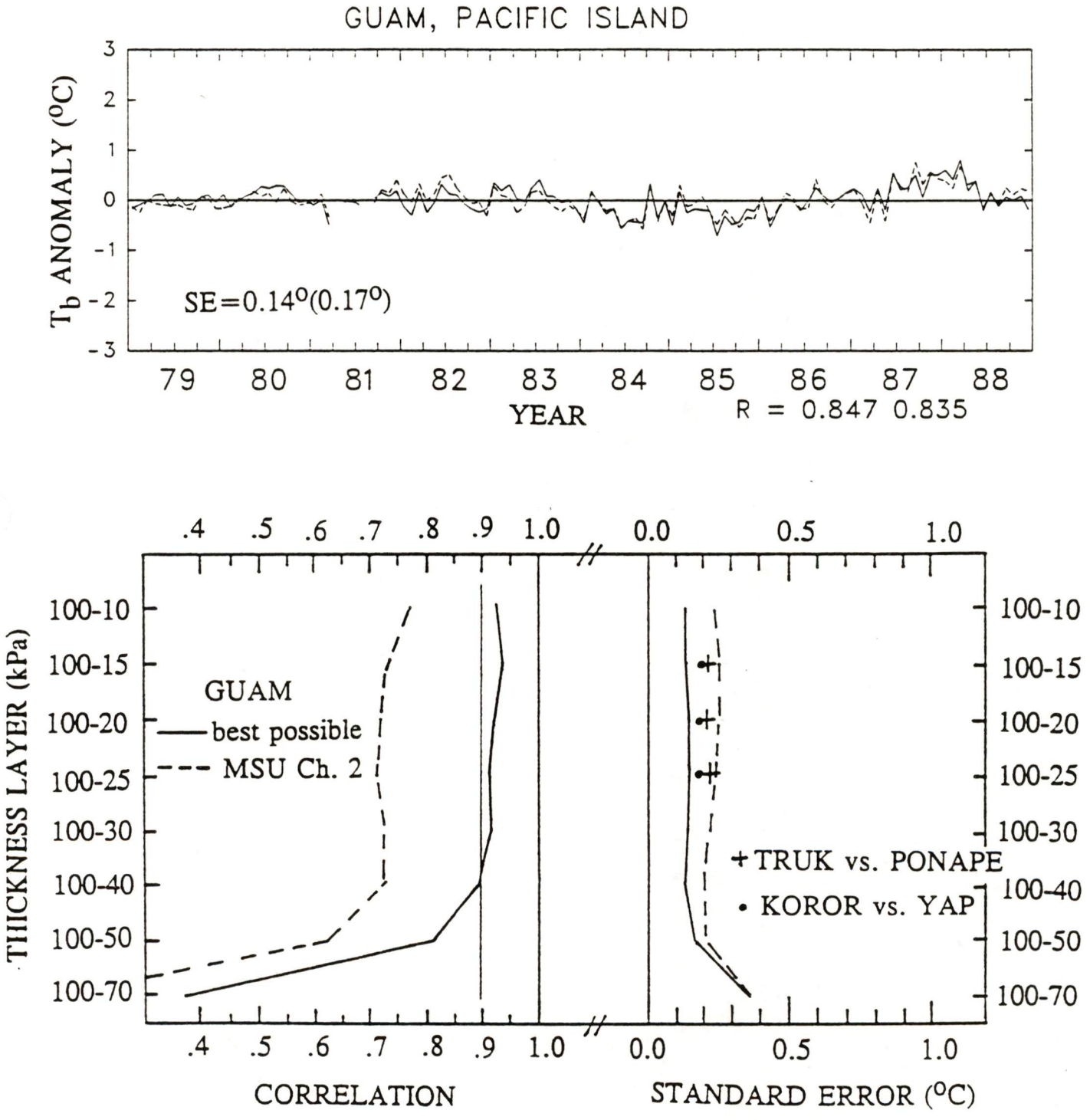

GUAM, PACIFIC ISLAND
T_b ANOMALY (°C)
3
2
1
0
-1
-2
-3
SE=0.14°(0.17°)
79
80
81
82
83
84
85
86
87
88
YEAR
R = 0.847 0.835
.4
.5
.6
.7
.8
.9
1.0
0.0
0.5
1.0
THICKNESS LAYER (kPa)
100-10
100-15
100-20
100-25
100-30
100-40
100-50
100-70
GUAM
best possible
MSU Ch. 2
+ TRUK vs. PONAPE
• KOROR vs. YAP
CORRELATION
STANDARD ERROR (°C)

Fig. 10


TIROSN
NOAA-6
NOAA-7
NOAA-8 X
NOAA-9
NOAA-10
NOAA-11
1979
1980
1981
1982
1983
1984
1985
1986
1987
1988
1989
1990
YEAR

Fig. A1

Precision and Radiosonde Validation of Satellite Gridpoint Temperature Anomalies, Part II: A Tropospheric Retrieval and Trends during 1979-90

by

Roy W. Spencer

ES43 Earth Science and Applications Division

NASA Marshall Space Flight Center

Alabama 35812

John R. Christy

Johnson Research Center

University of Alabama in Huntsville

Huntsville, Alabama 35899

submitted to

Journal of Climate

April 1991

ABSTRACT

TIROS-N satellite Microwave Sounding Unit (MSU) channel 2 data from different view angles across the MSU scan swath are combined to remove the influence of the lower stratosphere and much of the upper troposphere on the measured brightness temperatures. The retrieval provides a sharper averaging kernel than the raw channel 2 weighting function, with a peak lowered from 50 kPa to 70 kPa and with only slightly more surface influence than raw channel 2. Monthly 2.5° gridpoint anomalies of this tropospheric retrieval compared between simultaneously operating satellites indicates close agreement. The agreement is not as close as with raw channel 2 anomalies because synoptic scale temperature gradients across the 2000 km swath of the MSU are averaged out in the retrieval procedure, and because the retrieval involves the magnification of a small difference between two large numbers. Single gridpoint monthly anomaly correlations between the satellite measurements and the radiosonde calculations range from around 0.95 at high latitudes to below 0.8 in the tropical west Pacific, with standard errors of estimate of 0.16°C at Guam to around 0.50°C at high latitude continental stations. Calculation of radiosonde temperatures with a static weighting function instead of the radiative transfer equation degrades the standard errors by an average of less than 0.04°C. Of various standard tropospheric layers, the channel 2 retrieval anomalies correlate best with radiosonde 100-50 or 100-40 kPa thickness anomalies. A comparison between global and hemispheric anomalies computed for raw channel 2 data versus the tropospheric retrieval show a correction in the 1979-1990 time series for the stratospheric warming of 1982-83, which was independently observed by MSU channel 4. This correction leads to a slightly greater tropospheric warming trend in the twelve year time series (1979-1990) for the tropospheric retrieval (+0.048°C/decade) than for channel 2 alone (+0.015° C/decade).

1. Background

In Part I we showed the excellent agreement between separate TIROS-N satellites when independently measuring monthly anomalies of MSU channel 2 T_b at the 2.5° gridpoint level. The average gridpoint agreement between satellites was better than 0.1°C over the tropical oceans, and better than 0.2°C virtually everywhere else on the Earth. This level of agreement was shown to be at least as good as adjacent tropical oceanic radiosonde stations provide. When the satellite measurements were compared to radiosonde measurements of ten years of monthly anomalies, nearly as good agreement was found with many correlations over 0.95 and standard errors of estimate of 0.15°C in the tropics to 0.25°C at high latitudes. In terms of conventionally measured atmospheric layers, the channel 2 anomalies correlated best with 100-15 kPa thickness anomalies. Decadal trends in both the satellite and radiosonde time series showed no significant trend in their difference, indicating stability of MSU channel 2 long-term monitoring.

However, the possibility of cooling in the lower stratosphere coupled with significant energy being received from above this level by MSU channel 2 (Fig. 1), suggests that MSU channel 2 trends and anomalies might not accurately reflect temperature trends in the lower and middle troposphere. Examination of ten year radiosonde temperature trends for different layers of the atmosphere (Table 1) reveals that different trends can be experienced depending upon the layer in question, even within the troposphere. Most of these regions, with the exception of the tropical Pacific, experienced considerable difference in trends above versus below the 30 kPa level. Note also that these ten-year trends are quite variable from region to region, making the lack of radiosonde data in remote regions a significant source of uncertainty in monitoring "global" temperature trends with radiosonde data. These differences suggest the need to remove as much of the upper troposphere and lower stratosphere as possible from the satellite measurements if maximum utility of the satel-

lite is to be made for monitoring a single layer which is expected to behave more uniformly (e.g. the lower and middle troposphere).

We can examine the global temperature variability in the lower stratosphere during the period 1979-90 by applying the same procedures outlined in Part I of this study to MSU channel 4. All inter-satellite statistics on monthly agreement and long-term stability of MSU channel 4 (not shown) are even better than those reported for channel 2 in Part I, making channel 4 a superb resource for monitoring global lower stratospheric temperature trends. When we compute the channel 4 temperature anomalies for the period 1979-90 (Fig. 2) we find a relatively intense warm event during 1982-83. This appears to be superimposed upon an average cooling trend, although this cooling appears to have leveled off since 1985. The 1982-83 warming is generally attributed to solar heating of volcanic dust injected into the stratosphere by El Chichon volcano in early 1982 and by an equatorial African volcano in December 1981. This warm event happened to occur during the tropospheric El Nino Southern Oscillation (ENSO) warm event as seen by MSU channel 2 (also in Fig. 2). Since MSU channel 2 was viewing the tropospheric warmth "through" the stratospheric warmth, to the extent that the MSU channel 2 and 4 weighting functions in Fig. 1 overlap, the channel 2 warming might be partially due to the stratospheric event. We say "might be" because it is not proven that the warming seen by either channel 2 or 4 was contributed to by the overlap region of the weighting functions (although this would seem unlikely). Correction for any stratospheric influence would be increasingly important at high latitudes where the base of the stratosphere is much lower than in the tropics.

Fortunately, it is possible to combine MSU channel 2 data from various view angles in such a way as to cancel out any stratospheric contribution, and achieve a vertical weighting distribution which is sharper than a single channel can offer. Here we describe a method for removing most of the stratospheric influence on channel 2 based upon the differencing of MSU channel 2

near-nadir and limb measurements through the "averaging kernel" concept. This concept was originally described in the context of atmospheric temperature retrievals by Conrath (1972), where weighting functions can be linearly combined to achieve different vertical distributions of weighting. This is the fundamental basis for any satellite temperature retrieval procedures, and is in effect a deconvolution of overlapping weighting functions. This technique was discussed more recently by Grody (1980). Also, updated tropospheric time series of both channel 2 and the tropospheric retrieval are presented for the period 1979-90.

2. Multi-Angular retrievals of deep-layer temperature

a. retrieval philosophy

Retrieval of temperature information from the MSU (or other satellite sounding radiometers) is usually performed for specific pressure levels through various retrieval procedures which in effect deconvolve overlapping weighting functions into a sharper averaging kernel. The retrieval of specific pressure level information has provided conformity with traditional radiosonde measurements, and with numerical weather prediction models which have been tailored to accept radiosonde data. Unfortunately (as discussed in Part I) even though deconvolution of these weighting functions can achieve an averaging kernel which is sharper than the original weighting functions, it is not possible to compress the depth of the deconvolved layer beyond certain limits imposed by the finite number of channels and the existence of noise in those channels. Thus, a retrieval for a specific pressure level will always use information gathered from a relatively deep atmospheric layer. These attempts to retrieve a temperature for a specific pressure level exploit average statistical relationships which naturally exist between temperatures in different atmospheric layers. Because of their assumed time-invariant nature, these average statistical relationships have little use in climate monitoring.

Therefore, we assume at the outset that we wish to retrieve a deep-layer temperature measurement from the satellite (since it is not possible to reduce the thickness of the satellite measured layer beyond certain limits anyway). For climate monitoring this seems preferable since it would be unlikely that different climate trends would exist in adjacent, very thin layers of the troposphere. The individual channel weighting functions can in principle be used by themselves (as we saw in Part I), provided that their vertical weighting distribution is considered useful.

Removal of the stratospheric influence on MSU channel 2 might be accomplished through some deconvolution from MSU channel 3, which has information from the layer whose influence we wish to remove (Fig. 1). Unfortunately, our analysis of twelve years (1979-90) of MSU channel 3 data reveals that one or more MSUs show some sizeable calibration drifts in channel 3, evidenced by a trend in their difference (Fig. 3). While this drift is actually the difference in drifts between the two sensors, we have seen evidence to suggest that it is the NOAA-6 channel 3 which is drifting, which over the period represented in Fig. 3 would amount to 0.3°C. (The step function character of the drift in channel 3 is a result of the removal of a one year annual cycle (1982) which was not detrended. The drift by itself seems to be continuous and linear in time.) This amount of instrumental drift is too large to accept for climate monitoring purposes. Channel 3 drift problems were found for at least one other satellite. We have been unsuccessful in quantifying these drifts either through radiosonde comparisons or satellite intercomparisons. As a consequence of these drift problems, use of MSU channel 3 for any type of long-term climate monitoring should be done with extreme caution.

b. the tropospheric retrieval and its global precision

Fortunately, it turns out that if the goal is the removal of the stratospheric influence on MSU channel 2, then a combination of channel 2 data from different view angles provides better stratospheric canceling than any combination of channels 2 and 3. This is shown in Fig. 4, where the view angles corresponding to

MSU scan positions (#1,2,10,11) and (#3,4,8,9) can be combined with appropriate weighting to yield a new weighting function which removes most of the stratospheric influence, lowers and sharpens the peak of the averaging kernel, and results in only slightly more sensitivity to the surface than even the channel 2 nadir scan position (#6) provides. (SCG addressed the contaminating non-thermometric influence of surface processes on MSU channel 2). The use of eight scan positions was chosen to minimize measurement retrieval noise, which is greater than raw channel 2 noise because the retrieval involves the magnification of small differences between two large numbers. Separate retrievals for the two halves of the swath were attempted, but showed poor results.

This lower tropospheric retrieval (which for brevity we will call channel 2R) wipes out any horizontal temperature gradients across the 2000 km wide MSU swath. This gradient information had been retained in our channel 2 study (Part I) through the limb correction procedure. Thus, we can not expect channel 2R to provide very useful synoptic scale temperature information on short time scales. For our simple linear retrieval, after a ratio of weights is chosen which provides stratospheric canceling of the individual scan angle weighting functions in Fig. 4, the weights can then be adjusted so that their sum equals 1. This results in the retrieval being a brightness temperature, accurate for the averaging kernel distribution of weighting. The small amount of negative area under the channel 2R averaging kernel in Fig. 4, although probably insignificant in comparison to uncertainties in the oxygen absorption theory, would lead to a miniscule warming in the channel 2R T_b if stratospheric cooling occurs, and vice versa.

The same procedures for gridpoint assignment, satellite intercalibration, and anomaly calculation at both the 2.5° gridpoint and zonal levels were used as described for raw channel 2 data in Part I. However, since the full swath of data is required for the retrieval, no limb corrections are applied to the individual MSU scan positions. The channel 2R T_b were assigned

to only the middle three MSU scan position locations. From this point onward all daily gridpoint assignment and interpolation to empty gridsquares, monthly averaging, satellite intercalibration, and annual cycle removal follow the same procedures as were described in Part I for channel 2.

3. Gridpoint Channel 2R Validation

a. satellite intercomparisons

Despite the expected poorer performance of channel 2R for gridpoint comparisons, hemispheric and global averaging of the data again reveals excellent agreement between concurrently operating satellites during overlap periods (Table 2). It can be seen through comparison of this table with Table A1 of Part I that the monthly global signal to noise is is not as good for the tropospheric retrieval anomalies as it is for raw channel 2 anomalies. The standard deviation of the difference between satellites for single-satellite monthly global anomalies is often closer to $0.02^{o}C$ compared to $0.01^{o}C$ for channel 2 anomalies. This is, however, sufficiently good for the multi-month overlap periods to allow accurate intercalibration between satellites for long-term monitoring on at least a global basis. It should be emphasized that when two satellites are operating our final anomaly fields are an average of the two satellites fields, thus further reducing the noise by $2^{0.5}$.

As we did in Part I for channel 2 anomalies, we present a simple example of the precision of the monthly gridpoint retrieval anomalies by computing a difference between February 1983 and February 1982 channel 2R T_b fields (Fig. 5). Again we see that these monthly anomaly patterns measured separately by NOAA-6 and NOAA-7 are very similar, although the similarity is not quite as striking as the channel 2 anomaly fields. Any difference between the two satellites for channel 2R is almost always one of anomaly magnitude, and not of sign. The retrieval anomalies are larger at high latitudes than are the channel 2 anomalies from Fig. 3 of Part I. This is due to both removal of the stratospheric influence (which is usually negatively corre-

lated with tropospheric temperature variations) and to the greater variability of temperature variations at lower tropospheric levels. The tropical retrieval anomaly magnitudes are not, however, greater than the channel 2 anomalies. This is due to both the tropical stratosphere being much higher, and the fact that tropical oceanic temperature anomalies are often slightly weaker in the lower troposphere than they are in the middle troposphere.

A notable exception to the lower troposphere/stronger anomaly rule at high latitudes is seen in the cold anomaly over Western Europe in Fig. 5. Comparison with the corresponding channel 2 cold pattern (Fig. 2 in Part I) reveals that, if anything, the retrieval anomaly is actually weaker than the channel 2 anomaly. The reason for this is seen in an image of the MSU channel 4 (lower stratosphere) difference fields for the February 1983-82 periods (Fig. 5c). Here we find that the channel 2 cold anomaly over Europe was contributed to by a very cold anomaly in the lower stratosphere. The retrieval removed this stratospheric influence, which by itself would have resulted in a weaker channel 2R cold anomaly, but combined with the typically stronger cold anomaly in the lower troposphere, the channel 2R anomaly ended up being not much different from the channel 2 anomaly. This gives empirical evidence that stratospheric effects are indeed being removed by the retrieval.

b. single-station radiosonde comparisons

The monthly gridpoint channel 2R anomalies were compared to radiosonde data with the same three methods used for the channel 2 anomalies in Part I. Radiosonde computations of channel 2R were performed with (1) the radiative transfer equation, and (2) a constant (standard atmosphere) weighting profile (Fig. 4) in combination with Eq. 2 from Part I. A third method involved comparisons to standard pressure level thicknesses. As in Part I, we computed thickness anomalies for all combinations of layers having bases at either 100 or 85 kPa, and tops ranging from 70 to 10 kPa. Consistent with Part I, we present comparisons between channel 2R and the radiosonde channel 2R and thickness tempera-

ture anomalies at Cold Bay, Alaska (Fig. 6); St. Cloud, Minnesota (Fig. 7); Oakland, California (Fig. 8); Lihue, Hawaii (Fig. 9); San Juan, Puerto Rico (Fig. 10); and Guam (Fig. 11).

At Cold Bay (Fig. 6), we find a monthly correlation of 0.94 and SE=0.50°C between the MSU measured anomalies and the radiosonde anomalies calculated with the radiative transfer equation. When the static weighting method is applied to the radiosonde temperature profile, the SE degrades by only 0.02°C to 0.52°C. When compared to the standard layers measured by radiosondes, the layers starting at 100 kPa, rather than 85 kPa, had the best correlations with the MSU. This is to be expected from the weighting profile shown in Fig. 4. For Cold Bay, as well as all other stations, we find that the best correlations to the retrieval exist with either the 100-50 kPa or 100-40 kPa layers.

At St. Cloud, Minnesota (Fig. 7) R=0.97 and SE=0.48°C, results which are similar to Cold Bay, Alaska. The static weighting method resulted in only 0.01°C degradation in the standard error. The 100-40 kPa layer had the best correlation of all conventionally measured radiosonde layers, with R=0.95 and SE=0.54°C.

At Oakland, California (Fig. 8) R=0.91 and SE=0.54°C. Use of the static weighting function method leads to SE=0.58°C. Highest correlation with a standard layer is the 100-50 kPa layer with R=0.91 and SE=0.70°C.

In Lihue, Hawaii (Fig. 9) R=0.89 and SE=0.25°C. Use of the static weighting function yields SE=0.32°C. Highest correlation with a standard radiosonde layer is 0.88 and SE=0.31°C.

At San Juan, Puerto Rico (Fig. 10) R=0.84 and SE=0.29°C. Slight degradation to SE=0.33°C is seen when the standard atmosphere weighting function is applied to the radiosonde temperature profile. Correlation to the 100-40 kPa thickness anomalies is 0.84 also, with SE=0.35°C.

The worst correlations are seen for Guam (Fig. 11, R=0.74), but as was the case for the channel 2 comparisons, this is because the monthly anomaly signal is so small that it approaches

the noise of the radiosonde and satellite systems. In fact, the correlation with the satellite is about the same as between adjacent tropical radiosonde stations for the 100-40 kPa layer (0.76), while the standard error of estimate the satellite provides (0.16°C) is at the limit of the radiosondes ability to measure monthly anomalies anyway, as discussed in Part I. Use of the static weighting function method gives SE=0.20°C. The layer of highest correlation is 100-40 kPa with R=0.66 and SE=0.21°C.

c. composite station radiosonde comparisons

As was done for channel 2 in Part I, we computed statistics for radiosonde station grouping from several regions (Table 2). We find that these station grouping improve the levels of agreement considerably, with standard errors ranging from 0.11° over the tropical west Pacific to around 0.35°C at high latitudes and correlations sometimes exceeding 0.95 at high latitudes. These results suggest that, while individual gridpoint satellite data are good, the full 10,000 gridpoint dataset should allow low-noise estimates of global temperature anomalies even on a monthly time scale.

4. Retrieved Tropospheric Trends 1979-90

The good quality of the channel 2R gridpoint anomalies, combined with the small (0.02°C) monthly disagreement between simultaneously operating satellites (Table 1) suggests that hemispheric and global temperature trends in the lower half of the tropospheric can be monitored with this retrieval. The tropospheric retrieval temperature anomalies for 1979-90 are shown in Fig. 12 superimposed upon the channel 2 anomalies. The largest difference between channels 2 and 2R is seen in 1982-83, where the stratospheric warm event's influence has now been removed. Other differences can also be seen throughout the time series which, since apparently not stratospheric adjustments, probably indicate variations in globally-averaged tropospheric stability. That most of these differences between channel 2 and 2R are real

is supported by their large magnitude (0.1°C - 0.2°C) relative to the monthly level of channel 2R disagreement between simultaneously operating satellites in Table 1 (0.01° to 0.02°C).

Of some importance is the finding that the long-term trend of the data is somewhat warmer for the retrieval time series (+0.032°C) than it is for the raw channel 2 time series (+0.015°C). This was a combination of a Northern Hemisphere trend of +0.058.°C, and a Southern Hemisphere trend of -0.026°C. The removal of the stratospheric influence on MSU channel 2 during 1982-83 is probably the major reason for the difference in long-term trends between channel 2 and 2R since it occurred in the first half of the twelve year record.

5. Conclusions

A procedure for removal of the stratospheric influence on MSU channel 2 for more useful long-term tropospheric temperature monitoring has been applied to MSU channel 2 data from 1979-90, and tested with radiosonde data during 1979-88. Single gridpoint comparisons with individual radiosonde stations give correlations ranging from 0.97 (SE=0.48°C) at St. Cloud, Minnesota where the monthly tropospheric temperature anomaly signal is strong, to 0.74 (SE=0.16°C) at Guam where the signal is very weak compared to the limiting accuracy of both the radiosonde and satellite systems. Groupings of stations improve the standard errors to 0.11°C over the west Pacific to SE=0.35°C at high latitudes, with correlations ranging from 0.83 to 0.98, respectively. As was the case for the channel 2 results in Part I, the tropical standard errors reach the levels of agreement displayed by adjacent radiosonde stations. Best agreement with standard layers which radiosondes traditionally measure is with either 100-50 or 100-40 kPa layer anomalies.

For tropospheric temperature trends, the tropospheric retrieval shows some differences with raw channel 2 data, particularly during 1982-83 when stratospheric warming exaggerated the MSU channel 2 warm signal of the 1982-83 ENSO event. Other differences between channel 2 and 2R variations are probably re-

lated to variations in tropospheric stability. The satellite record trends for the retrieval differ from the channel 2 trends by only 0.01°C, with a tropospheric retrieval trend of +0.032°/decade and a channel 2 trend of +0.015°C/decade for the period 1979-90.

6. References

Conrath, B.J., 1972: Vertical resolution of temperature profiles obtained from remote radiation measurements. *J. Atmos. Sci.*, **29**, 1262-1271.

Grody, N.C., 1980: Analysis of satellite-based microwave retrievals of temperature and thermal winds: Effects of channel selection and a-priori mean on retrieval accuracy. *Remote Sensing of the Atmosphere and Oceans*, A. Deepak, Ed., Academic Press, 381-410.

Spencer, R.W. and J.R. Christy, 1990: Precise monitoring of global temperature trends from satellites. *Science*, **247**, 1558-1562.

Spencer, R.W., J.R. Christy, and N.C. Grody, 1990: Global atmospheric temperature monitoring with satellite microwave measurements: Method and results, 1979-84. *J. Climate.*, **3**, 1111-1128.

Acknowledgments

We thank Norman Grody (NOAA/NESDIS) for helpful advice during this study.

List of Figures

Figure 1. MSU channel 2, 3 and 4 weighting functions for a nadir view through a U.S. Standard Atmosphere.

Figure 2. MSU channel 4 (stratosphere) and channel 2 (troposphere) temperature anomalies during 1979-90, assembled by the method described in the Appendix of Part I. Anomalies have been low-pass filtered.

Figure 3. Time series of globally averaged NOAA-6 and NOAA-7 sums (widely varying line) and differences (slightly varying line) of daily MSU channels 2, 3, and 4 T_b anomalies. Drift in channel 3 is evident in the difference time series.

Figure 4. Scan-angle averaged MSU channel 2 weighting functions for scan positions #1,2,10,11, #3,4,8,9, and a retrieval averaging kernel (channel 2R) computed through a linear combination of functions the other two weighting functions.

Figure 5. Gridpoint MSU channel 2 T_b anomaly differences for February 1983 minus February 1982, as measured separately by (a) NOAA-6, and (b) NOAA-7; and channel 4 anomaly differences measured by NOAA-6.

Figure 6. Time series (a) of MSU channel 2R anomalies and radiosonde-calculated channel 2R anomalies; and correlations and standard errors (b) with radiosonde thickness temperature anomalies for Cold Bay, Alaska during 1979 through 1988. In (a) the solid line is MSU-measured, the dashed line is radiosonde-measured, and the correlations (R) are for the monthly and yearly anomalies, respectively. In (b) the solid line shows the best agreement possible based upon MSU channel 2R T_b being computed

from the radiosonde data, and the dashed line shows the satellite-measured agreement with the radiosonde thickness temperature anomalies.

Figure 7. As in Fig. 6, except St. Cloud, Minnesota.

Figure 8. As in Fig. 6, except Oakland, California.

Figure 9. As in Fig. 6, except Lihue, Hawaii.

Figure 10. As in Fig. 6, except San Juan, Puerto Rico.

Figure 11. As in Fig. 6, except Guam.

Figure 12. MSU channel 2 (thin line) and tropospheric retrieval (thick line) T_b time series for the globe, Northern Hemisphere, and Southern Hemisphere during 1979-90. Series have been low pass filtered.

Table 1. Composited radiosonde layer average temperature trends for the ten year period 1979-88 for different regions.

Layer	Florida[1]	NW U.S.[2]	NE U.S.[3]	Great Lakes[4]	Caribbean[5]	West Pacific[6]
30-15 kPa	-0.48°	-1.28°	-0.53°	-0.92°	-0.29°	+0.14°
50-30 kPa	-0.06°	+1.34°	+0.85°	+1.14°	-0.02°	+0.10°
70-50 kPa	-0.05°	+1.37°	+0.80°	+1.31°	+0.04°	+0.07°
85-70 kPa	0.00°	+1.37°	+0.84°	+1.67°	+0.19°	+0.25°

[1]Apalachicola, Tampa, Miami, Key West
[2]Salem, Oregon; Quillayute, Washington
[3]Caribou, Maine; Chatham, Massachusetts; Buffalo, New York; Albany, New York; Portland, Maine
[4]Flint, Michigan; Peoria, Illinois; Green Bay, Wisconsin; International Falls, Minnesota; St. Cloud, Minnesota; Huron, South Dakota
[5]Christ Church, Barbados; Santo Domingo, Dominican Republic; Piarco, Trinidad; San Juan, Puerto Rico; Curacao, Netherland Antilles
[6]Yap Island; Koror Island; Ponape Island; Truk Island; Majuro Island; Guam; Wake Island

Table 2. Global statistics of all overlaps between MSUs for the channel 2 tropospheric temperature retrieval.

Satellite route to NOAA-6		Overlap Dates	#days	daily error (1 sat/2 sat)	daily S/N	30-day error (1 sat/2 sat)	30-day S/N
TIROS-N	to NOAA-6	7/1/79-1/19/80	156	.093°/.066°	7.0	.024°/.017°	20.4
NOAA-6	BASE						
NOAA-7	to NOAA-6	6/26/81-4/16/83	566	.087°/.061°	8.4	.015°/.011°	124.8
NOAA-9	to NOAA-6	10/30/85-11/4/86	228	.087°/.061°	17.7	.015°/.011°	74.1
NOAA-10	thru NOAA-9	11/26/86-3/7/87	96	.092°/.065°	11.9	.013°/.009°	300.5
NOAA-11	thru NOAA-10	10/23/88-12/31/90	678	.088°/.062°	8.3	.029°/.020°	40.7

Table 3. Station composite correlations and standard errors of satellite versus radiosonde monthly anomalies in channel 2R. Numbers in parentheses are the corresponding single-station values from the stations represented in Figs. 5-10.

Region	R	SE
Alaska(15)	.97(.94)	.31°(.50°)
Great Lakes(6)	.98(.97)	.37°(.48°)
West Coast(4)	.95(.91)	.35°(.54°)
Caribbean(6)	.91(.84)	.16°(.29°)
West Pacific(7)	.83(.74)	.11°(.16°)

Alaska:(15) Anette, Yakutat, Kodiak, King Salmon, Cold Bay, Adak, St. Paul Island, Anchorage, Fairbanks, McGrath, Bethel, Kotzebue, Nome, Barter Island, Barrow. **Great Lakes:**(6) Sault Ste. Marie, MI; International Falls, MN; Green Bay, WI; St. Cloud, MN, Huron, SD. **U.S. West Coast:**(4) Quillayute, WA; Salem, OR; Oakland, CA; San Diego, CA. **Tropical West Pacific:**(7) Koror, Yap, Majuro, Wake, Guam, Truk, Ponape. **Caribbean:**(6) Christ Church, Barbados; Santo Domingo, Dominican Republic; Piarco, Trinidad; San Juan, Puerto Rico; Curacao, Netherland Antilles; Roberts, Cayman Islands

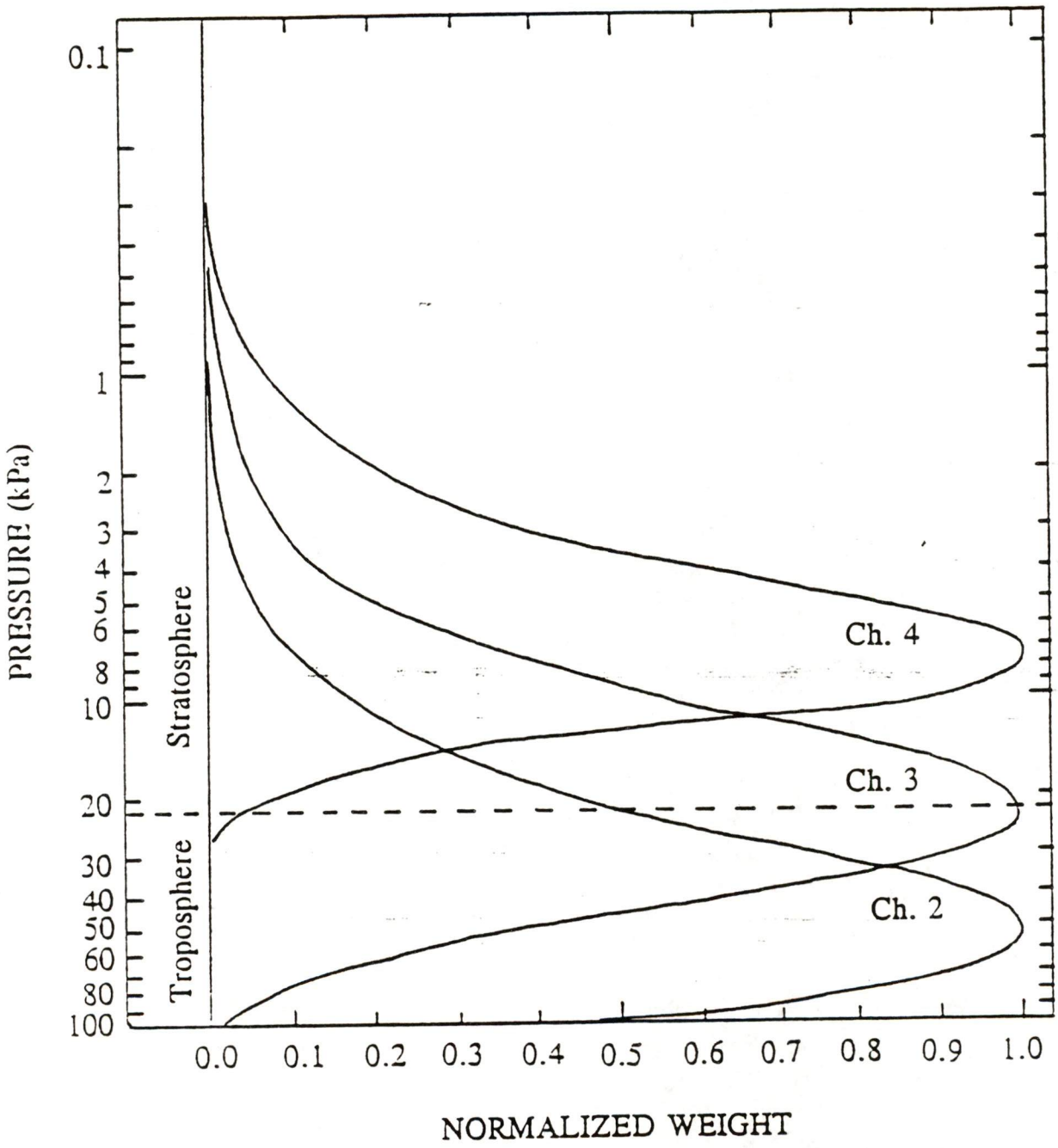

0.1
1
2
3
4
5
6
8
10
20
30
40
50
60
80
100
PRESSURE (kPa)
Stratosphere
Troposphere
Ch. 4
Ch. 3
Ch. 2
0.0
0.1
0.2
0.3
0.4
0.5
0.6
0.7
0.8
0.9
1.0
NORMALIZED WEIGHT

Fig. 1

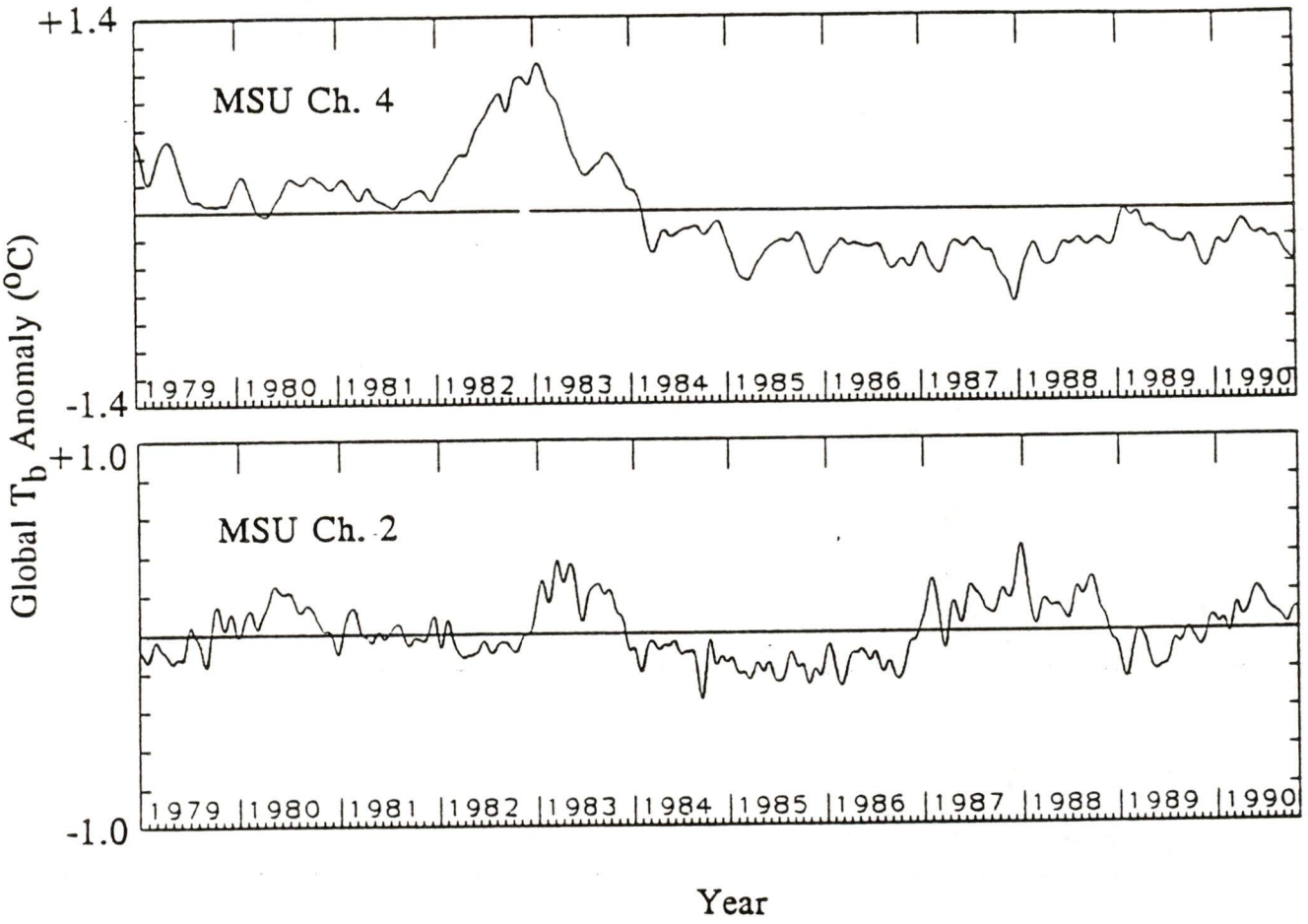

+1.4
MSU Ch. 4
-1.4
1979 1980 1981 1982 1983 1984 1985 1986 1987 1988 1989 1990
+1.0
MSU Ch. 2
-1.0
1979 1980 1981 1982 1983 1984 1985 1986 1987 1988 1989 1990
Global T_b Anomaly (°C)
Year

Fig. 2

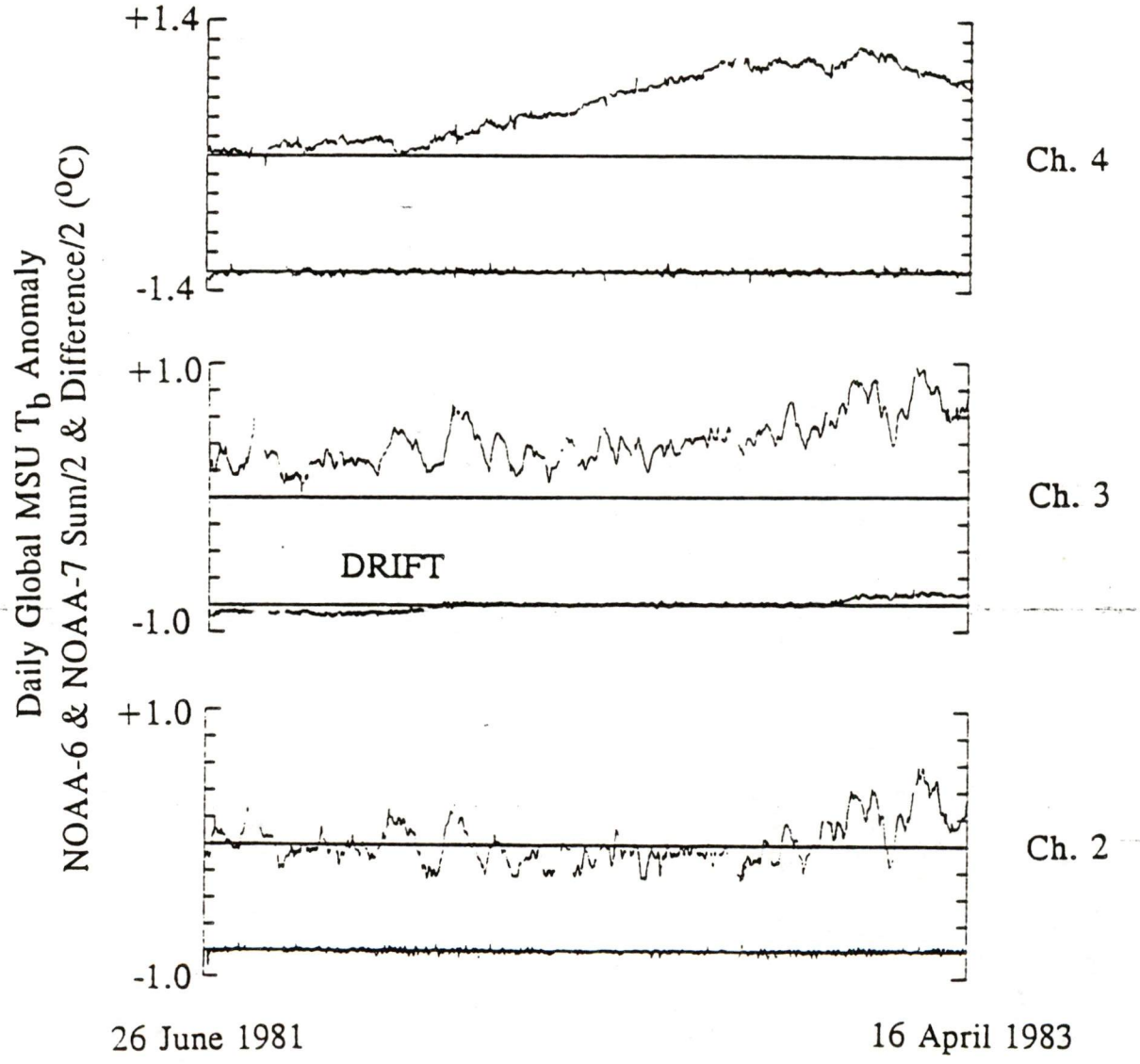

Daily Global MSU T_b Anomaly
NOAA-6 & NOAA-7 Sum/2 & Difference/2 (°C)
+1.4
-1.4
Ch. 4
+1.0
-1.0
Ch. 3
DRIFT
+1.0
-1.0
Ch. 2
26 June 1981
16 April 1983

Fig. 3

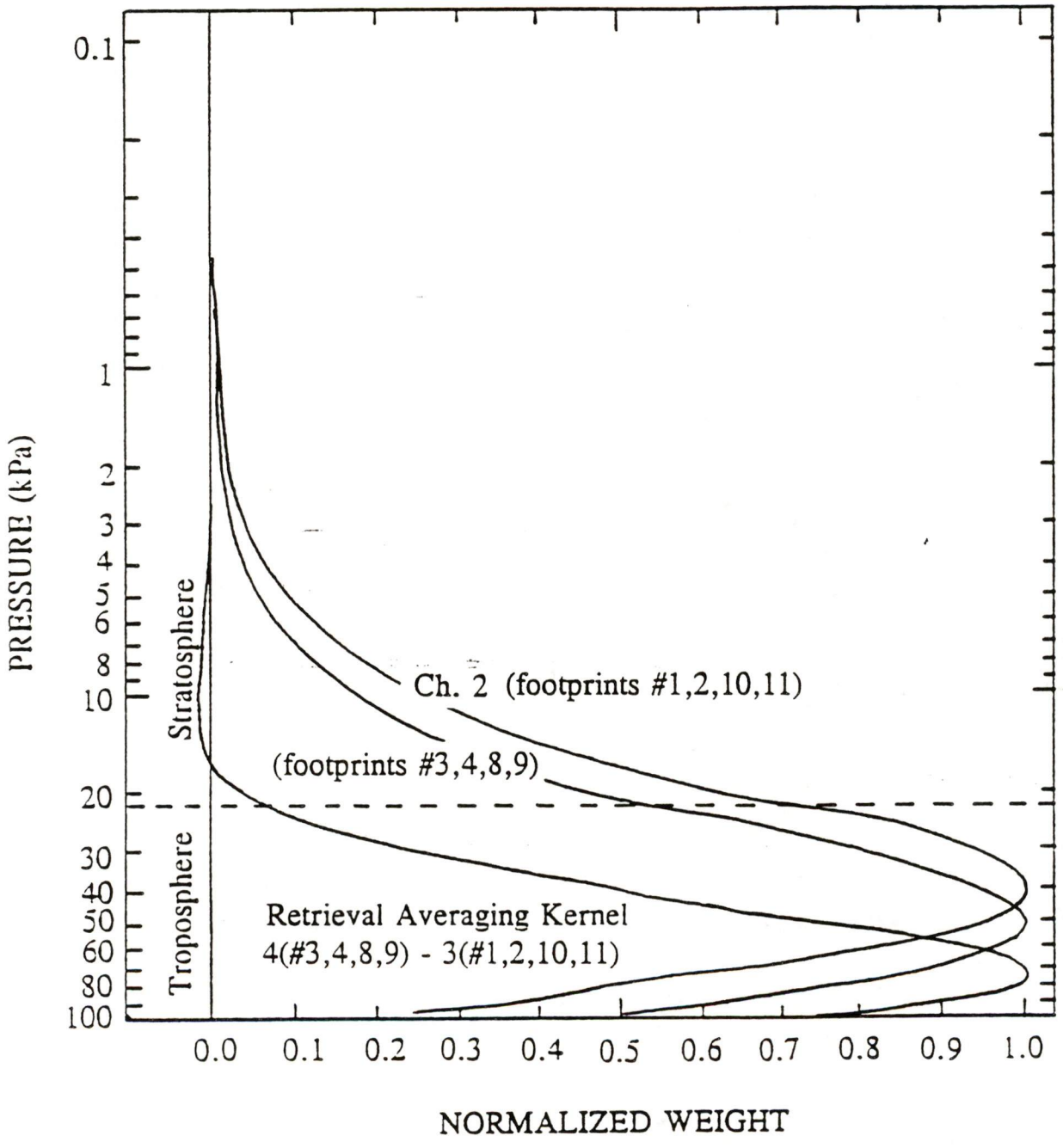

PRESSURE (kPa)
0.1
1
2
3
4
5
6
8
10
20
30
40
50
60
80
100
Stratosphere
Troposphere
Ch. 2 (footprints #1,2,10,11)
(footprints #3,4,8,9)
Retrieval Averaging Kernel
4(#3,4,8,9) - 3(#1,2,10,11)
0.0
0.1
0.2
0.3
0.4
0.5
0.6
0.7
0.8
0.9
1.0
NORMALIZED WEIGHT

Fig. 4

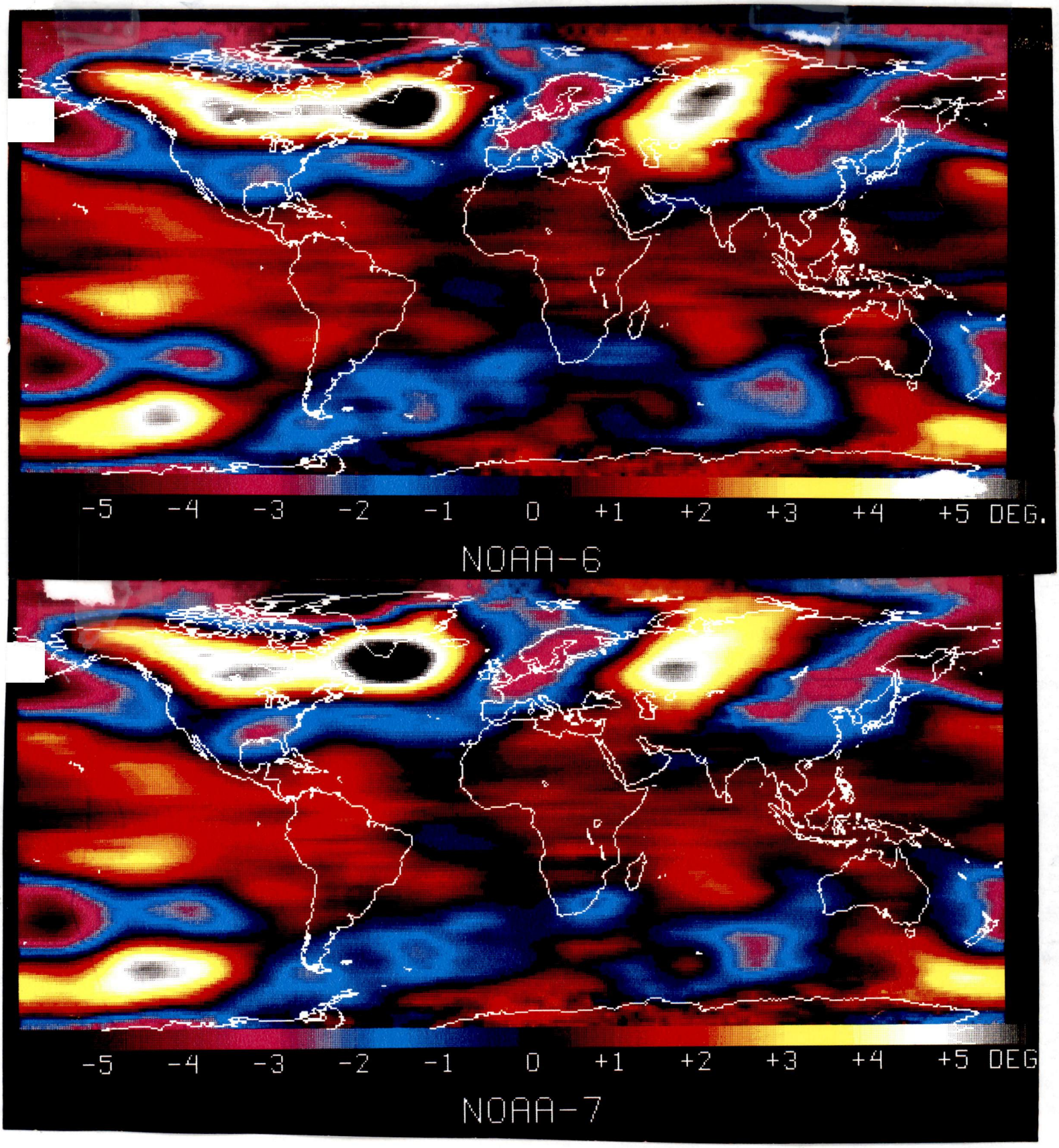
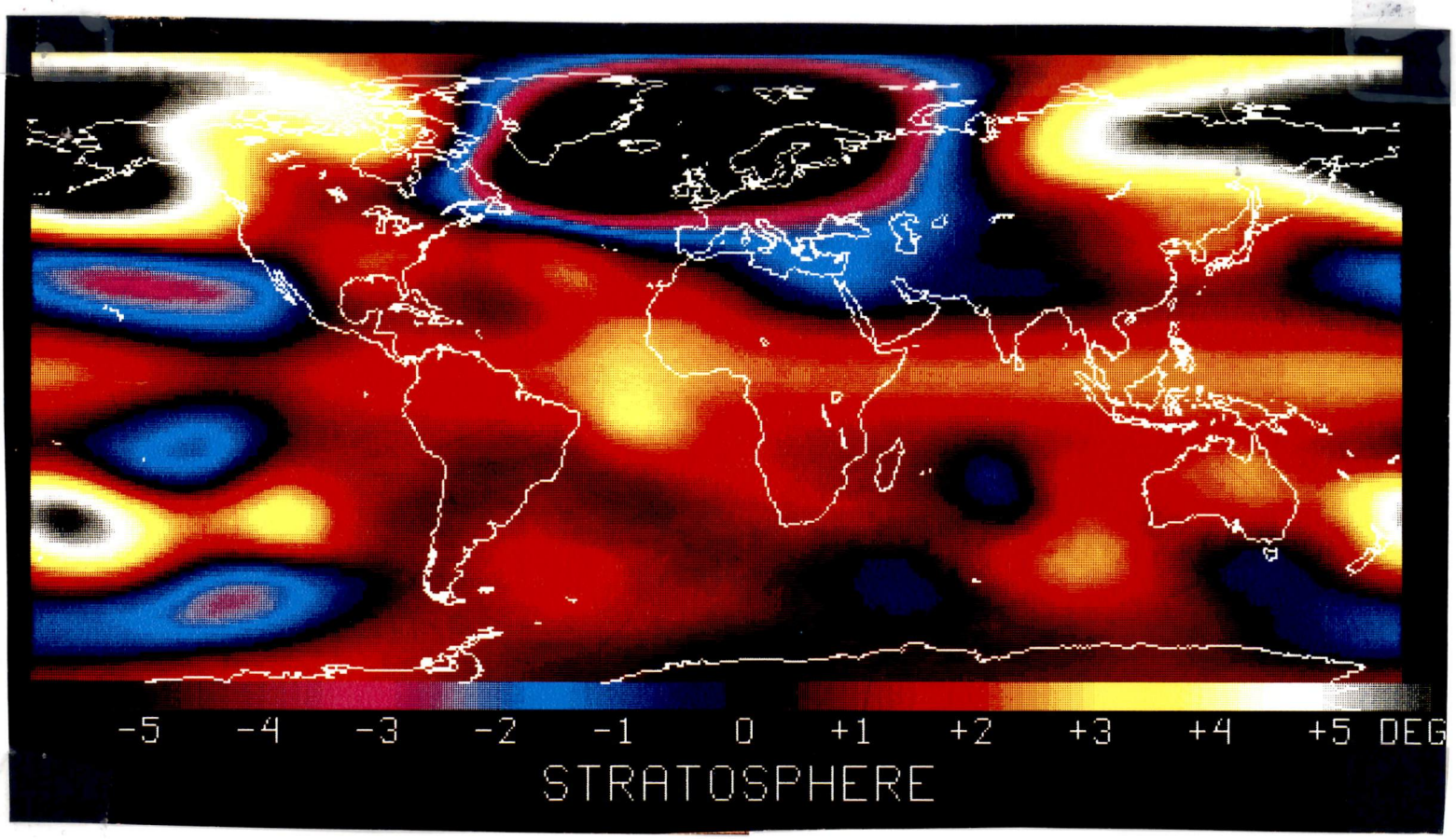
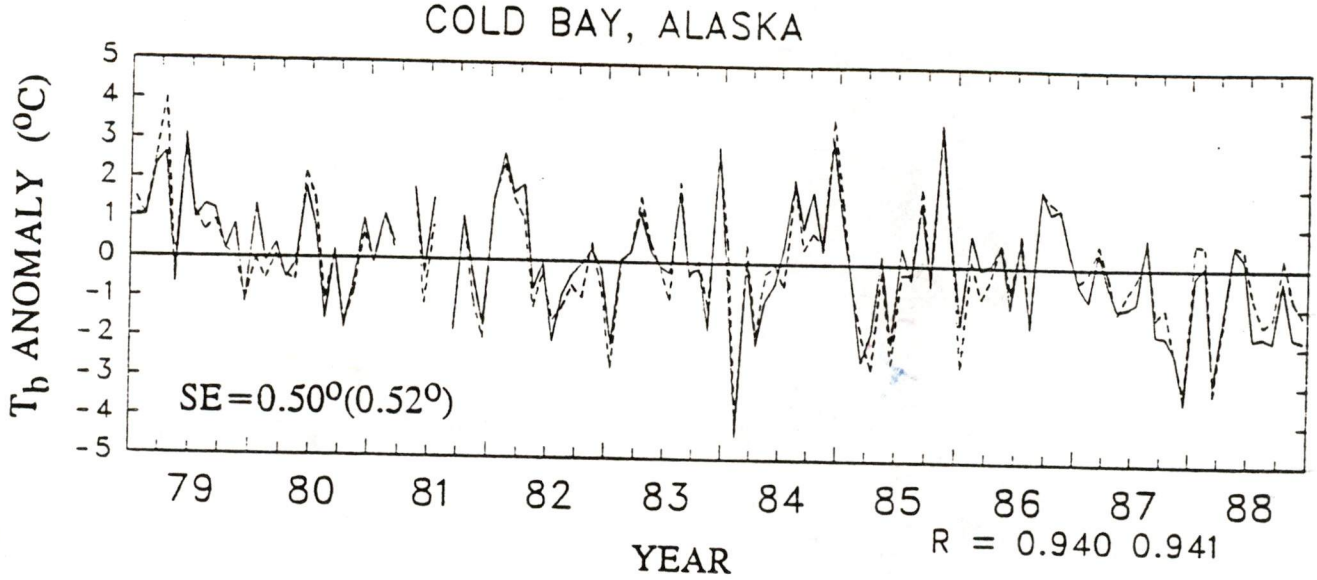


Fig. 5 a,b,c (overlay)


-5 -4 -3 -2 -1 0 +1 +2 +3 +4 +5 DEG
STRATOSPHERE


COLD BAY, ALASKA
T_b ANOMALY (°C)
5
4
3
2
1
0
-1
-2
-3
-4
-5
SE=0.50°(0.52°)
79
80
81
82
83
84
85
86
87
88
YEAR
R = 0.940 0.941

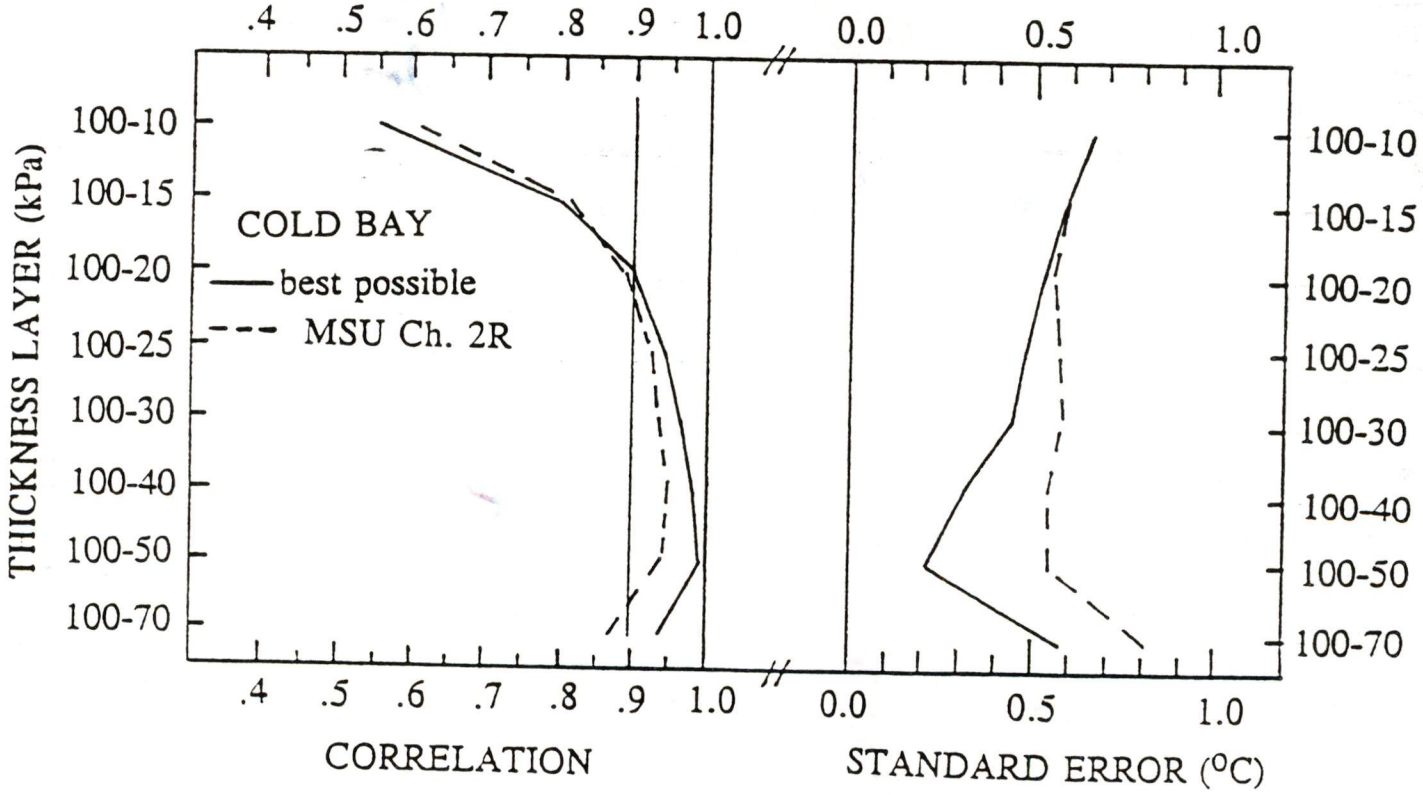

.4
.5
.6
.7
.8
.9
1.0
0.0
0.5
1.0
100-10
100-15
100-20
100-25
100-30
100-40
100-50
100-70
THICKNESS LAYER (kPa)
COLD BAY
best possible
MSU Ch. 2R
CORRELATION
STANDARD ERROR (°C)

Fig. 6

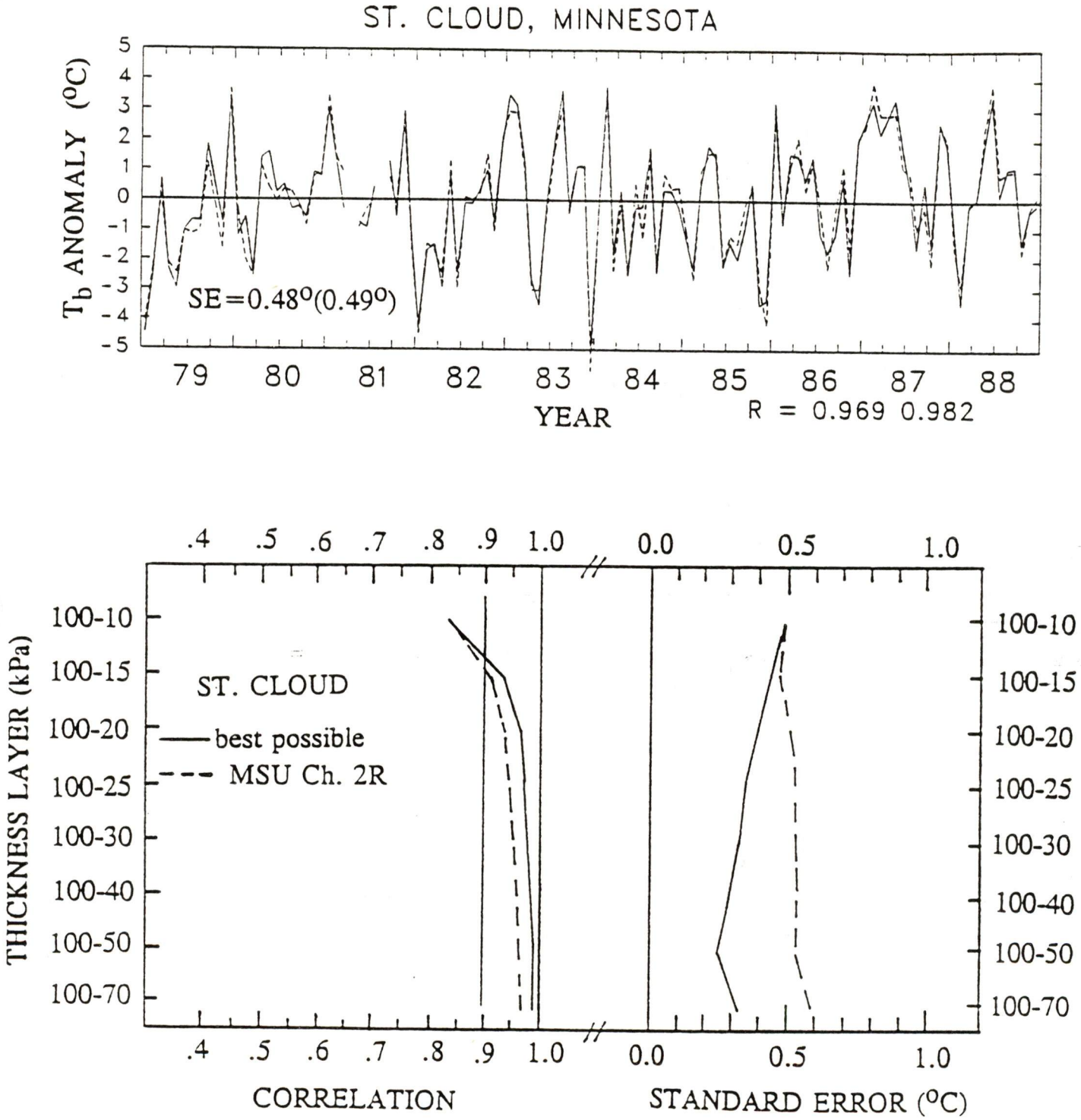

ST. CLOUD, MINNESOTA
T_b ANOMALY (°C)
5
4
3
2
1
0
-1
-2
-3
-4
-5
SE=0.48°(0.49°)
79
80
81
82
83
84
85
86
87
88
YEAR
R = 0.969 0.982
.4
.5
.6
.7
.8
.9
1.0
0.0
0.5
1.0
100-10
100-15
100-20
100-25
100-30
100-40
100-50
100-70
THICKNESS LAYER (kPa)
ST. CLOUD
best possible
MSU Ch. 2R
CORRELATION
STANDARD ERROR (°C)

Fig. 7

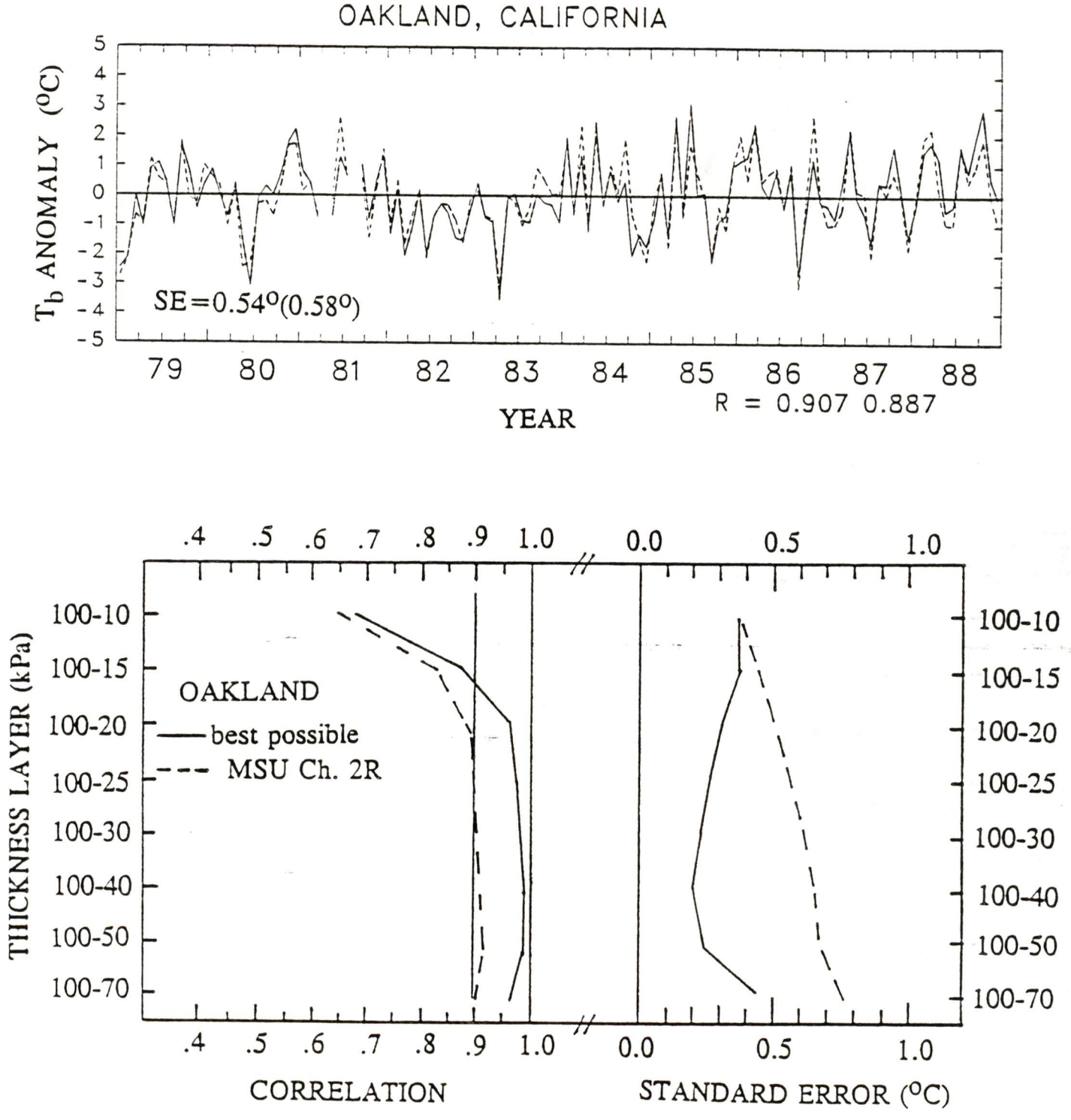
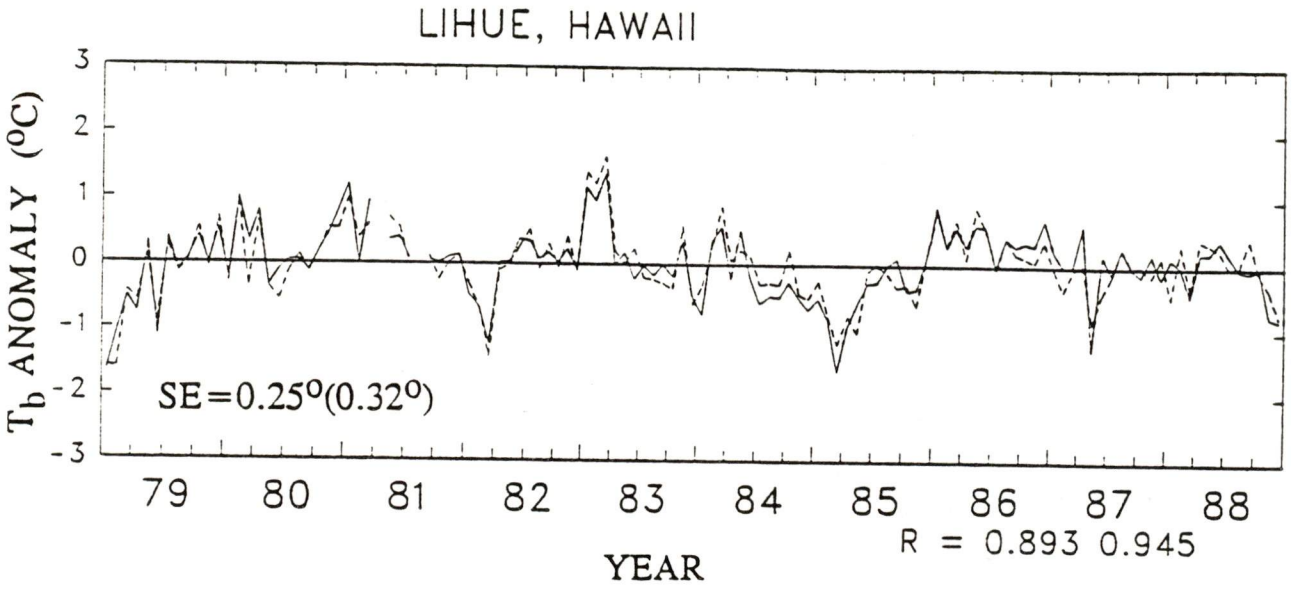

OAKLAND, CALIFORNIA
T_b ANOMALY (°C)
5
4
3
2
1
0
-1
-2
-3
-4
-5
SE=0.54°(0.58°)
79
80
81
82
83
84
85
86
87
88
YEAR
R = 0.907 0.887
.4
.5
.6
.7
.8
.9
1.0
0.0
0.5
1.0
100-10
100-15
100-20
100-25
100-30
100-40
100-50
100-70
THICKNESS LAYER (kPa)
OAKLAND
best possible
MSU Ch. 2R
CORRELATION
STANDARD ERROR (°C)

Fig. 8


LIHUE, HAWAII
T_b ANOMALY (°C)
3
2
1
0
-1
-2
-3
SE=0.25°(0.32°)
79
80
81
82
83
84
85
86
87
88
YEAR
R = 0.893 0.945

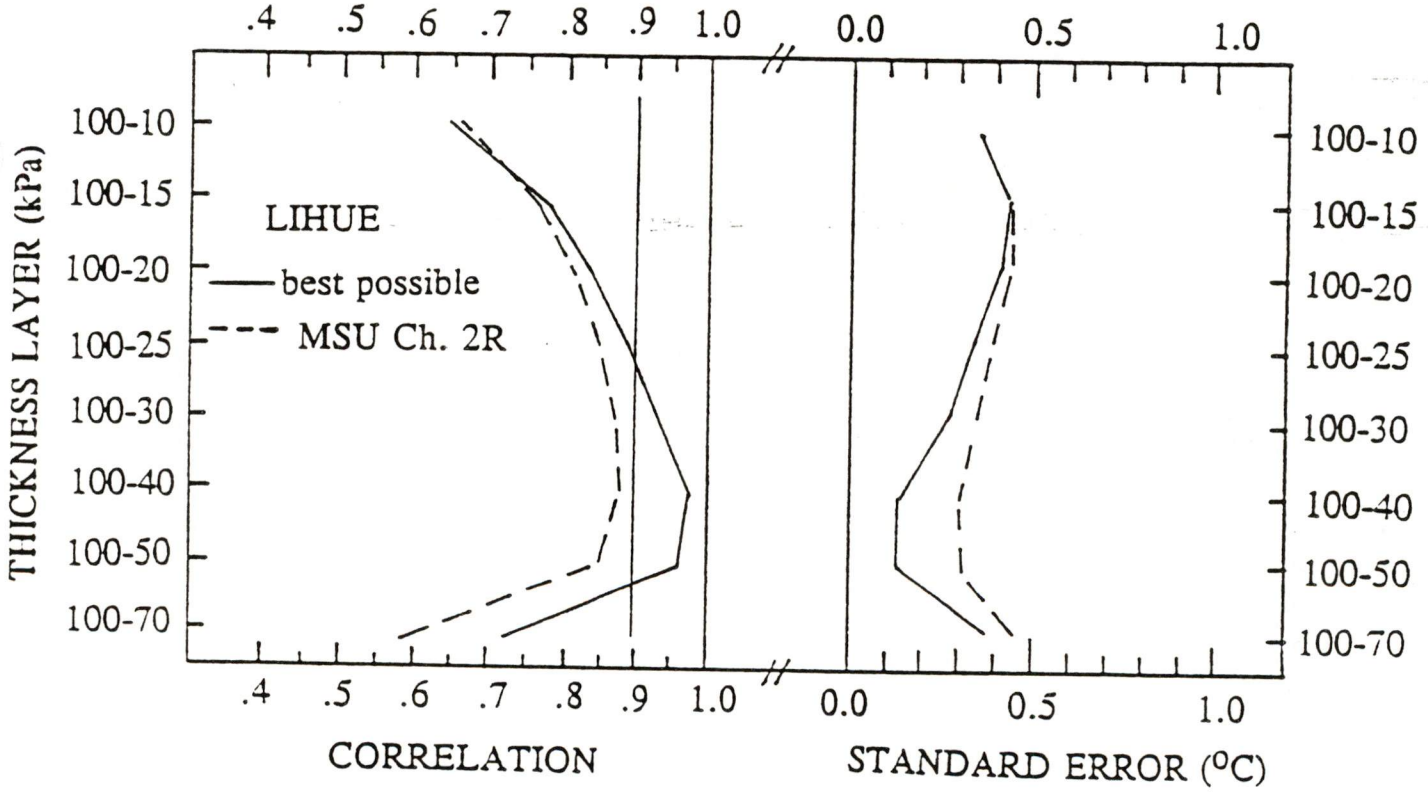

.4
.5
.6
.7
.8
.9
1.0
0.0
0.5
1.0
100-10
100-15
100-20
100-25
100-30
100-40
100-50
100-70
THICKNESS LAYER (kPa)
LIHUE
best possible
MSU Ch. 2R
CORRELATION
STANDARD ERROR (°C)

Fig. 9

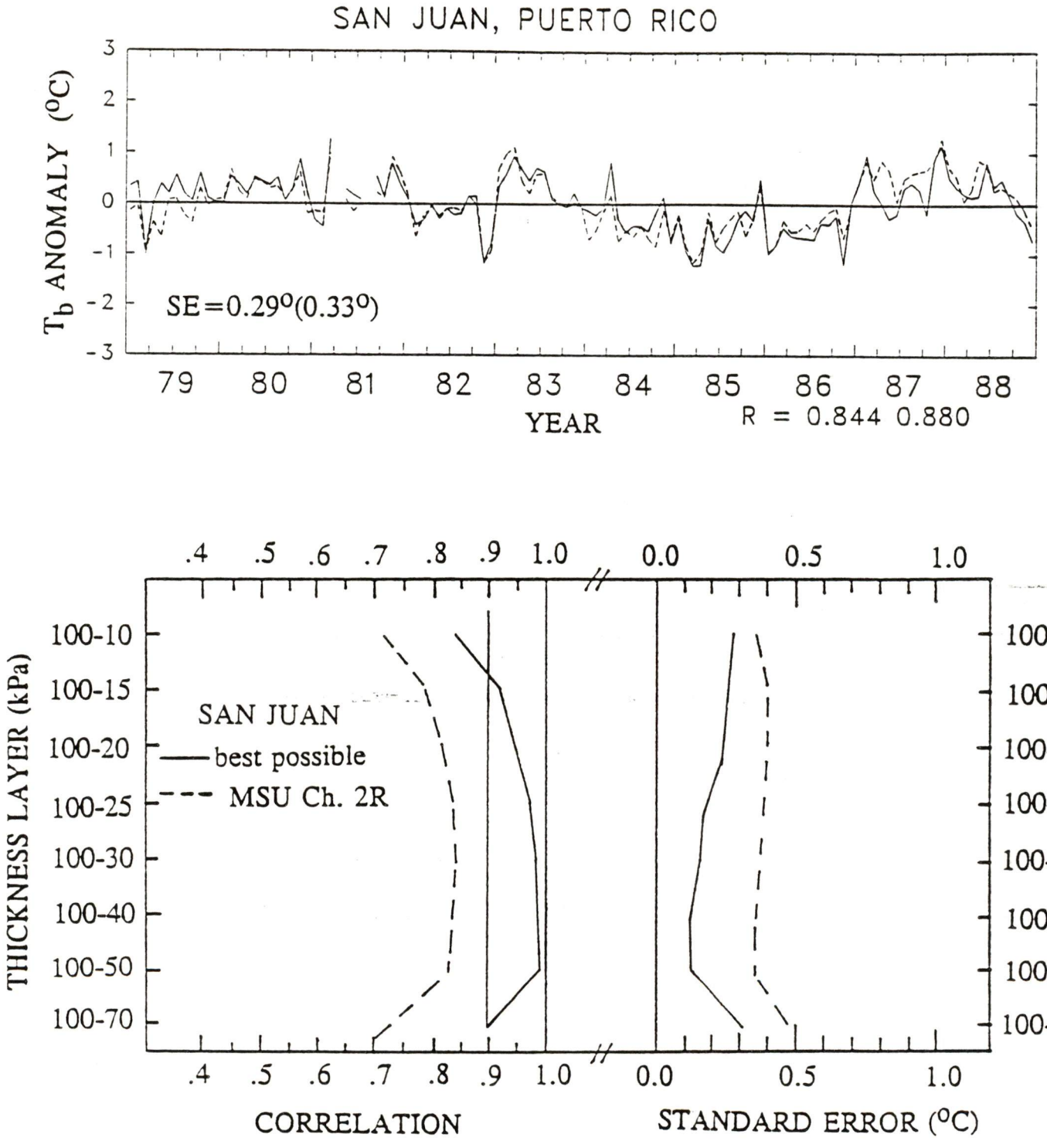

SAN JUAN, PUERTO RICO
T_b ANOMALY (°C)
3
2
1
0
-1
-2
-3
SE=0.29°(0.33°)
79
80
81
82
83
84
85
86
87
88
YEAR
R = 0.844 0.880
.4
.5
.6
.7
.8
.9
1.0
0.0
0.5
1.0
THICKNESS LAYER (kPa)
100-10
100-15
100-20
100-25
100-30
100-40
100-50
100-70
SAN JUAN
best possible
MSU Ch. 2R
CORRELATION
STANDARD ERROR (°C)

Fig. 10

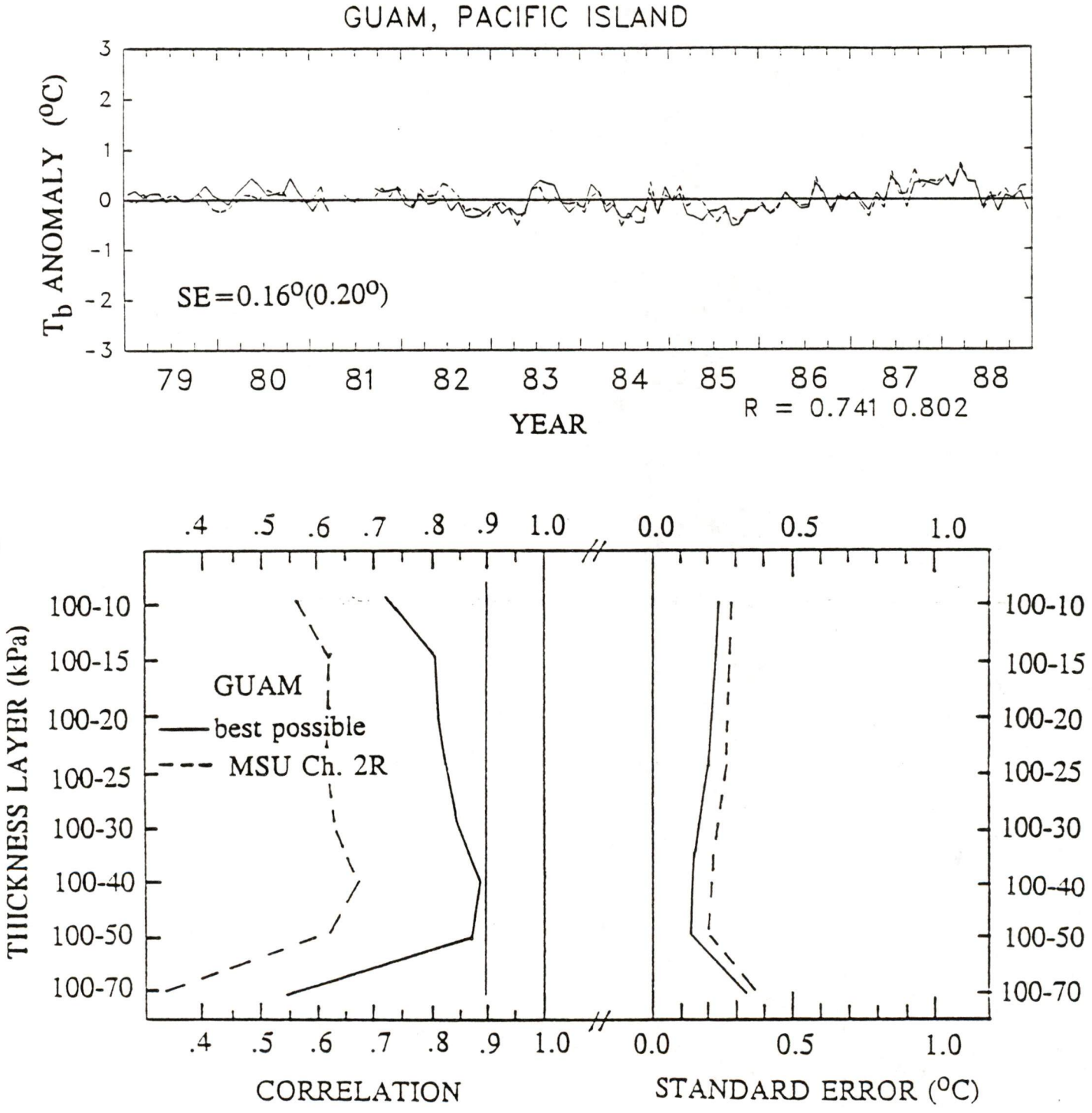

GUAM, PACIFIC ISLAND
T_b ANOMALY (°C)
3
2
1
0
-1
-2
-3
SE=0.16°(0.20°)
79
80
81
82
83
84
85
86
87
88
YEAR
R = 0.741 0.802
.4
.5
.6
.7
.8
.9
1.0
0.0
0.5
1.0
THICKNESS LAYER (kPa)
100-10
100-15
100-20
100-25
100-30
100-40
100-50
100-70
GUAM
best possible
MSU Ch. 2R
CORRELATION
STANDARD ERROR (°C)

Fig. 11

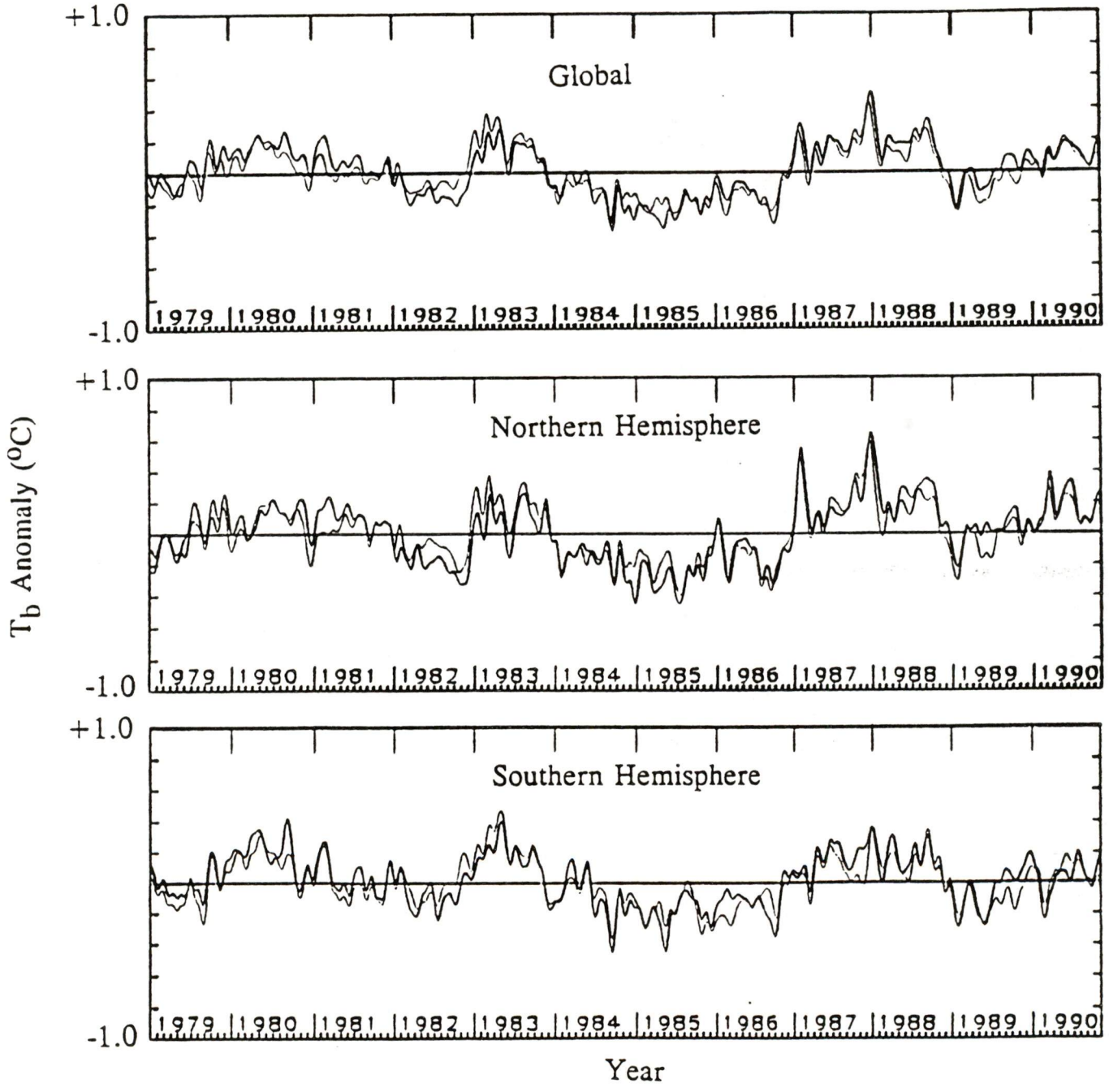

+1.0
Global
-1.0
1979 1980 1981 1982 1983 1984 1985 1986 1987 1988 1989 1990
+1.0
Northern Hemisphere
-1.0
1979 1980 1981 1982 1983 1984 1985 1986 1987 1988 1989 1990
+1.0
Southern Hemisphere
-1.0
1979 1980 1981 1982 1983 1984 1985 1986 1987 1988 1989 1990
T_b Anomaly (°C)
Year

Fig. 12

JUN 07 '91 17:44 CDC ASHVL, NC P.7

Reprinted from Nature, Vol. 347, No. 6289, pp. 169–172, 13th September, 1990

© Macmillan Magazines Ltd., 1990

Assessment of urbanization effects in time series of surface air temperature over land

P. D. Jones*, P. Ya. Groisman†, M. Coughlan‡, N. Plummer‡, W-C. Wang§ & T. R. Karl‖

* Climatic Research Unit, School of Environmental Sciences, University of East Anglia, Norwich NR4 7TJ, UK
† State Hydrological Institute, Leningrad, USSR
‡ Bureau of Meteorology, Melbourne, Australia
§ Atmospheric Sciences Research Center, State University of New York, Albany, New York 12205, USA
‖ National Climate Data Center, Asheville, North Carolina 28801, USA

RECORDS of hemispheric average temperatures from land regions for the past 100 years provide crucial input to the debate over global warming[1–4]. Despite careful use of the basic station data in some of these compilations of hemispheric temperature[1,2,4–6], there have been suggestions[7,8] that a proportion of the 0.5 °C warming seen on a century timescale may be related to urbanization influences—local warming caused by the effects of urban development. We examine here an extensive set of rural-station temperature data for three regions of the world: European parts of the Soviet Union, eastern Australia and eastern China. When combined with similar analyses for the contiguous United States[9,10], the results are representative of 20% of the land area of the Northern Hemisphere and 10% of the Southern Hemisphere. The results show that the urbanization influence in two of the most widely used hemispheric data sets[1,2,4] is, at most, an order of magnitude less than the warming seen on a century timescale.

Significant urbanization effects have been noted at many cities[7,11]. Two factors must be considered, however, when comparing individual city 'heat island' magnitudes with hemispheric warming trends. First, many of the extreme urban biases that have been quoted are the largest daily occurrences, perhaps happening during still evenings or intense inversions. The effect on station monthly mean temperatures is sure to be considerably smaller. Second, in any gridded temperature data set, a single affected station is unlikely to have a large influence on the time series of the nearest grid-point, because this is generally a weighted average of between 5 and 20 station records[1,2].

The most comprehensive attempt to assess the significance of urbanization on large-scale temperature trends has been made for the contiguous United States by Karl *et al.*[12]. In this analysis the Historical Climate Network (HCN)[13] of 1,219 stations was used to assign stations to pairs of rural and urban sites. Karl *et al.* showed that an urbanization influence could be detected in many records, with the urban bias being a nonlinear function of population. To assess the influence of urbanization on regional averages developed from the gridded data sets[1–3], the average for the contiguous United States derived from the HCN data set of principally rural stations was compared with the gridded series. The gridded series make use of some of the temperature data that have been assembled over the present century from sources such as World Weather Records and Monthly Climatic Data for the World (see ref. 5 for details of these sources). Some of these records come from large cities and could be affected by urbanization-related trends. Comparison of the gridded and the HCN series revealed that the gridded time series shows a warming of ~0.1 °C over the period 1901–84[9]. It can be argued[10], however, that the rate of urbanization growth in the United States is atypical compared with many other parts of the world. We have therefore attempted to assess the urbanization influence in other regions of the world using specially developed rural-station temperature series.

Western Soviet Union. For the western part of the Soviet Union we selected a network of 35 stations from sites in non-urbanized areas with long records (Fig. 1*a*). The sites include isolated [illegible] meteorological stations, lighthouses, villages and other small

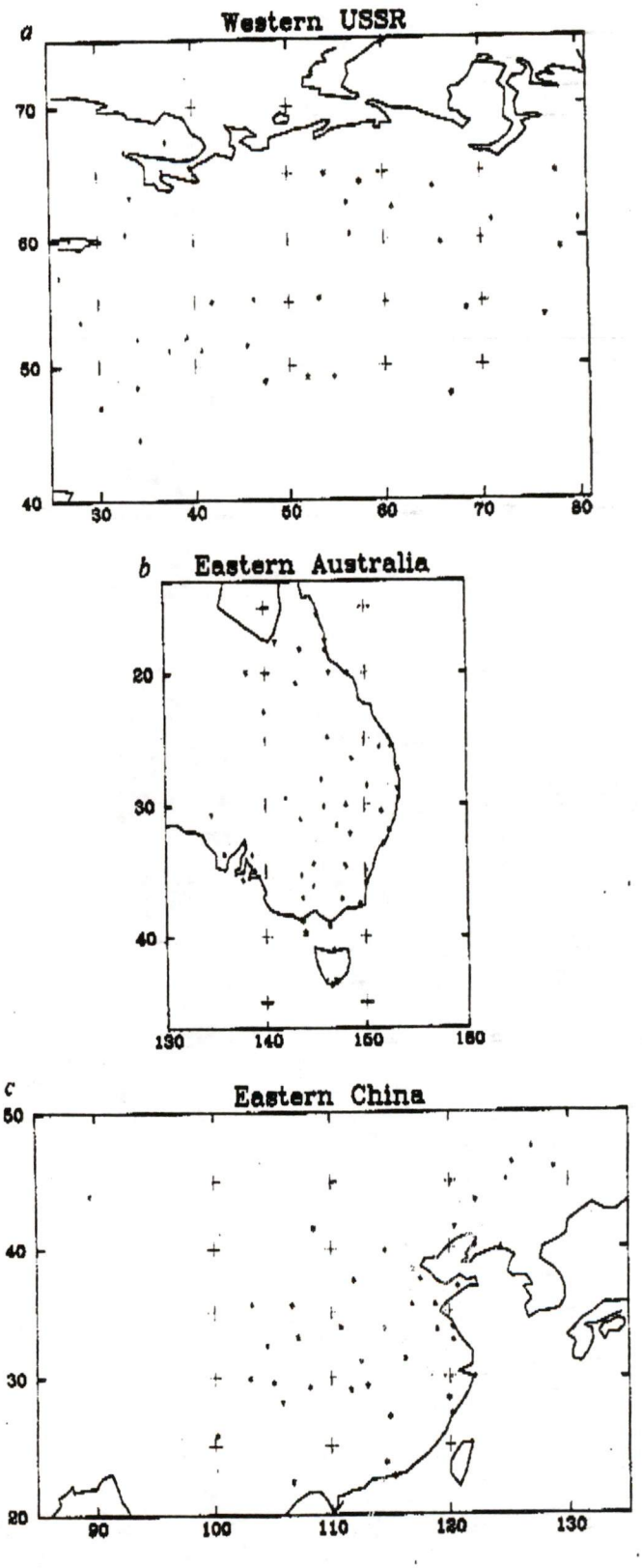


FIG. 1 Study regions, showing the rural stations (*) and the grid points (+). *a*, Western USSR; *b*, Eastern Australia; *c*, Eastern China. Details of the rural station networks are included in the text. The grid points are taken from the data set of refs 1 and 2, which interpolate station data onto a 5° latitude by 10° longitude grid. Station data used in the gridding extend 2.5° of latitude and 5° of longitude away from each grid point. For the western USSR, 60 station records were used to construct the grid-point series. There were 25 stations in operation by 1901 and 32 were operating in 1987. For eastern Australia 20 stations were used, 7 of which were operating during the 1930s [illegible]

settlements. The largest populated sites are nine towns with populations of the order of 10,000 people. All nine towns are located at least 80 km away from major cities. All the site records were assessed for artefacts due to factors such as site moves or changing methods used to calculate monthly mean temperatures. At twelve sites the observing station was moved slightly. Comparisons with neighbouring sites were made before and after each change, and where necessary, corrections were made to ensure homogeneity of the rural-station record. No corrections were deemed necessary for the remaining 26 stations, where no station moves were reported.

Data from the 38 stations were then converted to anomalies from the 1951–75 average and combined using the inverse-distance weighting gridding scheme used in ref. 1. By using the same averaging scheme as for the gridded data, any differences between this average and the gridded average will be the result of data differences and not due to differing interpolation methods. The resulting series (RUSSR, Fig. 2*a*) is an average for the European part of the Soviet Union, parts of western Siberia and Kazakhstan.

Using the gridded data from ref. 1, we developed a regional time series (JUSSR) for the region using 22 gridpoints (see Fig. 1*a*). Similarly, we developed a regional time series (VUSSR) for this region using the hemispheric data set from ref. 4. An optimum interpolation procedure was employed by Vinnikov *et al.*[4] to produce their annual hemispheric average time series, using about one-third the number of stations that were used in ref. 1. In this procedure, interpolation of station data to grid points was not undertaken, the published data being available only as annual hemispheric averages. For our study, regional time series were constructed from the data of ref. 4 using this same optimum interpolation scheme. The stations used extend beyond the bounds of the rural network, unlike those used in ref. 1.

The rural-network average was compared with the two gridded data series over two periods, 1901–87 and 1930–87. Intercorrelation between the three series over these two periods is exceedingly high, with all correlations between 0.98 and 0.99. Comparisons of the standard deviation and linear trend are given in Table 1. The similarity between the statistics for all three series over both periods is remarkable. Over the 1930–87 period, a cooling of ~0.2 °C in RUSSR is observed. This cooling is about 0.1 °C smaller in JUSSR, but there are no statistically significant differences between the two series. Given that all three data sets make use of different station networks, slight differences between the time series and their trends are to be expected.

Eastern Australia. We assembled a network of 49 stations in the eastern half of Australia, from the states of Queensland, New South Wales, Victoria and the southeastern quarter of South Australia (Fig. 1*b*). All stations are rural or small village sites and all encompass the period 1930–88. The average population of the stations is 5,775; the maximum population is 33,368 and there were seven lighthouse sites which were assumed to have a negligible population. The series from all stations were reduced to anomalies from the 1951–80 period before being combined into a regional series (RAUS, Fig. 2*b*) using the same inverse-distance gridding scheme.

A regional time series (JAUS) was developed for this region from ref. 2, using grid points (Fig. 1*b*). We also used the data in ref. 4 to derive a regional series (VAUS) for the region, which incorporated between 7 and 27 stations.

The correlation coefficients between the RAUS, JAUS and VAUS series over the 1930–88 period are all between 0.95 and 0.96. Comparisons of the standard deviation and linear trend are shown in Table 1. The results indicate that neither JAUS nor VAUS differ significantly from the rural time series RAUS. For VAUS, the warming over the region is similar to that from the rural series. In all three series, warming over the 59-year period is statistically significant at the 5% level.

The rural data set for Australia can be split into time series based on maximum and minimum temperatures. Examination of

TABLE 1 Comparison of temperature trends

Series	Period	Standard deviation (°C)	Linear trend (°C over period)
Western USSR			
RUSSR (rural)	1901–1987	0.82	0.36
JUSSR	1901–1987	0.79	0.38
VUSSR	1901–1987	0.81	0.31
RUSSR (rural)	1930–1987	0.84	−0.21
JUSSR	1930–1987	0.82	−0.09
VUSSR	1930–1987	0.85	−0.20
Eastern Australia			
RAUS (rural)	1930–1988	0.34	0.58*
JAUS	1930–1988	0.31	0.60*
VAUS	1930–1987	0.34	0.55*
Eastern China			
RCHI (rural)	1954–1983	0.30	0.23
JCHI	1954–1983	0.27	0.19
VCHI	1954–1983	0.37	0.13
UCHI	1954–1983	0.32	0.39*
Contiguous United States			
Rural[8,10]	1901–1984	0.42	0.16
Grid[8,10]	1901–1984	0.39	0.31

* Significant trend at the 5% level.

trends for these series shows that the 1930–88 warming is greater for the minimum temperatures (a 0.81 °C rise) than for the maximum temperatures (a 0.30 °C rise). This result indicates a reduction in the daily temperature range from this region, a feature noted for the United States by Karl *et al.*[14]. It is unfortunate that separate maximum and minimum temperature data sets are not more widely available. Many countries calculate mean monthly temperatures using observations from a number of fixed hours per day, without recording the daily maximum and minimum temperatures.

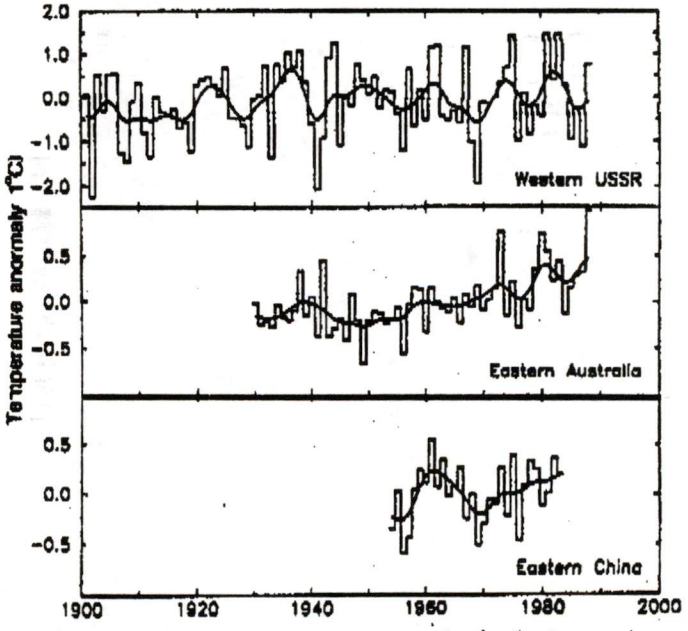


FIG. 2 Time series of annual temperature anomalies for the three regions: a, Western USSR (1901–88); b, Eastern Australia (1930–88); c, Eastern China (1954–83). The smooth curves were obtained using a gaussian filter designed to suppress variations on timescales of less than 10 years. The base periods for the three regions are 1951–75, 1951–80 and 1954–83, respectively. For the Chinese region all the rural stations are available for every year. For Eastern Australia, 3% of the annual station values are missing. For the Soviet series, there were only 20 of the 38 stations contributing in 1901. Seven stations began reporting after 1930. For the

tern China. We assembled a network of 42 station pairs of l and urban sites in the eastern half of China (Fig. 1*c*). The ata cover the period 1954–83. The 84 stations were selected from a 260-station temperature set recently compiled under the US Department of Energy and People's Republic of China Academy of Sciences Joint Project on the Greenhouse Effect[15]. The stations were selected on the basis of station history: we chose those with few, if any, changes in instrumentation, location or observation times. All 84 records were complete for the 30-year period. The urban stations were in regions with populations of over 0.5 million, whereas for the rural stations populations mostly less than 0.1 million (according to 1984 population statistics). From the 42-station rural network, we formed an average (RCHI, Fig. 2*c*) for eastern China using the inverse-weighting gridding scheme. The 42-station urban network (UCHI) was averaged in the same way. Using the gridded data from ref. 1, a regional time series (JCHI) was developed for the region encompassing 15 grid points (see Fig. 1*c*). An average series (VCHI) for the region, making use of 32 stations, was developed from the data in ref. 4.

The correlation between the RCHI and JCHI series over the 1954–83 period is 0.90, and there is a lower correlation of 0.81 between RCHI and VCHI. Comparisons of the standard deviation and linear trend are shown in Table 1. Although the results indicate that both gridded series show a slight cooling relative to the Chinese rural network (RCHI) over the 30-year period, differences between all three series are not statistically significant. Slight differences are to be expected given that the various series make use of different sets of raw station data. The warming in UCHI is 0.39 °C, considerably higher than that in RCHI. For this region, UCHI is the only series for which arming is statistically significant. The Chinese results may, at glance, seem somewhat surprising, as 24 of the stations d in ref. 1 are among the 42 urban sites. In refs 1 and 4, average temperatures for these sites generally come from airport sites, which may be in rural areas. In many parts of the world, city-centre observatories were relocated to airport sites during the 1950s and 1960s. That temperature records from many sites are a combination of information from various locations within a city or town emphasizes the need to assess the homogeneity of individual site records[5,6].

In none of the three regions studied here is there any indication of significant urban influence in either of the two gridded series[1,2,4] relative to the rural series. Earlier work on the contiguous United States[9,10] showed an urban influence of 0.15 °C over the period 1901–84. (The results of this work are summarized in Table 1.) The United States result therefore does seem to be somewhat atypical compared with other industrialized regions of the world. The results from the United States clearly represent an upper limit to the urban influence on hemispheric temperature trends.

In total, the three regions and the contiguous United States encompass 82 grid points (22 over the western USSR, 14 over eastern Australia, 16 over eastern China and 30 over the contiguous United States) on a resolution of 5° latitude by 10° longitude. The three Northern Hemisphere regions in total comprise about 20% of the landmass of the hemisphere, and the eastern Australian region comprises 10% of the landmass in the Southern Hemisphere. Thus there seems to be little urbanization influence in three regions of the world that, when taken together, are twice the size of the contiguous United States.

It is unlikely that the remaining unsampled areas of the developing countries in tropical climates, or other highly populated parts of Europe, could significantly increase the overall urban bias above 0.05 °C during the twentieth century. A bias of this order is an order of magnitude smaller than the hemispheric and global-scale warming trend observed over the last 100 years. The bias will be further halved in hemispheric and global temperature estimates that incorporate marine as well as land temperatures.

We emphasize, however, that our results do not imply that urban warming influences in observations of local temperature will remain inconsequential in global averages in the future. Indeed, careful selection, inspection and monitoring for urbanization influences in the climate record will be required. This concern could be greatly lessened by an international effort to monitor and place observing stations outside urban areas. □

Received 5 April; accepted 24 July 1990.

1. Jones, P. D. *et al. J. Clim. appl. Met.* **25**, 161–179 (1986).
2. Jones, P. D., Raper, S. C. B. & Wigley, T. M. L. *J. Clim. appl. Met.* **25**, 1213–1230 (1986).
3. Hansen, J. & Lebedeff, S. *J. geophys. Res.* **92**, 13345–13372 (1987).
4. Vinnikov, K. Ya, Groisman, P.Ya. & Lugina, K. M. *J. Clim.* **3**, 662–677 (1990).
5. Jones, P. D. *et al. A grid point surface air temperature data set for the Northern Hemisphere* Tech. Rep. TR022 (US Department of Energy, Washington, DC, 1985).
6. Jones, P. D., Raper, S. C. B., Goodess, C. M., Cherry, B. S. G. & Wigley, T. M. L. *A grid point surface air temperature data set for the Southern Hemisphere* Tech. Rep. TR027 (US Department of Energy, Washington DC, 1986).
7. Kukla, G., Gavin, J. & Karl, T. R. *J. Clim. appl. Met.* **25**, 1265–1270 (1986).
8. Wood, F. B. *Clim. Change* **13**, 297–312 (1988).
9. Karl, T. R. & Jones, P. D. *Bull. Am. met. Soc.* **70**, 265–270 (1989).
10. Jones, P. D., Kelly, P. M., Goodess, C. M. & Karl, T. R. *J. Clim.* **2**, 285–290 (1989).
11. Oke, T. R. (ed.) *Proceedings of the Technical Conference: Urban Climatology and its applications with special regard to tropical areas* WMO-No. 652 (World Meteorological Organization, Geneva, 1984).
12. Karl, T. R., Diaz, H. F. & Kukla, G. *J. Clim.* **1**, 1099–1123 (1988).
13. Quinlan, F. T., Karl, T. R. & Williams, C. N. Jr *United States Historical Climatology Network (HCN) Temperature and Precipitation Data* NDP-019 (CDIAC, Oak Ridge, 1987).
14. Karl, T. R., Kukla, G. & Gavin, J. *J. Clim. appl. Met.* **23**, 1489–1504 (1984).
15. Koomanoff, F. *et al. Bull. Am. met. Soc.* **69**, 1301–1308 (1988).

ACKNOWLEDGEMENTS. This work was funded partly by the US Department of Energy, Carbon Dioxide Research Division and through NOAA/DOE Interagency Agreement. The collaboration of the many individuals in this work was initiated by a meeting of one of the subgroups of Working Group 1 (WG1) of the Intergovernmental Panel on Climatic Change (IPCC) in December 1989.

Global Warming: Evidence for Asymmetric Diurnal Trends

T.N REVIEW
"SCIENCE"

Thomas R. Karl[1]

George Kukla[2]

Vyacheslav N. Razuvayev[3]

Michael J. Changery[1]

Robert G. Quayle[1]

Richard R. Heim, Jr.[1]

MAY 1991

1 NOAA/NESDIS/National Climatic Data Center
Global Climate Laboratory
Federal Building
Asheville, NC 28801 USA

2 Lamont/Doherty Geological Observatory of Columbia University
Palisades, NY 10964 USA

3 All-Union Research Institute of Hydrometeorological Information
6, Korolev St.
Obninsk, Kaluga, 249020, USSR

Global Warming: Evidence for Asymmetric Diurnal Trends

ABSTRACT

Analyses of the surface thermometric record over three large countries in the Northern Hemisphere (the United States, the Soviet Union, and the People's Republic of China) indicate that virtually all of the warming which has occurred in these regions over the past four decades can be attributed to an increase of mean daily minimum (nighttime) temperatures. Mean daily maximum (daytime) temperatures display little or no warming. In the USA and the USSR (no data available in China) similar characteristics are also reflected in the trends of extreme seasonal temperatures, e.g., positive trends in extreme minimum temperatures and little or no trend in extreme maximum temperatures. Nighttime warming is particularly strong in the USA and the USSR during the warm season, but it is most pronounced in China during winter. The cause(s) of the asymmetric trends are uncertain and may be directly or indirectly related to greenhouse effects. Evidence suggests that changes in cloud cover likely play a direct role (where increases in cloudiness result in reduced maximum and higher minimum temperatures), but these changes may stem from a variety of causes, e.g. greenhouse forcing, SO_x emissions, natural climate fluctuations.

JUN 07 '91 17:40 ECDC ASHVL.NC P.1
JUN 07 '91 17:40 ECDC ASHVL.NC P.2

Reprint Series
1 March 1991, Volume 251, pp. 1058–1061

SCIENCE

The Greenhouse Effect in Central North America: If Not Now, When?

THOMAS R. KARL, RICHARD R. HEIM, JR., AND ROBERT G. QUAYLE

Copyright © 1991 by the American Association for the Advancement of Science

The Greenhouse Effect in Central North America: If Not Now, When?

THOMAS R. KARL, RICHARD R. HEIM, JR., ROBERT G. QUAYLE

Climate models with enhanced greenhouse gas concentrations have projected temperature increases of 2° to 4°C, winter precipitation increases of up to 15 percent, and summer precipitation decreases of 5 to 10 percent in the central United States by the year 2030. An analysis of the climate record over the past 95 years for this region was undertaken in order to evaluate these projections. Results indicate that temperature has increased and precipitation decreased both during winter and summer, and that the ratio of winter-to-summer precipitation has decreased. The signs of some trends are consistent with the projections whereas others are not, but none of the changes is statistically significant except for maximum and minimum temperatures, which were not among the parameters predicted by the models. Statistical models indicate that the greenhouse winter and summer precipitation signal could have been masked by natural climate variability, whereas the increase in the ratio of winter-to-summer precipitation and the higher rates of temperature change probably should have already been detected. If the models are correct it will likely take at least another 40 years before statistically significant precipitation changes are detected and another decade or two to detect the projected changes of temperature.

ADEQUATE SUPPLIES OF WATER FOR crops and livestock are of primary importance to the central North America region (*1*). Severe droughts of the 20th century have affected both the biophysical and socioeconomic systems of the region (*2*). One of the more ominous scenarios that has been suggested on the basis of several climate model simulations in an enhanced greenhouse world is the decrease of summertime precipitation and an increase of temperature across central North America (*3*). The model predictions admittedly suffer from potentially significant limitations. For example, some regional phenomena such as the El Niño–Southern Oscillation (ENSO) are not adequately simulated by these models, but do appear to have linkages with regional surface temperature and precipitation variations in the United States (*4*). Nonetheless, if the projected climate occurs, it would certainly have a deleterious impact, and the region would have a difficult time adapting. In this report, we use observational records and purely statistical methods to review temperature and precipitation trends over the past century and assess the likelihood that climate projections will be verified by current climate monitoring techniques if contemporary climate model predictions are basically correct.

Global Climate Laboratory, National Climatic Data Center, National Environmental Satellite, Data, and Information Service, National Oceanic and Atmospheric Administration, Department of Commerce, Federal Building, Asheville, NC 28801.

Areally averaged seasonal mean temperature and precipitation over the IPCC Central region (Fig. 1A) bounded by the latitudes 35° to 50°N and longitudes 80° to 105°W (less a small part of land over the Canadian Provinces) were used to determine past changes (*5*). This is one of the regions where projections of temperature and precipitation change have been issued (*3*). The data are derived from the climate division averages of temperature and precipitation (*6*). A slightly different region referred to as "Central" (Fig. 1B) was used to examine past changes in the seasonal mean daily maximum and minimum temperatures (*7*, *8*), for which projections were not made by the IPCC. The seasonal mean daily maximum and minimum temperatures are area averages over the period 1901 to 1987 derived from 147 stations (*8*).

We analyzed changes of seasonal mean temperature and precipitation over the IPCC Central region using tests of significance of linear trends, the nonparametric Wilcoxon sign-rank test, and the two-phase regression test described by Solow (*9*). The two-phase regression can be used to test for a change point in the linear trends. Use of the two-phase regression helps ensure against undetected nonlinear trends. Similar tests were also applied for changes of the seasonal mean daily maximum and minimum temperatures.

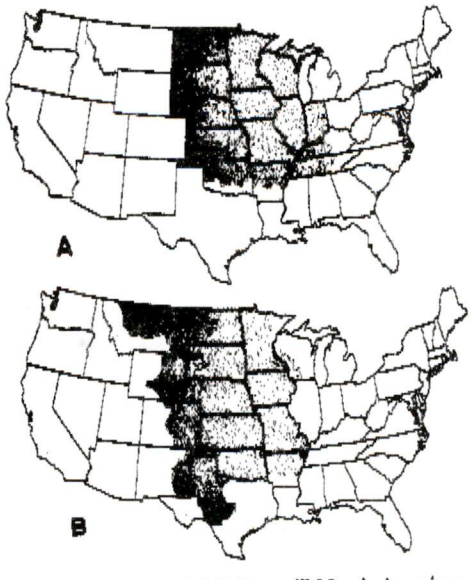


Fig. 1. (**A**) The "IPCC Central" North American region; (**B**) the "Central" United States region.

We developed autoregressive moving-average (ARMA) models using the seasonal time series of the precipitation and temperature records for the IPCC Central region. The data were transformed to standardized departures for temperature and precipitation by use of the normal and gamma statistical distributions, respectively. Five models were developed. Two were models for seasonal temperature (one for winter and one for summer) and two were for precipitation. The fifth model pertained to the ratio of winter to following summer precipitation. The models can be written as

$$Y_t = \sum_{i=1}^{p} \phi_i Y_{t-i} + \sum_{j=1}^{q} \theta_j a_{t-j} + a_t$$

where Y_t is the value of the time series at time t; ϕ_i is the ith autoregressive (AR) coefficient; θ_j is the jth moving average (MA) coefficient; and a_t is random noise (or a shock) at a time t. The order of the model is expressed as the sum of p and q and represented as ARMA (p, q). We assumed that a_t had a normal distribution with mean zero and standard deviation σ_a. Most stationary processes can be fitted by an ARMA model (*10*).

The Akaike information criterion (AIC) and the Bayesian information criterion (BIC) were both considered in the selection of the appropriate model order. Each model was tested up to order 12. After inspection of the residual mean squares of each of the models, a decision was made to use the AIC in the one instance where the two information criteria provided conflicting advice (the ratio of winter-to-summer precipitation). The AIC is known to somewhat overspecify a model (*11*), but in our analysis only one of the models had an order as high as two, and none of the models deviated greatly from white noise process. Four of the models are ARMA(0,1), whereas the ratio of winter-to-summer precipitation is an ARMA(1,1).

The time series generated from these models (if the models are perfectly specified) reproduce data that have all the characteristics of the observations. For each model, 1000 time series were generated of length 41 years (regarded as spanning the years 1990 to 2030) and 95 years (regarded as spanning the years 1895 to 1989). Linear trends (a convenient simplification used in the absence of any compelling reasons to suggest otherwise) were superimposed on the output from these models. The trends consisted of various percentages of the projected changes given in Table 1. The first time in which a significant trend could be detected was calculated by use of the empirically based 0.05 significance level. This statistical significance level was derived from the distribution of the slopes of the linear trends in 1000 simulations of the ARMA models without trends imposed.

No significant trends, even at the 0.10 significance level, could be found in the seasonal means of temperature, precipitation, or the ratio of winter-to-summer precipitation over the 1895 to 1989 time period. We looked for both linear trends and trends with one change point (*9*) (Table 2). No significant trends were observed even though substantial changes of temperature and precipitation over this region could have been anticipated on the basis of the model projections. For example, winter precipitation is expected to increase by as much as 15% (Table 1), but it has fallen at a rate slightly greater than 4% per century (Table 2). Summer precipitation has shown a slight decrease, but the magnitude is small, less than 1% per century (Table 2), despite projections of a decrease in precipitation by 5 to 10% by 2030. The ratio of winter-to-summer precipitation is projected to increase over this region, but it has decreased at a rate of nearly 4% per century. At least the direction of temperature change in both winter and summer is consistent with the projections, increasing by 0.23° and 0.43°C per century, respectively. None of the changes, however, are statistically significant. The hypothesis that all of the time series are stationary ARMA processes cannot be rejected, and thus ARMA models are appropriate tools for further analysis of these data.

We also considered the possibility that a greenhouse gas signal was masked by the natural climate variability in this region. To answer this question we imposed trends of various magnitudes on the 1000 simulations representing the years 1895 to 1989 for each of the five parameters of interest and calculated the probability that those trends would not be detected by our tests. The magnitudes of the trends imposed were 7, 14, and 28% of the total projected changes (Table 1). The rationale for these magnitudes is that global temperatures have risen by nearly 0.5°C since the 19th century (*3*), and this is 28% of the projected warming (1.8°C) expected by the year 2030 (*3*). The 7 and 14% changes correspond to potential undetectable greenhouse gas–induced changes that are only a fraction (0.25 and 0.50) of that corresponding to the 0.5°C global mean temperature increase. The IPCC concluded that the observed warming of nearly 0.5°C is already at the low end of the sensitivity of current climate models to greenhouse-induced warming.

For the projected rates of summer (three of three models) and winter (two of three models) warming, it is unlikely, but still possible (probability between 0.05 and 0.25, depending on the model used), that the changes projected would have been undetected if the rates of change in IPCC Central were proportional to the rate of global warming (28% of the value projected by the year 2030, Fig. 2A). Only for the winter projections from the GFDL (*3*) model (2°C warming by 2030) did we find it probable that changes could have been masked by natural variability. If climate model sensitivity were reduced by a factor of 2, we would likely (probability greater than 0.50) be unable to detect any of the greenhouse signals in the 95 years of thermometric records.

For winter and summer total precipitation (Fig. 2B), the natural variability of the climate record makes it unlikely that we would be able to detect the changes projected by the climate models, even if they were correct. In contrast, for the projected change in the ratio of winter-to-summer precipitation, at least for two of the models in which large changes in that ratio are projected, we should have already detected the changes. Once again, this conclusion is strictly valid

Table 1. Estimates of changes in areal means of surface air temperature (Temp) and precipitation (Precip) over central North America (35° to 50°N, 80° to 105°W) from preindustrial times to 2030, for the IPCC "business as usual" (*3*) emission scenario. These projections have been scaled to correspond to a global mean warming of 1.8°C by 2030. Model abbreviations are the Canadian Climate Center (CCC), Geophysics Fluid Dynamic Laboratory–USA NOAA (GFDL), and the United Kingdom Meteorological Office (UKMO) as provided by IPCC (*3*).

Parameter	Season	Model		
		CCC	GFDL	UKMO
Temp (°C)	Winter	4	2	4
Temp (°C)	Summer	2	2	3
Precip (%)	Winter	0	15	10
Precip (%)	Summer	−5	−5	−10
Precip (%) ratio	Winter/summer	5	21	22

Table 2. Observed trends of seasonal mean temperature (Temp) and total precipitation (Precip) from 1895 to 1989. No trends are statistically significant at the 0.10 level. Both a parametric test and a nonparametric test were used. Slopes are percent per 100 years for precipitation and degrees centigrade per 100 years for temperature.

Parameter	Season	Slope
Precip	Winter	−4.2
Precip	Summer	−0.7
Temp	Winter	0.23
Temp	Summer	0.43
Precip ratio	Winter/summer	−3.7

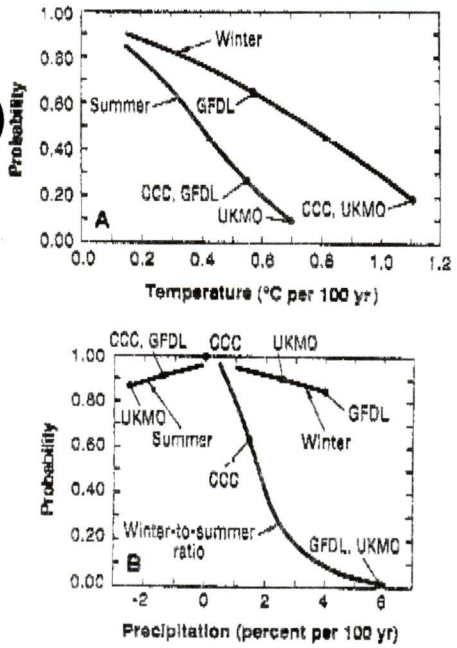


Fig. 2. Probability that trends of various magnitudes would have gone undetected over the IPCC Central North American region during the period 1895 to 1989: (**A**) temperature and (**B**) precipitation. Large dots indicate the trends that are consistent with projections from each of three climate models when these projections are reduced to the fraction of global warming already observed compared with that projected in the year 2030 (reduced, that is, to 28% of total projections). Abbreviations are defined in Table 1.

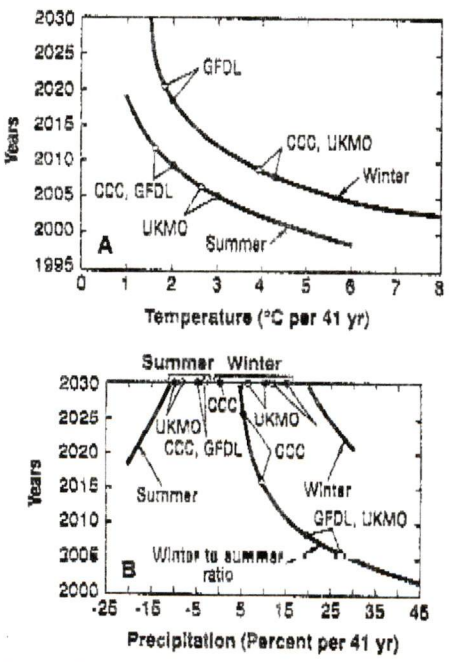


Fig. 3. The year in which detecting trends (at the 0.05 significance level) of various magnitudes becomes more likely than not (probability >0.5). (**A**) Temperature; (**B**) precipitation. Trends begin in the year 1990. The solid dots represent the magnitudes that would be equivalent to the projections of CCC, GFDL, and UKMO from the beginning of the industrial revolution to 2030 as given by the IPCC (*3*). The open circles represent similar magnitudes after consideration of the changes already observed since 1895.

only if the changes were proceeding at a rate in concert with the increase of global mean temperature (and if the increase of global mean temperature is indeed greenhouse-induced), that is, if we have experienced about 28% of the projected greenhouse-induced changes in temperature and precipitation as of 1990.

Assuming that all of the IPCC projections are correct and that the observed record to date is trend-free, we calculated when detection of the projected changes during the next 41 years would be likely. Another 15 to 20 years would be required for the detection of summer temperature changes (Fig. 3A). Between 15 and 30 years would be required for the detection of winter changes, depending on the projection and whether the warming that has already occurred is considered. Detection of the projected change for precipitation is less likely than for temperature during the next four decades (Fig. 3B) because of the large year-to-year variability. If the precipitation changes were about twice as large as those projected, we probably (probability >0.5) could detect the changes by about 2020. For the expected change in the ratio of winter-to-summer precipitation even though we should have already detected the larger rates of change projected by the GFDL and UKMO models during the past 95 years, it would not be until around 2005 that we would be able to detect the projected changes if they were to begin in 1990 and proceed at an approximately linear rate.

Although the general circulation model results we used do not project changes in the extremes of temperature, such extremes are useful diagnostic tools. Seasonal mean daily minimum temperature has increased in the central United States (Fig. 1B and Table 3) during all seasons and at a significant rate during spring and summer. The rise of the minimum is stronger than that of the maximum in all seasons. Differential changes in the seasonal mean maximum and minimum temperatures indicate that because of a focus on changes of seasonal mean temperature alone, many important aspects of climate change are being overlooked. Recent work (*12*) implies that the differential changes of maximum and minimum are related to increases of cloudiness.

These results suggest that it is difficult to dismiss outright many of the IPCC projections as inconsistent with the observations, except for the change in the ratio of winter-to-summer precipitation and the rates of summer temperature increase as projected by the UKMO model. If these latter projections were correct, we probably should have already detected some statistically significant changes. Furthermore, except for the expected change in the ratio of winter-to-summer precipitation, even if all the changes began to occur in 1990, it is unlikely that we will be able to detect these signals over the next few decades. Recently, Briffa *et al.* (*13*) have made similar conclusions for temperature changes in the Fennoscandia regions.

Table 3. Observed trends of the seasonal mean daily maximum and minimum temperatures over the central region of the United States for the period 1901 to 1987. Trends that are statistically significant at the 0.10 significance level are indicated by an asterisk (parametric test). None were significant according to the nonparametric test. The years of significant change points are listed along with the sign of the associated shift in the time rate of change.

Parameter	Season	Slope (°C/100 years)	Year of change point
Maximum	Winter	0.20	None
Minimum	Winter	0.59	None
Maximum	Spring	0.38	None
Minimum	Spring	*0.94	None
Maximum	Summer	0.45	1934(−)
Minimum	Summer	*0.98	1935(−)
Maximum	Fall	−0.55	None
Minimum	Fall	0.35	None

These analyses leave planners and policy makers in an unenviable position. They must decide to use or not use the IPCC projections without a clear rejection or acceptance of many of those projections and only a fuzzy notion that the projections may be overly sensitive to greenhouse increases when compared to the observed climate record in this region. To compound the dilemma, significant changes have now taken place with respect to increases of the seasonal mean daily minimum temperatures (which appear to be related to increased cloud cover), but we do not yet have a sound understanding of how these changes may or may not be related to the greenhouse effect.

REFERENCES AND NOTES

1. W. E. Riebsame, S. A. Changnon, T. R. Karl, *Drought and Natural Resources Management in the United States: Impacts and Implications of the 1987–1989 Drought* (Westview, Boulder, CO, 1990); A. D. Hecht, *J. Clim. Appl. Meteorol.* **22**, 51 (1983).
2. R. W. Kates, J. H. Ausubel, M. Barberian, Eds., *Climate Impact Assessment* (Wiley, New York, 1985).
3. Intergovernmental Panel on Climate Change (IPCC), *Scientific Assessment of Climate Change* (World Meteorological Organization, United Nations Environment Programme, Geneva, Switzerland, 1990).
4. K. E. Trenberth, G. W. Branstator, P. A. Arkin, *Science* **242**, 1640 (1988); K. E. Trenberth, *Bull. Am. Meteorol. Soc.* **71**, 988 (1990).
5. Seasons are defined as follows: winter is December, January, and February; spring is March, April, and May; summer is June, July, and August; fall is September, October, and November.
6. T. R. Karl, *Clim. Change* **12**, 179 (1988).
7. ____ and R. W. Knight, *Historical Climatology Series 3–14* (National Climatic Data Center, Asheville, NC, 1985); T. R. Karl, L. K. Metcalf, M. L. Nicodemus, R. G. Quayle, *ibid.* 6-1 (National Climatic Data

Center, Asheville, NC, 1983).
7. T. R. Karl and C. N. Williams, Jr., *J. Clim. Appl. Meteorol.* **26**, 1744 (1987).
8. T. R. Karl, R. G. Baldwin, M. G. Burgin, *Historical Climatology Series 4–5* (National Climatic Data Center, Asheville, NC, 1989).
9. A. R. Solow, *J. Clim. Appl. Meteorol.* **27**, 1401 (1987).
10. M. B. Priestly, *Spectral Analysis and Time Series* (Academic Press, Orlando, FL, 1981).
11. R. W. Katz, *J. Atmos. Sci.* **39**, 1446 (1982).
12. M. S. Plantico, T. R. Karl, G. Kukla, J. Gavin, *J. Geophys. Res.* **95**, 16617 (1990).
13. K. R. Briffa *et al.*, *Nature* **346**, 434 (1990).
14. This work was partially supported by the Department of Energy National Oceanographic and Atmospheric Administration Interagency Agreement DE-A105-90ER60952.

9 October 1990; accepted 28 December 1990

The Great Global Conveyor

Wallace S. Broecker
Lamont-Doherty Geological Observatory of
Columbia University
Palisades, New York 10964

Submitted to
Oceanography
May 1991

INTRODUCTION

A diagram depicting the ocean's "conveyor belt" has been widely adopted as a logo for the Global Change research initiative. This diagram (see figure 1) first appeared as an illustration in an article about the Younger Dryas event which appeared in the November 1987 issue of Natural History. It was designed as a cartoon to help the largely lay readership of this magazine to comprehend one of the elements of the deep sea's circulation system. Had I suspected that it would be widely adopted as a logo, I would have tried to "improve" its accuracy. In hindsight such repairs would likely have ruined the diagram both for the readers of Natural History and for use as a logo.

The lure of this logo is that it symbolizes the importance of linkages between realms of the Earth's climate system. The ocean's conveyor is driven by the salt left behind as the result of the transport of water vapor through the atmosphere from the Atlantic Basin to the Pacific Basin. A byproduct of its operation is the heat which maintains the anomolously warm winter air temperatures enjoyed by northern Europe. A millinneum of very cold conditions known as the Younger Dryas appears to have been the result of a temporary shutdown of the conveyor. Thus the conveyor logo portrays the concern which led to the launching of the Global Change research initiatives; namely devilishly complex interconnections among the elements of our Earth's climate system will greatly complicate our task of predicting the consequences of global pollution.

The objective of this paper is to provide a readable summary, from my prospective, of the conveyor's operation present and past.

IT'S PATH

The main problem with the logo is that it implies that if one were to inject a tracer substance into one of the conveyor's segments it would travel around the loop as a neat package eventually returning to its starting point. As we all know this is hardly the case.

Other circulation "loops" exist in the ocean and mixing occurs among the waters traveling along these intersecting pathways. The logo symbolizes a far more complex situation.

To understand the logo's message, let's start at the point of origin of its lower limb and work our way around the ocean. Waters in the vicinity of Iceland are cooled through contact with the cold winter air masses which sweep in from the Canadian Arctic. The cooling densifies the surface water to the point where it can sink to the abyss and flow southward forming the conveyor's lower limb. In the logo this flow is depicted as a ribbon of water which jets its way through the deep Atlantic from the vicinity of Iceland to the tip of Africa. In reality it is a sluggish mass which fills most of the deep Atlantic. Its flow is more akin to that in a slow moving river than to that in a fast moving mountain stream. This water mass, known to oceanographers as the North Atlantic Deep Water (NADW), stands out as a tongue of high salinity, low nutrient content and high $^{14}C/^{12}C$ ratio water in sections drawn along the Atlantic's length (see Figure 2). Its only competitor for space in the deep Atlantic is a wedge of Antarctic Bottom Water (AABW) which underrides the NADW mass. This intruding water is mixed upward into the southward flowing NADW, increasing the transport by the conveyor's lower limb.

Southward of 30°S the lower limb of the conveyor joins a rapidly moving deep current which encircles the Antarctic continent. This current serves as the great mix-master of the world ocean. It blends the NADW exiting the Atlantic with new deep water generated along the perimeter of the Antarctic continent and also with old deep waters recirculated back into the Antarctic from the deep Pacific and Indian Oceans. So efficient is this blending that the NADW entering from the Atlantic loses its identity before it passes even one half of a revolution around the Antarctic!

A rough quantification of the contribution of NADW to the deep waters of world ocean is provided by a property called PO_4^* (Broecker, et al., 1991) which is defined as follows

$$PO_4^* = PO_4 + \frac{O_2}{175} - 1.95\ \mu m/kg$$

where PO_4 and O_2 are the measured phosphate and dissolved oxygen gas concentrations in a given water sample. The coefficient, 175 is the global Redfield coefficient relating O_2 consumption to PO_4 release during respiration (Broecker, et al., 1985) and the coefficient 1.95 is arbitrarily introduced in order to bring the values of PO_4^* into the range of deep water PO_4 concentrations. To the extent that the respiration coefficient is a constant, PO_4^* constitutes a conservative property of any given deep water parcel; the increase in PO_4 due to the oxidation of organic material is exactly balanced by the decrease in $O_2/175$. PO_4^* is attractive as an indicator of the contribution of NADW because deep waters formed in the northern Atlantic have much lower PO_4^* values than those formed in the Southern Ocean. Further the range of PO_4^* values for the northern source waters (0.73 ± 0.03) and for southern source waters (1.67 ± 0.10) is small compared to the difference between the means for these end member values ($1.67 - 0.73 = 0.94$). The nomogram in figure 3 permits the conversion of deep sea PO_4^* values into percentage contribution of NADW.

As can be seen in the map in figure 4, at a depth of 3 kilometers the contribution of NADW to the deep water mix remains strong throughout the Atlantic, but after the conveyor's lower limb passes around the southern tip of Africa into the Antarctic it rapidly becomes blended with the high PO_4^* deep water generated along the edge of the Antarctic continent. In this way an ambient deep water mix with a PO_4^* value of 1.37 is produced (see histograms in figure 4). This blend which consists of 1 part deep water produced in the northern Atlantic with about 2 parts of deep water produced in the Antarctic floods the deep Pacific and Indian Oceans.

A more complete picture of the geometry of the blending process is given by the PO_4^* sections in figure 5. As can be seen, the more dense and higher PO_4^* waters produced in the Antarctic mix upward and northward into the less dense and lower PO_4^* waters entering from the Atlantic. By the time the water reaches the deep Indian, the deep Pacific and the Drake Passage, these endmember waters have been well blended.

As depicted in the logo the lower limb water returns to the surface in the northern Indian and Pacific Oceans. In reality this upwelling is widely spread with a large amount taking place in the Antarctic. The logo also suggests that the major route for return flow to the Atlantic (i.e the conveyor's upper limb) is through the Indonesian archipelago and around the tip of Africa. This view was impressed on my brain by enthusiastic presentations by our society's president who stressed the role of the Agulhas current in global circulation (Gordon and Piola, 1983; Gordon, 1985 and 1986). As discussed below, this route probably accounts for only about one quarter of the return flow. A more important pathway is that through the Antarctic via the Drake Passage into the South Atlantic. These additional upwelling and return flow pathways are portrayed in figure 6.

ITS FLUX

It is my view that the magnitude of transport by the conveyor is best constrained by radiocarbon measurements on samples of deep water from the Atlantic Ocean. Some physical oceanographers might dispute this claim and opt instead for estimates derived from a combination of current meter measurements and geostrophic flow calculations. Fortunately the two approaches yield similar answers.

The radiocarbon based estimate of the flux of NADW into the deep Atlantic is obtained by dividing the volume of water contained in the deep Atlantic by the radiodecay based mean residence time. This estimate must be corrected for the contribution made by

AABW to the conveyor's lower limb. It must also be corrected for the impact of temporal changes in the $^{14}C/C$ ratio for atmospheric CO_2.

The major obstacle to calculation from radiocarbon measurements of residence times for water in the deep Atlantic is the determination of the initial $^{14}C/C$ ratio for each parcel. The reason is that all waters in the deep Atlantic are mixtures of northern component water with a comparatively high $^{14}C/C$ ratio ($\Delta^{14}C = -68‰$) and of southern component water with a comparatively low $^{14}C/C$ ratio ($\Delta^{14}C = -158‰$). Because of the large difference in the $\Delta^{14}C$ values for these end members much of the variation in $^{14}C/C$ ratio within the deep Atlantic is created by differences in the end member blend. As shown by Broecker et al. (1991a), PO_4^* provides a quite accurate means of establishing the proportions of northern and southern component water in the sample analyzed for radiocarbon. The measured radiocarbon concentration is then subtracted from the initial concentration calculated for the mixture yielding the deficiency attributable to radiodecay. An example of this calculation is shown in Table 1. The radiocarbon measurements used in this analysis were made in the laboratories of Gote Ostlund at the University of Miami and Minze Stuiver at the University of Washington.

Water column averages for radiodecay deficiencies are shown in figure 7 for all the stations occupied during the GEOSECS, TTO, TAS and SAVE expeditions. Little information is lost by this vertical averaging because significant trends with depth are not found for any of the stations. The vertically averaged deficiencies do however show a pronounced geographic trend. The lowest values (<10‰) are found along the western margin of the Atlantic and the highest values (>30‰) along the eastern margin. As radiocarbon decays by 1‰ in 8.27 years, the isolation times corresponding to these radiocarbon deficiencies range from near zero for the western boundary in North Atlantic to as high as 300 years along the eastern boundary. This suggests rapid ventilation from both

ends of the Atlantic along the western boundary coupled with more leisurely dispersion into the interior. The radiocarbon deficiency for the entire deep Atlantic averages about 22‰. This corresponds to a residence time of about 180 years.

The volume of the deep Atlantic reservoir is 1.55×10^{17} m^3 (i.e., 2500m mean thickness with an area of 6.2×10^{13} m^2). Hence to achieve this residence time requires a ventilation flux of 8.6×10^{14} m^3/yr or 27 Sverdrups (1 Sverdrup = $10^6 m^3$/sec). As the flux of AABW is about 4 Sverdrups, the flux of NADW is estimated to be 23 Sverdrups.

This calculation assumes the system to be at steady state. While we have no way to know whether this is true for the water fluxes, we do know that the atmosphere's $^{14}C/C$ ratio has changed with time. When these changes are taken into account, the flux has to be reduced by a factor of about 0.88 (Broecker et al. 1991b). Hence, we get a flux of close to 20 Sverdrups for the northern component (i.e., NADW). It is difficult to assess the error in this estimate but it is probably on the order of 25% (i.e., ± 5 Sverdrups). To appreciate the immense magnitude of this flux it is important to be reminded that it is 20 times the combined flow of all the world's river and somewhat larger than the rainfall over the entire globe!

ITS DRIVE

My contention is that the conveyor is driven by the excess salt left behind in the Atlantic as the result of vapor export (Broecker, et al., 1985). As can be seen from the map in figure 8, the surface waters of the Atlantic are on the average 1 gm/liter higher in salt content than those in the Pacific. For sea water with temperatures in the range of those constituting the NADW mass (i.e. 2 to 4°C) one gram per liter extra salt has the same impact on the water's density as a cooling of 2 to 3°C. The salinity contrast between surface waters in the northern Atlantic and those at comparable latitudes in the northern Pacific is even larger, ranging from 2 to 3 grams per liter. This difference is so large that

surface waters in the northern Pacific even when cooled to their freezing point (i.e -1.8°C), sink to a depth of only a few hundred meters before reaching their buoyancy limit. Hence no deep water can form in the northern Pacific.

Three means are available by which the magnitude of the vapor export flux can be estimated. The first approach is based on the water budget for the Atlantic Ocean and its continental drainage basin (see figure 9). Baumgartner and Reichel (1975) have constructed a water budget based on estimates of rainfall and evaporation over the Atlantic Ocean and runoff from its drainage basin. Their result is that vapor is being lost from the Atlantic basin at a rate averaging 0.45 Sverdrups.

A second approach is to estimate the vapor export necessary to maintain the salinity differences in the sea against mixing among the ocean's water masses which tends to homogenize the sea's salt. If the mixing rates within can be determined and incorporated into an ocean mixing model, the fresh water budget for any region of the ocean can be determined. Broecker et al., (1990a) adopted this approach. Using a radiocarbon calibrated ocean box model they obtain a flux of 0.25 Sverdrups. The Princeton ocean GCM yields a water vapor loss of 0.45 Sverdrups (Manabe and Stauffer, 1988) and the Hamburg ocean GCM 0.20 Sverdrups (Ernst Maier-Reimer, personal communication).

The third approach involves the determination of the net fluxes of water vapor across segments of boundary separating the Atlantic's drainage basin from the remainder of the world. To do this, Zaucker and Broecker (in press) have used wind and humidity data summarized by Oort (1983) to calculate vertically integrated and annually averaged vapor transports for all positions on the globe (using the 4° x 5° grid 11 level eggcrate geometry employed by GISS). They obtain in this way a net vapor loss from the Atlantic of 0.32 Sverdrups. In addition to providing an estimate of the magnitude of the vapor loss, this approach also yields the routes for this loss. As is shown in figure 10, vapor loss occurs

both in the belt of northern hemispheres westerlies and in the belt of tropical easterlies. For the westerlies substantially more vapor is exported across Eurasia than is imported across the North American cordilera. For the easterlies substantially more vapor is exported across Central America than is imported across Africa.

Based on these results we estimate that the rate of vapor loss from the Atlantic basin is 0.35 ± 0.12 Sverdrups. To put this flux in context it helps to be reminded that it is about twice that for the Amazon River. Over the course of a year vapor export removes an amount of water equal to that in a 15 cm. thick layer covering the entire Atlantic!

ITS SALT BUDGET

Adopting a 20 Sverdrup export rate for lower limb water and an 0.35 Sverdrup fresh water loss from the Atlantic, it is of interest to see what combination of return flow water could balance the Atlantic's salt budget. As the outgoing lower limb water has a salinity of about 34.9‰ and the outgoing water vapor a salinity of 0.0‰, the aggregate salinity of the return flow water must be about 34.3‰ (see figure 11) or 0.6‰ lower than that of the outflowing lower limb water. Thus the salinity contrast between sea water and water vapor is about 60 times larger than the salinity contrast between the waters being traded between the Atlantic and the remainder of the ocean! It is for this reason that a measly 0.35 Sverdrup vapor loss can drive a mighty 20 Sverdrup ocean current! It should be kept in mind in this regard that were the salt buildup to go uncompensated, the salinity of the entire Atlantic would increase at the rate of about 1.4 gm/liter per millennium. As we shall see below, the conveyor appears to have been running more or less as it does today for the last 9000 years. Had the salt buildup not been compensated, the Atlantic's salinity would have increased during that time by a staggering 13‰. Clearly this can not have been the case. Rather, on the average over this period of time the export of salt via the conveyor's lower limb must have balanced the enrichment of salt by vapor loss.

The "remainder water," which feeds the upper limb of the Atlantic, has three components; Antarctic surface waters passing through the Drake Passage ($S \cong 33.8‰$), Indian surface water passing around the tip of Africa via the Agulhas Current ($S \cong 35.1‰$) and intermediate waters formed at the northern perimeter of the Atlantic segment of the Antarctic ($S \cong 34.3‰$). The salinity of the intermediate water matches that required to achieve salt balance. However this salinity could also be achieved by mixing 1.6 parts Drake Passage surface water with 1 part Agulhas water. So, based on salinity alone it is not possible to say how much of the remainder water enters the South Atlantic at intermediate depth and how much enters at the surface.

A rough idea of the proportions of intermediate water on one hand and the Drake-Agulhas mix on the other can be obtained by invoking another constraint, namely, that the element phosphorus be conserved within the Atlantic. The reason is that the residence time of phosphorus in the ocean (several tens of thousands of years) is roughly 100 times the residence time of water in the Atlantic (several hundreds of years). Hence, there can be no significant gain or loss of phosphorus during a single ventilation cycle; in other words, the phosphorus contained in the exported water must match that contained in the imported water. Before employing this constraint I must point out that it has a possible flaw. While we assume in our calculations that phosphorus is transported only in inorganic form (i.e., PO_4), the finding by Suzuki, et al.,1985, that sizable amounts of organic nitrogen are contained in low nutrient surface waters, opens the possibility that phosphorus is contained in the large molecules or fine particles thought to carry the organic nitrogen. If phosphorus is being shuttled back and forth between organic and inorganic forms, then the constraint suggested here becomes invalid.

The phosphorus constraint stems from the fact that only Agulhas Water carries less PO_4 than outgoing lower limb water; the other contributors to the return flow have 20 to

50% higher phosphate concentrations. Agulhas water carries no PO_4 and Drake Passage water carries about 1.5 μm/kg PO_4; hence the Agulhas-Drake Passage mix required to yield the right salinity (1 part to 1.6 parts) carries about 0.9 μm/kg. Intermediate water carries about 1.8 μm/kg of PO_4. Hence to match the 1.3 μm/kg of PO_4 carried by the outgoing lower limb water requires a mix of about 56% Agulhas-Drake Passage component and about 44% intermediate water. This then suggests that the 15.35 Sverdrups of remainder water is made up of 6.7 Sverdrups intermediate water, 5.3 Sverdrups of Drake Passage water and 3.3. Sverdrups of Agulhas water. However because of the many simplifications required in order to make this calculation, these fluxes must be taken with a grain of salt (and perhaps also a dram of phosphorus).

ITS BENEFITS

The benefit provided by the conveyor is the heat it releases to the atmosphere over the northern Atlantic. This heat is responsible for Europe's surprisingly mild winters. The amount of heat released to the atmosphere is given by the product of the conveyor's flux and the temperature change required to convert upper limb water to lower limb water (i.e., to create NADW). The temperature of NADW averages about 3°C. As will be shown below, the temperature of the upper limb water averages about 10°C. Thus each cubic centimeter of upper limb water releases 7 calories of heat to the atmosphere during its conversion to deep water. At an average flux of 20 Sverdrups this totals 4×10^{21} calories each year, an amount of heat equal to 35% of that received from Sun by the Atlantic north of 40° latitude!

Manabe and Stauffer (1988) have shown that indeed the thermohaline circulation of the Atlantic maintains high surface water temperatures in the northern Atlantic. Using the GFDL ocean GCM, they demonstrate that circulation in the Atlantic can assume two quite different modes; one with a strong thermohaline component akin to the conveyor and one

with no thermohaline circulation. The difference between surface water temperatures maintained by these modes is shown in figure 12. As can be seen when the conveyor is operative, the temperature of surface waters in the northern Atlantic average 5°C warmer than when it is off. Considering that strength of the thermohaline circulation in the Manabe and Stauffers' conveyor-on mode is only 12 Sverdrups, this warming should be even greater in the real ocean with its 20 Sverdrup thermohaline circulation.

Rind et al., (1986) have used the GISS atmospheric GCM to estimate the geographical pattern of the winter air temperature change supported by the conveyors heat output. They adopted for the surface water temperature difference between the conveyor-on and conveyor-off modes that reconstructed by the CLIMAP group for glacial surface water relative to today's. As shown in figure 13, the air temperature anomaly obtained in this way extends across Europe into Siberia. As we will discuss below this geographic pattern matches very nicely that for the Younger Dryas cooling.

Now let us return to the problem of estimating the temperature of the upper limb water supplying deep water formation in the northern Atlantic. The major supplier of water to the region of deep water formation is the Gulf Stream. As the roots of this great current extend to a depth of 1500 or so meters, the properties of the water supplied to the NADW source region depend strongly on the depth at which the major transport takes place. A large contrast exists between the water from depths of less than 500 meters and water from depths of greater 800 meters (see figure 14). For example, the upper waters have too high a salinity and the deep waters too low a salinity to match that needed to generate NADW. As summarized in figure 15, when the inputs into the northern region of low salinity Bering Sea water and of fresh water (through river runoff and the excess of precipitation over evaporation) are taken into account the salinity of the aggregate upper limb supply water must be about 35.6‰. This value is intermediate between those for upper and lower

Gulf Stream water. A similar situation exists for the nutrient constituents phosphate and silica. The deeper portion of the Gulf Stream carries too high concentrations and the upper portion too low concentrations to match that in outgoing NADW. Thus it appears that a mixture of upper and lower Gulf Stream water is required to create the salinity and nutrient content of new NADW.

Radiocarbon provides a crosscheck on this conclusion (see Broecker, in press a). The prenuclear $\Delta^{14}C$ value for new NADW was close to -66‰. The feed water for NADW production should have a value 6‰ more negative than this (i.e., -66 - 6 = -72‰). The reason is that CO_2 exchange with the atmosphere adds more radiocarbon to the source region than is lost by radiodecay during residence in the source region. CO_2 exchange raises the $\Delta^{14}C$ value by 11‰ while radiodecay lowers it by only 5‰. The prenuclear $\Delta^{14}C$ value for Gulf Stream water was about -50‰; and that for lower Gulf stream water about -80‰. In order to obtain the desired input value of -72‰ requires that about 1 part upper Gulf Stream water be mixed with 2 parts thermocline water carried beneath the Gulf Stream. These proportions match reasonably well those required to create the phosphate and silicate contents of new NADW.

While the proportions of upper and lower Gulf Stream water necessary to achieve the salinity nutrient and radiocarbon contents of new NADW are not well defined, the temperature of the input water should lie between that of about 18°C for the upper water and that of about 6°C for the lower water. A 1 parts upper - 2 parts lower water mixture would have a temperature of 10°C.

ITS ACHILLES HEEL

The addition of fresh water to the northern Atlantic poses a constant threat to the conveyor. Northward of 40°N in the Atlantic precipitation and continental runoff exceed evaporation by about 0.30 Sverdrups (Baumgartner and Reichel, 1975). In addition, the 1 Sverdrup of low salinity ($S \cong 33.0‰$) water entering the Arctic arm of the Atlantic through the Bering Straits contributes the equivalent of 0.06 Sverdrups of fresh water bringing the total to 0.36 Sverdrups. When the conveyor is running at its current strength of 20 Sverdrups, this fresh water is efficiently swept away causing only an 0.63‰ reduction in the conveyor water's salinity as it passes through the northern Atlantic. If the conveyor were to progressively weaken, this salinity reduction would grow. It would be 0.94‰ at 15 Sverdrups, 1.26‰ at 10 Sverdrups... At some point the salinity reduction would become so large that deep water could no longer form. The conveyor would shut down. Were this to happen, fresh water would pool at the surface of the northern Atlantic much as it currently does in the northern Pacific creating a severe barrier to deep water formation.

Ocean GCM simulations by Manabe and Stauffer (1988) clearly demonstrates the role of this fresh water input. As shown in figure 12, for the conveyor-off mode pooling of fresh waters reduces the salinity surface waters in the northern Atlantic by about 3‰. Maier Reimer and Mikolajewicz, 1989, using the Hamburg ocean GCM show that a modest dose of excess fresh water to the source region of NADW can kill the model's thermohaline circulation. Furthermore, the demise is abrupt occurring on the time scale of a few decades. The rapidity of this response is not surprising for it depends on the residence time of water in the source region. At a flushing rate of 20 Sverdrups the entire volume of water contained in the Atlantic north of 45°N can be replaced in two decades!

We know of no ocean GCM experiment which shows how the conveyor circulation might be restarted. Because of the strong barrier created by the pooling of fresh water, this

may prove to be a tricky task. Microprocesses such as densification through brine formation beneath sea ice may have to be invoked.

ITS HISTORY

The best indicator of the past operation of the conveyor is the air temperature in the northern Atlantic basin. The reason is that as we have already shown turning on and off the conveyor causes 5 to 8°C changes in the air temperatures over Greenland and Europe. The most detailed record of air temperature in the northern Atlantic basin is the isotope record preserved in the Greenland ice cap. This record (see figures 16 and 17) had different character during the last period of glaciation than during the present period of interglaciation (Dansgaard et al., 1971, Hammer et al., 1985). During glacial time air temperatures over Greenland underwent excursions of the magnitude and abruptness expected if the conveyor were turning on and off on an millennial time scale. By contrast, during the 9 or so thousand years since the period of glaciation came to a close, Greenland's air temperature has remained nearly constant. The impression I get from this is that a frenetic glacial conveyor became firmly locked in the on-position at the beginning of post glacial time and has remained so ever since.

A possible explanation for the behavior of the conveyor during glacial time is that when the northern end of the Atlantic Basin is surrounded by ice sheets, stable operation of Atlantic's circulation system is not possible (Broecker, et al., 1990b). Rather, because the ice sheets constitute a tremendous source of fresh water, circulation in the Atlantic tends to flip back and forth between the conveyor-on and conveyor-off modes.. When the conveyor is operative its heat output tends to melt back the ice releasing large amounts of fresh water to the Atlantic. The conveyor also efficiently exports excess salt from the Atlantic. The combination of meltwater dilution and salt export drives down the density of waters in the Atlantic until the point is reached where the conveyor can no longer function.

It goes off. With the conveyor inoperative, the export of salt and the dilution with meltwater are reduced to the point where water vapor export once again begins to enrich salt in the Atlantic. The salt content and hence also the density of Atlantic waters steadily rise until the conveyor turns on again. This cycle repeats over and over again.

Although a rigorous demonstration that such an oscillator did operate is not possible, the facts we do have lend strong support to this scenario. First of all, we know that the 40 million cubic kilometers of excess ice present in the ice sheets of the northern hemisphere during peak glacial time began to melt about 13,000 years ago and was gone by about 8000 years ago. Thus the average flux of meltwater during this interval must have been about 0.25 Sverdrups. Assuming this to be the magnitude of the melting rate during the proposed conveyor-on episodes then the dilution of salt due to meltwater would have been comparable to today's rate of vapor export. If the assumption is made that then as now the conveyor was exporting salt at a rate comparable to the rate it was being enriched through vapor export, then during the conveyor-on episodes, salt would have been diluted at a rate corresponding to the input of meltwater. When the conveyor was off the dominant important term in the salt budget would be vapor export. As yet we do not have an adequate estimate of the rate of water vapor export in the presence of an ice sheet. However, since vapor export is dictated by the interaction of planetary winds with mountain ranges, the rate may not have been very different from today's.

Additional support comes from the observation that the average duration of individual warm and cold episodes recorded in Greenland ice ranges from about one half to two millennia. This spacing is consistent with that expected from the salt oscillation hypothesis. A vapor loss of 0.35 Sverdrups removes a layer 15 cm thick from the Atlantic each year. If uncompensated by salt export, the salt content of Atlantic waters will rise 1.4 gm/liter per millennium! As a salt buildup or reduction of 1 to 2 gm/liter for the Atlantic is

about what is needed to tip the balance between conveyor-on and conveyor-off, a match exists between the observed timing and that predicted timing (Birchfield and Broecker, 1990). This is a strong point in favor of the oscillator hypothesis!

For an oscillator to function requires a combination of a long time constant drift (in this case the buildup or drawdown of salt) and a short time constant stablization mechanism. In the previous section it was shown that a tendency exists for fresh water to pool at the surface of the northern Atlantic. When the conveyor comes on this pool is quickly destroyed raising the salinity in NADW source region. This stabilizes the conveyor in its on-position. Similarly when the conveyor stops the pool quickly reappears stabilizing the conveyor in its off position.

As can be seen in figure 17, many of the Greenland temperature cycles are characterized by abrupt warmings followed by more gradual coolings. The salt oscillator hypothesis provides a natural explanation for this shape (see Broecker, in press b). The abrupt warmings are caused by turn-ons of the conveyor. Immediately following such a reinitiation, the conveyor runs with extra vigor. The reason is that in order to overcome the fresh water pool present in the northern Atlantic when the conveyor is inoperative, the salinity of the Atlantic would have to rise above the level required for steady state operation. Thus when the conveyor comes on the buoyancy contrast between deep water formed in the northern Atlantic and deep water present in the remainder of the ocean will be unusually large. This excess density will drive the conveyor at an unusually high rate. As a consequence, a greater amount of heat will be released to the atmosphere over the north Atlantic. However, once operative, the conveyor's strength will steadily wane. The reason is that the combination of dilution with meltwater and export of excess salt will lessen the buoyancy contrast between deep waters inside and outside the Atlantic. As the strength of the conveyor wanes, the amount of heat given off to the atmosphere over the

northern Atlantic will also decrease causing air temperatures to drop. Eventually the conveyor will shut down abruptly cutting off the supply of ocean heat. The atmospheric temperature cycle generated in this way resembles that seen in the ice core record (see figure 18).

Only for the most recent of these cycles do we have sufficient auxiliary evidence to add muscle to this scenario. The abrupt warmings at about 12,700 and at about 10,000 radiocarbon years ago, provide smoking guns in this regard. Not only the oxygen isotope record in ice cores (Dansgaard, et al., 1989) but also that in lake sediments on the European continent (Lötter and Zbinden, 1989) demonstrate that both of these warmings were accomplished in only 50 years! Further, the geographic pattern of these temperature changes associated with Younger Dryas is as expected if they were caused by conveyor turn ons. Pronounced changes are confined to latitudes greater than 40°N and extend from the maritime provinces of Canada and the ice cap of Greenland on the west across the northern Atlantic, the British Isles and Scandinavia into Russia on the east (see Rind, et al., 1986 for summary). Finally, Boyle and Keigwin 1987, have shown based on carbon isotope and cadmium concentration measurements on benthic foraminifera shells from a deep sea core from the vicinity of Bermuda that water of Antarctic origin flooded the western basin of deep Atlantic during Younger Dryas time, confirming that a shutdown of deep water formation accompanied this cold event.

ITS FUTURE

When the Natural History article containing the great global conveyor belt diagram appeared, the editor put a sales "stimulator" on the cover which stated "Europe beware: the big chill may be coming." At the time I was much annoyed because no mention of the conveyor's future was made in the article. To make matters worse, even after reading the article itself, many people were left with the impression that I was warning of an imminent

conveyor shutdown. The fact is that at that time I thought that the coming greenhouse warming would, if anything, strengthen the conveyor by increasing the rate of vapor loss from the Atlantic Basin. I had not given serious thought to the question as to whether any changes associated with man's activities might threaten the conveyor.

The first activity which comes to mind in this regard is the rerouting of water for agricultural use. Irrigation projects increase the recycling of water on the continents and thereby change the point at which a given water molecule reenters the ocean. Of particular interest in this regard is the Russian proposal to divert the great northward flowing Siberian Rivers to the south for agricultural use. The result of such a diversion would be to increase the vapor loss from the Atlantic Basin for instead of flowing out of river mouths into the Arctic, the water would move through the atmosphere across Asia into the Pacific Basin. The longterm result would be to strengthen the conveyor.

In addition to increasing vapor export from the Atlantic Basin, the greenhouse warming will increase the transport of fresh water to the northern Atlantic. On the short term (i.e. decades), the salinity decrease created in northern surface waters would be more important than the Atlantic-wide salinity increase caused by increased vapor loss from the Atlantic Basin. The reason is that the replacement time for waters in the northern Atlantic is shorter than the replacement time for waters in the upper limb of the conveyor. So if a threat to the conveyor is in the making, it is most likely to come in this way. To be on guard we should pay close attention to the climate and oceanography of the northern Atlantic Basin. The finding by Brewer et al., 1983 that the salinity of Atlantic deep waters to the north of 50°N declined between 1972 and 1981 and the finding by Schlosser et al., 1991 that deep ventilation of the Greenland Sea was shutdown during the 1980's are indications that changes do occur. Unfortunately we have no way to tell whether these changes signal natural fluctuations or anthropogenically driven trends.

CONCLUSIONS

The conveyor is only one of many elements which together constitute the Earth's climatic system. It stands out because of its dramatic impact on the climate of a single region on our planet. We must keep in mind however, that the abrupt global warmings which heralded the termination of the last major glaciation can certainly not be explained by the conveyor alone (Broecker and Denton, 1989, 1990). Rather, elements of the system, such as the Hadley cell, which influence cloudiness and atmospheric water vapor content must also have been involved. The challenge of the Global Change Research Initiative is to understand the complex web of interactions which tie together the operation of these diverse elements.

ACKNOWLEDGEMENTS

I would like to thank the Exxon Corporation and Livermore National Laboratory for their generous support of my research. Instead of requiring me to write long proposals and reports, they encourage me instead to put this effort into articles such as this. My research on ocean chemistry is supported by DOE's CO_2 program grant no. LLNL B130547; that on the climate history of the Atlantic by NSF Climate Dynamics grant no. ATM 89-21306 and by NOAA grant no. NA90-AA-D-AC520; and that on atmospheric vapor transport by EPRI grant RP 2333-6.

Table 1. Example of radiocarbon deficiency calculation

GEOSECS STATION 113 (11°N, 20°W, 4741m)

O_2 µm/kg	PO_4 µm/kg	$\Delta^{14}C$ ‰
239	0.91	-120

$$PO_4^* = \frac{O_2}{175} + PO_4 - 195$$
$$= \frac{239}{175} + 0.91 - 1.95$$
$$= 0.91 \text{ µm/kg}$$

$$\text{frac. no. comp.} = \frac{1.67 - PO_4^*}{1.67 - 0.73} = \frac{1.67 - 0.91}{1.67 - 0.73}$$
$$= 0.81$$

$$\text{frac. so. comp.} = 1 - 0.81$$
$$= 0.19$$

$$\Delta^{14}C_{initial} = 0.81(-68) + 0.19(-158)$$
$$= -84‰$$

$$\Delta\Delta^{14}C = \Delta^{14}C_{initial} - \Delta^{14}C_{measured}$$
$$= (-84) - (-120)$$
$$= 36‰$$

$$\text{apparent age} = 36‰ \times 8.27 \text{ yr/‰}$$
$$\cong 300 \text{ years}$$

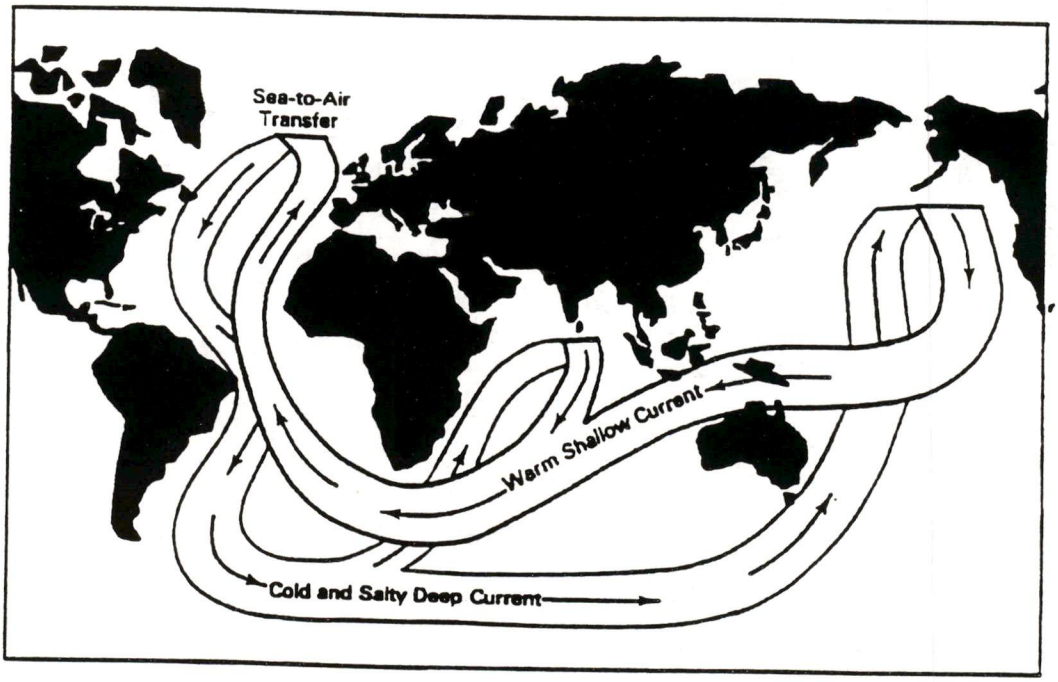


Figure 1. The great ocean conveyor logo (Broecker, 1987).

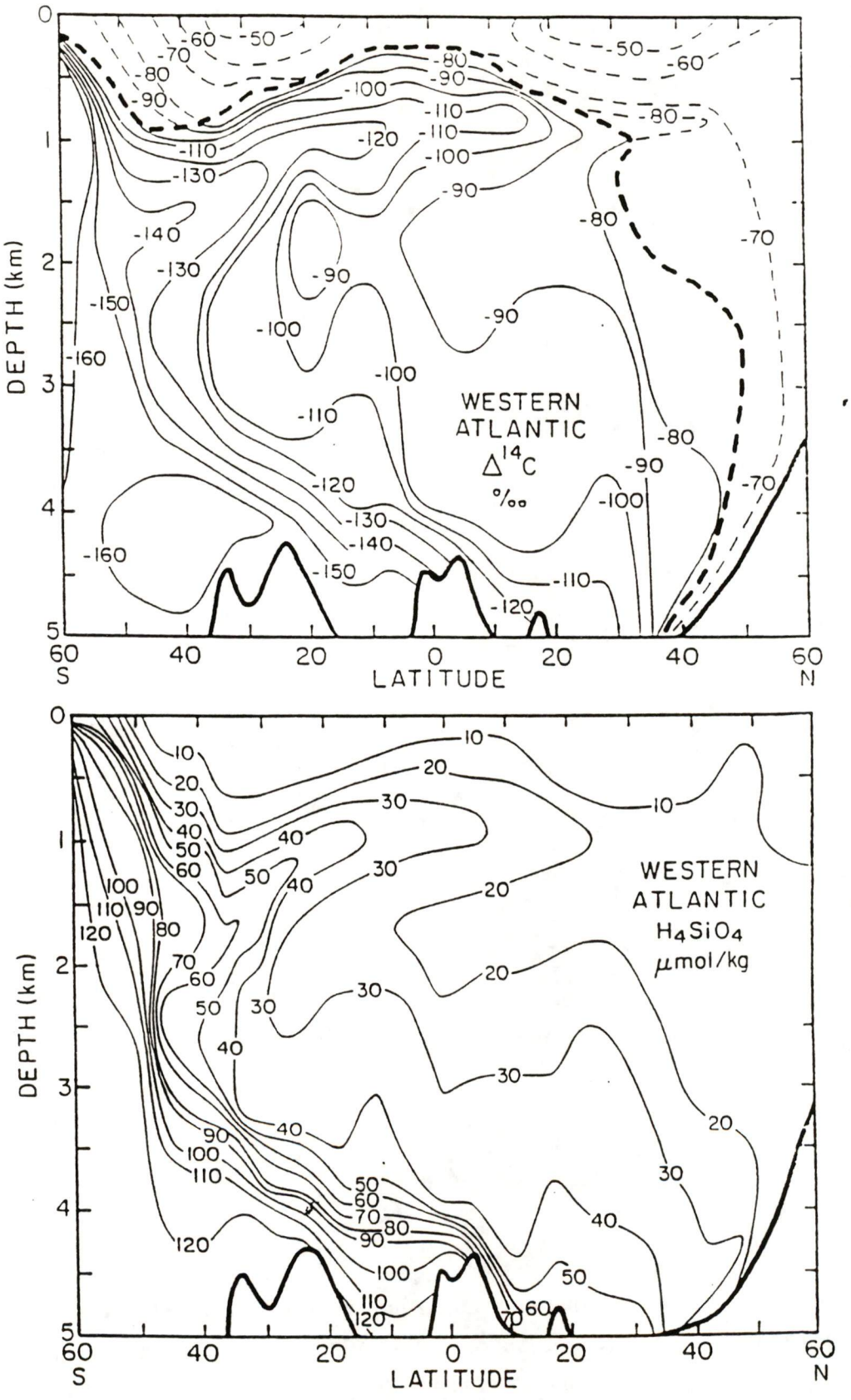
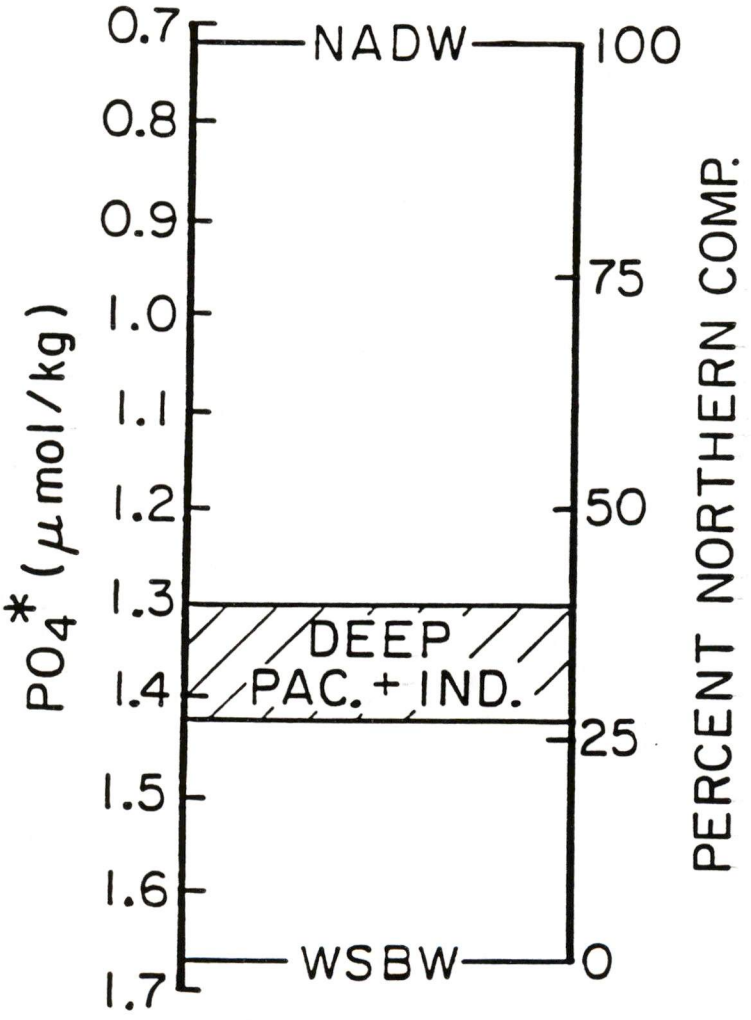


Figure 2. Sections of radiocarbon and of dissolved silicate in the western Atlantic based on measurements made as part of the GEOSECS program. In both the North Atlantic Deep Water clearly stands out from the over and underlying waters of Antarctic origin. The intermediate and bottom waters which enter the Atlantic from the Antarctic have higher in silica concentrations and lower $^{14}C/C$ ratios than the NADW which constitutes the conveyor's lower limb.



$$PO_4^* = PO_4 + \frac{O_2}{175} - 1.95$$

Figure 3. Nomogram showing the relationship between PO_4^* value (Broecker, et al., 1991a) and the percentage contribution of NADW to waters in the deep sea mix. Deep waters formed in the northern Atlantic have nearly uniform low PO_4^* values (0.73 ± 0.03 μm/kg). Those which form around the Antarctic continent have high values (between 1.6 and 1.7 μm/kg). Bottom water formed in the Weddell Sea (WSBW) has a PO_4^* value close to 1.67 μm/kg. The deep Pacific and Indian Oceans are flooded with a nearly uniform mix of these two end members (33% NADW + 67% WSBW).

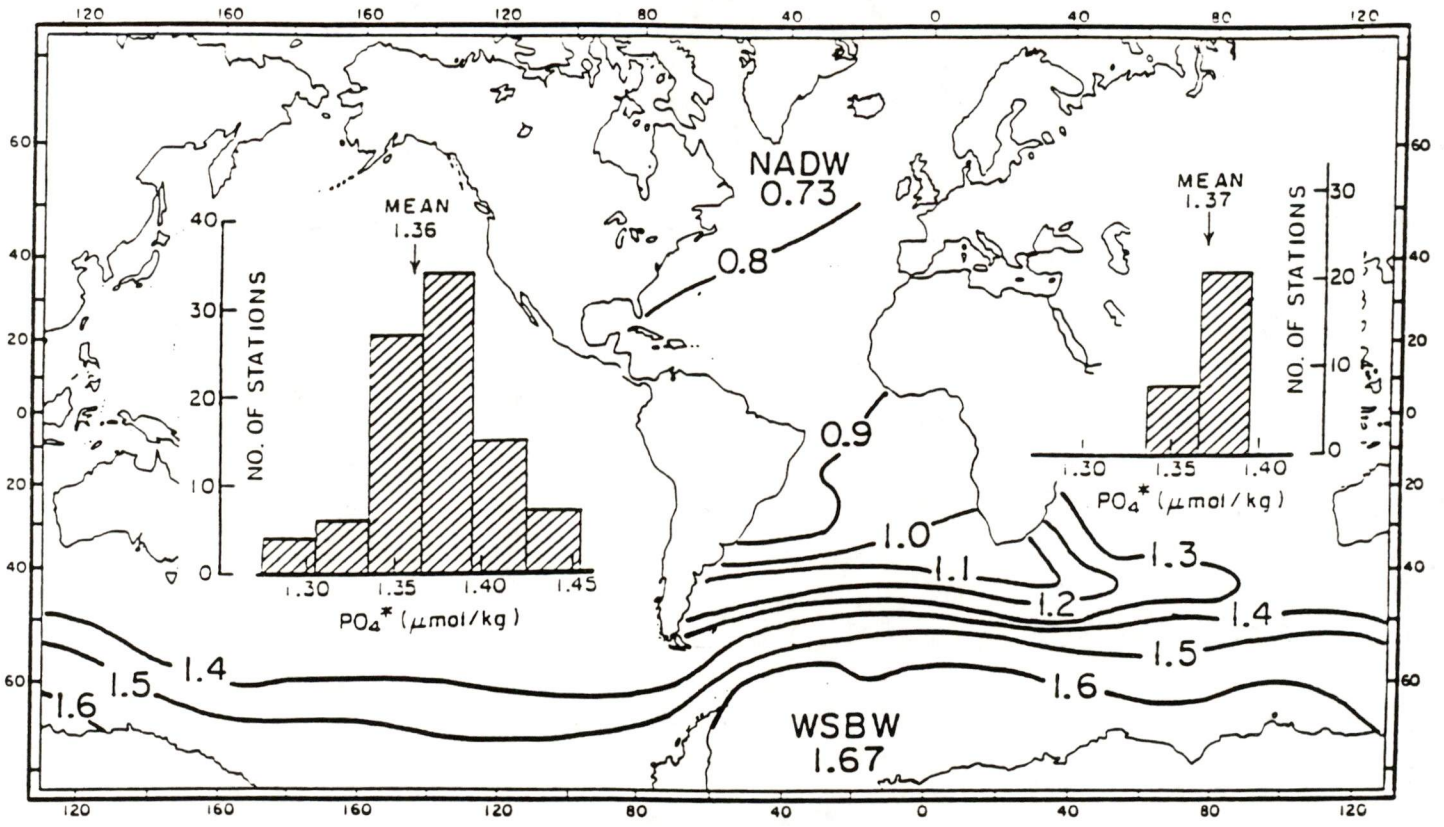


Figure 4. Map of PO_4^* values at 3 kilometers depth. The deep water source in the northern Atlantic has a PO_4^* value of 0.73 μm/kg. and that in the Antarctic a value of about 1.67μm/kg. As shown by the histograms, waters on this depth horizon in the Indian and Pacific Oceans have nearly constant PO_4^* values. Although the Pacific GEOSECS stations shows a range of PO_4^* values, the lack of geographic coherence suggests that this spread is the result of station to station shifts in the calibration of the nutrient analyses system.

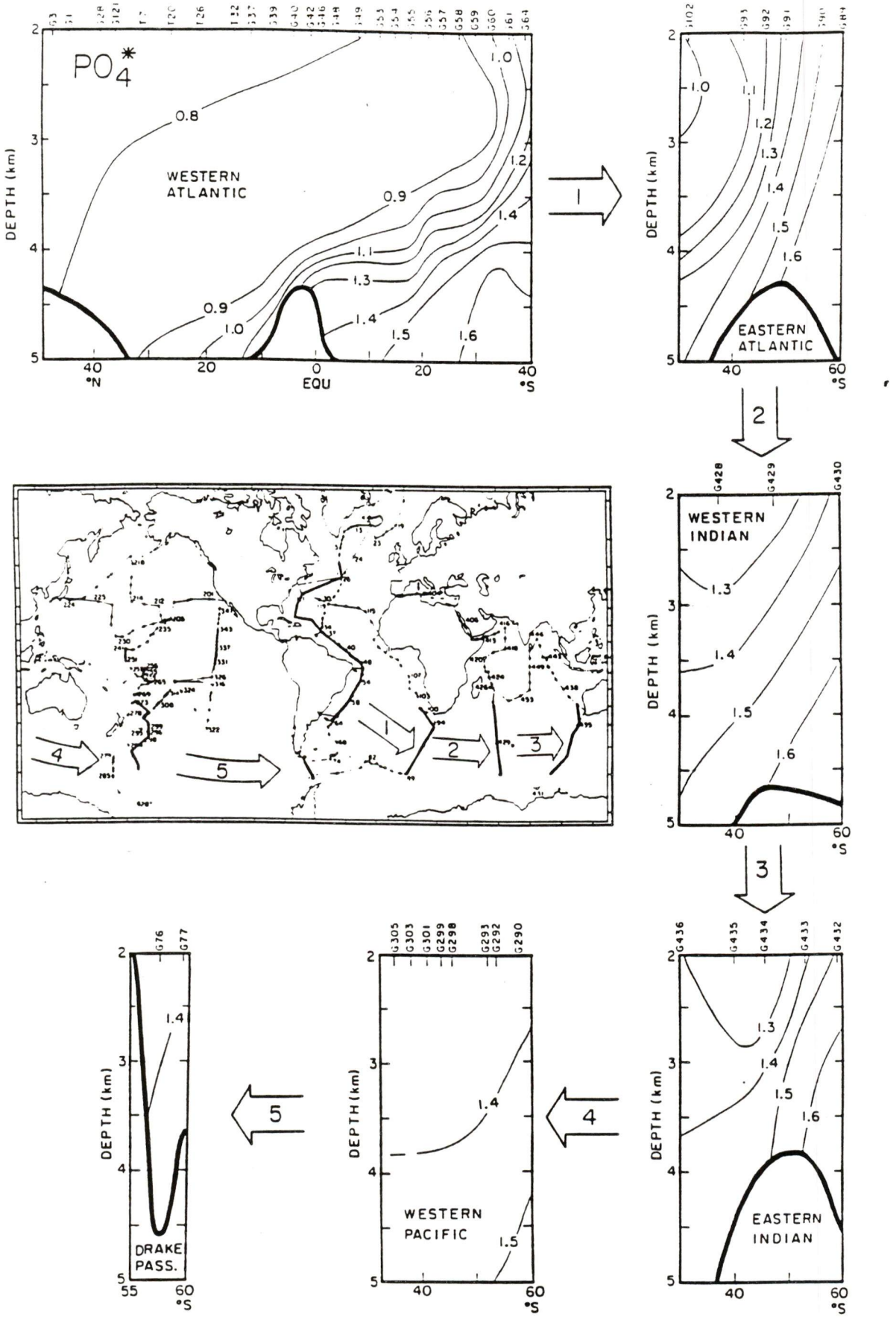


Figure 5. Sections of PO_4^* down the western basin of the Atlantic and around the Southern Ocean. The map shows the location of the GEOSECS stations and of the sections. Note how the <1.3 μm/kg and the >1.6 μm/kg waters blend as they move around the Antarctic continent eventually producing a nearly uniform mix with a PO_4^* value close to 1.4 μm/kg.

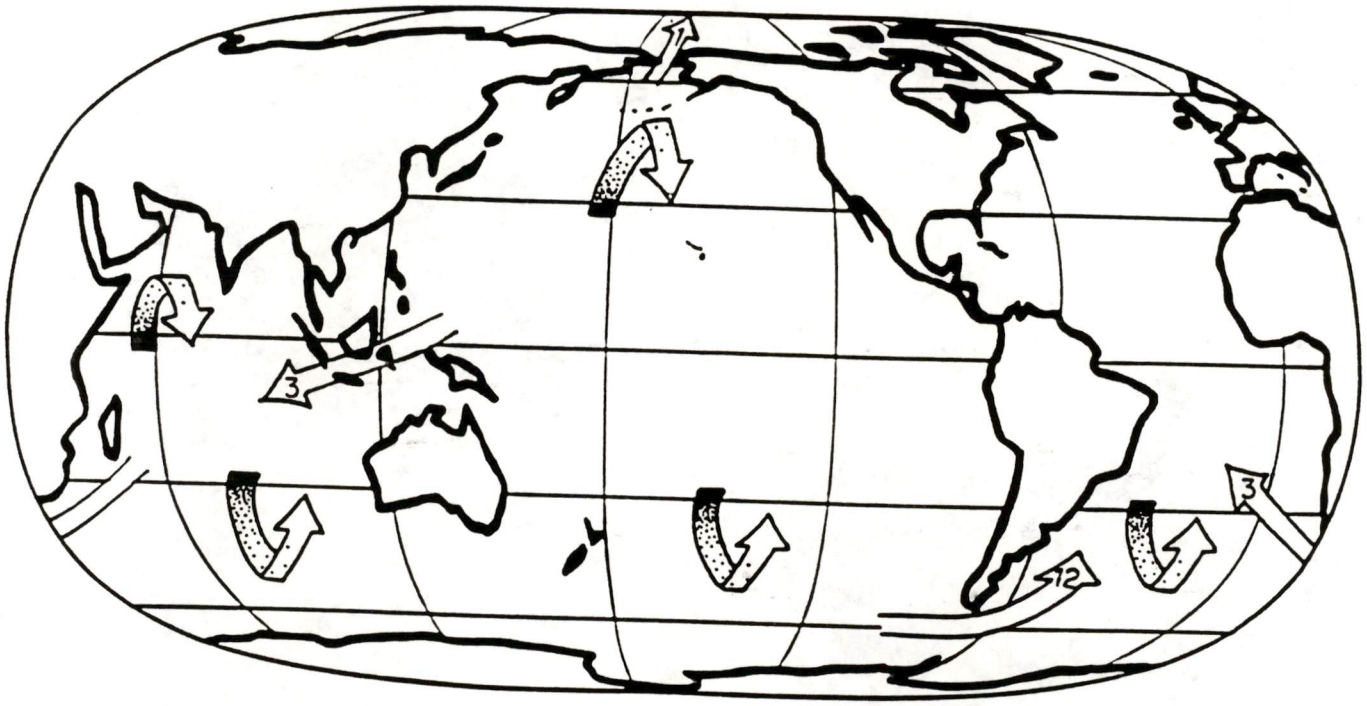


Figure 6. The dotted arrows show the location where intense upwelling of deep water occurs. The clear arrows show the upper ocean routes of return flow which balance the outflow from the Atlantic of lower limb water. The numbers in the arrowheads represent the rough estimates of the magnitude of the fluxes (in Sverdrups). In addition to the features portrayed by the logo, this diagram shows that much of the upwelling occurs in the Antarctic and that much of the return flow occurs through Drake Passage.

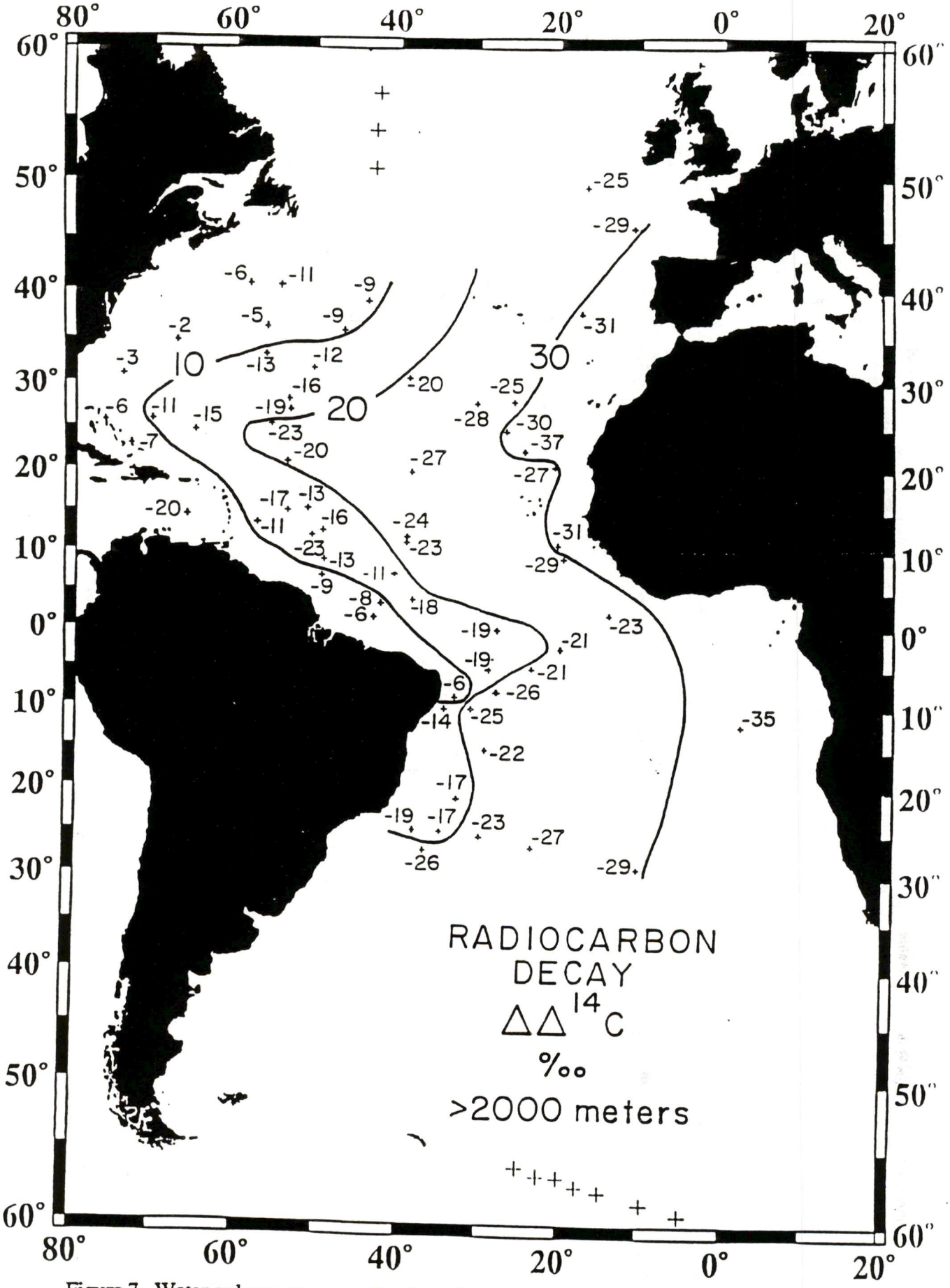


Figure 7. Water column averages for the radiodecay induced ^{14}C deficiency (Broecker, et al., 1991a) at stations occupied during the GEOSECS, TTO, TAS and SAVE expeditions. The major gradient is from low deficiencies along the western margin to high deficiencies along the eastern margin. The residence times corresponding to the 10, 20 and 30‰ deficiency contours are respectively 83, 166 and 249 years. The mean deficiency for this entire region of the Atlantic is estimated to be 22‰ which corresponds to an isolation time of about 180 years.

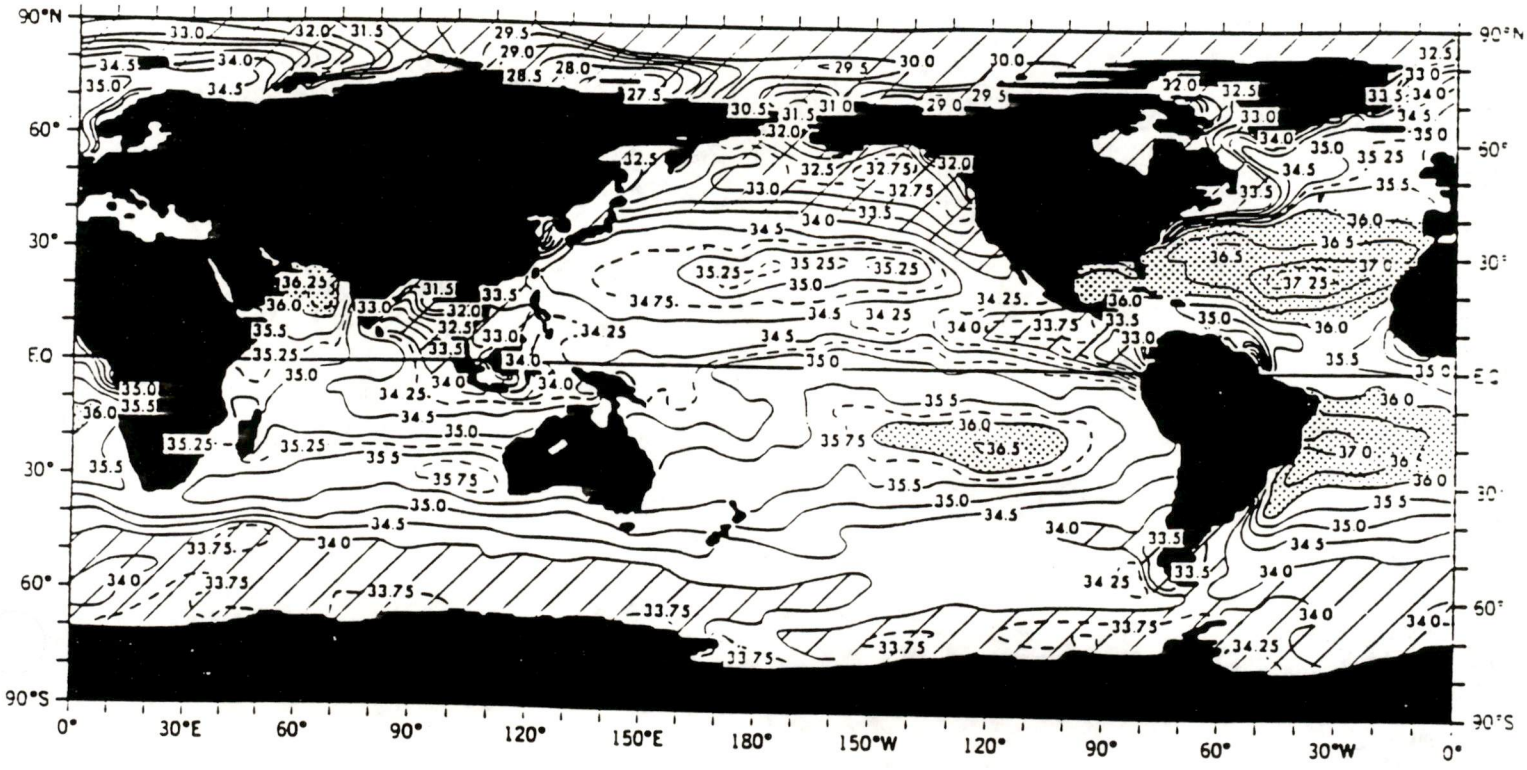


Figure 8. Map of surface ocean salinity (Levitus, 1982). Regions of low salinity (i.e. S<34‰) are cross hatched. Regions of high salinity (i.e. S > 36‰) are dotted. Note that on the average surface waters in the Atlantic are about 1‰ higher in salinity that their Pacific counterparts. For the high northern latitudes the difference is even larger averaging about 2‰.

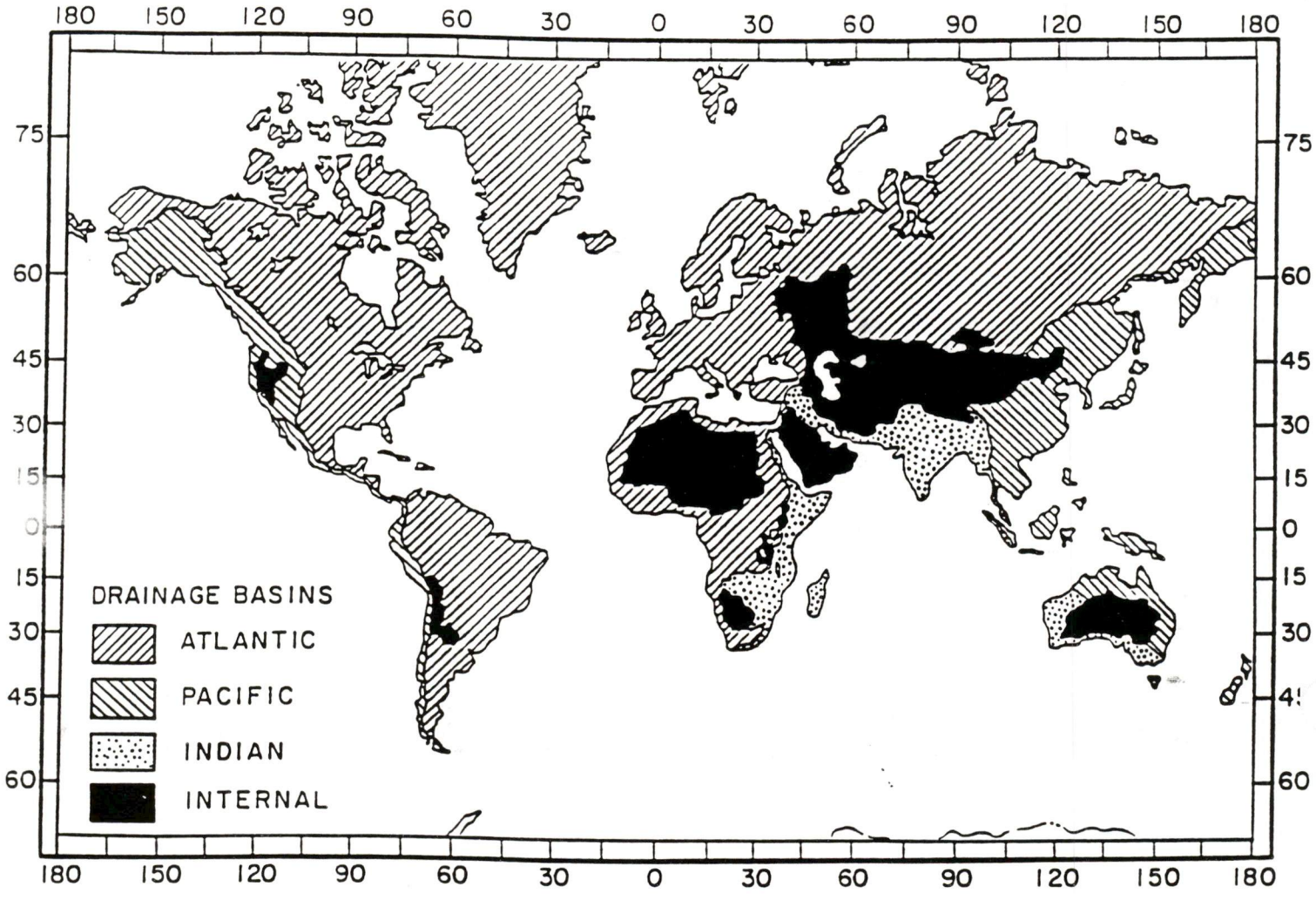


Figure 9. Map showing continental areas whose drainage reaches the Atlantic, Pacific and Indian Oceans. The black areas are deserts from which no drainage to the sea occurs. About 0.35 Sverdrups of fresh water are transported from the Atlantic to the Pacific Ocean moving as vapor in part across Central America and in part across Africa.

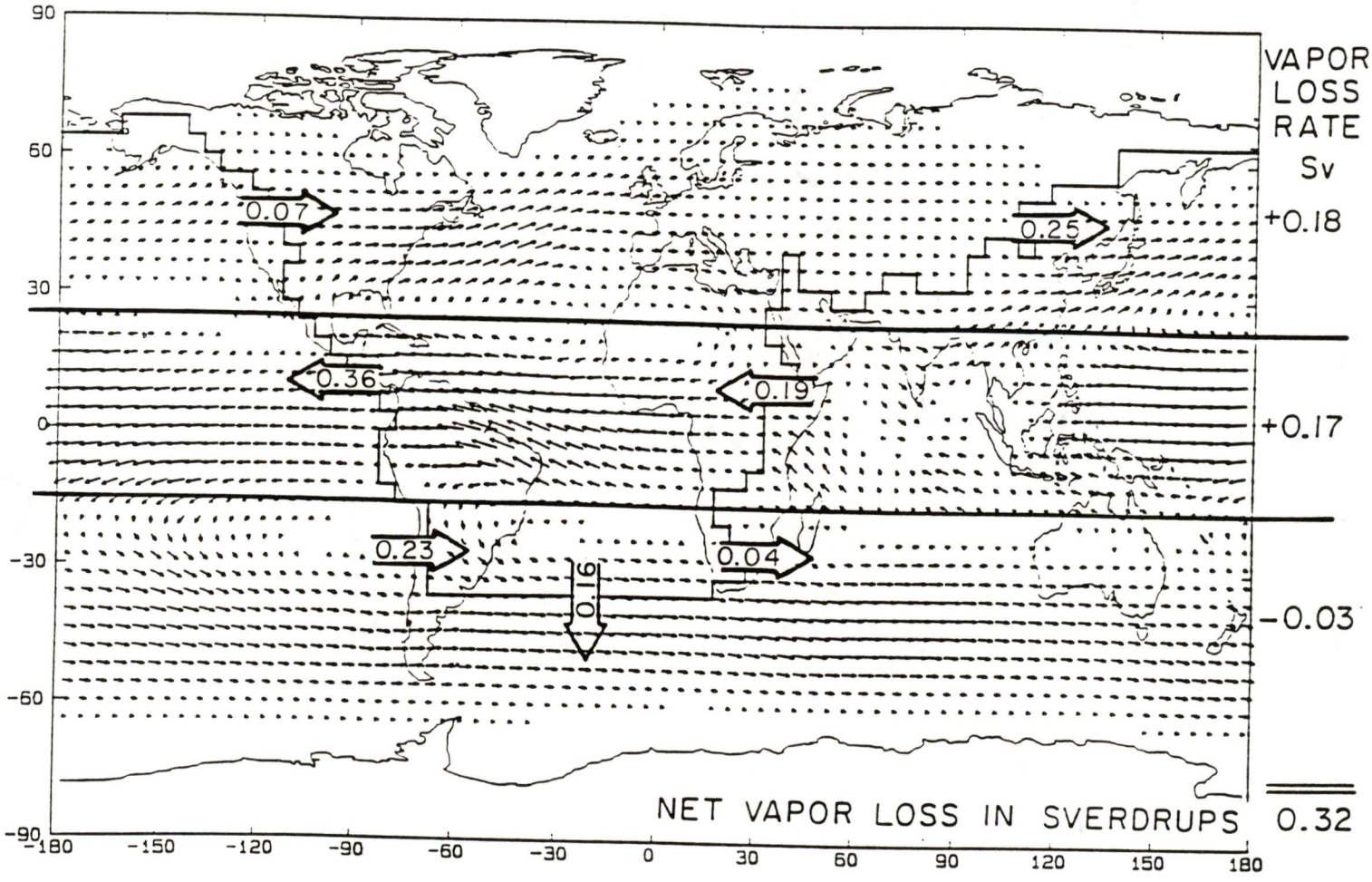
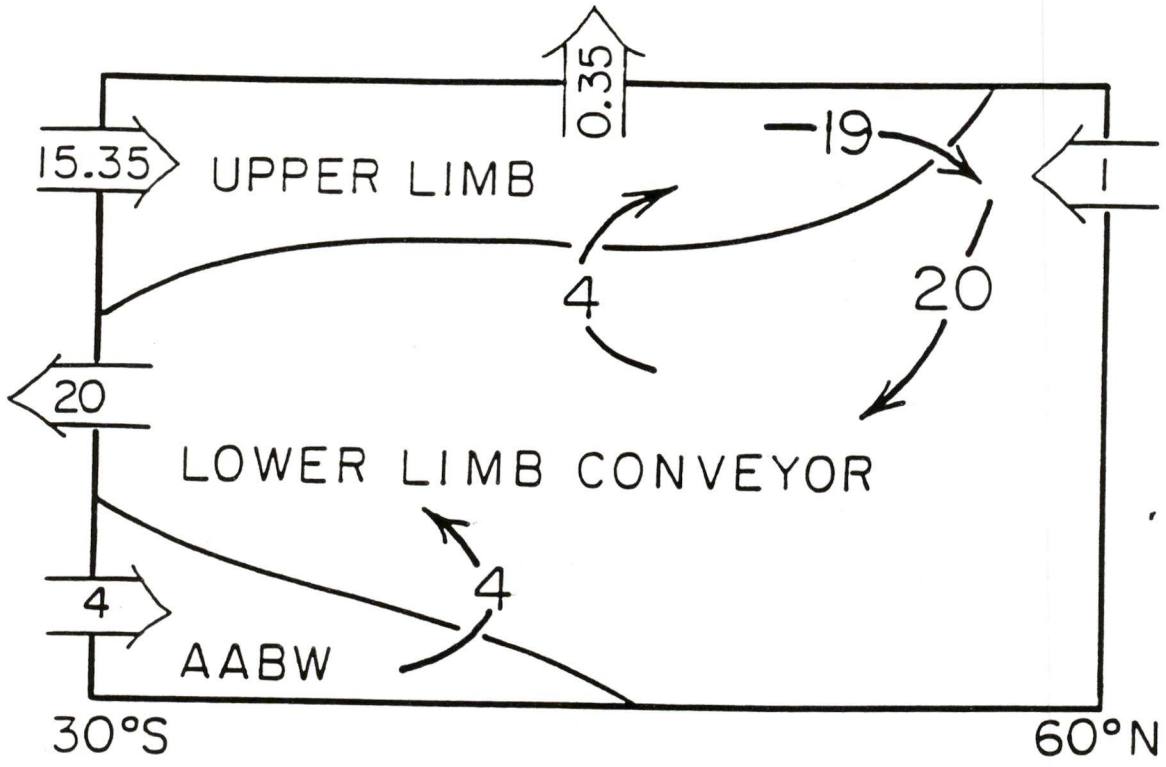


Figure 10. Map showing vertically integrated and annually average water vapor flux vectors compiled by Oort (1983). Also shown is the boundary of the Atlantic's drainage basin and net fluxes across segments of this boundary. The tropical easterlies carry out more water vapor of the Atlantic basin across Central America than they bring in via Africa. So also do the northern westerlies; more water escapes across Asia than enters across the American cordilera. For the entire basin the rate of water vapor loss is 0.32 Sverdrups (see Zaucker and Broecker, in press).



ATLANTIC'S SALT BUDGET

	SALINITY ‰	FLUX Sv
OUT		
NADW	34.9	20.0
VAPOR	0.0	0.35
TOTAL	34.3	20.35
IN		
BERING STS	33.0	1.0
AABW	34.7	4.0
REMAINDER	34.3	15.35
TOTAL	34.3	20.35

Figure 11. Approximate water and salt budget for the Atlantic Ocean. The fluxes of Bering Sea surface water and of AABW are independently determined. The remainder water must then have a flux of 19.35 minus the amount of NADW recirculated within the Atlantic. With the guess of 4 Sverdrups recirculation adopted here the remainder water flux becomes 15.35 Sverdrups. The aggregate return water must have a salinity of 34.3‰ to balance the Atlantic's salt budget. Since the combined Bering Sea (Coachman and Aagaard, 1988)and AABW inputs have a salinity of 34.3‰, the remainder water must also have this salinity.

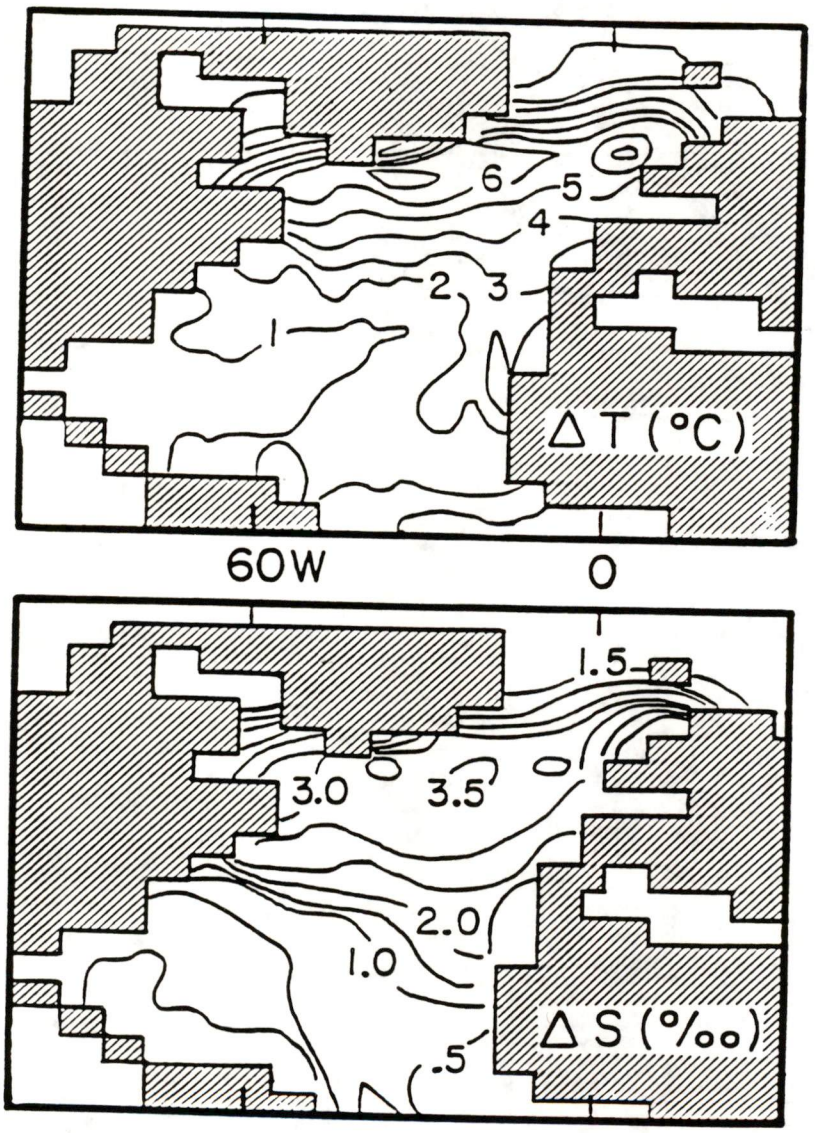


Figure 12. Maps showing the difference in North Atlantic surface water temperature (upper) and surface water salinity (lower) between the Manabe and Stauffer (1988) model circulation schemes with and without thermohaline circulation. As can be seen, a turnoff of thermohaline circulation leads to a pronounced cooling and freshening of the waters in the northern Atlantic.

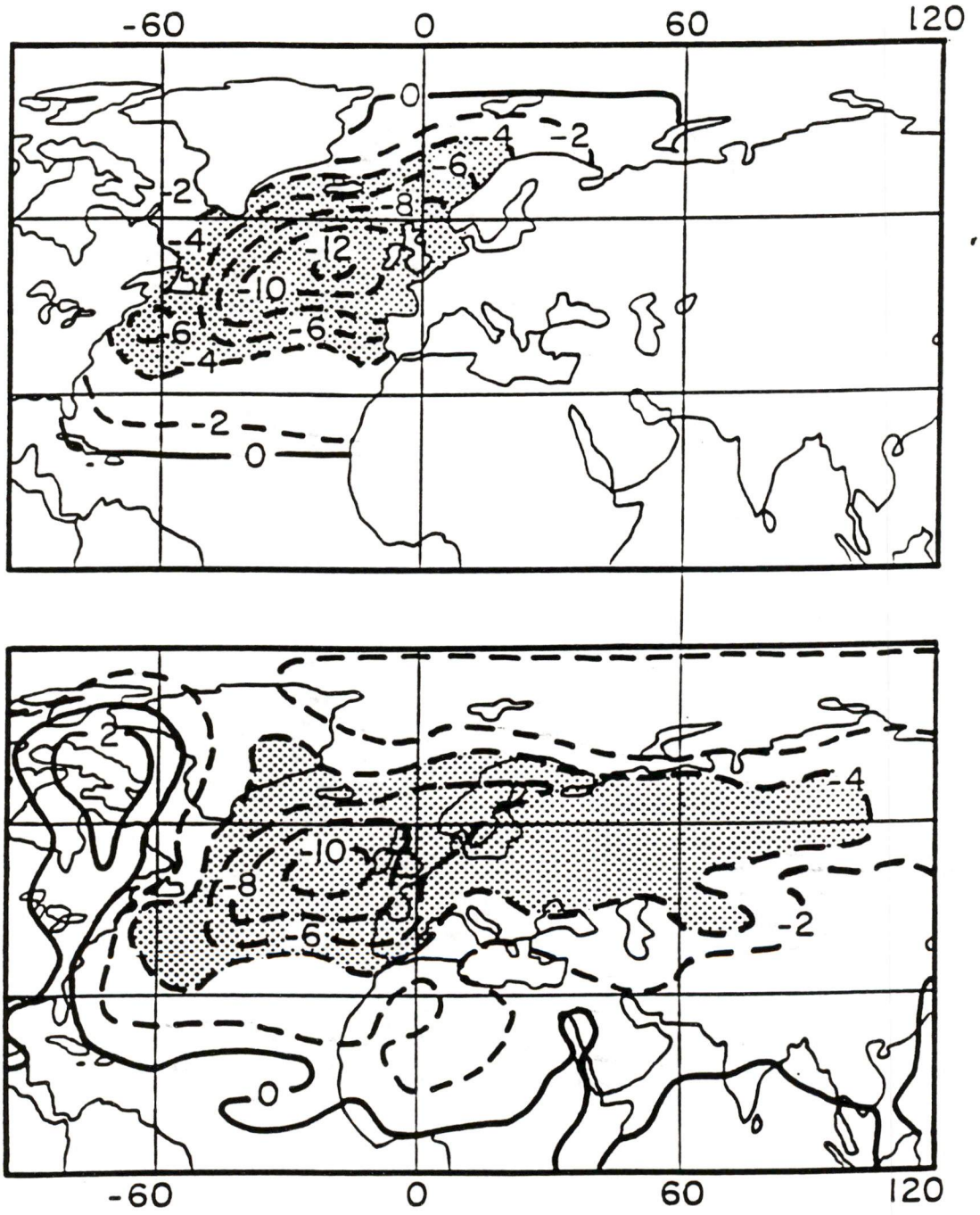


Figure 13. Results of an experiment carried out using the GISS atmospheric GCM (Rind et. al, 1986). Two runs were made which differed only in the surface ocean temperature assigned to the northern Atlantic (see upper panel). The resulting winter air temperature change produced by this ocean temperature change is shown in the lower panel.

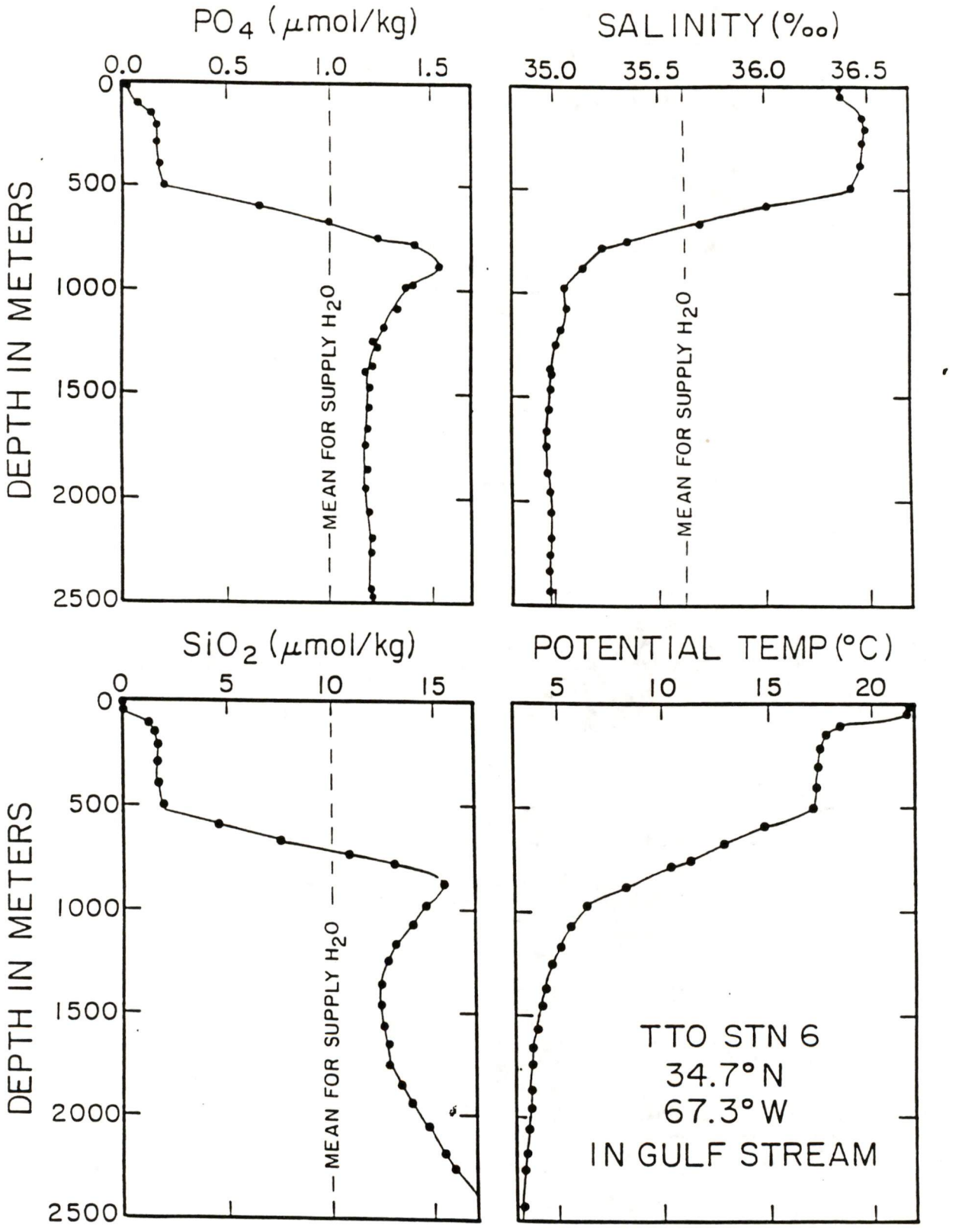
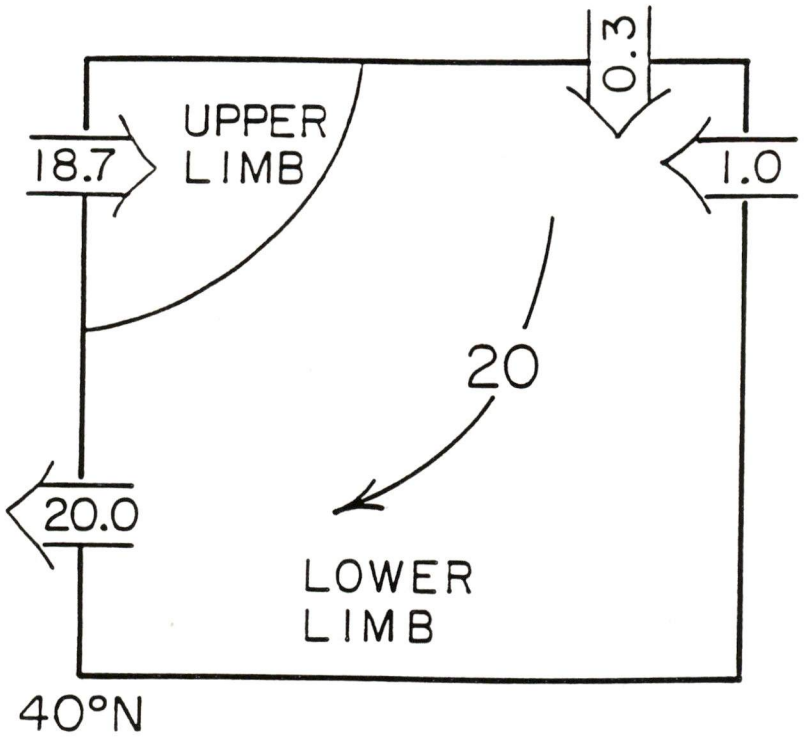


Figure 14. Phosphate, silica, salinity and potential temperature profiles at TTO station 6 in the Gulf Stream. Shown for comparison are the average values for these constituents required for the water constituting the upper limb source for NADW production (vertical dashed line).



NORTHERN ATLANTIC'S SALT BUDGET

		SALINITY ‰	FLUX Sv
OUT			
	NADW	34.95	20.0
	TOTAL	34.95	20.0
IN			
	BERING STS	33.0	1.0
	VAPOR	0.0	0.3
	UPPER LIMB	35.6	18.7
	TOTAL	34.95	20.0

Figure 15. Water and salt budgets for the region in the northern Atlantic where NADW forms. The fluxes and salinities of new NADW, Bering Straits input and fresh water input are known. The water flux and salinity for the upper limb are obtained by difference.

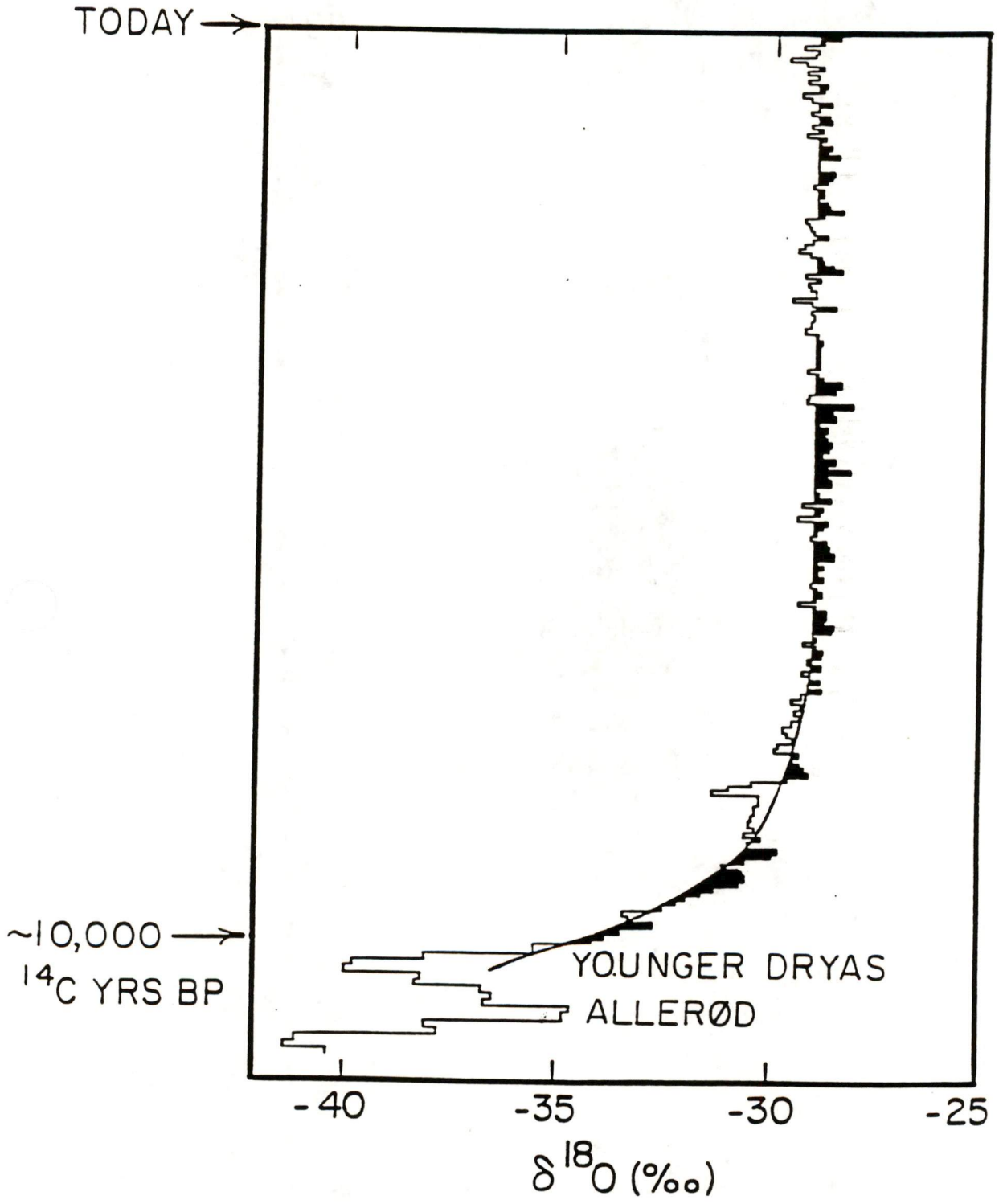


Figure 16. Oxygen isotope record for the Camp Century Greenland ice core (Dansgaard et al., 1971) covering the period from about 13,000 radiocarbon years B.P. to the present.

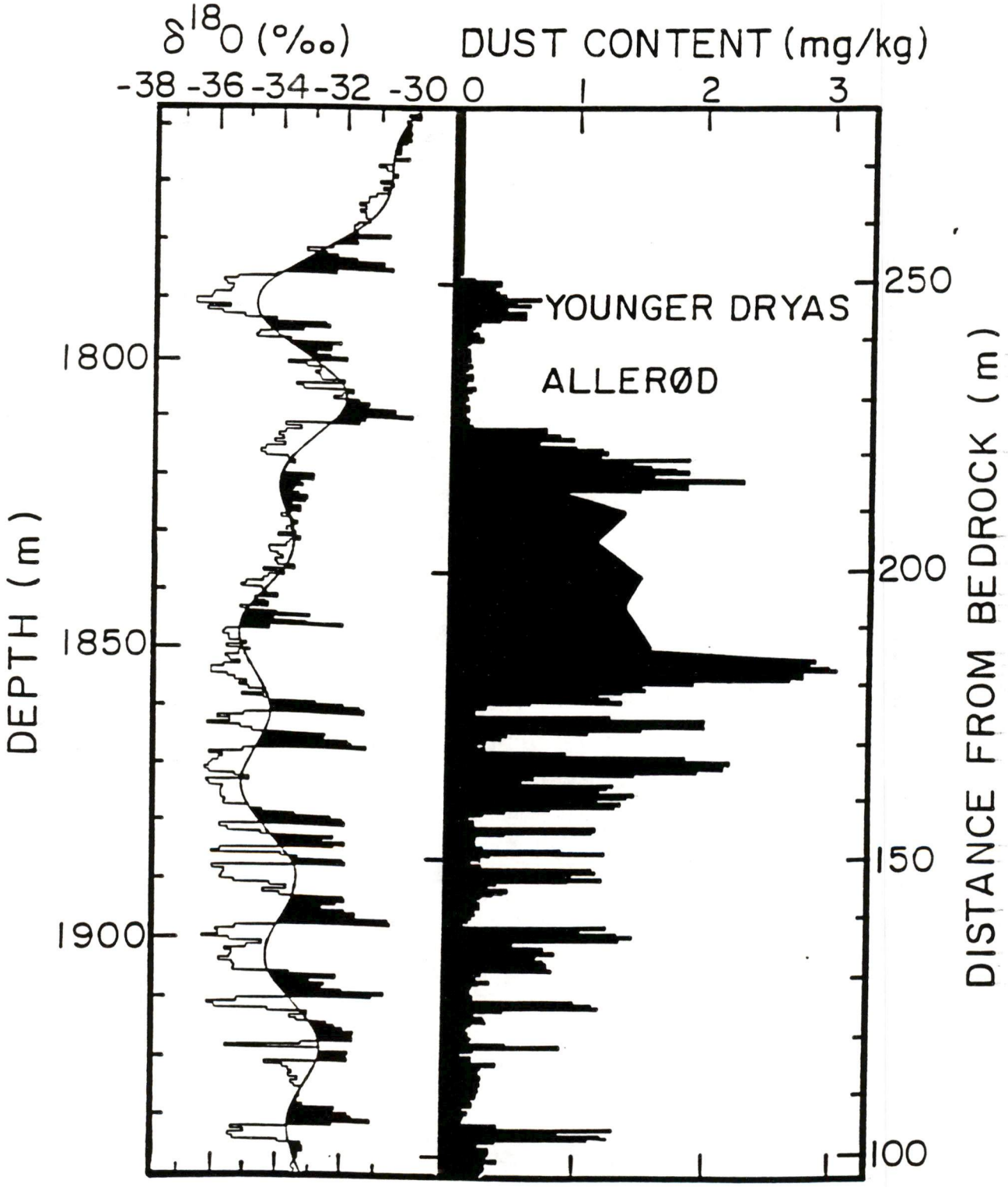


Figure 17. Oxygen isotope and dust records for that part of the Dye 3 Greenland ice core covering the time period ~45,000 to ~8000 years B.P. (Hammer et al., 1985). Note that many of the oxygen isotope events are characterized by rapid warmings followed by more gradual coolings.

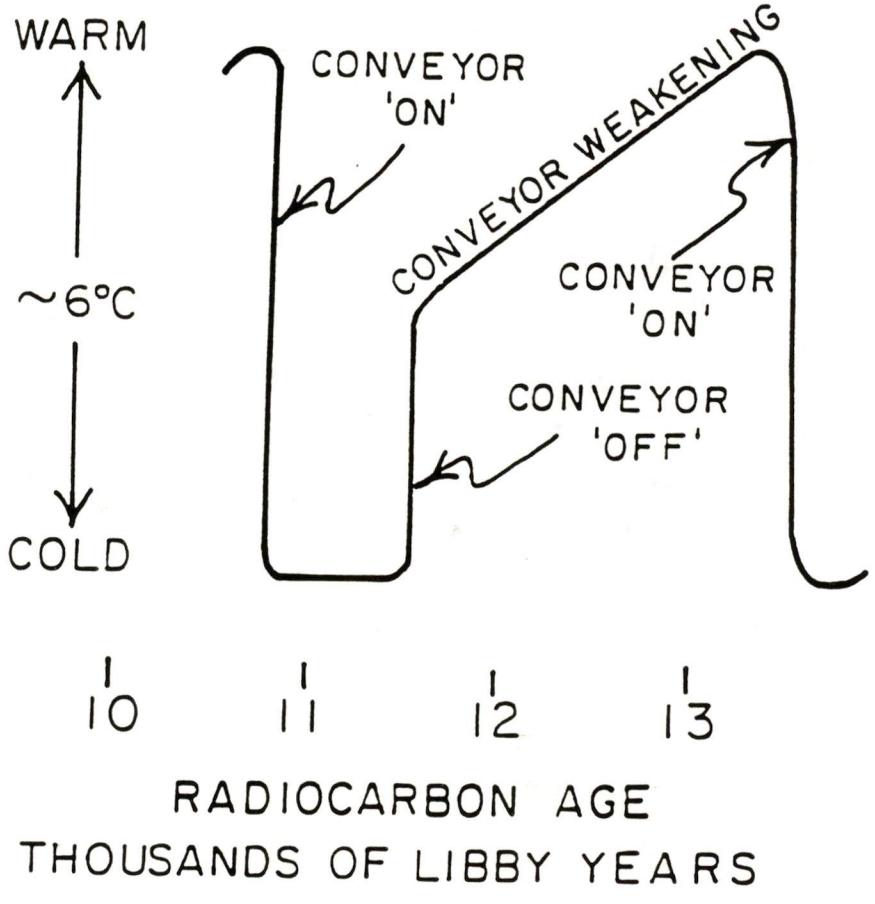


Figure 18. Diagrammatic representation of the temperature record for the northern Atlantic basin from just before 13,000 to just after 10,000 radiocarbon years before present. The features shown in this diagram appear in records of ^{18}O in ice, of ^{18}O in lake sediment, of ocean planktonic foraminifera (Ruddiman and McIntyre, 1981), of pollen and of beetles (Atkinson et al., 1987). Of particular interest is rapidity of the warmings at 12,700 years BP and at 10,000 years BP. Detailed measurements in the Dye 3 ice core and in varved lake sediments reveal that these warmings took place in about 50 years!

REFERENCES

Atkinson, T.C., K.R. Briffa and G.R. Coope, Seasonal temperatures in Britain during the past 22,000 years, reconstructed using beetle remains, Nature, vol. 325, February, 1987.

Baumgartner, A. and Reichel, E., Die Weltwasserbilanz, Oldenbourg, München, 1975.

Birchfield, G.E., W.S. Broecker, A salt oscillator in the glacial northern Atlantic? Part II: A 'Scale Analysis' Model, Paleoceanography, vol. 5, no. 6, 835-843, Dec. 1990.

Boyle, E.A. and L. Keigwin, North Atlantic thermohaline circulation during the past 20,000 years linked to high-latitude surface temperature, Nature, 330, 35-40, 1987.

Brewer, P.G., W.S. Broecker, W.J. Jenkins, P.B. Rhines, C.G. Rooth, J.H. Swift, T. Takahashi, and R.T. Williams, A Climatic freshening of the deep Atlantic north of 50°N over the past 20 years, Science, 222:1237-1239, 1983.

Broecker, W.S., D. Peteet and D. Rind, Does the ocean-atmosphere have more than one stable mode of operation? Nature, 315:21-25, 1985.

Broecker, W.S., The Biggest Chill, Natural History Magazine, p. 74-82, Oct. 1987.

Broecker, W.S., and G.H. Denton, The role of ocean-atmosphere reorganizations in glacial cycles, Geochimica et Cosmochimica Acta, 53:2465-2501, October, 1989.

Broecker, W.S. and G.H. Denton, What Drives Glacial Cycles? Scientific American, Jan. 1990.

Broecker, W.S., T.-H. Peng, J. Jouzel, and G. Russell, The magnitude of global fresh water transports of importance to ocean circulation, Climate Dynamics, 4:73-79, 1990a.

Broecker, W.S., G. Bond, M. Klas, G. Bonani, and W. Wolfli, A salt oscillator in the glacial North Atlantic? 1. The Concept, Paleoceanography, vol. 5, no. 4:469-477, August 1990b.

Broecker, W.S., S. Blanton, and T. Takahashi, W. Smethie and G. Ostlund, Radiocarbon decay and oxygen utilization in the dep Atlantic Ocean, submitted to Global Biogeochemical Cycles, vol. 5, 87-117, March, 1991a.

Broecker, W.S., A. Virgilio, and T.-H. Peng, Radiocarbon Age of Water in the Deep Atlantic Revisited, Geophys. Res. Lett., vol. 18, no. 1, 1-3, Jan. 1991b.

Broecker, W.S., The Conveyor's Upper Limb: The Source for North Atlantic Deep Water, in press a, Jour. Geophysical Research.

Broecker, W.S., The Strength of the Nordic Heat Pump, 13,500 to 9500 B.P., in press, Erice volume.

Coachman, L.K., and K. Aargaard, Transports through Bering Strait: Annual and Internannual Variability, Jour. Geophys. Research, vol. 93, no. C12, 15,535-15,539, 1988.

Dansgaard, W., S.J. Johnsen, H.B. Clausen, and C.C. Langway, Jr., in The Late Cenozoic Glacial Ages, (ed. by Karl K. Turekian), New Haven and London, Yale Univ. Press, pp. 37-56, 1971.

Dansgaard, W., J.W.C. White, and S.J. Johnson, The abrupt termination of the Younger Dryas climate event, Nature, 339:532-533, 1989.

Gordon, A.L., and A.R. Piola, Atlantic Ocean upper layer salinity budget, Jour. Phys. Oceanogr., 13, 1293-1300, 1983.

Gordon, A.L., Indian-Atlantic Transfer of Thermocline water at the Agulhas retroflection, Science, 227, 1030-1033, 1985.

Gordon, A. Interocean Exchange of Thermocline Water, Jour. Geophys. Research, vol. 91, no. C4, 5037-5046, 1986.

Hammer, C.U., H.B. Clausen, W. Dansgaard, A. Neftel, P. Kristinsdottir, and E. Johnson, Continuous impurity analysis along the Dye 3 deep core. In Greenland Ice Core: Geophysics, Geochemistry, and the Environment (eds. C.C. Langway, H. Oeschger, and W. Dansgaard); Amer. Geophys. Union Mon. 33, pp. 90-94.

Levitus, S., Climatological Atlas of the World Ocean, NOAA Professional Paper No. 13, (U.S. GPO, Washington, DC)., 1982.

Lotter, A.F. and H. Zbinden, Late-Glacial pollen analysis, oxygen-isotope record, and radiocarbon stratigraphy from Rotsee (Lucerne), Central Swiss Plateau, Eclogae geol. Helv. 82/1: 191-202, 1989.

Maier-Reimer, E. and U. Mikolajewicz, Experiments with and OGCM on the cause of the Younger Dryas, in Oceanography, (A. Ayala-Castanares, W. Wooster, and A. Yanez-Arancibia, ed.), 87-100, UNAM Press, Mexico, 1989.

Manabe S., and R.J. Stauffer, Two stable equilibria of a coupled ocean-coupled ocean-atmosphere model, J. Climate, 1:841-866, 1988.

Oort , A.H., Global atmospheric circulation statistics, 1958-1973, NOAA Professional Paper 14, 1983.

Rind, D. D. Peteet, W.S. Broecker, A. McIntyre and W. Ruddiman, The impact of cold North Atlantic sea surface temperatures on climate: Implications for the Younger Dryas cooling (11-10k), Climate Dynamics, 1:3-33, 1986.

Ruddiman, W.F. and A. McIntyre, The North Atlantic Ocean during the last deglaciation, Paleogeogr., Palaeoclim., Palaeoecol, 35:145-214, 1981.

Schlosser, P, G. Bönisch, M. Rhein and R. Bayer, Reduction of Deepwater Formation in the Greenland Sea during the 1980s: Evidence from Tracer Data, Science, 251:1054-1056, 1991.

Suzuki, Y. and Y. Sugimura and T. Itoh, A Catalytic Oxidation Method for the Determination of Total Nitrogen Dissolved in Seawater, Marine Chemistry, 16, 83-97, 1985.

Zaucker, F. and W.S. Broecker, Atmospheric water vapor transport from a general circulation model, in press, Jour. Geophysical Research.

What Drives Glacial Cycles?

Massive reorganizations of the ocean-atmosphere system, the authors argue, are the key events that link cyclic changes in the earth's orbit to the advance and retreat of ice sheets

by Wallace S. Broecker and George H. Denton

Eight times within the past million years, something in the earth's climatic equation has changed, allowing snow in the mountains and the northern latitudes to remain where it had previously melted away. The snow compacted into ice, and the ice built up into glaciers and ice sheets. Over tens of thousands of years, the ice sheets reached thicknesses of several kilometers; they planed, scoured and scarred the landscape as far south as central Europe and the midwestern U.S. And then each glacial cycle came to an abrupt end. Within a few thousand years, the ice sheets shrank back to their present-day configurations.

Over the past 30 years, evidence has mounted that these glacial cycles are ultimately driven by astronomical factors: slow, cyclic changes in the eccentricity of the earth's orbit and in the tilt and orientation of its spin axis. By altering the intensity of the seasons, the astronomical cycles somehow tip the balance between glacial buildup and glacial retreat. But what is the link between astronomy and the ice ages? How are the seasonality changes leveraged into global changes in climate?

Any answer must contend with the vast array of evidence that has accumulated about the nature, timing and extent of the climatic shifts that accompanied ice buildup and retreat. Many workers have proposed that the seasonality changes act directly on the ice sheets of the Northern Hemisphere. A reduction in summer sunshine allows ice to build up, and an increase melts it away; the ice in turn alters the earth's climate. In contrast, we think the ice sheets were a consequence of broader climatic events. By altering patterns of evaporation and rainfall, the changes in seasonal intensity appear to have caused the ocean and atmosphere (a single, coupled system) to flip from one mode of operation to another, very different mode. With each flip, ocean circulation changed and heat was carried around the globe differently, the properties of the atmosphere were altered, climate changed—and the ice sheets grew or shrank.

ICE FIELD IN PATAGONIA ends in a deep glacial lake. Such Southern Hemisphere glaciers have grown and shrunk in concert with the great northern ice sheets, according to radiocarbon dating of vegetation (such as the trees in the foreground) that was overwhelmed by advancing glaciers or that took root after their retreat. The timing is a puzzle because the intensity of summer sunshine, which is thought to influence ice growth, changes on quite different schedules at middle latitudes in the two hemispheres.

Our proposal is not a rejection of the astronomical theory of the ice ages but an extension of it. The hypothesis was first proposed in 1842, just a few years after the Swiss-American naturalist Louis Agassiz argued that polished and scarred rocks and heaps of detritus in the Alps recorded some past age of glaciers. In that year the French mathematician Joseph A. Adhémar suggested that astronomically driven changes in the intensity of the seasons might periodically trigger glaciation.

The Yugoslav astronomer Milutin Milankovitch refined and formalized the hypothesis in the 1920's and 1930's. The astronomical pacemaker he advocated has three components, two that change the intensity of the seasons and a third that affects the interaction between the two driving factors. The first is the tilt of the earth's spin axis. Currently about 23.5 degrees from the vertical, it fluctuates from 21.5 degrees to 24.5 degrees and back every 41,000 years. The greater the tilt is, the more intense seasons in both hemispheres become: summers get hotter and winters colder.

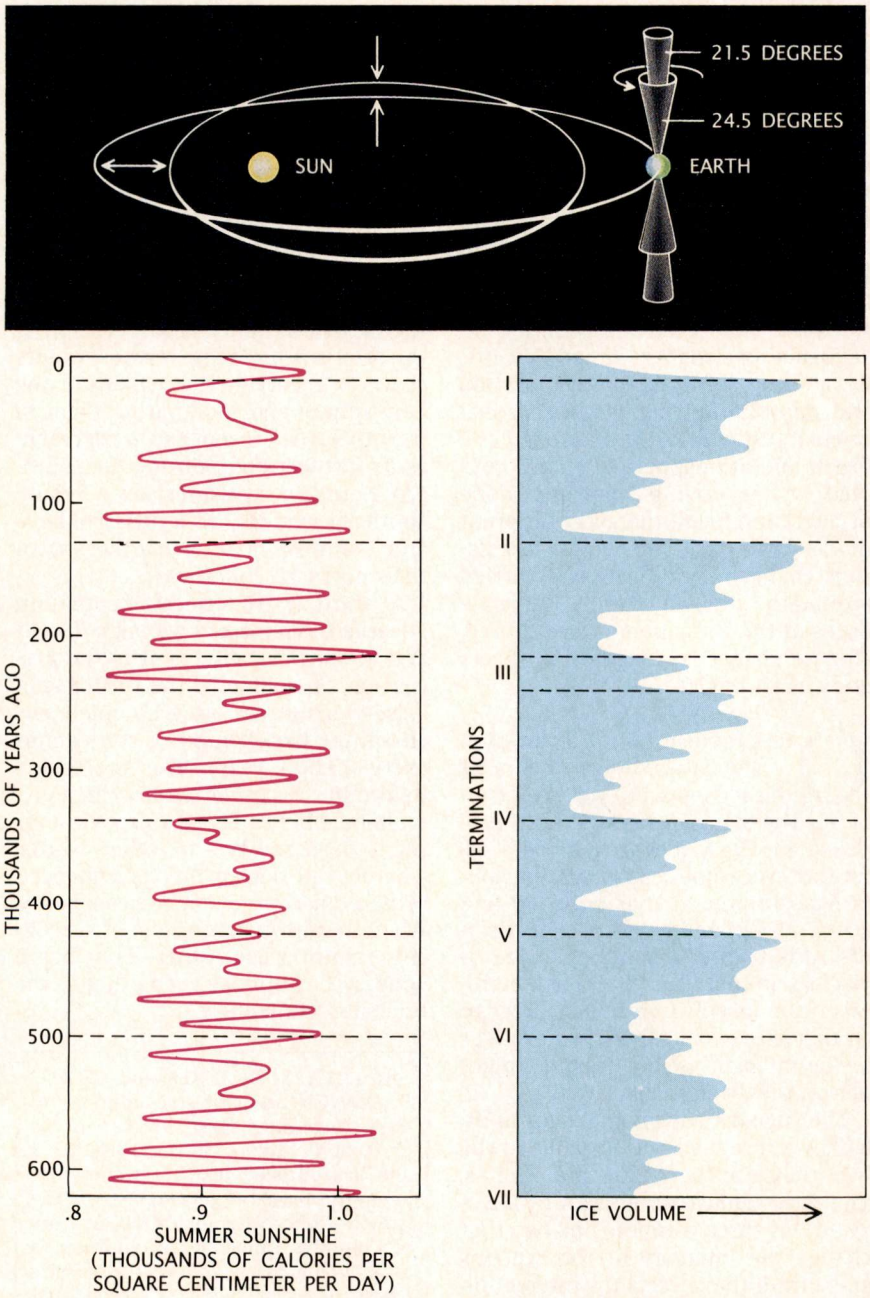
The second, weaker factor controlling seasonality is the shape of the earth's orbit. Over a period of 100,000 years, the orbit stretches into a more eccentric ellipse and then grows more nearly circular again. As the orbital eccentricity increases, the difference in the earth's distance from the sun at the orbit's nearest and farthest points grows, intensifying the seasons in one hemisphere and moderating them in the other. (At present the earth reaches its farthest point during the Southern Hemisphere winter; as a result, southern winters are a little colder—and summers a little warmer—than their northern counterparts.)

A third astronomical fluctuation governs the interplay between the tilt and eccentricity effects. It is the precession, or wobble, of the earth's spin axis, which traces out a complete circle on the background of stars about every 23,000 years. The precession determines whether summer in a given hemisphere falls at a near or a far point in the orbit—in other words, whether tilt seasonality is enhanced or weakened by distance seasonality. When these two controllers of seasonality reinforce each other in one hemisphere, they oppose each other in the opposite hemisphere.

WALLACE S. BROECKER and GEORGE H. DENTON bring diverse interests to their study of ice ages. Broecker got his Ph.D. at Columbia University in 1958 and has pursued his career there. He is now professor of geochemistry at the Lamont-Doherty Geological Observatory of Columbia University. In addition to ancient climates, he follows research interests in ocean chemistry, isotope dating and environmental science. Denton is professor of geology at the University of Maine. After earning a Ph.D. at Yale University in 1965, he did postdoctoral work at the University of Stockholm and then moved to Maine. He has spent 36 seasons in the field studying the timing and extent of glacial advances, 22 of them in Antarctica and elsewhere in the Southern Hemisphere.

Milankovitch calculated that these three factors work together to vary the amount of sunshine reaching the high northern latitudes in summer over a range of some 20 percent—enough, he argued, to allow the great ice sheets that advanced across the northern continents to grow during intervals of cool summers and mild winters. For many years, however, the lack of an independent record of ice-age timing made the hypothesis untestable.

In the early 1950's Cesare Emiliani, working in Harold C. Urey's laboratory at the University of Chicago, produced the first complete record of the waxings and wanings of past glaciations. It came from a seemingly odd place, the sea floor. Single-cell marine organisms called foraminifera house themselves in shells made of calcium carbonate. When the foraminifera die, sink to the bottom and contribute to the sea-floor sediments, the carbonate of their shells preserves certain characteristics of the seawater they inhabited. In particular, the ratio of a heavy isotope of oxygen (oxygen 18) to ordinary oxygen (oxygen 16) in the carbonate preserves the ratio of the two oxygens in the water molecules.

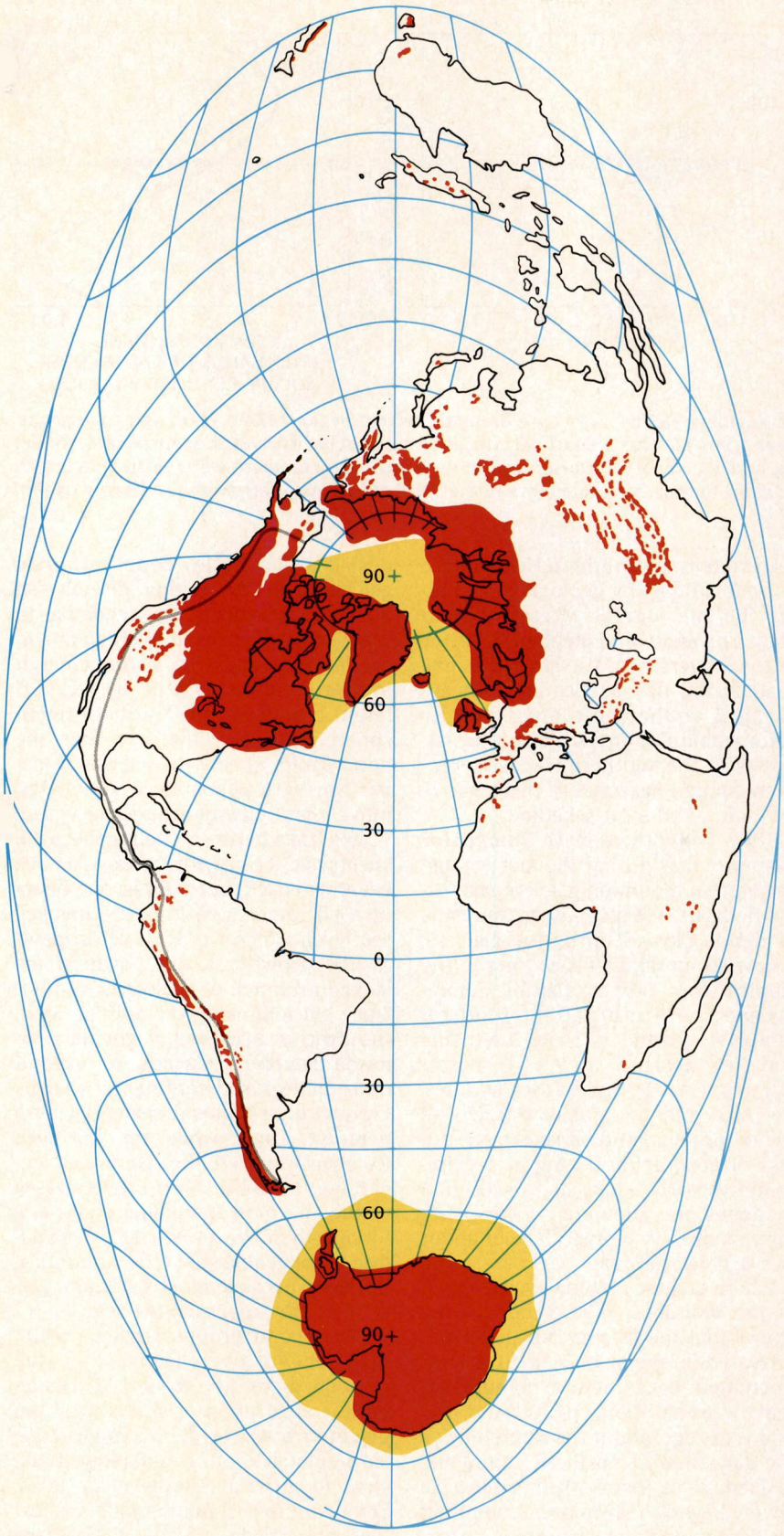


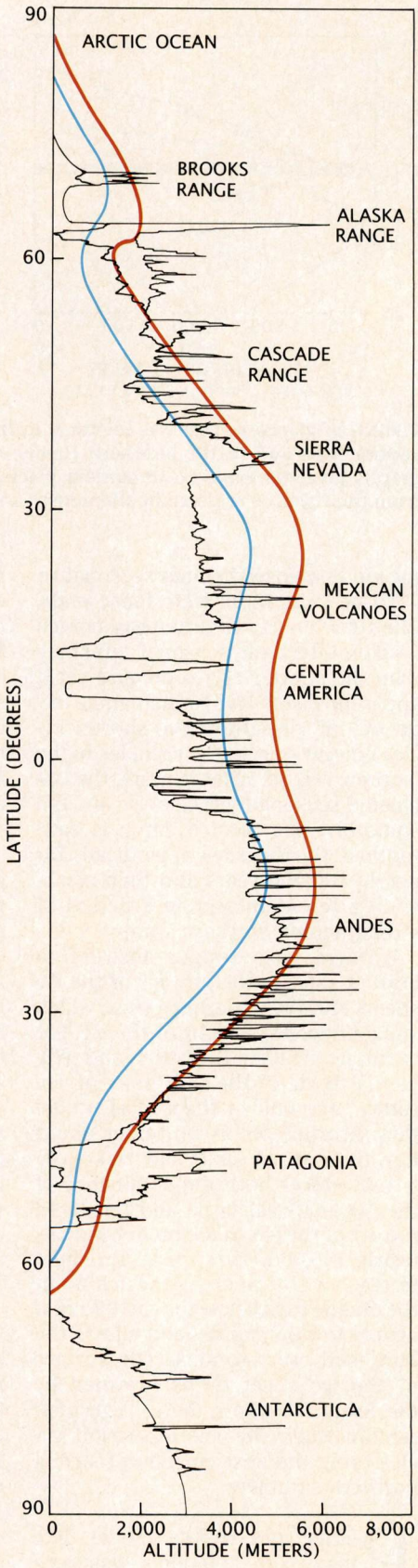
ASTRONOMICAL CYCLES (*top*) are the pacemaker of glaciation. The cycles—23,000 to 100,000 years in length—affect the eccentricity of the earth's orbit, the orientation of its spin axis (which slowly traces out a cone in space) and the tilt of the axis (which affects the width of the cone). The effect of the changes on the intensity of summer sunshine at high northern latitudes is shown at the left. The curve at the right indicates the volume of the earth's ice sheets, determined from isotopic studies of sea-floor sediments. Ice volume climbs gradually for about 100,000 years and then falls abruptly in ice-age terminations that correspond to episodes of increasing summer sunshine at northern latitudes. (Seasonality varies differently in the Southern Hemisphere, which suggests that northern seasonality must be what drives ice ages.)

It is now understood that the ratio of oxygen isotopes in seawater closely tracks the proportion of the world's water that is locked up in glaciers and ice sheets. A kind of meteorological distillation accounts for the link. Water molecules containing the heavier isotope tend to condense and fall as precipitation a tiny bit more readily than molecules containing the lighter isotope. Hence, as water vapor evaporated from warm oceans moves away from the source, its oxygen 18 preferentially returns to the oceans in precipitation. What ultimately falls as snow on ice sheets and mountain glaciers is relatively depleted of oxygen 18. As the oxygen 18-poor ice builds up, the oceans become relatively enriched in the isotope. The larger the ice sheets grow, the higher the proportion of oxygen 18 becomes in seawater—and hence in the sediments.

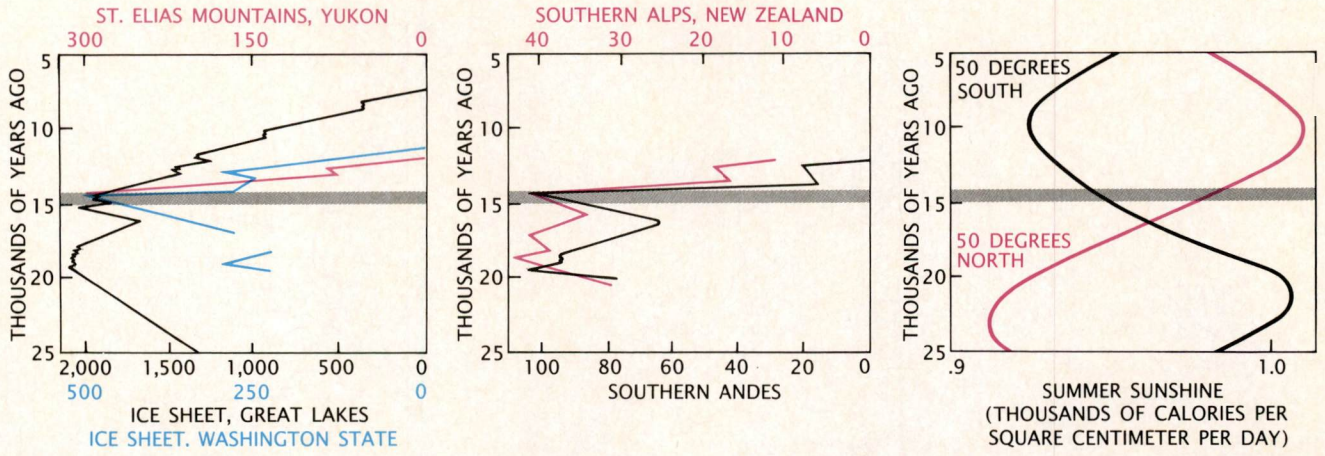
Analyzing cores drilled from sea-floor sediments, Emiliani found that the isotopic ratio rose and fell in rough accord with the cycles Milankovitch had predicted. Since that pioneering observation, oxygen-isotope measurements have been made on hundreds of cores. A chronology for the combined record enabled James D. Hays of Columbia University, John Imbrie of Brown University and Nicholas Shackleton of the University of Cambridge to show in 1976 that the record contains the very same periodicities as the orbital processes.

Over the past 800,000 years, the global ice volume has peaked every 100,000 years, matching the period of the eccentricity variation. In addition, "wrinkles" superposed on each cycle—small decreases or surges in ice volume—have come at intervals of roughly 23,000 and 41,000 years, in keeping with the precession and tilt frequencies. Imbrie, working with a group called SPECMAP, later strengthened the case for the astronomical theory even more when he showed that the amplitude of the shorter-period signals has varied exactly as one would expect if the signals were be-





ICE SHEETS AND MOUNTAIN GLACIERS expanded in both hemispheres during the last ice age. The map (an unusual equal-area projection) shows the extent of land ice (*red*) and sea ice (*yellow*) on all the continents at peak glaciation some 19,500 years ago. (Land ice extended beyond some present coastlines because the sea level was lower.) The graph traces the average elevation of mountain snow lines on the American cordillera, plotted along the north-south transect indicated on the map. Ice-age snow lines (*blue line*) were about 1,000 meters lower than snow lines are today (*red*), regardless of latitude.



TIMING of glacial retreat was identical in the Northern Hemisphere (*left*) and in the Southern Hemisphere (*center*). The graphs give the extent of mountain glaciers and ice sheets from their source regions (in kilometers) and show that in every case dramatic retreat began 14,000 years ago. Changes in seasonal intensity could not have driven the retreat directly, because even though northern summers were getting stronger, summers in the Southern Hemisphere were weakening (*right*).

ing modulated by distance seasonality.

To be sure, there were loose ends. The 100,000-year variation has a much weaker effect on seasonal sunshine than the shorter cycles do, and yet it apparently sets the fundamental frequency of glaciation. The shorter cycles emerge only in the wrinkles in the isotopic record. What is more, the calculated seasonality cycles rise and fall smoothly, but the ice curve is sawtoothed: the ice grows episodically for nearly 100,000 years and then crashes in a few thousand, in a period of strengthening northern summers.

Workers have sought answers to both puzzles in the physics of the ice sheets and the underlying rock, which sinks under the weight of the ice. For example, William R. Peltier and William T. Hyde of the University of Toronto have built a theoretical model that incorporates assumptions about how the bedrock sinks and that closely reproduces both the dominance of the 100,000-year cycle and the rapid retreat of the ice. In the model, it takes nearly 100,000 years for an ice sheet to reach a critical size, at which point the ductile rock below the earth's crust begins to flow rapidly and allows the burdened crust to sink. The surface of the ice sheet drops; warmed by the lower elevation, the ice can melt rapidly when the shorter-period cycles bring the next episode of strong northern summers.

Peltier and Hyde's model, like many other models, assumes that Northern Hemisphere seasonality changes drive glacial advance and retreat directly, with bedrock response shaping each cycle and setting its length. Yet the assumption suffers a crucial problem: glaciers grew and retreated in the Southern Hemisphere as well. Studies by geologists, including the late John H. Mercer of Ohio State University and Stephen C. Porter of the University of Washington, show that during the last ice age, climate changed at the same times and by comparable amounts in the middle latitudes of the Southern Hemisphere—even though seasonality there varies on a quite different schedule.

They and others have found, for example, that during the last ice age the earth's mountain glaciers also expanded. The evidence—from the heaps of debris plowed up by the glaciers, known as moraines—is as clear in the tropics (New Guinea, Hawaii, Colombia and East Africa) and the southern temperate latitudes (Chile, Tasmania and New Zealand) as it is in northern temperate latitudes (the Cascades, the Alps and the Himalayas). On all the mountains studied so far, regardless of geographic setting or precipitation rate, the snow line descended by about one kilometer, corresponding to a drop in temperature of about five degrees Celsius.

Where organic material was trapped in the moraines, radiocarbon dating shows that the glaciers advanced and retreated on the same schedule. They fluctuated near their maximum extent between about 19,500 and 14,000 years ago, about the same time as the glaciation of northern continents peaked. Then, just as the northern ice sheets began to shrink, the mountain glaciers underwent a dramatic retreat that sharply reduced their size by about 12,500 years ago.

How could changes in summer sunshine at the latitude of Iceland have caused glaciers to grow and retreat in New Zealand and the southern Andes? If orbital cycles do indeed drive glacial cycles by acting directly on northern ice sheets, the response to seasonality changes in the high northern latitudes must be strong enough to override the effects of the very different changes in the Southern Hemisphere. One possibility is that the northern ice sheets themselves translate Northern Hemisphere seasonality into climatic change around the world.

Two links between the northern ice sheets and ice growth worldwide have been proposed, but neither one bears up well under scrutiny. One invokes sea level, which would have dropped as the growth of the northern ice locked up much of the world's water. Since glaciers can grow only on land, the drop in sea level might have allowed southern glaciers to expand onto the exposed continental shelves even without a global change in temperature. Later, when the northern ice sheets melted, the rise in sea level might have broken up the margins of the Southern Hemisphere glaciers, forcing them to retreat. The explanation is plausible only for Antarctica, however, because most mountain glaciers do not approach the sea.

The second proposal relies on the high albedo, or reflectivity, of the vast northern ice sheets. By reducing the absorption of sunlight by the planet as a whole, the ice might have led to global cooling and allowed glaciers to grow at southern latitudes. Yet computer climate models show that the albedo effects of Northern Hemisphere ice sheets should be confined to northern latitudes. Also, if ice albedo does drive global climatic change, one would expect to find a pronounced north-to-south gradient in the mountain-glacier record,

with mountains adjacent to the northern ice sheets recording the greatest snow-line lowering and the Andes, say, showing very little change. No such gradient is seen.

Any causal link between the ice sheets and global climatic change also must contend with the timing of the mountain-glacier retreat. Both the northern ice sheets and the mountain glaciers began their retreat from the last glacial maximum at the same time, about 14,000 years ago. The continental glaciers took about 7,000 years to melt away, whereas the mountain glaciers shrank much more quickly. The disparity suggests that the northern ice sheets cannot be calling the tune for climate over the rest of the earth.

If the ice sheets themselves cannot link the astronomical cycles to the climatic shifts, what can? Clues come from core samples drilled from depths of as much as two kilometers in the ice that still blankets Greenland and Antarctica. The first thing the ice cores offer is confirmation of the global and synchronous character of ice-age climatic changes.

The oxygen 18 content of glacial ice is depleted in general, but the exact content records the local temperature at the time the ice was laid down. (The colder a parcel of air becomes, the more of its water vapor is likely to have fallen already in precipitation, reducing the oxygen 18 content of the remaining vapor.) Isotopic studies of the Greenland and Antarctic cores show that during the last glaciation both poles cooled—to as much as 10 degrees C below today's temperatures—and warmed in step.

The ice also revealed something much more intriguing. Groups led by Hans Oeschger of the University of Bern and Claude Lorius of the Laboratory of Glaciology and Geophysics of the Environment, near Grenoble, measured the carbon dioxide content of the tiny bubbles of ancient air trapped in the ice. They found that during the last glaciation the carbon dioxide concentration of the atmosphere was about two thirds of its interglacial level. The carbon dioxide curve pointed to a missing ingredient in the climatic recipe: the ocean.

Only a major shift in the ocean's operation could account for such a dramatic change in atmospheric composition. After all, the oceans hold 60 times as much carbon dioxide as the atmosphere; because the gas readily diffuses between the ocean surface and the atmosphere, its concentration in surface waters regulates the atmospheric concentration.

Living things in turn control the surface-water concentration, by acting as a biological pump that transfers carbon dioxide from the surface to the ocean depths. In the course of photosynthesis, the tiny green plants of the ocean's sunlit upper layers capture dissolved carbon dioxide to form organic tissue. Some of the plant matter, as well as animal tissue nourished by the plants, eventually sinks into the deep sea, where bacteria oxidize it back to carbon dioxide. Thus, the gas is continuously pumped into the abyss, together with nutrients such as phosphate and nitrate.

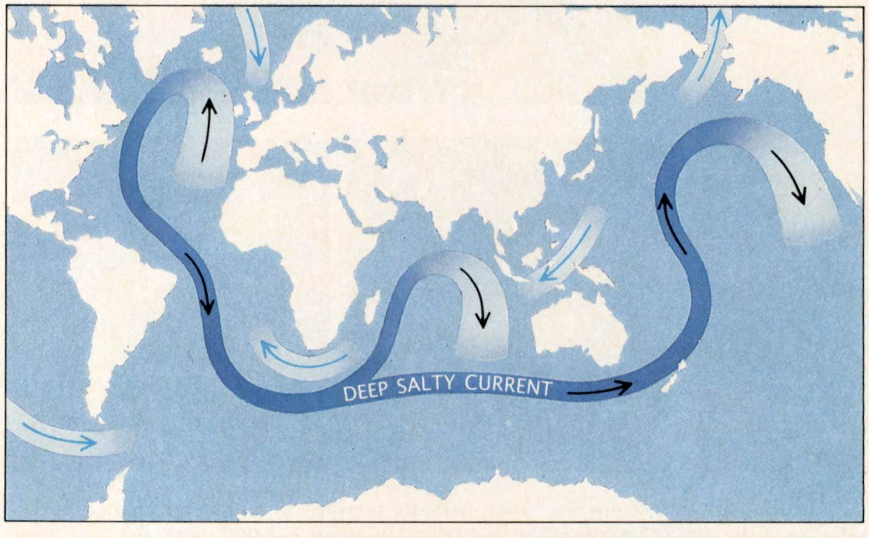
The efficiency of this pump depends not only on the surface community's population and species but also on vertical mixing patterns. The exact link between pumping efficiency and ocean circulation is controversial, but one can imagine, for example, that if the mixing of deep waters with the surface is slowed, surface plant life will have more time to deplete the shallow water of carbon dioxide before more of the gas is stirred up from the depths. During glacial time, some combination of altered mixing and changes in ecology must have made the biological pump more efficient.

The first indications that the ice-age ocean did operate differently came from fossil evidence: changes in the populations of microorganisms that inhabit water masses of specific temperature and salinity, studied by William F. Ruddiman and Andrew McIntyre of Columbia University and by Detmar F. Schnitker of the University of Maine. More recently a geochemical technique pioneered by Edward A. Boyle of the Massachusetts Institute of Technology provided dramatic and direct confirmation that the ocean circulated differently during the last glaciation.

Boyle discovered that, for unknown reasons, the distribution of cadmium in today's oceans closely matches that of phosphate and nitrate nutrients. Because the cadmium ion has the same charge and size as calcium, Boyle guessed that cadmium might substitute for calcium in the calcium carbonate of foraminiferal shells. If it does, measurements of cadmium in shells from sediment cores might reveal the distribution of nitrate and phosphate in the glacial ocean.

Boyle's intuition proved correct when he found that foraminifera in the present-day ocean do incorporate cadmium in a constant proportion to its abundance in seawater. He then measured cadmium in sediment cores. The result was exciting: a key signature of the Atlantic's present-day circulation was missing during glacial time, until about 14,000 years ago.

Currently the Atlantic's deep water contains only about half as much phosphate and nitrate as the deep waters of the Pacific and Indian oceans. The



DEEP SALTY CURRENT threads the world's oceans, compensating for the transport of water vapor by the atmosphere. (Light blue arrows indicate shallow return flow.) The current originates in the North Atlantic, where northward-flowing warm water that is unusually saline (and therefore dense) because of excess evaporation is chilled, which increases its density further. It sinks into the abyss and flows southward, out of the Atlantic. Most of the salty water that is supplied by this Atlantic "conveyor" mixes upward in the Pacific, making up for excess precipitation there. The Atlantic conveyor—and probably the entire system—was disrupted during glacial time.

low nutrient content reflects the water's recent sojourn near the surface (where biological activity depletes the nutrients). Every winter at about the latitude of Iceland, water of relatively high salinity, flowing northward at intermediate depths (perhaps 800 meters), rises as winds sweep the surface waters aside. Exposed to the chill air, the water releases heat, cooling from 10 degrees C to two degrees. The water's high salinity together with the drop in temperature makes it unusually dense, and it sinks again, this time all the way to the ocean bottom.

The formation of the North Atlantic deep water, as it is called, gives off a staggering amount of heat. Equal to about 30 percent of the yearly direct input of solar energy to the surface of the northern Atlantic, this bonus of heat accounts for the surprisingly mild winters of Western Europe. (The warming is often mistakenly ascribed to the Gulf Stream, which ends well to the south.) The magnitude of the vertical circulation is also immense, averaging 20 times the combined flow of all the world's rivers. Indeed, much of the deep water in the world's oceans ultimately originates here. From its source the water floods the deep Atlantic, curves around the southern tip of Africa and joins the deep current that circles Antarctica and distributes deep water to the other oceans.

As the deep water ages and travels away from the site of its formation, it collects sinking phosphate and nitrate, which results in a gradient of increasing nutrient levels. By measuring the cadmium content of foraminifera that lived near the bottom, Boyle found that during glacial time the nutrients were more uniformly distributed through the depths of the world's oceans. In addition, the concentration in the glacial Atlantic peaked in the deepest parts rather than at intermediate depths, as it does today.

These results bore out the implication of the earlier microfossil studies. The Atlantic "conveyor," which releases vast quantities of heat to the North Atlantic and sends immense volumes of water into the abyss, was shut down until the last ice age ended 14,000 years ago. In the absence of this key component, worldwide ocean circulation must have looked very different.

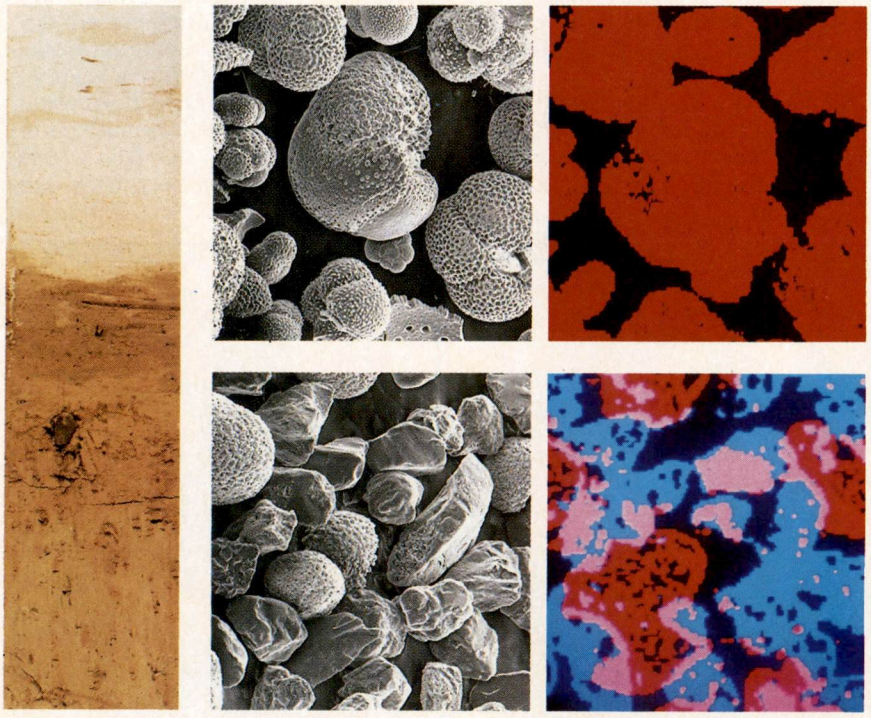
The sea and land evidence together points to a simultaneous change in the operation of the ocean and the atmosphere 14,000 years ago. The pattern of ocean circulation shifted dramatically; glaciers in both hemispheres began retreating, signaling global warming; and the carbon dioxide content of the atmosphere started to rise to interglacial levels. We think these events indicate a major reorganization of the joint ocean-atmosphere system—a jump from a glacial mode of operation to an interglacial mode. Indeed, we believe that abrupt jumps among several ocean-atmosphere modes may underlie glacial cycles in general.

We propose that changes in seasonality are the ultimate causes of these mode shifts. Although we can suggest no simple mechanisms linking seasonality, the ocean-atmosphere system and global climate, we can offer some insights.

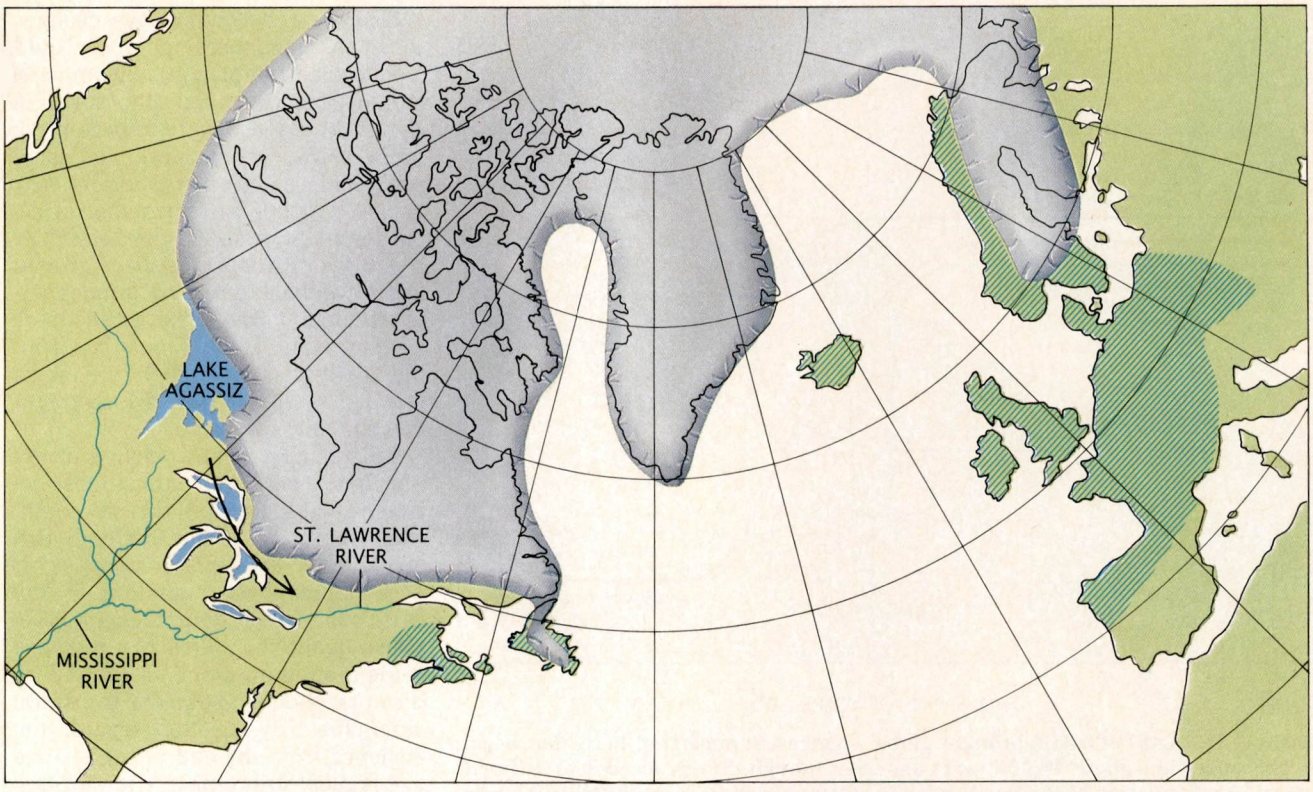
The atmosphere, which would certainly feel the effects of seasonality changes, strongly influences the circulation of the ocean. The link involves the distribution of salt. Prevailing winds transfer water evaporated from one part of the ocean to another region, where it falls as precipitation. The transport of vapor leaves a heritage of salt in the first region and dilutes the salinity of the second.

Now, the tendency of surface waters to sink into the depths and initiate a vertical conveyor belt like that of the North Atlantic depends on their density. Density reflects both temperature and salinity, but salinity is the decisive factor. (Surface water cools almost to the freezing point throughout the high latitudes in winter, but only where it is unusually saline does it sink into the abyss.) The system has a built-in nonlinearity: a gradual shift in atmospheric circulation, by changing salinity in regions such as the North Atlantic, could dramatically alter the global circulation pattern. Indeed, the Atlantic conveyor appears to be the most vulnerable part of the system, which may explain why it is Northern Hemisphere seasonality that drives global climatic changes.

A climatic event called the Younger Dryas, which took place several thousand years after the glaciers started to retreat, provides a smoking gun for this part of our case. It vividly illustrates the link between the transport of fresh water—in this case liquid water and not vapor—and ocean circulation. About 11,000 years ago the re-



SEDIMENT CORE (*left*) from the North Atlantic testifies to an abrupt change in circulation at the end of the penultimate glaciation about 128,000 years ago. The transition (identified by Gerard C. Bond of Columbia University) spans a few millimeters and represents about 50 years. A scanning electron micrograph of coarse material from the dark sediments (*bottom*) reveals abundant rock fragments, rich in silicon (*blue in an X-ray map*), presumably dropped by melting icebergs. The light-colored sediments (*top*) include almost no rock and are made up mainly of shells, rich in calcium (*red*), from marine organisms that inhabit warm waters. (Shells in the dark sediments came from cold-water species.) The sudden revival of the Atlantic conveyor must have warmed the surface, eliminating icebergs and altering ecology.



DIVERSION OF MELTWATER during the retreat of the North American ice sheet some 11,000 years ago may explain the 1,000-year cold spell known as the Younger Dryas. Lake Agassiz, fed by meltwater, had been draining down the Mississippi River to the Gulf of Mexico. When the retreat of the ice opened a channel to the east, however, the water flooded across the region of the Great Lakes to the St. Lawrence River (*arrow*). The influx of fresh water to the North Atlantic diluted the salinity of surface water, reducing its density and preventing it from sinking. The Atlantic conveyor was shut down: warm water could no longer flow northward, and a broad region around the North Atlantic was chilled (*hatched area*).

treat of the glaciers was well under way, and temperatures had risen to their interglacial levels. Suddenly, in as little as 100 years, northern Europe and northeastern North America reverted to glacial conditions. Pollen records show that the forests that had colonized postglacial Europe gave way to arctic grasses and shrubs (including the Dryas flower, for which the period is named), and the Greenland ice core records a local cooling of six degrees C. About 1,000 years later, this cold spell ended abruptly—in as little as 20 years, recent work by Willi Dansgaard of the University of Copenhagen suggests.

Boyle's cadmium measurements, together with the record of surface-water foraminifera in the North Atlantic, tell what happened. Both indicators return to their glacial state at the onset of the Younger Dryas. The conveyor belt had shut down once again. Deep-water formation had stopped, and so the warm intermediate-depth water that supplies Europe's bonus of heat could no longer flow northward. The chill over the region was dispelled only when the conveyor began running again 1,000 years later.

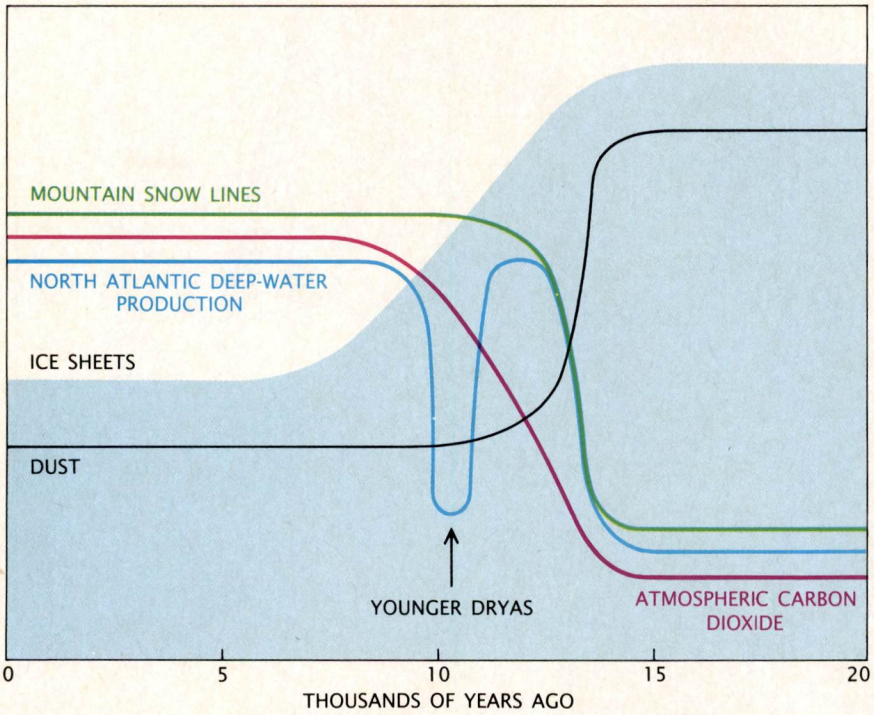
A massive influx of fresh water from the melting North American ice sheet seems to have killed the conveyor and precipitated the Younger Dryas. The ice sheet started shrinking 14,000 years ago; for the 7,000 years it took to melt away, it must have released fresh water at about the same rate as today's Amazon River. At first nearly all the meltwater from the southern edge of the massive ice sheet flowed down the Mississippi River to the Gulf of Mexico. About 11,000 years ago, however, a major diversion sent meltwater in torrents down the St. Lawrence River to the Atlantic.

A vast clearinghouse for meltwater, known as Lake Agassiz, had formed in the bedrock depression at the edge of the retreating ice sheet in what is now southern Manitoba. Until 11,000 years ago the lake, larger than any of the existing Great Lakes, had overflowed a bedrock lip to the south and drained down the Mississippi. Then the retreat of the ice opened a channel to the east. The water level in Lake Agassiz dropped by 40 meters as water flowed across the region of the Great Lakes and down the St. Lawrence.

Foraminifera from surface waters of the Gulf of Mexico record this diversion. Their oxygen 18 content had been anomalously low, reflecting the oxygen 16–rich meltwater discharging from the Mississippi. About 11,000 years ago the isotopic ratio increased abruptly as the Lake Agassiz diversion shut off the meltwater flow to the Gulf.

The meltwater, meanwhile, poured into the North Atlantic close to the site of deep-water formation. There it reduced the salinity of surface waters (and hence their density) by so much that, in spite of severe winter cooling, they could not sink into the abyss. The conveyor belt stayed off until 1,000 years later, when a lobe of ice advanced across the western end of the Lake Superior basin and once again blocked the exit to the east. Lake Agassiz rose again by 40 meters, diverting the meltwater back down the Mississippi. The conveyor belt was reactivated, and Europe warmed up again.

The Younger Dryas links freshwater flow, ocean circulation and climate—but only regional climate. Only around the North Atlantic did the episode bring a sharp cooling; elsewhere its effects were slight



END OF THE LAST ICE AGE brought global changes, summarized here, that began at the same time about 14,000 years ago even though they proceeded at different rates. The circulation of the North Atlantic shifted abruptly from glacial to interglacial conditions (with a brief relapse during the Younger Dryas cold snap) as deep-water production resumed. At the same time, the amount of dust in the atmosphere dropped and the concentration of carbon dioxide started to increase. The shifts may have been part of a larger reorganization of the ocean and atmosphere that warmed the planet and caused mountain glaciers and ice sheets to start retreating.

or absent. Unlike the glaciations, the Younger Dryas affected only the transport of heat (from low latitudes to the North Atlantic) and not the global climate. How could a change in ocean-atmosphere operation during the ice ages have cooled the world as a whole?

The Greenland and Antarctic ice cores suggest part of an answer. The lower level of atmospheric carbon dioxide they record for the last glaciation would certainly have contributed to the cooling: carbon dioxide is a greenhouse gas that warms the earth's surface by trapping solar energy. Computer climate simulations suggest, however, that the global cooling caused by the observed drop in carbon dioxide would be at most two degrees C—less than half of what is recorded in the mountain glaciers.

Two other changes recorded in the ice cores must also have contributed. Ice-age air contains only half the post-glacial level of methane. Methane, too, is a greenhouse gas, although the ice-age cooling attributable to reduced methane amounts to just a few tenths of a degree. In addition, dust is about 30 times as abundant in glacial-age ice as in more recent layers, confirming evidence from other sites that the ice-age atmosphere was exceedingly dusty. Dust, too, could have contributed to the cooling, by reflecting sunlight. Unfortunately, its effect is hard to quantify.

The dustiness and low methane content of the ice-age air do suggest that the glacial mode of ocean-atmosphere operation had imposed a dry climate. Dust, after all, blows from areas where vegetation is sparse, whereas methane is produced in swamps. Dry conditions (which are also recorded in ice-age landforms, such as sand dunes, and in pollen deposits) would have had their own effect on global temperatures. Temperature falls more rapidly with increasing altitude in a drier atmosphere; hence, the drying could have contributed to the depression of mountain snow lines.

Even added together, the impacts of carbon dioxide, methane, dust and drying may come up short in accounting for the temperature difference between the glacial and the interglacial planet. What else could have contributed? One possibility is that the ocean-atmosphere reorganization changed the characteristics of clouds and made them more reflective.

Clearly, our account of how changes in ocean-atmosphere operation could have cooled the planet is incomplete. Moreover, since we appeal to Northern Hemisphere seasonality to pace these mode shifts, we encounter the same problem faced by other theorists: Why is the 100,000-year astronomical cycle dominant when it is the weakest of the three? Perhaps ice-sheet growth has a feedback effect on atmospheric circulation. The ocean-atmosphere system might become most susceptible to a mode shift once the ice sheets reached a critical size—which might take 100,000 years.

Still, much recent evidence favors our basic proposal: transitions between glacial and interglacial conditions represent jumps between two stable but very different modes of ocean-atmosphere operation. If the earth's climate system does jump between quantized states, like the electrons around an atom, all climate indicators should register a transition simultaneously. In this regard, the evidence from the end of the last ice age is most impressive. The warming of North Atlantic surface waters, the onset of melting in the northern ice sheets and the mountain glaciers of the Andes, the reappearance of trees in Europe and changes in plankton ecology near Antarctica and in the South China Sea—all took place between 14,000 and 13,000 years ago.

If the global climate system does prove to have quantized states, climatologists will have gained new insight into the way astronomical forcing, acting mainly in high northern latitudes, could transform climate worldwide. They will also have new cause for concern over the earth's climatic future. Just as 14,000 years ago the earth was feeling the gradual forcing effect of stronger northern summers, so now it is subject to gradual forcing as human activity releases carbon dioxide and other greenhouse gases into the atmosphere. Will the climate system again respond abruptly, by flipping to an entirely new mode?

FURTHER READING

THE OCEAN. Wallace S. Broecker in *Scientific American*, Vol. 249, No. 3, pages 146–160; September, 1983.

ICE AGES: SOLVING THE MYSTERY. John Imbrie and Katherine O. Imbrie. Harvard University Press, 1986.

THE ROLE OF OCEAN-ATMOSPHERE REORGANIZATIONS IN GLACIAL CYCLES. Wallace S. Broecker and George H. Denton in *Geochimica et Cosmochima Acta*, Vol. 53, No. 10, pages 2465–2501; October, 1989.

an Article from

SCIENTIFIC AMERICAN

JANUARY, 1990 VOL. 262 NO. 1

COPYRIGHT © 1990 BY SCIENTIFIC AMERICAN, INC. ALL RIGHTS RESERVED

Video Science Course for Children

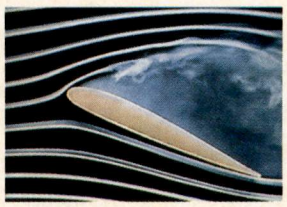
Winner of the Association for the Advancement of Science Award

"Only 8 Years Old...And *He's* Teaching *Me* About Science!"

First Time in the U.S. on Home Video. Not Sold in Stores!



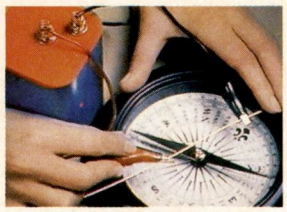
"Look, Dad. Static electricity can actually bend water!"



Learn what makes an airplane fly.



Learn how machines work.



Learn about the powers of magnetism.

Acclaimed Video Science Course for Children Gives Your Child a Critical Early Advantage

A Head Start in Science for Children Ages 7-12.

It's no secret: American schools are failing science. The National Science Foundation and the U.S. Dept. of Education have reported this time and again. The *average* European or Japanese student gets *3 times* more science instruction than the best U.S. science student!

World Ranking of Science Student Achievement*

1. England	5. Japan	9. Sweden
2. Hong Kong	6. Poland	10. Finland
3. Singapore	7. Norway	11. **United States**
4. Hungary	8. Australia	12. Canada

*Source — National Science Foundation
(Performance in physical sciences, 4th-12th grades.)

In tomorrow's super-tech world, science will be essential for success. U.S. kids are already being left behind. But now there's something you can do about it.

Turn Your TV into a Teacher.

the first time ever, your child can start learning science from the same learn-at-home video program proven in Europe.

Adventures Into Science is entertaining and effective. Winner of the prestigious Advancement of Science Award! Kids learn about the fantastic powers of light, gravity, magnetism, inertia, electricity — and much more. The *London Times* calls it "the most imaginative educational video program yet!"

Dozens of dazzling experiments and demonstrations excite kids' curiosity, and teach basic scientific principles.

Give Your Child What the Schools Aren't Providing.

Adventures Into Science includes everything to master basic scientific principles. Twelve colorful video lessons on six 50-minute videos that kids will watch over and over. Emphasizes the "hands-on" learning too absent in U.S. schools. A special Parent's Guide includes safe experiments for you and your children to do at home. You'll be thrilled when your child starts explaining science to you! Be delighted with his excited progress.

Satisfaction Guaranteed.

Adventures Into Science is priced affordably — just $26.95 per video. And there's no risk: you may return the set within 15 days for a full refund. Order today! Give your child a critical early advantage in a competitive world.

© 1989 MBI

Early Advantage
47 Richards Avenue
Norwalk, Conn. 06857

Satisfaction guaranteed

Call Toll-Free: 1-800-367-4534

Yes! Please send me the Adventures Into Science Home Video Course for Children. I understand only VHS format is available.

Name_____
PLEASE PRINT CLEARLY

Address_____

City/State/Zip_____

Signature_____
(All orders subject to acceptance.)

Charge each of six monthly installments of $27.74* to my credit card:
☐ VISA ☐ MasterCard ☐ Diners Club ☐ American Express

Credit Card No. Exp. Date

☐ I prefer not to use my credit card and will pay by check. Enclosed is my deposit of $55.48* for each set. I will pay the balance as billed in four monthly installments of $27.74* each.

*Includes one-time $4.75 shipping/handling charge.
CT residents add 8%; TN residents add 7¾% sales tax.
Allow 2 to 4 weeks for shipment.

490-4819



PALEOCEANOGRAPHY, VOL. 5, NO. 4, PAGES 469-477, AUGUST 1990

A SALT OSCILLATOR IN THE GLACIAL ATLANTIC? 1. THE CONCEPT

Wallace S. Broecker, Gerard Bond, and Millie Klas

Lamont-Doherty Geological Observatory of Columbia University, Palisades, New York

Georges Bonani and Willy Wolfli

Institut fur Mittelenergiephysik, ETH Honggerberg, Zurich, Switzerland

Abstract. As shown by the work of Dansgaard and his colleagues, climate oscillations of one or so millennia duration punctuate much of glacial section of the Greenland ice cores. These oscillations are characterized by 5°C air temperature changes, severalfold dust content changes and 50 ppm CO_2 changes. Both the temperature and CO_2 change are best explained by changes in the mode of operation of the ocean. In this paper we provide evidence which suggests that oscillations in surface water conditions of similar duration are present in the record from a deep sea core at 50°N. Based on this finding, we suggest that the Greenland climate changes are driven by oscillations in the salinity of the Atlantic Ocean which modulate the strength of the Atlantic's conveyor circulation.

INTRODUCTION

One of the most puzzling features of the ice core records from Greenland is the series of large and rather abrupt changes in oxygen isotope composition during the last period of glaciation [Dansgaard et al., 1971, 1982, 1989]. Based on the correlation between the $\delta^{18}O$ in present-day precipitation and mean annual temperature for high-latitude stations, these changes translate into 5°C jumps in air temperature. Correlating with the oxygen isotope changes are severalfold changes in the dust content of the ice (see Figure 1), 50 ppm changes in the CO_2 content of the air trapped in the ice [Stauffer et al., 1984], changes in the SO_4 concentration in the ice [Finkle and Langway, 1985] and changes in ^{10}Be content of the ice [Beer et al., 1984]. As the ^{18}O signature for these events has now been found in three Greenland ice cores (Camp Century [Dansgaard et al., 1971], Dye 3 [Dansgaard et al., 1982], and Renland (W. Dansgaard personal communication, 1990)), they must be real climatic events. However, the validity of the CO_2 signal as a record of atmospheric composition remains in limbo. The reason is that similar events were not found in a study of an Antarctic ice core [Neftel et al., 1988]. As discussed by Dansgaard and Oeschger [1989], this absence could reflect either a smoothing of the record in low deposition Antarctic record or meltwater layers in the Dye 3 ice. Oeschger et al. [1984], first suggested that the Greenland events constitute jumps between two modes of operation of the climate system. Broecker et al. [1985] went a step further and postulated that Oeschger's modes involved a turning on and off of the Atlantic's conveyor circulation system.

Rather than pursuing the cause of the entire series of oscillations, recent attention has been focused on a single event, the Younger Dryas, which followed upon the heels of the last glacial termination. This event has roughly the same shape, amplitude, and duration as those during the glacial period. The lure of the Younger Dryas is that in contrast to the others it is well documented in pollen records from the lands surrounding the northern Atlantic [Watts, 1980; Rind et al., 1986] and in foraminifera records from the northern Atlantic itself [Ruddiman et al., 1977; Ruddiman and McIntyre, 1981]. A case has been made that the Younger Dryas event was triggered by a diversion of

Copyright 1990
by the American Geophysical Union.

Paper number 90PA01194.
0883-8305/90/90PA-01194 $10.00

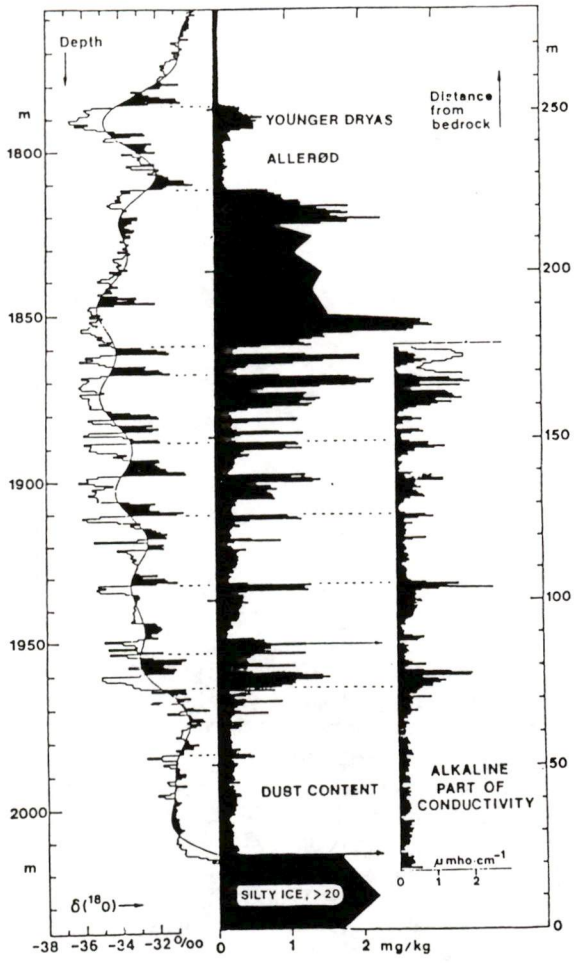


Fig. 1. Oxygen isotope composition, dust content, and alkalinity versus depth for the bottom 300 m of the Dye 3 Greenland ice core [Hammer et al., 1985] covering the time interval from about 8000 to at least 80,000 years ago. Each cold event (i.e., more negative $\delta^{18}O$ values) is accompanied by a severalfold increase in dust content of the ice and an increase in the alkalinity of the ice.

meltwater from the Mississippi drainage to the St. Lawrence drainage which led to the drowning of deep-water production in the northern Atlantic [Broecker et al., 1988a]. Radiocarbon dating of the paleoshorelines of Lake Agassiz and of the oxygen isotope record in the Gulf of Mexico sediments supports a synchroneity between the timing of the diversion of meltwater discharge and the onset of the Younger Dryas [Broecker et al., 1989]. The problem with this focus is that its logical extension is to postulate that each of the series of Greenland climate jumps during the last glacial period was caused by a diversion of meltwater. Such an origin is quite unlikely. In fact, the recent documentation by Fairbanks [1989] that the rate of sea level rise immediately before and immediately after the Younger Dryas was several times more rapid than that during the Younger Dryas requires a reexamination of the diversion theory for the cause of the Younger Dryas.

In this paper we provide evidence that the climatic oscillations seen in the Greenland ice core record have equivalents in the marine sediment record for the northern Atlantic and propose that these events are the result of an oscillation in the salt content of the Atlantic Ocean. Further, we propose that while the Younger Dryas was likely just another of these salt oscillations, its onset and demise were paced by meltwater diversions.

EVIDENCE FROM THE SEAFLOOR

While abundant evidence for the Younger Dryas event has been found in sediments from the northern Atlantic, equivalents of the series of events recorded in the glacial section of the Greenland ice cores have yet to be documented in the marine record [Broecker et al., 1988b]. Working with M. Kominz on the color record in deep-sea sediments, one of us (G. Bond), demonstrated that a fine structure exists in the gray tone record extracted from photos of cores from Deep Sea Drilling Project (DSDP) site 609 at 50°N -24°W in the eastern Atlantic (see Figure 2). As shown in Figure 3, the fine structure in this gray tone record resembles that in the ^{18}O record in the Camp Century core.

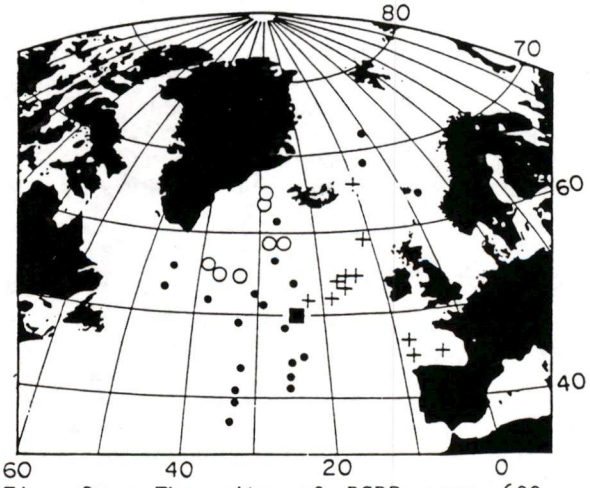


Fig. 2. The site of DSDP core 609 (square) is placed on a map showing the location of sites at which an Neogloboquadrina pachyderma (left coiling) abundance peak corresponding to the Younger Dryas is present (pluses) and is absent (open circle) in deep-sea cores. The sites (solid circles) at which the sedimentation rate is too slow for the recording of the Younger Dryas are also shown [from Broecker et al.,1988a].

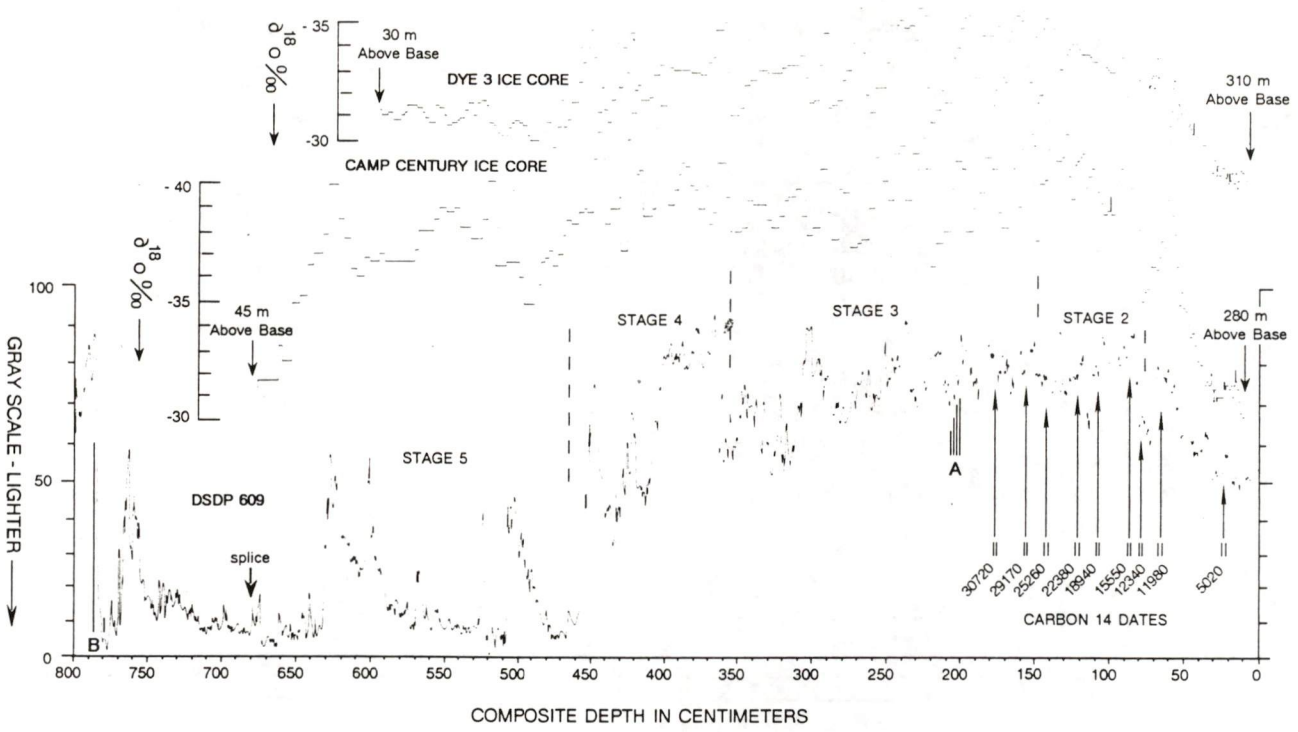


Fig. 3. Comparison of the gray scale record for DSDP site 609 from 50°N in the eastern Atlantic with the oxygen isotope records from the two Greenland ice cores [Dansgaard et al., 1971, 1982]. The radiocarbon ages were determined on hand-picked foraminifera shells by the AMS technique described by Suter et al.[1984]. The ice core record has been "stretched" to compensate for flow induced foreshortening and scaled to best match the marine record. B designates the location of termination II and A the couplet on which foraminiferal and lithic fragments counts were made. The depths in the ice core are measured above bed rock. Note that the upper ~1700 m (i.e., the last 8000 years) of each ice core record is not included.

In order to test whether these gray tone variations represent changes in surface water conditions, we examined the greater than 150 μm size fraction from six site 609 samples, using color as a guide to their positioning. The results are listed in Table 1. One pair of samples spans termination II which occurs at about 780 cm depth in the composite section (see B in Figure 3). Samples B1 and B2 are only a few millimeters apart, one from just below and the other from just above the color change which marks the termination. As can be seen in Table 1, the sample from just below the boundary consists of roughly equal number of lithic fragments and foraminifera shells. The lithic fragments are dominated by quartz grains with lesser amounts of feldspar and a few dark minerals. As these grains are too bulky to have been carried by the wind, they were presumably dropped from melting icebergs. The foraminifera shells in this sample are 90% Neogloboquadrina pachyderma (left coiling) signifying cold water conditions. By contrast, the sample from just above the color boundary is nearly free of lithic fragments and only 2% of the forams are N. pachyderma (left coiling). The remainder are warmer water species akin to those dwelling at this locale today. Both the disappearance of ice rafted debris and the shift in foram ecology suggest that the waters at this site underwent an abrupt warming which marked the termination of a major cold period (i.e., marine stage 6). If sedimentation was continuous, then at the ambient sedimentation rate of about 6 cm/1000 years (see Table 2), this transition from cold conditions to warm conditions must have occurred in less than one century! That this boundary is sharp was demonstrated long ago by Ruddiman et al. [1977] who studied six cores from the 50°N to 54°N latitude range in the northern Atlantic. They found that the faunal change associated with termination II occurred over a depth range of as little as a few centimeters which translates to a time interval as short as 1000 years. It remains to be determined whether the termination II in the 609 record has been sharpened by an erosional event or whether the record in the other cores has been blurred by bioturbation.

Broecker and Denton [1989] have proposed that deglaciations are triggered by reorganizations of the ocean-atmosphere system. In particular, they point to a sudden resumption of conveyor circulation in the Atlantic as a key ingredient of such reorganizations. As the conveyor brings vast amounts of warm water to the surface of the northern Atlantic its resumption

TABLE 1. Analyses of Coarse Fraction (>150 μm) Sieved From Samples From ODP Site 609 (50°N, 24°W, 3.9 km)

Sample	Depth in Core, cm	Coarse* Fraction, %	Total Forams, g^{-1}	N pach(L) Forams, g^{-1}	Other** Forams, g^{-1}	Lithic Frags, g^{-1}	N pach(L) Total Forams	Lithic Frags Total Forams	Gray Scale+
				Couplet (~40,000 years B.P.)					
A-1	201.0	14.4	3300	1680	1620	1430	0.51	0.42	darker
A-2	202.5	14.6	3740	1350	2390	720	0.36	0.19	intermediate
A-3	204.2	15.5	3170	1190	1980	850	0.38	0.27	intermediate
A-4	206.5	10.8	3990	550	3400	440	0.14	0.11	lighter
				Termination II (~128,000 years B.P.)					
B-1	just above 780	9.1	3600	85	3515	80	0.02	0.02	lightest
B-2	just below 780	20.6	2890	2600	290	2590	0.90	0.90	darkest

*>63μm; percent by weight
**Inflata, Bulloides, Glutinata, Pachyderma (R), etc.
+See Figure 2.

TABLE 2. AMS Radiocarbon Ages on Hand-Picked Foraminifera Shells From DSDP Core 609 (49° 53'N, 24° 14'W, 3884 m)

Depth, cm	Species	Radiocarbon Age, years	Corrected Age, years	Accumulation Rate cm/10^3 years
21-23	G. bulloides	5420± 80	5020	
63-65	G. inflata	12380±120	11880	
79-81	G. inflata	12740±140	12340	
105-107	N. pachyderma	19340±220	18940	Mean
112-113	N. pachyderma	21510±220	21110	
115-115	N. pachyderma	21770±220	21370	
118-120	N. pachyderma	22780±340	22380	5.95
139-141	G. bulloides	25660±440	25260	
153-155	N. pachyderma	29570±660	25170	
174-176	G. bulloides	31120±730	30720	
780	--	128,000*		6.09

*Age of Termination II

would explain not only the rapidity of the change associated with termination II but also its magnitude.

Since the meltback of the northern hemisphere ice sheets triggered by such a reorganization required about 7000 years for completion, icebergs must have been discharged into the Atlantic long after the termination event recorded by the site 609 color record. The absence of lithic fragments above the color change then suggests that the southward drifting icebergs melted away before drifting this far to the south (i.e., 50°N).

The remaining four samples come from the gray scale couplet located at about 2 meters depth in the core (age ~35,000 years; see A in Figure 3). One (A-1) is from the lightest portion of the couplet. Another (A-4) is from the darkest portion of the couplet. The other two (A-2 and A-3) are from the zone of gradation between these extremes. The four samples span 6 cm suggesting a duration of 1000 years for the half cycle. As listed in Table 1 and shown graphically in Figure 4, these samples have N. pachyderma (left coiling) and lithic fragment to total foraminifera ratios lying between those for the two samples spanning termination II. Further, the light portion of the couplet and the dark portion of the couplet differ in the same sense as do the samples on either side of termination II; i.e., the darker sample is richer in N. pachyderma (left coiling) and in lithic fragments than the lighter sample. However, the range of the difference is only about 40% of that seen across termination II (see Figure 4). Hence while the fine scale color changes do indeed record water temperature changes at the site of core 609 (i.e,, 50°N), these changes are not as extreme as those across the transition from full glacial to full interglacial conditions.

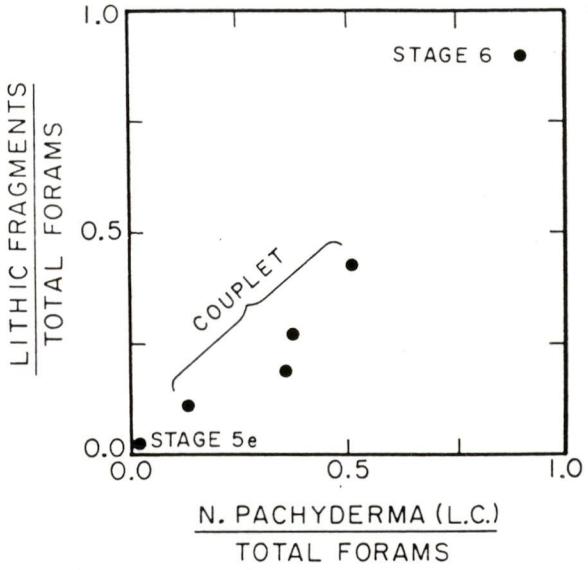


Fig. 4. Plot of the lithic fragment to total foraminifera shell ratio versus the N. pachyderma (left coiling) to total foraminiferal shell ratio for the six DSDP site 609 samples listed in Table 1. The higher either ratio, the colder the surface waters.

In situations such as this, blurring created by bioturbation must be considered. Radiocarbon measurements demonstrate that for open ocean sites in the tropics, the sediment is currently being homogenized to a depth of 6-12 cm [Nozaki et al., 1977; Peng et al., 1977, 1979; Berger and Killingley, 1982]. However, studies by Ruddiman and Glover [1972, 1982] and by Ruddiman et al. [1980] clearly demonstrate that the depth of bioturbation must be considerably less in sediments from the northern Atlantic than in the tropical cores on which radiocarbon measurements were conducted. In core 609, no evidence for bioturbation can be seen at termination II. While in other portions of this core burrow like structures are present, the mixing may be stochastic rather than pervasive. At this point we cannot assess to what extent the changes associated with the couplets have been reduced by mixing.

Isotopic measurements (see Table 3) on foraminifera reveal no significant change across this couplet. The 1‰ higher $\delta^{18}O$ value for N. pachyderma than for Globorotalia inflata and G. bulloides suggests that the N. pachyderma grew in colder water than did the other two species. The important message from these results is that the isotopic evidence does not require any change in the temperature for either the water in which N. pachyderma grew or that in which the subpolar species grew. Rather, the evidence suggests that only the blend changed (i.e., during the dark portion of the couplet more material formed in polar water was incorporated and during the light portion) less (see Table 1). This change in blend could have been accomplished by mixing (through bioturbation) of sediment consisting of the pure polar end-member deposited during a conveyor "off" portion of the cycle and sediment consisting of pure subpolar endmember deposited during the conveyor "on" portion of the cycle. By contrast, Ruddiman and McIntyre [1981] and Duplessy et al. [1986] viewed the situation in terms of migration of a "front" separating polar and subpolar waters. Following their hypothesis the cycle could be more nearly sinisoidal and need not show the full glacial to interglacial amplitude. Evidence presented here could also be interpreted in terms front migration on time scales shorter than the duration of the couplet. During each half of the couplet, the site was alternately covered by each water mass. In this scenario, the dark portion of the couplet represents a period when the site was covered more

TABLE 3. Oxygen Isotope and Carbon-Isotope Measurements on Samples From Couplet A.

Depth cm	G. inflata	G. bulloides	N. pachyderma	
		Oxygen Isotopic Ratio (‰)		
201.0	1.69	1.94	2.93	darker
202.5	1.84	1.93	3.03	↓
204.3	--	1.94	3.06	↓
206.5	2.12	1.94	2.97	lighter
		Carbon Isotopic Ratio (‰)		
201.0	1.29	-0.28	-0.15	darker
202.5	1.04	-0.17	+0.05	↓
204.3	--	-0.36	-0.12	↓
206.5	0.90	-0.17	-0.01	lighter

Made by C. Charles in the Lamont-Doherty Geological Observatory laboratory of R. Fairbanks.

frequently by polar waters and the light portion of the couplet a period when the site was less frequently covered by polar waters. Until the record of these events has been studied in more detail in cores from several latitudes, it is premature to conclude which of these hypotheses is the correct one.

Boyle and Rosener [1990] consider this same question in connection with a study of the Cd/Ca record kept by benthic foraminifera from a deep sea core in the Bermuda area. They show that bioturbation could easily alter a rectangular signal to a low-amplitude sine wave.

THE ATLANTIC SALT OSCILLATOR

We propose here the framework of a mechanism which could create the events observed in the Greenland ice cores. It involves oscillations in the oceans thermohaline circulation. The theoretical basis for such oscillations is given in papers by Stommel, 1961; Welander, 1982, and Ruddick and Zhang, 1989. Schnitker [1982] purports to have found evidence for such changes based on benthic foraminifera records for cores from the northwestern Atlantic. Our hypothesis concerns changes in the operation of the Atlantic's conveyor circulation. For ease of presentation we speak in terms of the conveyor going from "on" to "off". By "on" we mean a mode of operation akin to today's. By "off" we mean a mode in which the heat release to the atmosphere over the northern Atlantic and the export of North Atlantic Deep Water (NADW) to the southern ocean were greatly reduced. It is possible that the conveyor is still operative in the "off" mode but runs much slower and forms a more nearly closed circulation loop within the Atlantic itself.

We propose that during glacial time the Atlantic's conveyor circulation was modulated by periods of salt buildup and periods of salt drain down. For such an oscillator to function a mechanism must be identified to change the salt content of the Atlantic on the time scale of a millenium. Such a mechanism exists. Currently, the Atlantic is losing fresh water (via vapor transport) at the rate of 0.35±0.10 Sv = 10^6 m^3/s [Broecker et al., 1990]. If uncompensated by the exchange of more salty Atlantic waters with less salty water from outside the Atlantic, the salt content of the Atlantic would rise at the rate of about 1‰ per 1000 years. The density change created by an increase of one or so salinity units is enough to tip the balance between the conveyor "off" and conveyor "on" situation.

With this in mind let us consider the hypothetical cycle shown in Figure 5. We start with the conveyor off. The assumption is made that in the conveyor-off mode the rate of salt export from the Atlantic is less than the rate of salt buildup due to vapor loss. Hence the salt content and also the density of the Atlantic water increases. Further, in the absence of the heat released by the conveyor to the atmosphere over the northern Atlantic, the ice sheets would undergo net

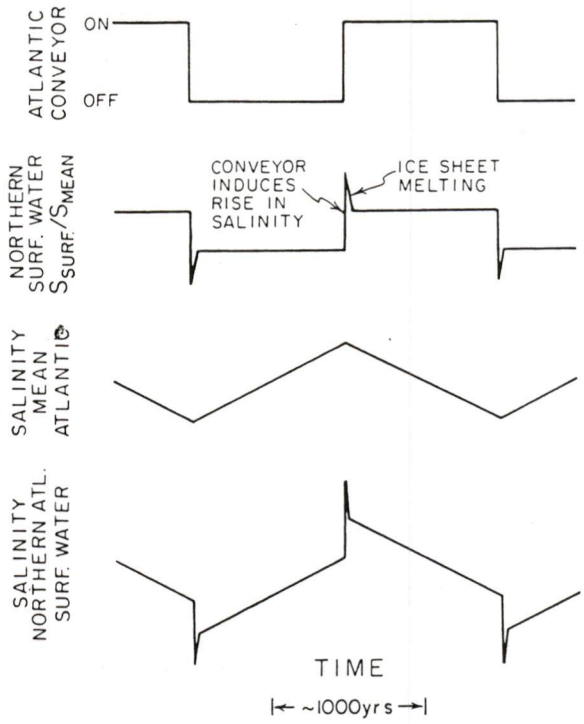


Fig. 5. Diagrammatic presentation of the salt oscillator proposed here. The conveyor is turned off by the decrease in Atlantic salinity caused by ice sheet melting and by conveyor export of salt. This shutdown causes the salinity of high latitude surface waters in the Atlantic to take a sudden drop thus stabilizing the shutdown (see second panel from top). The scale S_{SURF}/S_{MEAN} (second panel from the top) is the ratio for the salinity of surface waters in the northern Atlantic to the mean salinity for the Atlantic as a whole. The assumption is made that reduction in meltwater delivery which would follow closely on the heels of the shutdown would only partially compensate for the salinity drop associated with the shutdown (see second panel from top). During the next 1000 or so years the salinity of the Atlantic as a whole (see third panel from top) rises until the conveyor reinitiates. This reinitiation causes the salinity of high-latitude surface waters to undergo a sudden rise. This rise would be quickly countered by the introduction of meltwater. It is necessary to the success of this scenario that the compensation not be complete. In other words, the salinity reduction in high-latitude surface waters due to the inflow of meltwater cannot be larger than the salinity increase associated with the initiation of the conveyor.

growth (i.e., little meltwater would be added to the Atlantic). When a critical density threshold is reached, the conveyor springs into action. To reach this threshold, the deep water formed in the northern Atlantic must have a density great enough to push its way around the tip of Africa into the southern ocean.

Once in action the conveyor raises the salinity of northern Atlantic surface waters to a value much closer to the oceanic mean than was the case in the conveyor off mode [see Manabe and Stauffer, 1988]. Because of this the conveyor is self-stabilizing. However, this tendency toward stabilization would be countered by renewed meltwater input (driven by the heat released by the conveyor) which would dilute the salt in the surface waters in the region where deep waters form. An assumption necessary for the success of this scenario is that the salinity reduction in northern surface waters generated by the introduction of meltwater be smaller than the salinity enhancement in these waters created by the conveyor itself (see Broecker [1990] for discussion of this problem). In the conveyor "on" mode, the combination of salt export via the conveyor and meltwater input would gradually reduce the salinity of the entire Atlantic. Eventually the density would be reduced to the point where the conveyor would shut down. The shutdown would be self-stabilizing since it would cause a large drop in the salinity of the surface waters of the northern Atlantic. Of course, the cessation of meltwater input which would accompany the shutdown would counter this stabilization. Again, it is necessary to postulate that the salinity reduction associated with the shutdown was larger than the salinity increase associated with the stoppage of meltwater flow. This sequence of events is summarized in the appendix. In a separate paper (G. E. Birchfield and W.S. Broecker, A salt oscillator in the glacial Atlantic?, 2, A 'scale analysis' model, submitted to Paleoceanography, 1990) a mathematical representation of this oscillator will be presented.

IMPLICATIONS TO THE YOUNGER DRYAS

If the climatic events recorded in the glacial sections of the Greenland ice cores are the result of a salt oscillator operating in the Atlantic Ocean, then the question arises whether the Younger Dryas is yet another such oscillation. We suspect that this may be the case. During the warm interval preceding the Younger Dryas, the combination of meltwater input and salt export (via the conveyor) steadily reduced the salt content of the Atlantic culminating with a conveyor shutdown which brought on the Younger Dryas cold epoch. However, since this shutdown appears to have been triggered by the diversion of meltwater from the Mississippi to the St. Lawrence, we would have to postulate that this sudden input of this excess fresh water to the region where deep water formed crippled an already weakened conveyor. During the Younger Dryas the salt content of the Atlantic steadily increased until the conveyor reinitiated. Again, it appears that the diversion of meltwater back to the Mississippi allowed the salinity of northern Atlantic surface waters to achieve the value necessary for conveyor initiation. Hence the Younger Dryas may well have been yet another salt oscillation with the diversions of meltwater pacing the conveyor switches.

CONCLUSIONS

The claim by Fairbanks [1989] that the rate of meltwater generation during the Younger Dryas was much smaller than during the warm episodes immediately before and after this cold event forced us to rethink the cause of not only the Younger Dryas but also of the other rapid climate changes recorded in the Greenland ice cores. We propose that a salt oscillator operates in the Atlantic Ocean during times of major ice cover of the adjacent lands. When the Atlantic's conveyor system is operating, a combination of salt export and meltwater input cause the salinity and hence the density of Atlantic waters to decrease. When the density becomes sufficiently low that the deep water produced in the northern Atlantic no longer can force its way into the southern ocean, the conveyor stops. This stoppage greatly reduces the rate of salt export and reduces the rate of meltwater input causing the salt content of the Atlantic to increase until the conveyor is reinitiated. The Younger Dryas event was the last in a long series of these events. Its onset and demise were likely paced by diversions in the route of meltwater discharge.

APPENDIX: COMPARISON OF THE CONDITIONS ASSOCIATED WITH THE CONVEYOR "ON" AND "OFF" MODES OF THE ATLANTIC

Conveyor On

1. Warm water rising from the thermocline to the surface of the northern Atlantic releases heat to the overlying air. This extra heat causes the ice sheets surrounding the Atlantic to retreat.
2. The large throughput of conveyor water maintains the salinity of the surface waters in the northern Atlantic at values close to the mean for the Atlantic.
3. Deep water formed in the northern Atlantic carries excess salt the length of this ocean into the southern ocean.

Conveyor Off

1. In the absence of a strong inflow of warm water from the Atlantic's thermocline, surface waters of the northern Atlantic are much cooler. This permits a net growth of the ice sheets around the northern Atlantic.
2. In the absence of the strong throughput of conveyor water, the salinity of northern Atlantic surface waters drops well below the mean for Atlantic waters.
3. In the absence of the conveyor the export of salt from the Atlantic into the southern ocean is greatly reduced.

Acknowledgments. Funds provided by a gift from Exxon Research division and by the National Science Foundation Climate Dynamics Program made this work possible. Part of this work was funded by the Swiss National Science Foundation. Lamont-Doherty Geological Observatory of Columbia University contribution 4642.

REFERENCES

Beer, J., H. Oeschger, M. Andree, G. Bonani, M. Suter, W. Wolfli, and C.C. Langway, Jr., Temporal variations in the ^{10}Be concentration levels found in the Dye 3 ice core, Greenland, Ann. Glaciol., 5, 16-17, 1984.

Berger, W. H., and J. S. Killingley, Box cores from the equatorial Pacific: ^{14}C sedimentation rates and benthic mixing, Mar. Geol., 45, 93-125, 1982.

Boyle, E.A., and P. Rosener, Further evidence for a link between late Pleistocene North Atlantic surface temperatures and North Atlantic deep water production, Global Planet. Change, in press, 1990.

Broecker, W.S., and G. H. Denton, The role of ocean-atmosphere reorganizations in glacial cycles, Geochim. Cosmochim. Acta, 53, 2465-2501, 1989.

Broecker, W. S., D. Peteet, and D. Rind, Does the ocean-atmosphere have more than one stable mode of operation, Nature, 315, 21-25, 1985.

Broecker, W. S., M. Andree, W. Wolfli, H. Oeschger, G. Bonani, J. Kennett, and D. Peteet, The chronology of the last deglaciation: Implications to the cause of the Younger Dryas event, Paleoceanography, 3, 1-19, 1988a.

Broecker, W.S., M. Andree, G. Bonani, W. Wolfli, H. Oeschger, and M. Klas, Can the Greenland climatic jumps be identified in records from ocean and land?, Quat. Res., 30, 1-6, 1988b.

Broecker, W. S., J. P. Kennett, B. P. Flower, J. Teller, S. Trumbore, G. Bonani, and W. Wolfli, The routing of Laurentide ice-sheet meltwater during the Younger Dryas cold event, Nature, 341, 318-321, 1989.

Broecker, W. S., T.-H. Peng, J. Jouzel, and Gary Russell, The magnitude of global fresh water transports of importance to ocean circulation, Clim. Dyn., 4, 73-79, 1990.

Broecker, W.S., Salinity history of the northern Atlantic during the last deglaciation, Paleoceanography, in press, 1990.

Dansgaard, W., S. J. Johnsen, H. B. Clausen, and C. C. Langway, Climatic record revealed by the Camp Century ice core. Late Cenozoic Glacial Ages, edited by K.K. Turekian, pp. 37-56, Hartford Conn., Yale University Press, 1971.

Dansgaard, W., H.B. Clausen, N. Gundestrup, C.U. Hammer, S.J. Johnsen, P. Kristinsdottir, and N. Reeh, A new Greenland deep ice core, Science, 218, 1273-1277, 1982.

Dansgaard, W., J.W.C. White, and S.J. Johnson, The abrupt termination of the Younger Dryas climate event, Nature, 339, 532-533, 1989.

Dansgaard, W., and H . Oeschger, Past environmental long-term records from the Arctic, in The Environmental Record in Glaciers and Ice Sheets, edited by H. Oeschger and C. Langway, Jr., pp. 287-318, John Wiley, New York, 1989.

Duplessy, J.-C., M. Arnold, P. Maurice, E. Bard, J. Duprat, and J. Moyes, Direct dating of the oxygen-isotope record of the last deglaciation by ^{14}C accelerator mass spectrometry, Nature, 320, 350-352, 1986.

Fairbanks, R.G., A 17,000-year glacio-eustatic sea level record: influence of glacial melting rates on the Younger Dryas event and deep-ocean circulation, Nature, 342, 637-642, 1989.

Finkle, R.C., and C.C. Langway, Jr., Global and local influences on the chemical composition of snowfall at Dye 3, Greenland: The record between 10 ka B.P. and 40 ka B.P., Earth Planet. Sci. Lett., 73, 196-206, 1985.

Hammer, C.U., H.B. Clausen, W. Dansgaard, A. Neftel, P. Kristinsdottir, and E. Johnson, Continuous impurity analysis along the Dye 3 deep core. in Greenland Ice Core: Geophysics, Geochemistry, and the Environment, Geophys. Monogr. Ser., vol. 33, edited by C.C. Langway, H. Oeschger and W. Dansgaard, AGU, 90-94, Washington, 1985.

Manabe, S., and R.J. Stauffer, Two stable equilibria of a coupled ocean-coupled ocean-atmosphere model, J. Clim., 1, 841-866, 1988.

Neftel, A., H. Oeschger, T. Staffelbach, and B. Stauffer, CO_2 record in the Byrd ice core 50,000-5,000 years B.P., Nature, 331, 609-611, 1988.

Nozaki, Y., J. Cochran, K. Turekian, and G. Keller, Radiocarbon and ^{210}Pb distribution in submersible-taken deep-sea cores from Project FAMOUS, Earth Planet. Sci. Lett., 34, 167-173, 1977.

Oeschger, H., J. Beer, U. Siegenthaler, B. Stauffer, W. Dansgaard, and C.C. Langway, Jr., Late-Glacial climate history from ice cores, A. G. U., Geophys. Monogr. 29, Climate Processes and Climate Sensitivity (M. Ewing Ser.), 299-306, 1984.

Peng, T.-H., W.S. Broecker, G. Kipphut, and N. Shackleton, Benthic mixing in deep sea cores as determined by ^{14}C dating and its implications regarding climate stratigraphy and the fate of fossil fuel CO_2, in The Fate of Fossil Fuel CO_2 in the Ocean, edited by N. Anderson and A. Malahoff, pp. 355-374, Plenum, New York, 1977.

Peng, T.-H., W. S. Broecker, Rates of benthic mixing in deep-sea sediment as determined by radioactive tracers, Quat. Res., 11, 141-149, 1979.

Rind, D., D. Peteet, W. Broecker, A. McIntyre, and W. Ruddiman, The impact of cold North Atlantic sea surface temperatures on climate: Implications for the Younger Dryas cooling (11-10 k), Clim. Dyn., 1, 3-33, 1986.

Ruddick, B., and L. Zhang, The mythical thermohaline oscillator?, J. Mar. Res., 47, 717-746, 1989.

Ruddiman, W. F., and L.K. Glover, Vertical mixing of ice-rafted volcanic ash in North Atlantic sediments, Geol. Soc. Am. Bull., 83, 2817-2836, 1972.

Ruddiman, W.F., and A. McIntyre, The North Atlantic Ocean during the last deglaciation, Palaeogeogr. Palaeoclimatol. Palaoecol., 35, 145-214, 1981.

Ruddiman, W.F., and L.K. Glover, Mixing of volcanic ash zones in subpolar North Atlantic sediments, in The Ocean Floor, edited by R.A. Scrutton and M. Talwani, pp. 37-60, John Wiley, New York, 1982.

Ruddiman, W.F. , C.D. Sancetta, and M. McIntyre, Glacial/interglacial response rate of subpolar North Atlantic waters to climatic change: The record in ocean sediments, Philos. Trans. R. Soc. London, Ser. B, 280, 119-142, 1977.

Ruddiman, W.F., G.A. Jones, T.-H. Peng, L.K. Glover, B.P. Glass and P.J. Liebertz, Tests for size and shape dependency in deep-sea mixing, Sediment Geol., 25, 257-276, 1980.

Schnitker, D., Climate variability and deep ocean circulation: Evidence from the north Atlantic, Palaeogeogr. Palaeoclimatol. Palaeoecol., 40, 213-234, 1982.

Stauffer, B., H. Hofer, H. Oeschger, J. Schwander, and U. Siegenthaler, Atmospheric CO_2 concentration during the last glaciation, Ann. Glaciol., 5, 160-164, 1984.

Stommel, H., Thermohaline convection witth two stable regimes of flow, Tellus, 13, 224-228, 1961.

Suter, M., R. Balger, G. Bonani, H.J. Hofmann, E. Morenzoni, M. Nessi, W. Wolfli, M. Andree, J. Beer, and H. Oeschger. Precision measurements of ^{14}C in AMS--Some results and prospects, Nucl. Instrum. Methods Physics Res., 5, 117-122, 1984.

Watts, W. A., Regional variation in the response of vegetation of Lateglacial climatic events in Europe. in Studies in the Late Glacial of North-West Europe, edited by J.J. Lowe, J.M.Gray, J.E. Robinson, pp. 1-22, Pergamon, New York, 1980.

Welander, P., A simple heat-salt oscillator, Dyn. Atmos. Oceans, 6, 233-242, 1982.

G. Bonani and W. Wolfli, Institut fur Mittelenergiephysik, ETH Honggerberg, 8093 Zurich, Switzerland.

G. Bond, W.S. Broecker, and M. Klas, Lamont-Doherty Geological Observatory of Columbia University, Palisades, NY 10964.

(Received February 27, 1990;
revised May 22, 1990;
accepted May 24, 1990.)

The Biggest Chill

by Wallace S. Broecker

We, the inhabitants of planet Earth, are performing a gigantic climate experiment. Begun by our grandparents, its results will be recorded by our grandchildren. The experiment involves the production and release into the atmosphere of gaseous molecules made up of three or more atoms; the most important of these are carbon dioxide (CO_2), methane (CH_4), and the freons (CF_3Cl and CF_2Cl_2). Unlike the two-atom molecules, oxygen (O_2) and nitrogen (N_2), which make up 99 percent of our atmosphere, these multiatom molecules have the capacity to capture packets of outgoing radiation from the earth. Just as a blanket helps retain our body heat, these gases retain the earth's heat. Hence, the result of our experiment will be to make the surface of our planet warmer.

Unfortunately, our knowledge of the earth's climate system is still not good enough to reliably predict the effects of this heating on wildlife, agriculture, and a host of other matters important to humans. We will only know the results of the buildup of these "greenhouse" gases if our learning rate greatly accelerates.

In the face of such uncertainty, one might ask why the experiment is not declared dangerous to the well-being of the planet and abandoned. The reason is that the generation of greenhouse gases is not an enterprise designed by scientists. Rather, it is an inescapable byproduct of our civilization. Carbon dioxide is produced when coal, oil, and natural gas are burned. When carbon atoms, which make up the bulk of these fuels, combine with oxygen molecules from the atmosphere, an amount of CO_2 weighing roughly three times more than the fuel burned is generated. There is no feasible way to prevent this CO_2 from escaping into the atmosphere. Methane is produced by living organisms. The metabolic systems of steers and the bacteria in the mud of rice paddies are methane producers. Hence, some methane will be added to the atmosphere for each hamburger or bowl of rice we eat. Freons are manufactured by industry as foaming agents, refrigerants, and propellants. Except for the freons, the greenhouse gases are products of activities essential to human survival. If five or so billion people are to be maintained on our planet, we must continue the greenhouse experiment. We are hooked.

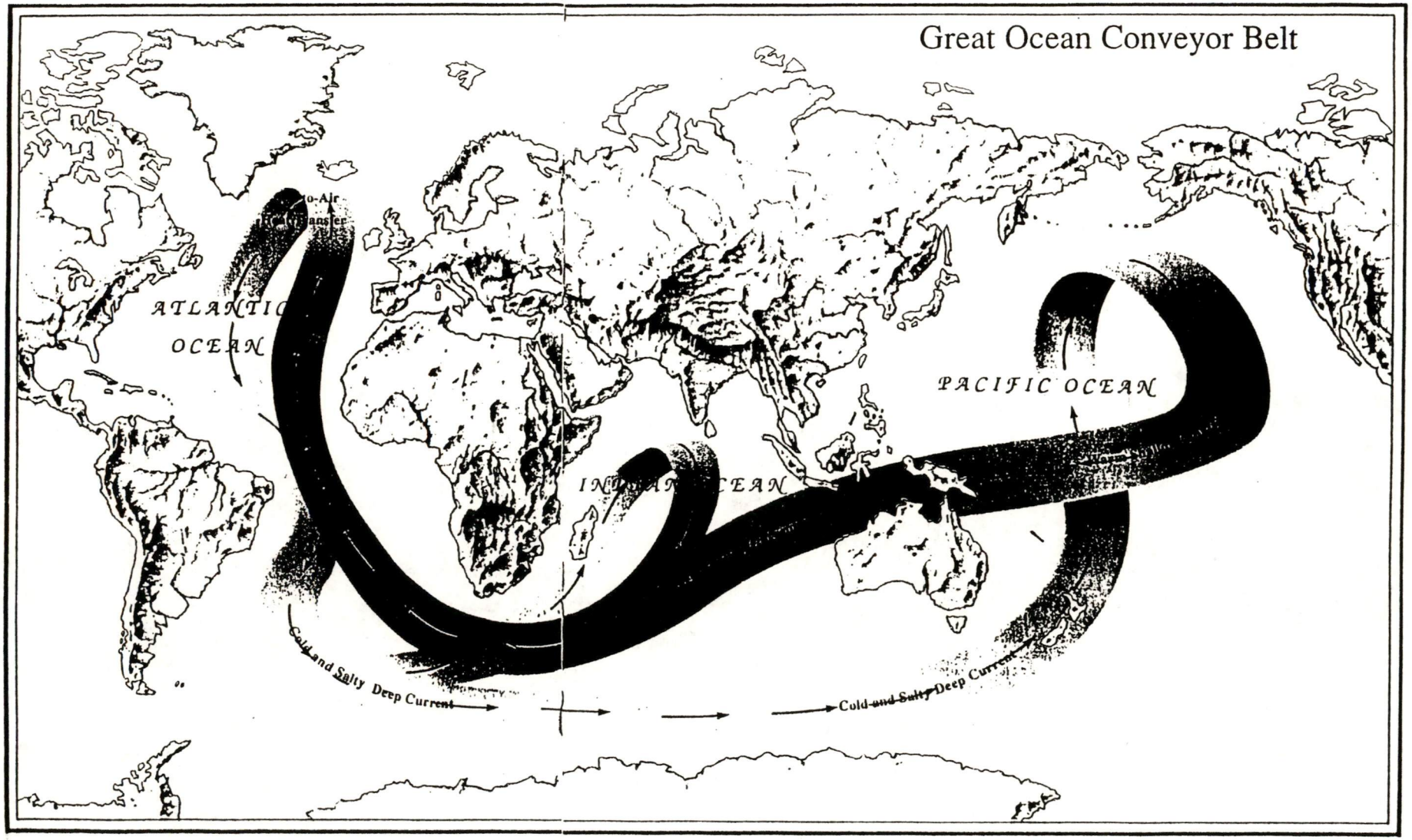
Scientists struggle to increase our understanding of how the earth's environmental system operates in the hope that we will be able to predict at least some of the coming consequences. If so, we can develop strategies to cope with the "bad" and take advantage of the "good" results of this experiment.

These inquiries have recently revealed a piece of disquieting information. Geological studies suggest the earth's climate system resists change until pushed beyond some threshold; then it leaps into a new mode of operation. The situation is akin to that of a radio with automatic frequency control. When the dial on such a radio is turned, instead of one station fading out and the next one fading in, the radio remains locked on one station until a threshold is crossed, at which point it suddenly jumps to another station. The implication of this finding for future climates is clear: the effects of the greenhouse gas buildup may come in sudden jumps, rather than gradually. Such jumps would pose great threats to humans and wildlife.

Our suspicion that the earth's climate changes in leaps comes from the evidence recorded in deep-sea sediments and in ice. The most studied of these records is the amount of heavy oxygen found in the preserved shells of microscopic animals on the ocean floor. The heavy form of oxygen in water vapor tends to be lost as atmospheric moisture is transported to the icecaps. The larger the icecap, the more heavy oxygen remains behind in the seawater. Thus, in eras when the icecaps were large, shelled organisms contained more heavy oxygen than they did when the icecaps were small; the shells therefore contain a history of the ice ages.

The oxygen isotope record tells us that over the last million years the polar icecaps have changed in a cyclic fashion, going from the rather small size of the current warm period to the very large size

Published in Natural History, Vol. 96, No. 10, October, 1987, pp. 74-82.



Illustrations by Joe Lelkonner

at the maximum of the last glaciation. More important, these fluctuations in ice volume have been shown to be in tune with periodic changes in the earth's orbit around the sun, generated by gravitational interactions among the objects making up our solar system. Because the timing of the oxygen isotope changes (as determined by age measurements on deep-sea sediment cores) matches what would be expected if the changes were driven by the earth's changing orbit, scientists are reasonably certain of the cause-and-effect relationship.

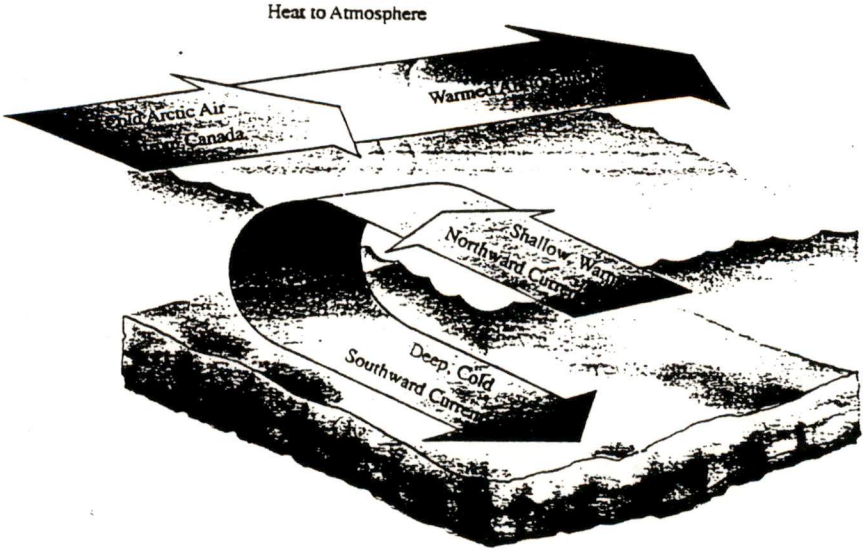
Why do changes in the characteristics of the earth's orbit have anything to do with climate? The answer is that these changes alter the earth's seasons. The relative amounts of each year's sunlight received during the winter months, as opposed to the summer months, changes in accordance with the changing orbit. Exactly how changes in the strength of the seasons drive the expansion and contraction of the earth's polar icecaps remains a matter of debate.

While the oxygen isotope record in the deep-sea sediments provided evidence pointing to the earth's orbital cycles as the pacemaker of glaciation, it also tended to lull scientists into concluding that the earth's climate responds gradually when pushed. This conclusion was drawn despite the realization that the response of polar icecaps to changing climate would have to be so sluggish that a smooth oxygen isotope record would be expected no matter how abrupt the changes in environmental conditions might be. So lulled were we that other clues in paleoclimatic records that pointed to abrupt response were largely disregarded.

The awakening came in the early 1980s when Hans Oeschger and his group at the university in Bern, Switzerland, carried out detailed measurements of the CO_2 content of air trapped in the ice from a deep boring made at a site in southern Greenland. These measurements concentrated on a section of the core on which earlier studies made by the Danish group of Willi Dansgaard had shown repeated leaps in Greenland's air temperature. To everyone's surprise, each of Dansgaard's jumps was accompanied by a 20 percent change in the CO_2 content of the air trapped in bubbles in the ice (and hence in the CO_2 content of air above Greenland at the time the ice formed).

Eyebrows were raised by Oeschger's CO_2 jumps because while the temperature jumps could be written off as a curiosity of Greenland, the CO_2 changes could not. The atmosphere's CO_2 is well mixed with its other gases, hence a measurement in Greenland typifies the entire globe. Furthermore, the changes in CO_2 content found by the Oeschger group occurred in times as short as a few hundred years. To bring about these changes in CO_2 requires some extraordinary change in the earth's chemical cycles, particularly those operating in the ocean. Scientists were therefore forced to the realization that the leaps in Greenland's climate were far-reaching, involving the workings of the ocean as well as those of the atmosphere.

The new look at the ocean triggered by the finding of the Oeschger group brought to the fore the potential importance of a curious tie that exists between the functioning of today's ocean and today's atmosphere. This tie results in a globe-straddling ocean current that keeps north-



Sea-to-Air Heat Transfer *At the northern Atlantic limit of the ocean conveyor belt, surface waters release heat into the atmosphere, greatly moderating Europe's climate.*

ern Europe unusually warm. Paris lies almost a full ten degrees farther north than New York, yet its mean annual temperature is similar to that of New York.

The extra heat received by northern Europe is carried by a conveyor-belt-like ocean current. The part of the conveyor closer to the surface moves to the north; the conveyor's deeper part moves to the south. The important point is that the water of the upper part is warm, while that of the lower part is cold. The temperature change occurs at the northern limit of the belt (in the region around Iceland). Here, during the winter months, water warmed during its passage through the tropical and temperate Atlantic meets air cooled during its passage over frigid Canada. The meeting results in the transfer of heat from the sea to the air. The amount of heat is staggering, measuring about 30 percent of that received by the surface of the North Atlantic from the sun. The result of this transfer is twofold. First, the sting of the cold Canadian air masses is removed before the air hits northern Europe. Second, the waters are cooled and consequently made more dense. The extra density allows the water to sink to the abyss and feeds the lower part of the conveyor. Thus the ocean current acts as a pump, extracting heat from low-latitude air and transferring it to high-latitude air.

The water that sinks to the bottom of the northern Atlantic flows down the full length of the Atlantic, around Africa, through the southern Indian Ocean, and finally up the Pacific Ocean. This deep current carries twenty times more water than the combined world rivers.

There is also an ocean conveyor belt in the North Pacific but it runs the opposite way around. Deep waters move toward the north and upwell to the surface. From there they move toward the equator in the upper ocean. So in today's world, the Atlantic Ocean conveyor belt carries tropical heat for delivery to the atmosphere at high northern latitudes, while the Pacific conveyor belt carries cold surface waters southward, pushing the invading warm waters back toward the equator. Today's major ocean current system thus heats the lands adjacent to the northern Atlantic.

While we don't have the complete answer to why our ocean operates in this fashion, we do have the first principles. The pattern of circulation is governed by the sea's salt. To understand this we must consider the transport of water through the atmosphere. The water that evaporates from the ocean falls eventually as rain or snow. Some of this precipitation reaches the land and some reaches the sea. Some precipitation that falls on land evaporates (mainly from plants) and some runs down the rivers and back to the sea. This cycle must exactly balance: for each molecule that evaporates from the sea, one molecule must return to it either by precipitation on its surface or from the mouth of a river. While this is true for the ocean as a whole, it need not be true for each part of the ocean. In fact, in today's world, an imbalance exists between the Atlantic and the Pacific. The Atlantic loses more water by means of evaporation than it gains by precipitation and continental runoff. The situation is reversed in the Pacific, which receives more water as rain and runoff than it loses by evaporation. While this imbalance is compensated for by a net flow of seawater from the Pacific to the Atlantic, it leaves a mark on the ocean's salt budget. Salt does not evaporate. Thus, the transport of water vapor from the Atlantic to the Pacific enriches the waters of the North Atlantic in salt content. The enrichment in salt must be compensated for by a flow of more salty water from the Atlantic to the Pacific. This is accomplished by the great conveyor belt: the water sinking to the abyss in the northern Atlantic carries excess salt.

The ocean conveyor system maintains higher surface water temperatures in the northern Atlantic than in the northern Pacific. Warmer waters have a higher vapor pressure and lose more water to the air by evaporation. Thus the rate of evaporation from the Atlantic is higher than that from the Pacific. This creates a global "still": water is extracted from the warm Atlantic and transferred through the atmosphere to the cool Pacific.

The phenomenon that maintains this situation is a devilish one; the circulation pattern is self-reinforcing and hence self-stabilizing. The deep current is driven by the extra density supplied to the waters of the northern Atlantic through the enrichment of salt. The enrichment of salt is driven by the heat carried by the water that flows northward in the upper Atlantic. Thus we have a classic chicken and egg situation; excess evaporation causes the deep current and the deep current causes excess evaporation.

The self-stabilization of this great conveyor belt is like the radio automatic frequency control already mentioned. And like that control, the mode of operation of the joint ocean–atmosphere operation will jump if pushed too far. The evidence contained in paleoclimatic records seems to be telling us that the conveyor of today's ocean did not function during the glacial time. Hence it is tempting to conjecture that the turning on and off of the conveyor constitutes an important link between the earth's orbits and our climate. When the belt is in operation, the warmth it delivers prevents ice from accumulating on the lands surrounding the northern Atlantic; when the conveyor is not in operation, these lands are sufficiently cold to permit their glaciation. If this is indeed the case, then the orbitally induced changes in seasonality must somehow alter the extent to which the water evaporating from the Atlantic Ocean escapes removal by the precipitation that falls on continental areas whose drainage is back into the Atlantic. Salt buildup is caused only by that fraction of the water evaporating from the Atlantic that escapes these basins and falls as rain in the Pacific or on continental drainage basins feeding the Pacific.

As we do not yet understand enough about the rules controlling the transport of water vapor through the atmosphere, we cannot say why changes in seasonality cause changes in the transport of water vapor from one ocean basin to another. We can only say that compelling evidence exists in the marine-sediment record for a flipping on and off of the ocean conveyor belt. Since the most vulnerable attribute of the conveyor is water-vapor transport from the Atlantic to the Pacific, some link between this transport and seasonality seems logical.

Evidence for rapid jumps in climate on the land surrounding the northern Atlantic was discovered many decades ago by scientists studying pollen grains preserved in sediments. The record from bogs created during the early phases of the retreat of the icecap that covered Scandinavia and the British Isles during the last glaciation (20,000 to 14,000 years ago) shows a transition from the herbaceous shrubs of the cold period back to the forests of a warmer period. Those early postglacial forests persisted for about 2,000 years and then were suddenly replaced by shrubs akin to those of glacial time. This intense cold snap lasted about 700 years and then just as suddenly came to an end, permitting the forests to return. This brief reversion to cold conditions, which punctuated the period of deglaciation, was named the Younger Dryas (dryas is one of the herbaceous plants that clothed the landscape during the glacial time).

Like other signs pointing to rapid climate change, this rather extraordinary and relatively short-lived return to cold conditions was not given very high billing until Oeschger's group found the rapid CO_2 changes. It then became the focus of attention because detailed records for many localities on the earth's surface were available for the time interval when the earth emerged from its last episode of

glaciation. Furthermore, the records from those sites showed that the Younger Dryas had a distinct geographic pattern. It is a prominent feature in records from the floor of the northern Atlantic and the surrounding continental areas (Maritime Canada, Greenland, and northern Europe). But it is not found in records from the continental United States.

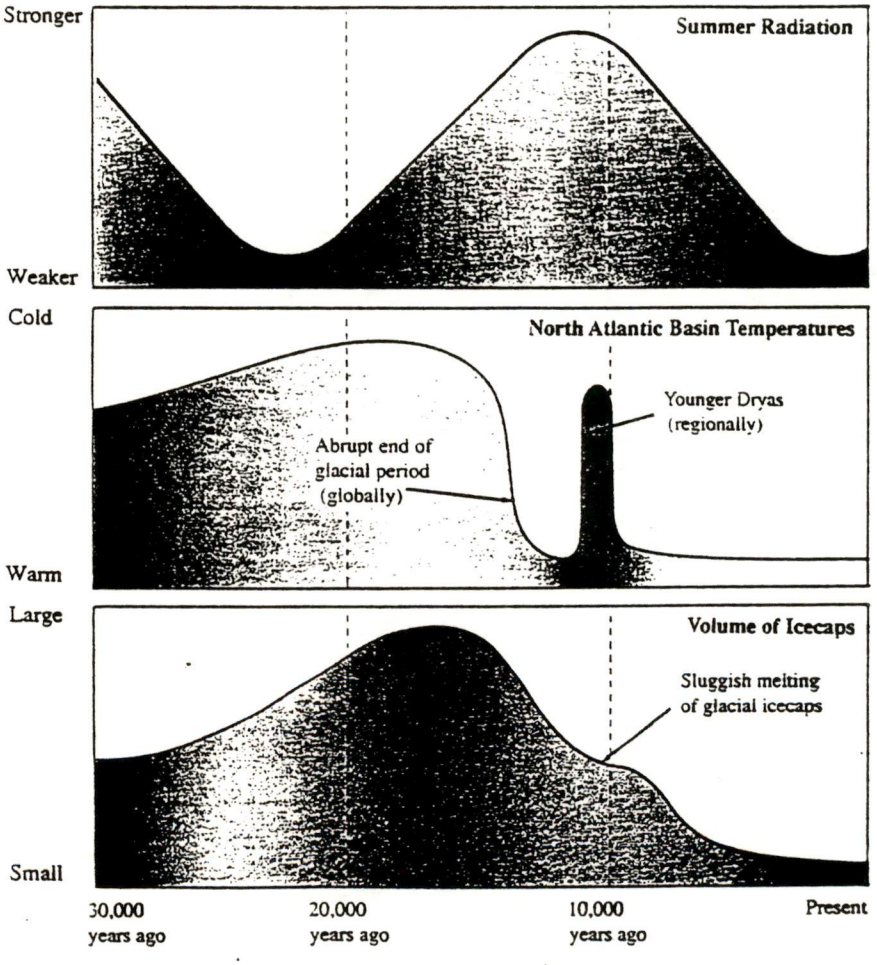
This geographic pattern has been shown by computer simulations of the global climate system to be what would be expected if the ocean conveyor belt were to be turned off (and with it the enormous amount of heat delivered to the atmosphere above the northern Atlantic). Air temperatures over the eastern fringe of Canada, over Greenland, and over much of western Europe would plunge about 15°F. By contrast, no significant change in temperature would be seen in the United States. Hence, the geographic pattern of the Younger Dryas event points to the ocean conveyor as the causal villain.

Evidence from ocean-sediment cores taken in the northern Atlantic strengthens this case. Not only do the shells of the surface-dwelling plankton show a dramatic shift back to cold-water species during the Younger Dryas interval but also, as shown by Edward Boyle of MIT, the content of the trace metal cadmium in the shells of bottom-dwelling foraminifera indicates that cold deep waters, akin to those present during glacial times, returned during the Younger Dryas.

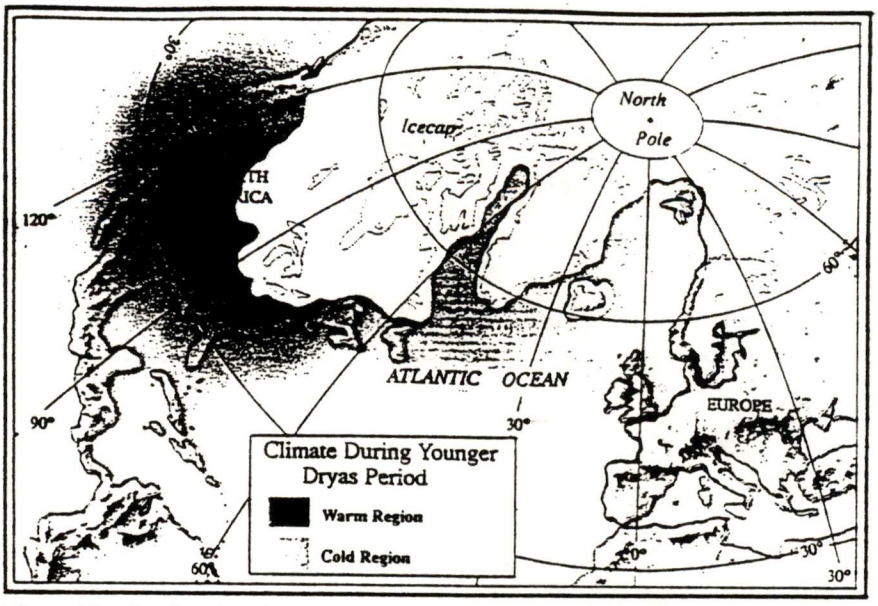
So we get the following picture. A full-fledged glaciation dominated our planet from about 20,000 to about 14,000 years ago. This corresponded to a time when the earth's orbital cycles gave rise to reduced seasonality at high latitudes in the Northern Hemisphere. During this time the ocean was "on another station," meaning its conveyor belt was not in operation. Then, as the orbits led to gradual strengthening of seasonality, the conveyor was switched back on. The heat released by the conveyor to the atmosphere over the northern Atlantic caused the great ice sheets to melt. But about 2,000 years later the conveyor came to an abrupt halt, bringing back cold conditions to the lands around the northern Atlantic. Then after a 700-year hiatus, the conveyor belt sprang back into action and has run steadily up to the present. Why the brief stoppage?

To understand what appears to be the answer to this question, we must first appreciate that a staggering 12-million cubic miles of water was bound up in the continental ice sheets of the Northern Hemisphere at the peak of the last glaciation. During the 5,000-year period when this ice melted away, the flow of meltwater must have averaged about half the current discharge of the Northern Hemisphere's combined rivers. Where it went would therefore have an important impact on the ocean's salt cycle.

Geologists studying the deposits left behind during the retreat of the largest of the glacial icecaps, the one that covered Canada from the Rocky Mountains to the Atlantic Ocean, have reconstructed the routes taken by the meltwater released from its southern margin. Their studies reveal that during the initial phases of melting, all routes converged on the Mississippi River and hence all the meltwater flowed into the Gulf of Mexico. However, starting about 11,800 years ago, those routes were captured one after another by eastward-leading channels that progressively opened as the ice front retreated to the north. First, the water entering the basins of what are now Lakes Erie and Ontario was diverted to the sea through the Hudson River valley. Then the water entering the basins of what are present-day Lakes Huron and Michigan was diverted to the Saint Lawrence River valley through a channel in the glacially depressed landscape north of Lake Erie. Finally, the biggest and most important of these diversions occurred when a lobe of ice blocking off the eastern end of what is now Lake Superior melted, allowing water to flow into Lake Huron and from there to the Saint Lawrence. At this point all the water melting from the southern margin of the Laurentide ice sheet was flowing eastward into the Atlantic. Nearly all of this water reached the Atlantic via the Saint Lawrence River. While the diversion of the meltwater from the Mississippi to the Saint Lawrence occurred in



Fluctuations in the earth's orbit, affecting how much summer sunlight the earth receives (top graph), have expanded and contracted the polar icecap, driving the Northern Hemisphere in and out of glacial (Ice Age) episodes. Although the volume of the ice changes sluggishly and gradually (bottom graph), an abrupt global warming has marked the end of each glacial period, indicating that ocean–atmosphere operation can change suddenly (middle). The Younger Dryas event, a 700-year return to glacial conditions that interrupted the present warm episode, is thought to have been caused by a sudden diversion of melting Canadian ice sheet waters from the Mississippi to the Saint Lawrence River.



The sudden, localized cooling of Europe and Maritime Canada during the Younger Dryas event indicates that the great ocean conveyor belt suddenly stopped operating.

several discrete steps over a period of about 800 years, the largest of these diversions was the last, involving the meltwater released from about 60 percent of the southern perimeter of the Laurentide ice sheet. As dated by the radiocarbon method, it occurred about 11,000 years ago. Within the margin of error of such age determinations, this corresponds to the time the Younger Dryas began.

Scientists understand why the sudden diversion of a large meltwater flow from the Mississippi River to the Saint Lawrence would affect the ocean conveyor. As stated above, an essential feature of this system is the densification through cooling of high salt content water in the northern Atlantic. Today, the sinking of this water feeds a globe-encircling deep current. The sudden influx directly into the northern Atlantic of an amount of water equivalent to that carried by the Amazon River would almost certainly diminish the salinity of surface waters in the northern Atlantic enough to disrupt the deep-water formation process. One might say that the Younger Dryas was not only a warning about the manner in which climate reacts when pushed but also clearly showed that the coupling between the transport of fresh water across the earth's surface and the transport of salt within the sea is a critical element in the earth's response to climate change.

If this reading of the paleoclimatic record is correct, then we must face up to the reality that our climatic system does not operate in an orderly manner. As the greenhouse gases we produce build up, the ocean–atmosphere system may leap to yet another mode of operation. Unfortunately, the paleoclimatic record provides no clues as to how the earth's climate system responds when warmed beyond its prevailing state. Over the period for which our paleoenvironmental records are sufficiently detailed to permit such reconstructions, climate has not been significantly warmer than today's. So we are pushing the earth into an unknown realm. We have no way to predict how the great ocean conveyor will respond, nor can we be sure of other important elements of the system, which are subject to dramatic change.

The computer simulations that have greatly improved our ability to predict weather have also told us some important things about the possible response to the greenhouse buildup. But because of their basic design, these computer models cannot tell us anything about the ocean–atmosphere system and leaping climates. At present no one knows how to incorporate the oceans into these simulations. Decades may pass before this can be done. Even then I doubt if computer simulations will offer much insight into the changes in climate that might be triggered by the greenhouse buildup.

The upshot is that we must take our greenhouse experiment more seriously. Rather than treating it as a cocktail hour curiosity, we must view it as a threat to human beings and wildlife that can be resolved only by serious study over many decades. We must expand our efforts to understand the operation of each of the units of the earth's climate system and how they interact. Only in this way will our grandchildren be able to prepare wisely for the changes that are bound to be wrought by our great experiment. □

The Biggest Chill

by Wallace S. Broecker

We, the inhabitants of planet Earth, are performing a gigantic climate experiment. Begun by our grandparents, its results will be recorded by our grandchildren. The experiment involves the production and release into the atmosphere of gaseous molecules made up of three or more atoms; the most important of these are carbon dioxide (CO_2), methane (CH_4), and the freons (CF_3Cl and CF_2Cl_2). Unlike the two-atom molecules, oxygen (O_2) and nitrogen (N_2), which make up 99 percent of our atmosphere, these multiatom molecules have the capacity to capture packets of outgoing radiation from the earth. Just as a blanket helps retain our body heat, these gases retain the earth's heat. Hence, the result of our experiment will be to make the surface of our planet warmer.

Unfortunately, our knowledge of the earth's climate system is still not good enough to reliably predict the effects of this heating on wildlife, agriculture, and a host of other matters important to humans. We will only know the results of the buildup of these "greenhouse" gases if our learning rate greatly accelerates.

In the face of such uncertainty, one might ask why the experiment is not declared dangerous to the well-being of the planet and abandoned. The reason is that the generation of greenhouse gases is not an enterprise designed by scientists. Rather, it is an inescapable byproduct of our civilization. Carbon dioxide is produced when coal, oil, and natural gas are burned. When carbon atoms, which make up the bulk of these fuels, combine with oxygen molecules from the atmosphere, an amount of CO_2 weighing roughly three times more than the fuel burned is generated. There is no feasible way to prevent this CO_2 from escaping into the atmosphere. Methane is produced by living organisms. The metabolic systems of steers and the bacteria in the mud of rice paddies are methane producers. Hence, some methane will be added to the atmosphere for each hamburger or bowl of rice we eat. Freons are manufactured by industry as foaming agents, refrigerants, and propellants. Except for the freons, the greenhouse gases are products of activities essential to human survival. If five or so billion people are to be maintained on our planet, we must continue the greenhouse experiment. We are hooked.

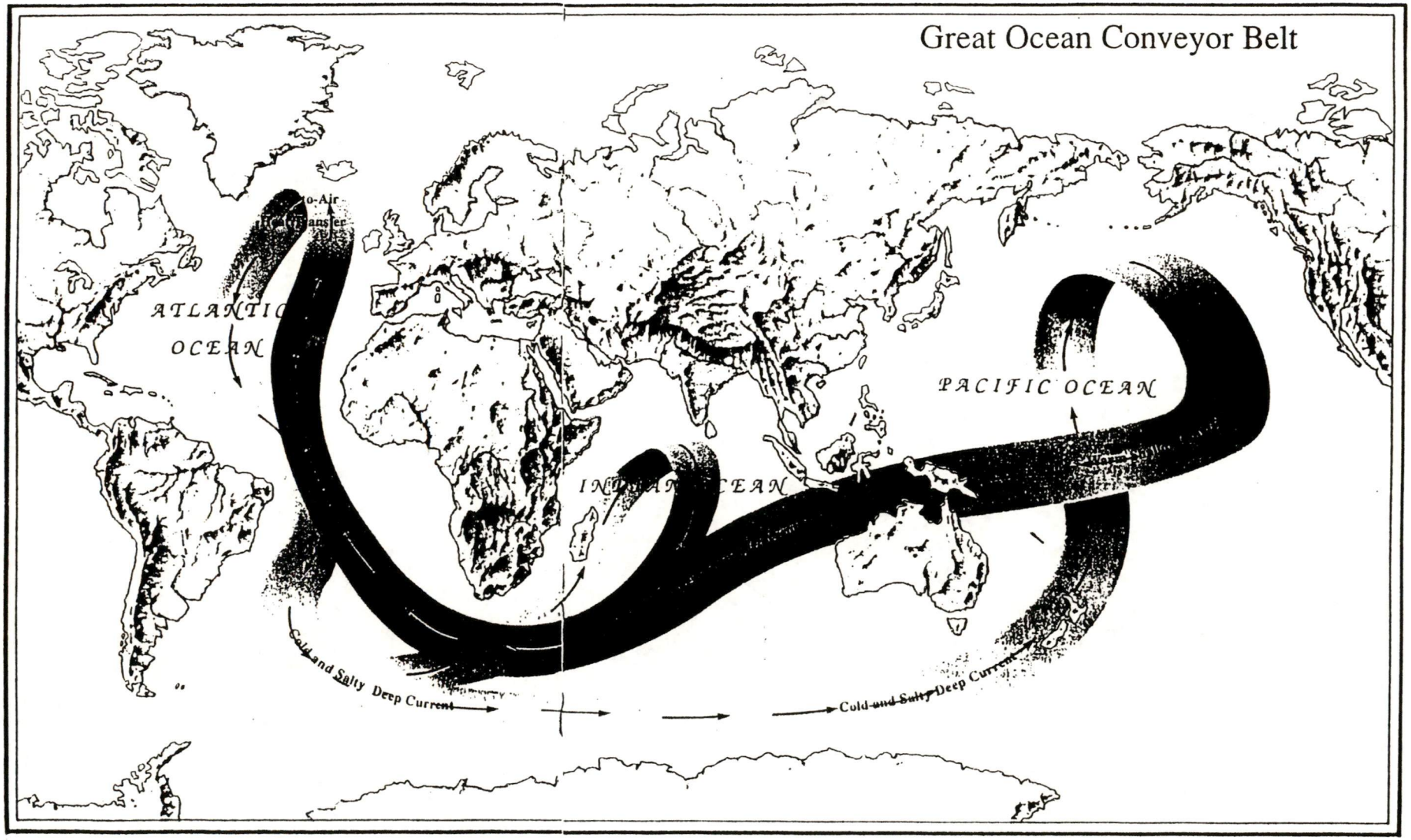
Scientists struggle to increase our understanding of how the earth's environmental system operates in the hope that we will be able to predict at least some of the coming consequences. If so, we can develop strategies to cope with the "bad" and take advantage of the "good" results of this experiment.

These inquiries have recently revealed a piece of disquieting information. Geological studies suggest the earth's climate system resists change until pushed beyond some threshold; then it leaps into a new mode of operation. The situation is akin to that of a radio with automatic frequency control. When the dial on such a radio is turned, instead of one station fading out and the next one fading in, the radio remains locked on one station until a threshold is crossed, at which point it suddenly jumps to another station. The implication of this finding for future climates is clear: the effects of the greenhouse gas buildup may come in sudden jumps, rather than gradually. Such jumps would pose great threats to humans and wildlife.

Our suspicion that the earth's climate changes in leaps comes from the evidence recorded in deep-sea sediments and in ice. The most studied of these records is the amount of heavy oxygen found in the preserved shells of microscopic animals on the ocean floor. The heavy form of oxygen in water vapor tends to be lost as atmospheric moisture is transported to the icecaps. The larger the icecap, the more heavy oxygen remains behind in the seawater. Thus, in eras when the icecaps were large, shelled organisms contained more heavy oxygen than they did when the icecaps were small; the shells therefore contain a history of the ice ages.

The oxygen isotope record tells us that over the last million years the polar icecaps have changed in a cyclic fashion, going from the rather small size of the current warm period to the very large size

Published in Natural History, Vol. 96, No. 10, October, 1987, pp. 74-82.



Illustrations by Joe LeMonnier

at the maximum of the last glaciation. More important, these fluctuations in ice volume have been shown to be in tune with periodic changes in the earth's orbit around the sun, generated by gravitational interactions among the objects making up our solar system. Because the timing of the oxygen isotope changes (as determined by age measurements on deep-sea sediment cores) matches what would be expected if the changes were driven by the earth's changing orbit, scientists are reasonably certain of the cause-and-effect relationship.

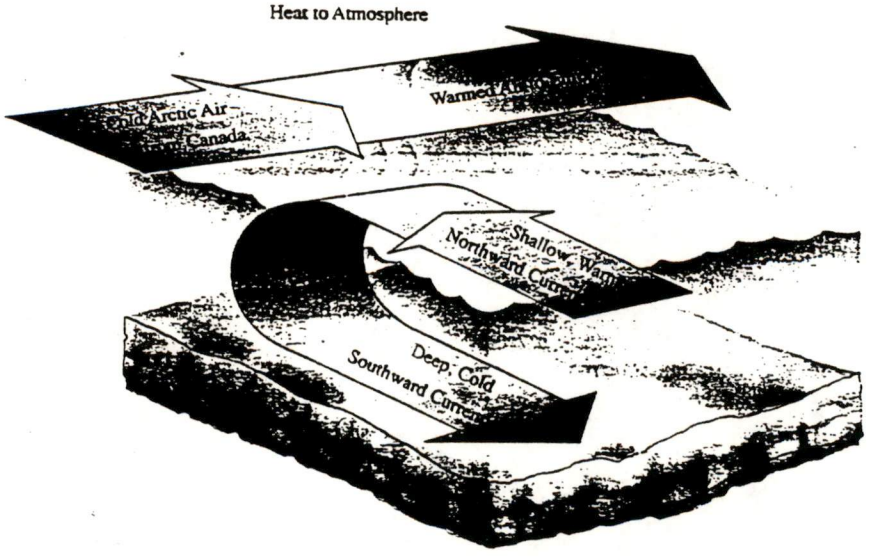
Why do changes in the characteristics of the earth's orbit have anything to do with climate? The answer is that these changes alter the earth's seasons. The relative amounts of each year's sunlight received during the winter months, as opposed to the summer months, changes in accordance with the changing orbit. Exactly how changes in the strength of the seasons drive the expansion and contraction of the earth's polar icecaps remains a matter of debate.

While the oxygen isotope record in the deep-sea sediments provided evidence pointing to the earth's orbital cycles as the pacemaker of glaciation, it also tended to lull scientists into concluding that the earth's climate responds gradually when pushed. This conclusion was drawn despite the realization that the response of polar icecaps to changing climate would have to be so sluggish that a smooth oxygen isotope record would be expected no matter how abrupt the changes in environmental conditions might be. So lulled were we that other clues in paleoclimatic records that pointed to abrupt response were largely disregarded.

The awakening came in the early 1980s when Hans Oeschger and his group at the university in Bern, Switzerland, carried out detailed measurements of the CO_2 content of air trapped in the ice from a deep boring made at a site in southern Greenland. These measurements concentrated on a section of the core on which earlier studies made by the Danish group of Willi Dansgaard had shown repeated leaps in Greenland's air temperature. To everyone's surprise, each of Dansgaard's jumps was accompanied by a 20 percent change in the CO_2 content of the air trapped in bubbles in the ice (and hence in the CO_2 content of air above Greenland at the time the ice formed).

Eyebrows were raised by Oeschger's CO_2 jumps because while the temperature jumps could be written off as a curiosity of Greenland, the CO_2 changes could not. The atmosphere's CO_2 is well mixed with its other gases, hence a measurement in Greenland typifies the entire globe. Furthermore, the changes in CO_2 content found by the Oeschger group occurred in times as short as a few hundred years. To bring about these changes in CO_2 requires some extraordinary change in the earth's chemical cycles, particularly those operating in the ocean. Scientists were therefore forced to the realization that the leaps in Greenland's climate were far-reaching, involving the workings of the ocean as well as those of the atmosphere.

The new look at the ocean triggered by the finding of the Oeschger group brought to the fore the potential importance of a curious tie that exists between the functioning of today's ocean and today's atmosphere. This tie results in a globe-straddling ocean current that keeps north-



Sea-to-Air Heat Transfer *At the northern Atlantic limit of the ocean conveyor belt, surface waters release heat into the atmosphere, greatly moderating Europe's climate.*

ern Europe unusually warm. Paris lies almost a full ten degrees farther north than New York, yet its mean annual temperature is similar to that of New York.

The extra heat received by northern Europe is carried by a conveyor-belt-like ocean current. The part of the conveyor closer to the surface moves to the north; the conveyor's deeper part moves to the south. The important point is that the water of the upper part is warm, while that of the lower part is cold. The temperature change occurs at the northern limit of the belt (in the region around Iceland). Here, during the winter months, water warmed during its passage through the tropical and temperate Atlantic meets air cooled during its passage over frigid Canada. The meeting results in the transfer of heat from the sea to the air. The amount of heat is staggering, measuring about 30 percent of that received by the surface of the North Atlantic from the sun. The result of this transfer is twofold. First, the sting of the cold Canadian air masses is removed before the air hits northern Europe. Second, the waters are cooled and consequently made more dense. The extra density allows the water to sink to the abyss and feeds the lower part of the conveyor. Thus the ocean current acts as a pump, extracting heat from low-latitude air and transferring it to high-latitude air.

The water that sinks to the bottom of the northern Atlantic flows down the full length of the Atlantic, around Africa, through the southern Indian Ocean, and finally up the Pacific Ocean. This deep current carries twenty times more water than the combined world rivers.

There is also an ocean conveyor belt in the North Pacific but it runs the opposite way around. Deep waters move toward the north and upwell to the surface. From there they move toward the equator in the upper ocean. So in today's world, the Atlantic Ocean conveyor belt carries tropical heat for delivery to the atmosphere at high northern latitudes, while the Pacific conveyor belt carries cold surface waters southward, pushing the invading warm waters back toward the equator. Today's major ocean current system thus heats the lands adjacent to the northern Atlantic.

While we don't have the complete answer to why our ocean operates in this fashion, we do have the first principles. The pattern of circulation is governed by the sea's salt. To understand this we must consider the transport of water through the atmosphere. The water that evaporates from the ocean falls eventually as rain or snow. Some of this precipitation reaches the land and some reaches the sea. Some precipitation that falls on land evaporates (mainly from plants) and some runs down the rivers and back to the sea. This cycle must exactly balance: for each molecule that evaporates from the sea, one molecule must return to it either by precipitation on its surface or from the mouth of a river. While this is true for the ocean as a whole, it need not be true for each part of the ocean. In fact, in today's world, an imbalance exists between the Atlantic and the Pacific. The Atlantic loses more water by means of evaporation than it gains by precipitation and continental runoff. The situation is reversed in the Pacific, which receives more water as rain and runoff than it loses by evaporation. While this imbalance is compensated for by a net flow of seawater from the Pacific to the Atlantic, it leaves a mark on the ocean's salt budget. Salt does not evaporate. Thus, the transport of water vapor from the Atlantic to the Pacific enriches the waters of the North Atlantic in salt content. The enrichment in salt must be compensated for by a flow of more salty water from the Atlantic to the Pacific. This is accomplished by the great conveyor belt: the water sinking to the abyss in the northern Atlantic carries excess salt.

The ocean conveyor system maintains higher surface water temperatures in the northern Atlantic than in the northern Pacific. Warmer waters have a higher vapor pressure and lose more water to the air by evaporation. Thus the rate of evaporation from the Atlantic is higher than that from the Pacific. This creates a global "still": water is extracted from the warm Atlantic and transferred through the atmosphere to the cool Pacific.

The phenomenon that maintains this situation is a devilish one; the circulation pattern is self-reinforcing and hence self-stabilizing. The deep current is driven by the extra density supplied to the waters of the northern Atlantic through the enrichment of salt. The enrichment of salt is driven by the heat carried by the water that flows northward in the upper Atlantic. Thus we have a classic chicken and egg situation; excess evaporation causes the deep current and the deep current causes excess evaporation.

The self-stabilization of this great conveyor belt is like the radio automatic frequency control already mentioned. And like that control, the mode of operation of the joint ocean–atmosphere operation will jump if pushed too far. The evidence contained in paleoclimatic records seems to be telling us that the conveyor of today's ocean did not function during the glacial time. Hence it is tempting to conjecture that the turning on and off of the conveyor constitutes an important link between the earth's orbits and our climate. When the belt is in operation, the warmth it delivers prevents ice from accumulating on the lands surrounding the northern Atlantic; when the conveyor is not in operation, these lands are sufficiently cold to permit their glaciation. If this is indeed the case, then the orbitally induced changes in seasonality must somehow alter the extent to which the water evaporating from the Atlantic Ocean escapes removal by the precipitation that falls on continental areas whose drainage is back into the Atlantic. Salt buildup is caused only by that fraction of the water evaporating from the Atlantic that escapes these basins and falls as rain in the Pacific or on continental drainage basins feeding the Pacific.

As we do not yet understand enough about the rules controlling the transport of water vapor through the atmosphere, we cannot say why changes in seasonality cause changes in the transport of water vapor from one ocean basin to another. We can only say that compelling evidence exists in the marine-sediment record for a flipping on and off of the ocean conveyor belt. Since the most vulnerable attribute of the conveyor is water-vapor transport from the Atlantic to the Pacific, some link between this transport and seasonality seems logical.

Evidence for rapid jumps in climate on the land surrounding the northern Atlantic was discovered many decades ago by scientists studying pollen grains preserved in sediments. The record from bogs created during the early phases of the retreat of the icecap that covered Scandinavia and the British Isles during the last glaciation (20,000 to 14,000 years ago) shows a transition from the herbaceous shrubs of the cold period back to the forests of a warmer period. Those early postglacial forests persisted for about 2,000 years and then were suddenly replaced by shrubs akin to those of glacial time. This intense cold snap lasted about 700 years and then just as suddenly came to an end, permitting the forests to return. This brief reversion to cold conditions, which punctuated the period of deglaciation, was named the Younger Dryas (dryas is one of the herbaceous plants that clothed the landscape during the glacial time).

Like other signs pointing to rapid climate change, this rather extraordinary and relatively short-lived return to cold conditions was not given very high billing until Oeschger's group found the rapid CO_2 changes. It then became the focus of attention because detailed records for many localities on the earth's surface were available for the time interval when the earth emerged from its last episode of

glaciation. Furthermore, the records from those sites showed that the Younger Dryas had a distinct geographic pattern. It is a prominent feature in records from the floor of the northern Atlantic and the surrounding continental areas (Maritime Canada, Greenland, and northern Europe). But it is not found in records from the continental United States.

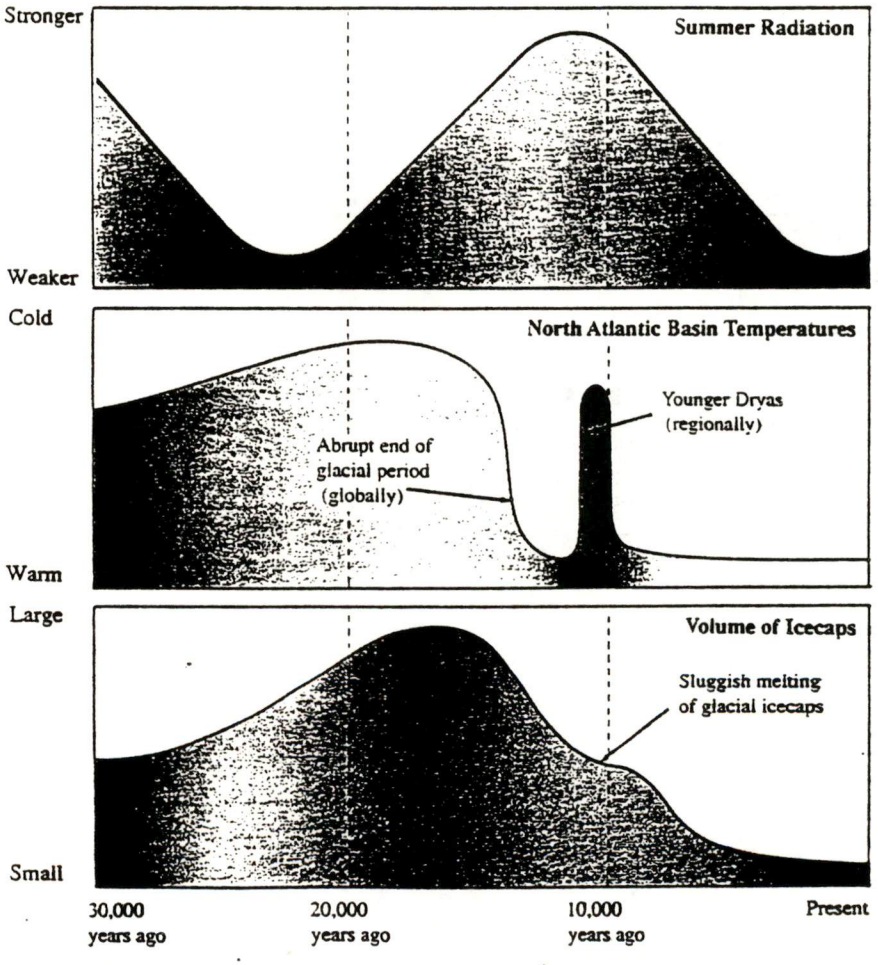
This geographic pattern has been shown by computer simulations of the global climate system to be what would be expected if the ocean conveyor belt were to be turned off (and with it the enormous amount of heat delivered to the atmosphere above the northern Atlantic). Air temperatures over the eastern fringe of Canada, over Greenland, and over much of western Europe would plunge about 15°F. By contrast, no significant change in temperature would be seen in the United States. Hence, the geographic pattern of the Younger Dryas event points to the ocean conveyor as the causal villain.

Evidence from ocean-sediment cores taken in the northern Atlantic strengthens this case. Not only do the shells of the surface-dwelling plankton show a dramatic shift back to cold-water species during the Younger Dryas interval but also, as shown by Edward Boyle of MIT, the content of the trace metal cadmium in the shells of bottom-dwelling foraminifera indicates that cold deep waters, akin to those present during glacial times, returned during the Younger Dryas.

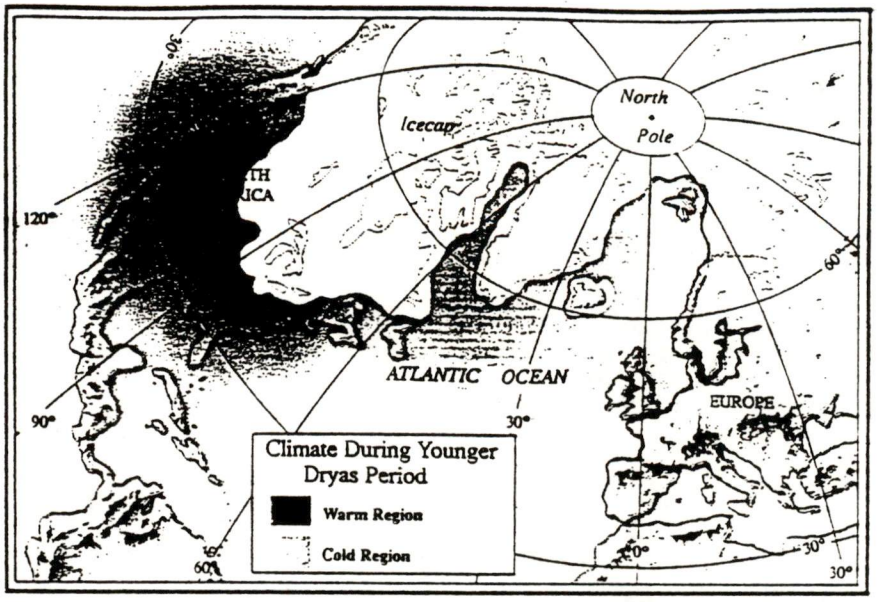
So we get the following picture. A full-fledged glaciation dominated our planet from about 20,000 to about 14,000 years ago. This corresponded to a time when the earth's orbital cycles gave rise to reduced seasonality at high latitudes in the Northern Hemisphere. During this time the ocean was "on another station," meaning its conveyor belt was not in operation. Then, as the orbits led to gradual strengthening of seasonality, the conveyor was switched back on. The heat released by the conveyor to the atmosphere over the northern Atlantic caused the great ice sheets to melt. But about 2,000 years later the conveyor came to an abrupt halt, bringing back cold conditions to the lands around the northern Atlantic. Then after a 700-year hiatus, the conveyor belt sprang back into action and has run steadily up to the present. Why the brief stoppage?

To understand what appears to be the answer to this question, we must first appreciate that a staggering 12-million cubic miles of water was bound up in the continental ice sheets of the Northern Hemisphere at the peak of the last glaciation. During the 5,000-year period when this ice melted away, the flow of meltwater must have averaged about half the current discharge of the Northern Hemisphere's combined rivers. Where it went would therefore have an important impact on the ocean's salt cycle.

Geologists studying the deposits left behind during the retreat of the largest of the glacial icecaps, the one that covered Canada from the Rocky Mountains to the Atlantic Ocean, have reconstructed the routes taken by the meltwater released from its southern margin. Their studies reveal that during the initial phases of melting, all routes converged on the Mississippi River and hence all the meltwater flowed into the Gulf of Mexico. However, starting about 11,800 years ago, those routes were captured one after another by eastward-leading channels that progressively opened as the ice front retreated to the north. First, the water entering the basins of what are now Lakes Erie and Ontario was diverted to the sea through the Hudson River valley. Then the water entering the basins of what are present-day Lakes Huron and Michigan was diverted to the Saint Lawrence River valley through a channel in the glacially depressed landscape north of Lake Erie. Finally, the biggest and most important of these diversions occurred when a lobe of ice blocking off the eastern end of what is now Lake Superior melted, allowing water to flow into Lake Huron and from there to the Saint Lawrence. At this point all the water melting from the southern margin of the Laurentide ice sheet was flowing eastward into the Atlantic. Nearly all of this water reached the Atlantic via the Saint Lawrence River. While the diversion of the meltwater from the Mississippi to the Saint Lawrence occurred in



Fluctuations in the earth's orbit, affecting how much summer sunlight the earth receives (top graph), have expanded and contracted the polar icecap, driving the Northern Hemisphere in and out of glacial (Ice Age) episodes. Although the volume of the ice changes sluggishly and gradually (bottom graph), an abrupt global warming has marked the end of each glacial period, indicating that ocean–atmosphere operation can change suddenly (middle). The Younger Dryas event, a 700-year return to glacial conditions that interrupted the present warm episode, is thought to have been caused by a sudden diversion of melting Canadian ice sheet waters from the Mississippi to the Saint Lawrence River.



The sudden, localized cooling of Europe and Maritime Canada during the Younger Dryas event indicates that the great ocean conveyor belt suddenly stopped operating.

several discrete steps over a period of about 800 years, the largest of these diversions was the last, involving the meltwater released from about 60 percent of the southern perimeter of the Laurentide ice sheet. As dated by the radiocarbon method, it occurred about 11,000 years ago. Within the margin of error of such age determinations, this corresponds to the time the Younger Dryas began.

Scientists understand why the sudden diversion of a large meltwater flow from the Mississippi River to the Saint Lawrence would affect the ocean conveyor. As stated above, an essential feature of this system is the densification through cooling of high salt content water in the northern Atlantic. Today, the sinking of this water feeds a globe-encircling deep current. The sudden influx directly into the northern Atlantic of an amount of water equivalent to that carried by the Amazon River would almost certainly diminish the salinity of surface waters in the northern Atlantic enough to disrupt the deep-water formation process. One might say that the Younger Dryas was not only a warning about the manner in which climate reacts when pushed but also clearly showed that the coupling between the transport of fresh water across the earth's surface and the transport of salt within the sea is a critical element in the earth's response to climate change.

If this reading of the paleoclimatic record is correct, then we must face up to the reality that our climatic system does not operate in an orderly manner. As the greenhouse gases we produce build up, the ocean–atmosphere system may leap to yet another mode of operation. Unfortunately, the paleoclimatic record provides no clues as to how the earth's climate system responds when warmed beyond its prevailing state. Over the period for which our paleoenvironmental records are sufficiently detailed to permit such reconstructions, climate has not been significantly warmer than today's. So we are pushing the earth into an unknown realm. We have no way to predict how the great ocean conveyor will respond, nor can we be sure of other important elements of the system, which are subject to dramatic change.

The computer simulations that have greatly improved our ability to predict weather have also told us some important things about the possible response to the greenhouse buildup. But because of their basic design, these computer models cannot tell us anything about the ocean–atmosphere system and leaping climates. At present no one knows how to incorporate the oceans into these simulations. Decades may pass before this can be done. Even then I doubt if computer simulations will offer much insight into the changes in climate that might be triggered by the greenhouse buildup.

The upshot is that we must take our greenhouse experiment more seriously. Rather than treating it as a cocktail hour curiosity, we must view it as a threat to human beings and wildlife that can be resolved only by serious study over many decades. We must expand our efforts to understand the operation of each of the units of the earth's climate system and how they interact. Only in this way will our grandchildren be able to prepare wisely for the changes that are bound to be wrought by our great experiment. □

National Aeronautics and
Space Administration

George C. Marshall Space Flight Center
Marshall Space Flight Center, Alabama 35812
AC(205)544-2121

NASA

Reply to Attn of: DA01

The Honorable Albert Gore, Jr.
United States Senate
Washington, DC 20510

Dear Senator Gore:

This letter is a continuation of our response to your October 1990, request to Dr. Roy Spencer, a scientist in the Remote Sensing Branch of the Marshall Space Flight Center's Space Science Laboratory, to keep you informed of his monitoring of global satellite temperature data. Our initial update was provided in January 1991, reflecting temperatures through October 1990.

As you can see from the results through February 1991, global temperatures are remaining above average, continuing the most recent warm period which began in late 1989. The net global trend for the last 12 years is now +0.03°C/decade, made up of a Northern Hemisphere trend of +0.09°C/decade and a Southern Hemisphere trend of -0.03°C/decade. The margin of error for the global temperature trend is ±0.02°C/decade, and ±0.03°C/decade for each Hemisphere. These measurements have been corrected for stratospheric influences.

I appreciate the opportunity to provide you with this information, and for your interest in Dr. Spencer's work and your support of the Marshall Center and NASA.

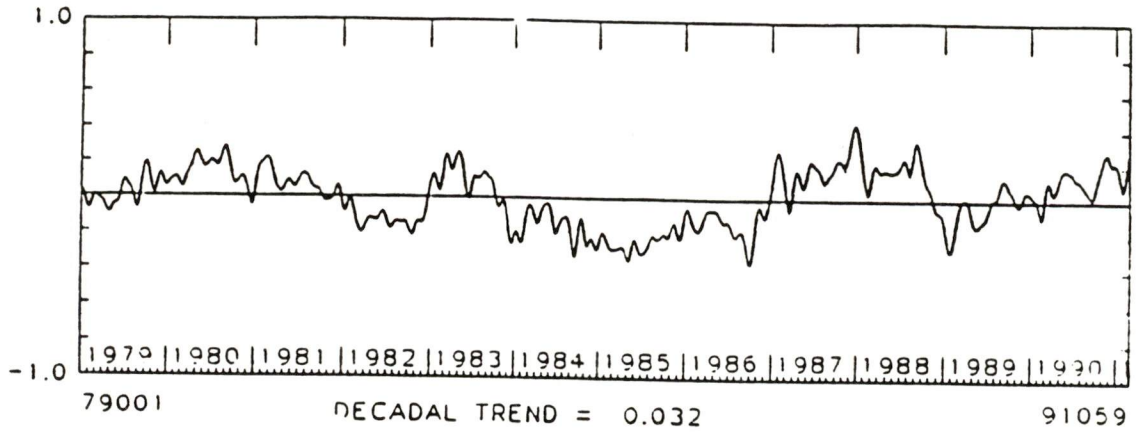
Sincerely,

T. J. Lee
Director

Enclosure

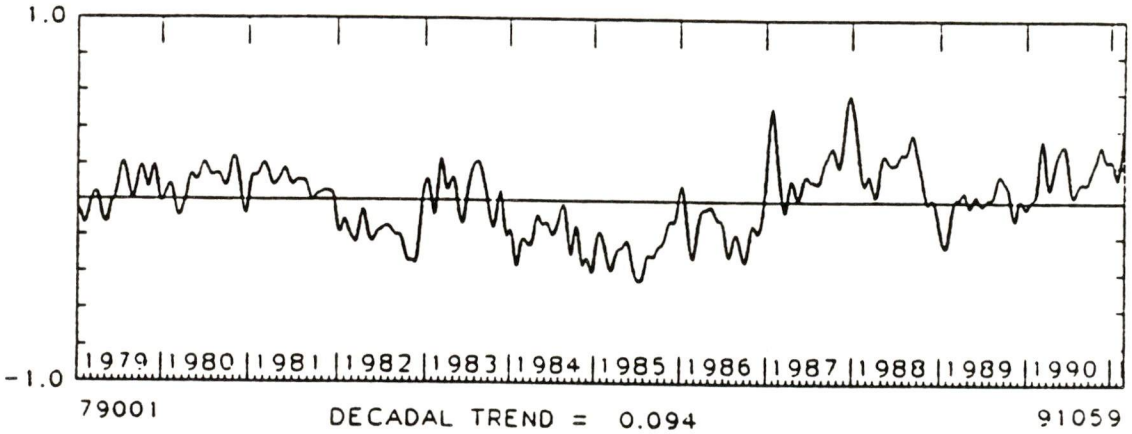
cc:
HDQS/S/Dr. Fisk
[redacted]/Dr. Tilford

GLOBAL



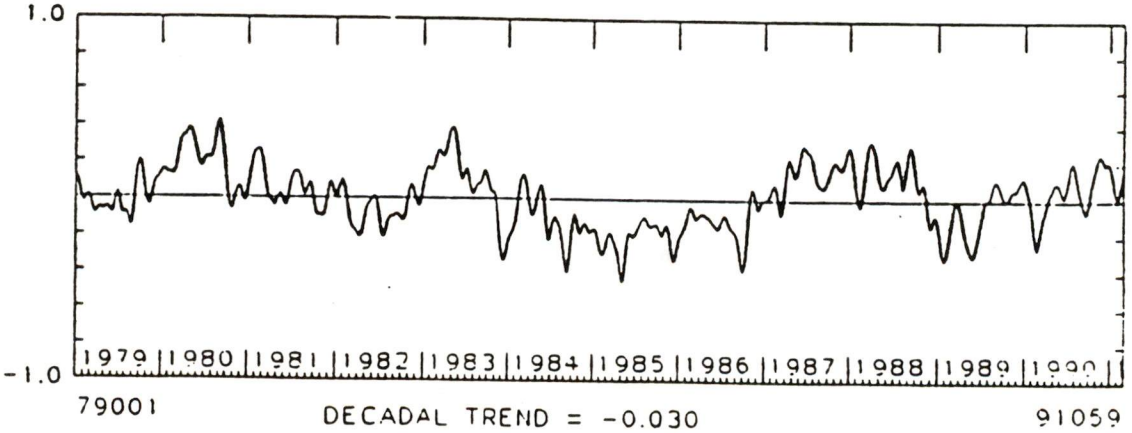
79001 DECADAL TREND = 0.032 91059

NO. HEMISPHERE



79001 DECADAL TREND = 0.094 91059

SO. HEMISPHERE



79001 DECADAL TREND = -0.030 91059

FILTER WIDTH = 61

Revised projection of future greenhouse warming

Michael E. Schlesinger & Xingjian Jiang

Department of Atmospheric Sciences, University of Illinois at Urbana-Champaign, 105 South Gregory Avenue, Urbana, Illinois 61801, USA

FOR the Intergovernmental Panel on Climate Change (IPCC) report[1], using a simple climate/ocean model, we made projections of the greenhouse warming to 2100. Projections were made for four greenhouse-gas scenarios, whose radiative effects in 2100, expressed in terms of an equivalent amount of CO_2, ranged from 2 to 5.5 times the pre-industrial CO_2 concentration. The projected global warming in 2100 for these scenarios, relative to 1990, ranged from 0.62–2.31 °C for the minimum assumed CO_2-doubling temperature sensitivity, $\Delta T_{2x} = 1.5$ °C, to 1.61–5.15 °C for the maximum sensitivity $\Delta T_{2x} = 4.5$ °C. Here we broaden these projections to include a recently suggested lower sensitivity, $\Delta T_{2x} = 0.5$ °C. We also revise all projections by prescribing, using the results of our analysis of simulations by a coupled atmosphere–ocean general circulation model, a lower value for a key parameter of the simple ocean model, Π, which indicates the warming of the polar ocean relative to the warming of the non-polar ocean. We find that, for any value of ΔT_{2x}, the atmospheric temperature increases more rapidly with time as a consequence of the reduction in Π. We also find that a delay of ten years in initiating a 20-year transition from the IPCC 'business-as-usual' scenario to any other IPCC scenario has only a small effect on the projected warming in 2100, regardless of the value of ΔT_{2x}. This indicates that the penalty for a 10-year delay is small.

Our earlier analysis for the IPCC report, and this revision thereof, both use an energy-balance climate/upwelling-diffusion ocean model (Fig. 1) similar to that introduced by Hoffert *et al.*[2] and used by Hoffert and Flannery[3] to predict CO_2-induced climate change. This simple climate/ocean model is used instead of our atmosphere-ocean general circulation model[4] because of the latter's large computational requirement.

The simple climate/ocean model (Fig. 1) determines the surface temperature of the atmosphere and the temperature of the ocean as a function of depth from the ocean surface to the ocean floor. In the model, the ocean is subdivided vertically into 40 layers, with the uppermost being the mixed layer and the deeper layers each being 100 m thick. The ocean is also subdivided horizontally into a polar region where bottom water is formed, and a non-polar region where there is vertical upwelling. In the non-polar region, heat is transported upwards toward the surface by the upwelling, and downwards by physical processes whose effects are treated as equivalent to diffusion. Heat is also removed from the mixed layer in the non-polar region by transport to the polar region and downwelling towards the ocean bottom—this heat is ultimately transported upwards from the ocean floor in the non-polar region. Five quantities must be prescribed in this simple climate/ocean model: the temperature sensitivity of the climate system, characterized by the equilibrium warming induced by a CO_2 doubling, ΔT_{2x}; the vertically uniform upwelling velocity for the global ocean, W; the vertically uniform thermal diffusivity, κ, by which all non-advective vertical heat transport in the ocean is parameterized; the depth of the oceanic mixed layer, h; and the warming of the polar ocean relative to the warming of the non-polar ocean, Π. For the IPCC report we chose three values of ΔT_{2x} (4.5, 2.5 and 1.5 °C) and $h = 70$ m, $W = 4$ m yr^{-1}, $\kappa = 0.63$ cm^2 s^{-1}, and $\Pi = 1.0$. We chose the latter value as a result of simulations by atmospheric GCM/mixed-layer ocean models of the equilibrium climate change induced by a doubling of the atmosphere CO_2 concentration[5]. These simulations show a poleward amplification of the surface temperature change in the winter hemisphere, thereby suggesting that Π should equal 1.0.

Here we prescribe Π based on our recent analysis[4] of the transient time evolutions of $1\times CO_2$ and $2\times CO_2$ simulations with an atmosphere-ocean GCM. Examining the changes in temperature in the polar (downwelling) and non-polar (upwelling) regions gives values of Π that range from 0.569 for the uppermost layer (a depth of 0–50 m) to 0.004 for the lowermost layer (a depth of 2,750–4,350 m), with a depth-averaged value of 0.161. The smallness of the depth-averaged value and the value of Π for the deep ocean are probably due to the brevity of the $1\times CO_2$ and $2\times CO_2$ simulations, each being only 20 years

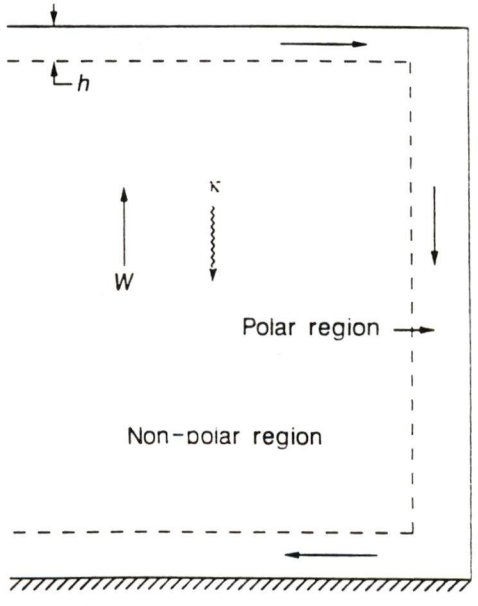


FIG. 1 Schematic representation of the energy-balance climate/upwelling-diffusion ocean model.

TABLE 1 Potential warming reduction in 2100 obtained by a linear transition from IPCC scenario A to IPCC scenario B, C or D during either 1990–2010 or 2000–2020

ΔT_{2x} (°C)	*Scenario A to B*		*Scenario A to C*		*Scenario A to D*	
	1990–2010 (°C)	2000–2020 (°C)	1990–2010 (°C)	2000–2020 (°C)	1990–2010 (°C)	2000–2020 (°C)
0.5	0.39	0.37 (96%)	0.55	0.52 (96%)	0.64	0.61 (96%)
1.5	1.04	0.99 (95%)	1.45	1.38 (96%)	1.71	1.63 (95%)
4.5	2.31	2.18 (95%)	3.17	3.00 (95%)	3.78	3.57 (95%)

long. It is therefore likely that $0.161 < \Pi < 0.569$, with a value closer to the mean of 0.365, and we accordingly choose $\Pi = 0.4$.

We have calculated the temperature change from 1765 to 1990 induced by the historical evolution of greenhouse gases (T. Wigley, personal communication), and from 1990 to 2100 for the four IPCC scenarios. These scenarios can be characterized by the year in which the radiative effect of greenhouse gases is equivalent to a doubling of the pre-industrial CO_2 concentration: A ('business-as-usual'), 2015; B, 2031; C, 2038 and D, 2100. We have performed these calculations for presumed temperature sensitivities of $\Delta T_{2x} = 4.5$, 1.5 and 0.5 °C, the first two values being the extremes adopted by IPCC, and the latter value proposed by Lindzen[6] (and personal communication, 1990). Comparing the calculated greenhouse-induced temperature changes for these different sensitivities with the observed global mean temperature changes from 1880 to 1990 (ref. 1) shows that the patterns of temperature change are not identical in shape or magnitude (Fig. 2). In particular, the calculated temperature changes increase monotonically in time and attain values of 1.30, 0.61 and 0.24 °C in 1990 relative to 1880 for the three sensitivities, respectively, but the observed global mean temperature does not increase monotonically in time, and is ~0.5 °C in 1990 relative to 1880. Thus, there are significant disparities between the observed and reconstructed temperature evolutions for both $\Delta T_{2x} = 4.5$ and 0.5 °C, with a best fit being obtained for $\Delta T_{2x} = 1.24$ °C, a value less than the minimum temperature sensitivity used in the IPCC calculations. This sensitivity is also below that for zero feedback (only radiative-convective adjustment of temperature without changes in other quantities such as water vapour, clouds and sea ice), $(\Delta T_{2x})_0 = 1.32$ °C, and implies a net negative feedback of $f = -0.06$ $[\Delta T_{2x}/(\Delta T_{2x})_0 = 1/(1-f)]$. But as discussed by Wigley and Raper[7], it is difficult to estimate ΔT_{2x} from the observed temperature record because of the unknown contribution from the climate's natural variability. Any estimate of ΔT_{2x} is further confounded by external forcing mechanisms, both natural (for example, volcanic and solar-irradiance variations) and anthropogenic (for example, sulphate emissions[8]), the magnitudes of which are also uncertain.

Our temperature projections to 2100 for the IPCC scenarios using $\Pi = 0.4$ give larger temperature increases than those using $\Pi = 1.0$, with the difference being larger for larger ΔT_{2x}. This occurs because less heat is transferred to the deep ocean as Π decreases, hence the warming of the upper ocean and atmosphere increases. For the business-as-usual scenario (A) and with $\Delta T_{2x} = 4.5$ °C, $T(2100) - T(1880) = 6.2$ °C for $\Pi = 1.0$, but 7.2 °C for $\Pi = 0.4$. The corresponding values for $\Delta T_{2x} = 1.5$ °C are 2.9 °C and 3.1 °C, whereas those for $\Delta T_{2x} = 0.5$ °C are both 1.1 °C. These results clearly show that the magnitude of the potential greenhouse-gas-induced climate change ranges from catastrophic to minor depending on the true value of ΔT_{2x} for the climate system. Consequently, it is imperative to narrow the range of possible values of ΔT_{2x}, for example, by determining the minimum possible value below which the Earth would not have undergone glacial–interglacial cycles. This can be done by model simulations of these cycles and comparison with paloclimate data.

We have calculated the temperature changes from 1990 to 2100 for the IPCC scenarios B, C and D, in which greenhouse gas emissions are reduced. These calculations show, as did our IPCC calculations, that reducing the future increase in greenhouse gases reduces the future increase in temperature, with the size of the reduction being larger for larger ΔT_{2x}. For example, the 1990–2100 temperature rise for scenario B is less than that for scenario A by 2.45, 1.08 and 0.40 °C for $\Delta T_{2x} = 4.5$, 1.5 and 0.5 °C, respectively. If a linear transition from 1990 to 2010 is

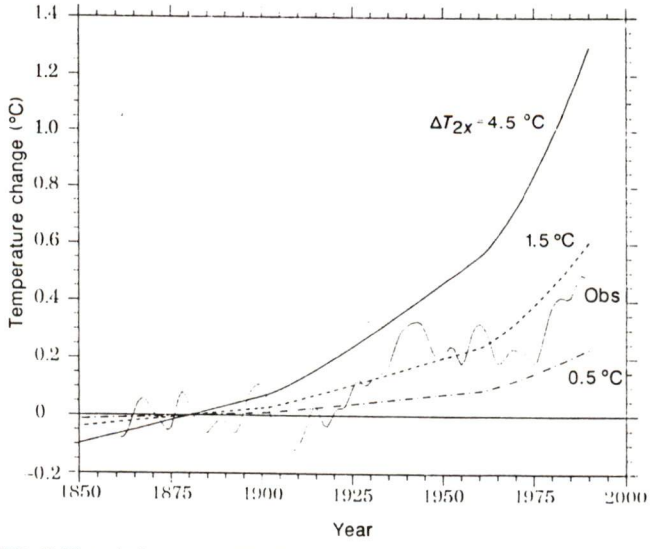


FIG. 2 Historical greenhouse-gas-induced temperature change calculated from 1765 to 1990 for prescribed climate sensitivities of $\Delta T_{2x} = 4.5$, 1.5, and 0.5 °C, together with the observed temperature change (Obs). All temperature changes have been referenced to 1880.

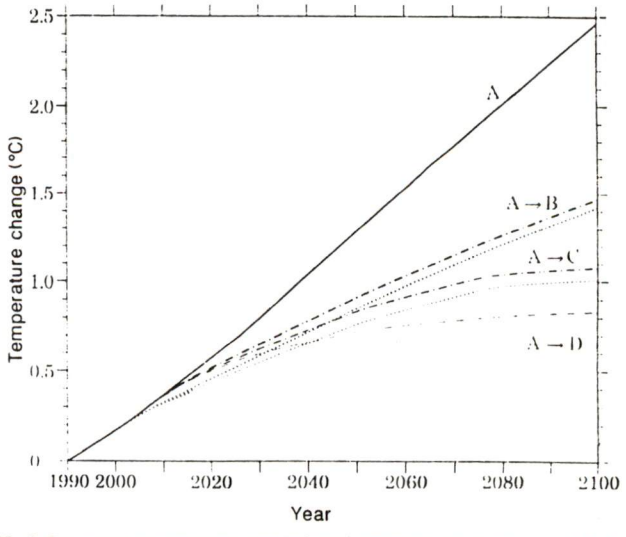


FIG. 3 Projected greenhouse-gas-induced temperature change to 2100 for a prescribed climate sensitivity of $\Delta T_{2x} = 1.5$ for: IPCC scenario A (solid line); a linear transition from 1990 to 2010 from IPCC scenario A to either IPCC scenario B, C or D (dotted lines); and a linear transition during 2000 to 2020 from IPCC scenario A to either IPCC scenario B, C or D (dash-dotted lines). All calculations begin in 1765 and all temperature changes are relative to 1990.

made from the emission rate of scenario A to the emission rate of scenario B, the reduction in temperature rise in 2100 is 2.31, 1.04 and 0.39 °C for $\Delta T_{2\times} = 4.5$, 1.5 and 0.5 °C, respectively (Fig. 3, Table 1). If the initiation of this transition in emission rate is deferred 10 years until 2000, the reduction in temperature rise in 2100 is 2.18, 0.99 and 0.37 °C; that is, at least 95% of that possible by not deferring the transition. The equivalent atmosphere CO_2 concentration in 2100 increases as a consequence of this deferral, thereby increasing the equilibrium temperature change (the 'committed warming,' approximately equal to the increase in temperature change shown in Fig. 3) by 0.15, 0.05 and 0.02 °C for $\Delta T_{2\times} = 4.5$, 1.5 and 0.5 °C, respectively. Corresponding results are obtained for 20-year linear transitions from the emission rate of scenario A to the emission rate of either scenario C or scenario D (Fig. 3), with the reduction in temperature rise in 2100 equal to at least 95% of that possible by not deferring the transition, regardless of the temperature sensitivity (Table 1). The corresponding increases in the committed warming in 2100 for a 10-year deferral in transitions from scenario A to C(D) are 0.22(0.28), 0.07(0.09) and 0.02(0.03)°C for $\Delta T_{2\times} = 4.5$, 1.5 and 0.5 °C, respectively. This indicates that the penalty is small for a 10-year delay in initiating the transition to a regime in which greenhouse-gas emissions are reduced.

To us this small penalty does not indicate that we should 'wait and see' and do nothing during this decade—quite the contrary. The study of the greenhouse effect, both theoretically and observationally, should be accelerated into a 'crash programme' so that we do not squander the time that nature has given us to obtain a realistic understanding of the climate response to increasing concentrations of greenhouse gases. □

Received 12 November 1990; accepted 28 January 1991.

1. Houghton, J. T., Jenkins, G. J. & Ephraums, J. J. (eds) *Climate Change: The IPCC Scientific Assessment* (Cambridge University Press, 1990).
2. Hoffert, M. I., Callegari, A. J. & Hsieh, C.-T. *J. geophys. Res.* **85**, 6667–6679 (1980).
3. Hoffert, M. I. & Flannery, B. P. in *Projecting the Climatic Effects of Increasing Carbon Dioxide* (eds MacCracken, M. C. & Luther, F. M.), 149–190 (US Department of Energy, Washington, DC 1985).
4. Schlesinger, M. E. & Jiang, X. *J. Clim.* **3**, 1297–1315 (1990).
5. Schlesinger, M. E. & Mitchell, J. F. B. *Rev. Geophys.* **25**, 760–798 (1987).
6. Lindzen, R. S. *Bull. Am. meteorol. Soc.* **71**, 288–299 (1990).
7. Wigley, T. M. L. & Raper, S. C. B. in *Greenhouse-gas-induced Climatic Change: A Critical Appraisal of Simulations and Observations* (ed. Schlesinger, M. E.) 471–482 (Elsevier, Amsterdam, 1991).
8. Charlson, R. J., Langner, J. & Rodhe, H. *Nature* **348**, 22 (1990).

ACKNOWLEDGEMENTS. This research was supported by the US NSF and the US Department of Energy Carbon Dioxide Research Program, Office of Health and Environmental Research.